Biofabrication Platforms for Increasing the Dimensionality of Electrospun Hydrogels

---

A dissertation presented to the faculty at the School of Engineering and Applied Science
University of Virginia

In partial fulfillment of the requirements for the degree of
Doctor of Philosophy in Chemical Engineering

By:

M. Gregory S. Grewal

August 2023

APPROVAL SHEET

This

Dissertation

is submitted in partial fulfillment of the requirements
for the degree of

Doctor of Philosophy

Author: M. Gregory Grewal

This Dissertation has been read and approved by the examing committee:

Advisor: Christopher Highley

Advisor:

Committee Member: Steven Caliari

Committee Member: Shayn Peirce-Cottler

Committee Member: Kyle Lampe

Committee Member: Rachel Letteri

Committee Member: Rebecca Pompano

Committee Member:

Accepted for the School of Engineering and Applied Science:

Jennifer L. West (signature)

Jennifer L. West, School of Engineering and Applied Science

August 2023

ABSTRACT

The extracellular matrix (ECM) is highly complex and dynamic, regulating cell functions through the presentation of various biophysical and biochemical signals. ECM composition is tissue system-dependent, but it generally consists of fibrous proteins that dictate tissue structure with additional amorphous interstitial material contributing to function and soft-tissue mechanics. Historically, there has been considerable focus on using hydrogels to model the ECM; however, these materials are often static and isotropic and therefore unable to recapitulate some of the complexities of natural tissue. Work to close this gap in biomaterials research includes a focus on hydrogel advances that aim to capture the highly structured and dynamic nature of the ECM. Processing hydrogel-forming biomaterials via electrospinning enables these advancements in dynamic hydrogels to be translated into a fibrous form, which offers opportunities to model some of the biochemical and biophysical attributes found in endogenous tissue environments. While it is possible to generate dynamic, fibrous hydrogel architectures in this way, they are often still limited in their dimensionality – both in 3D space and in dynamics across time. In light of this, the goal of this thesis was to develop new classes of biofabrication tools that address these limitations in electrospun systems based on hydrogels.

We leveraged hyaluronic acid (HA) and polyethylene glycol (PEG) as the base materials for this work and installed reactive groups (e.g., norbornene, methacrylate, vinyl sulfone) that enable spatially-controllable, photomediated crosslinking and biochemical functionalization of the resultant fibers. The flexibility offered by these reaction mechanisms, along with the geometry of the electrospun hydrogel fibers, are exploited

herein to develop the demonstrated biofabrication platforms. First, to address challenges in the time dimension, a peptide-based platform that enabled dynamic presentation of bioactive molecules on hydrogel (both isotropic and fibrous) substrates was demonstrated. User-defined, reversible presentation of these biomolecules was achieved through the formation and disruption of coiled coil complexes through toehold-mediated strand displacement. Next, towards the translation of electrospun fibers into 3D space, a novel granular hydrogel medium comprised of segmented electrospun hydrogel fibers was developed. These granular hydrogel materials exhibited unique mechanics with tunable viscoelasticity and stress relaxation properties – enabling not only injection/extrusion, but also serving as 3D, permissive culture environments for cell encapsulation. Finally, a foundational layer-by-layer biofabrication platform based on spatially-patternable electrospun substrates was investigated to enable the localization of cellular and material content at high resolution in 3D, macroscale constructs. Taken together, the electrospun hydrogel-based systems developed throughout this thesis offer new opportunities in designing functional biomaterials and address broad challenges in recapitulating complex biochemical and biophysical architectures in engineered tissues.

ACKNOWLEDGEMENTS

TABLE OF CONTENTS

LIST OF TABLES

LIST OF SCHEMES

LIST OF FIGURES

CHAPTER 2

CHAPTER 3

CHAPTER 4

CHAPTER 5

CHAPTER 6

CHAPTER 7

CHAPTER 1: SPECIFIC AIMS AND RESEARCH OVERVIEW

1.1. Overview

The extracellular matrix (ECM) is a complex, heterogenous material environment that comprises the acellular scaffolding within natural tissue that supports physiological function through the presentation of various biophysical and biochemical signals. While the specific composition of the ECM is highly dynamic and tissue-dependent, it generally consists of fibrous proteins that dictate the physical structure, with additional amorphous interstitial material that contributes to the soft, water-swollen characteristics of the tissue system. Hydrogel-forming biomaterials have seen considerable use in the tissue engineering space due to their ability to recapitulate some of the properties of soft tissue types; however, hydrogels are often static and isotropic and therefore unable to mimic some of the complexities of endogenous ECM. Work to close this gap in biomaterials research includes a focus on hydrogel advances that aim to capture the highly structured and dynamic nature of the ECM. Processing hydrogel-forming biomaterials via electrospinning enables these advancements in dynamic hydrogels to be translated into a fibrous form, which offers opportunities for modeling some of the biochemical and biophysical attributes found in natural tissue. While it is possible to generate dynamic, fibrous hydrogel architectures using electrospinning, the resultant fibers are often still limited in their dimensionality – both in 3D space and in dynamics across time. In response, there has been considerable work aiming to improve upon the dimensionality of electrospun fibers to engineer more dynamically complex models of the ECM.

Given the desire to improve electrospun hydrogel fibers for tissue engineering applications, the goal of this thesis was to develop biofabrication platforms that address

the time and space limitations of more traditional electrospun hydrogels. Hyaluronic acid (HA) and polyethylene glycol (PEG) were chosen as the base polymers for the electrospun fibers due to their inherent biocompatibility and amenability to chemical modifications that enable both crosslinking and downstream functionalizing with bioactive molecules. Specifically, these bodies of work leveraged well-established reactive moieties (e.g., norbornene, methacrylate, vinyl sulfone) to form HA or PEG fibers that were utilized as the building blocks for the biofabrication tools described herein. These HA and PEG fibers received different downstream processing treatments to realize new biochemical and biophysical complexities for engineering fibrous hydrogels with increased dimensionalities. The following three aims were developed to move towards biofabrication platforms that address the time and space constraints associated with conventional electrospun fibers.

1.2. Specific Aims

<u>Specific Aim 1:</u> **Design a material technology that enables control over both spatial and temporal presentation of bioactive molecules on isotropic hydrogels and electrospun hydrogel fibers.**

Hypothesis: Coiled coil-forming peptides can be designed to allow for both spatially-controlled conjugation to hydrogel substrates through photomediated thiol-ene reactions, and temporal control of biomolecule presentation via toehold-mediated strand displacement of the coiled coils.

To address this hypothesis, norbornene-modified HA and PEG derivatives (NorHA and PEGNB, respectively) were utilized to permit thiol-ene tethering of cysteine-

containing peptide sequences. Repeating heptads known to form coiled coils were synthesized with mismatched lengths to enable toehold-mediated strand displacement using traditional solid-phase methods. Three peptides were utilized in this study: the T-peptide (3 repeating heptads; tethers to the hydrogel substrate), the A-peptide (4 repeating heptads; contains either a fluorophore or bioactive sequence; associates with the T-peptide), and the D-peptide (4 repeating heptads; preferentially associates with the A-peptide; disrupts the T:A complex). The mismatched lengths allow for toehold-mediated strand displacement with the A:D association forming a preferred coiled coil complex compared to the T:A association. NorHA synthesis was confirmed with ^{1}H NMR. Successful peptide syntheses were confirmed using electrospray ionization mass spectrometry, secondary structures were analyzed using circular dichroism spectroscopy, and coiled coil complexation in solution was monitored via isothermal titration calorimetry.

Coiled coil-forming peptides were conjugated to NorHA hydrogels and PEGNB hydrogel fibers with spatial control through the photomediated thiol-ene click reaction. Temporal control via toehold-mediated strand displacement was quantified by measuring the fluorescence of the supernatant following the washing steps to remove a fluorophore-tagged analog of the bioactive peptide utilized in this coiled coil scheme. The fluorophore on the bioactive peptide is interchangeable and was next replaced with an RGD sequence to modulate the adhesion properties of the NorHA and PEGNB substrates and influence 3T3 fibroblast spreading.

Specific Aim 2: Design and characterize a fiber-based granular hydrogel medium that enables increased interparticle interactions between individual fibers for robust mechanical properties with tunable viscoelasticity and stress relaxation.

Hypothesis: Electrospun hydrogel fibers can be segmented and packed to yield a granular hydrogel where the "grains" are discrete fibers that interact and entangle at increased length scales, thus contributing unique mechanical profiles to the granular hydrogel medium.

To address this hypothesis, methacrylate-modified HA (MeHA) and PEGNB were utilized as the base materials to fabricate electrospun fibers. MeHA structure was confirmed via ^{1}H NMR. Resultant fibers were segmented to form discrete fiber lengths and assembled into granular hydrogels without secondary annealing via centrifuge-mediated packing at different packing densities (i.e., varying degrees of interstitial fluid between fibers). Physical properties and complex, time-dependent mechanics were evaluated using oscillatory shear rheology and filament stretching extensional rheology. Indeed, analyses of packed hydrogel microfiber scaffolds suggest unique mechanical properties (e.g., yield strains, extensibility, viscoelasticity, stress relaxation, etc.) compared to conventional hydrogel particle systems (i.e., spherical particles), which is attributed to their increased interparticle interactions afforded by fiber-fiber entanglement and reorganization. Adding secondary annealing mechanisms increases the elasticity of these materials, while concomitantly limiting fiber sliding and reorganization, thus restricting bulk scaffold time-dependent mechanics like stress relaxation. These fiber-based granular hydrogels were conceptualized and demonstrated as 3D, permissive cell

culture scaffolds; however, they also demonstrate utility as injectable biomaterial inks for extrusion printing applications.

Specific Aim 3: Design of a biofabrication platform for engineering tissue constructs with control over material and cellular architecture at near-cell-scale resolution throughout 3D space.

Hypothesis: Photopatternable electrospun scaffolds will enable near-single-cell resolution in the localization of bioactive molecules and cells, and a layer-by-layer assembly of multiple independently patterned scaffolds will enable the ability to dictate multiscale cellular and material composition in macroscale 3D constructs.

To address this hypothesis, MeHA and NorHA were leveraged as materials to fabricate thin, planar electrospun substrates. Successful syntheses were confirmed using ^{1}H NMR. Photomediated patterning capabilities were analyzed via ligating thiolated fluorophores onto electrospun HA scaffolds using photomasks with decreasing feature sizes down to 20 μm. Similarly, the ability to control cellular localization was determined by the same photopatterning process, albeit with a thiolated RGD adhesive ligand in addition to the thiolated fluorophore, and cell positioning was determined by counting cells within the RGD+ regions (RGD+ regions also fluoresce due to concurrent patterning of the fluorophore). Thiolated fluorophores were synthesized via traditional solid-phase methods.

Subsequently, MeHA and NorHA fibers were electrospun onto cyclic olefin copolymer (COC) substrates as supports for aligning individual fiber layers. COC films contained ablated regions to allow for fibers to span across void spaces and be in direct

contact with each other following layering (i.e., no COC material between fiber layers). Additionally, direct contact of fiber layers allows for holes to be spatially patterned into the HA-based fibers during crosslinking, which can theoretically be layered directly on top of each other to build out a material channel in 3D space as more layers are added. Finally, precise alignment was demonstrated utilizing 2 layers of fluorophore-patterned scaffolds that build out a 2-part image when layered. Taken together, these preliminary steps illustrate the possibilities afforded by a layer-by-layer biofabrication platform to control material and cellular architecture in macroscale 3D constructs.

1.3. Research Overview

Chapter 2 introduces the motivation for engineering dynamic electrospun hydrogels for tissue engineering applications. This chapter focuses on previously established methods to engineer complexities within the hydrogel fibers themselves, while briefly acknowledging platforms utilizing electrospun hydrogels in 3D. Expanding upon engineering dynamic complexities into electrospun hydrogels, **Chapter 3** describes the development of peptide-based system that enables user-defined, reversible presentation of bioactive molecules on hydrogel substrates (both nonfibrous and fibrous) through toehold-mediated strand displacement of coiled coil complexes. Notably, this chapter addresses the challenge of engineering time-dependent dynamic complexities into electrospun hydrogel scaffolds.

Next, the focus shifts from the time dimension to the spatial dimensions. Since natural tissue exists in both space and time, it is paramount to consider 3D space along with the time-based biofabrication platform described in Chapter 3. Electrospun fibers are traditionally 2D, dictated by the stochastic deposition of fibers onto a grounded collection surface, and were historically utilized as cell culture substrates with microscale topography dictated by the nano-to-microscale fibers that comprise the scaffold. In response, **Chapter 4** provides background for the research described in Chapters 5-7 and introduces established techniques to utilize electrospun fibers in 3D space. While early iterations of 3D electrospun fibers utilized thicker constructs as substrates, this chapter focuses primarily on electrospun fibers as next-generation 3D scaffolds for encapsulation cell culture – ranging from fiber:hydrogel composites with small amounts of embedded fibers, to 3D hydrogel media comprised largely of electrospun fibers.

Chapter 5 and **Chapter 6** describe the development of a fiber-based granular hydrogel strategy for 3D cell culture applications. In these granular hydrogel systems, each "particle" is a discrete hydrogel microfiber segment. The fiber segments are assembled into a bulk scaffold via centrifuge-mediated packing and present material properties that are unique among biomaterial systems currently in existence – due to interparticle interactions and entanglements between individual microfibers in the scaffold. More specifically, **Chapter 5** characterizes the mechanical and physical properties of packed hydrogel microfibers and demonstrates them as an injectable/extrudable biomaterial ink that is suitable for both 2D and 3D cell culture. **Chapter 6** focuses on tuning the complex, time-dependent physical properties of packed hydrogel microfibers for mechanically matching characteristics of natural tissue. These fiber-based hydrogel assemblies are advantageous for 3D cell culture models due to their permissive nature (i.e., ability to be reorganized at the cell-level in the absence of secondary annealing processes).

Due to the highly organized architecture and structuring of some tissue types, higher degrees of spatiotemporal control are needed when engineering ECM-mimetics *in vitro*. **Chapter 7** introduces a novel biofabrication platform that is grounded in the layer-by-layer assembly of thin, planar electrospun scaffolds. These electrospun fibrous scaffolds enable photomediated patterning of biomolecules at resolutions <100 μm and can influence cell position when the patterned biomolecule contains an adhesive ligand motif. These scaffolds can be independently patterned and seeded with cells, thus providing the ability to arbitrarily define 2D space on each layer. If the designs across

layers are designed to be related, precise control over cellular and material architecture is possible at high resolution in macroscale 3D constructs.

Finally, **Chapter 8** summarizes and also addresses some notable limitations of the works presented in this dissertation. Additionally, we identify some worthwhile future work building off of the technologies developed herein. Continuing to advance and apply these biofabrication tools will make them more generalizable and adoptable, thereby enabling the development of more complex tissue models for biological studies using dynamic electrospun hydrogel fibers.

CHAPTER 2: ELECTROSPUN HYDROGELS FOR DYNAMIC MODELS OF THE EXTRACELLULAR MATRIX: ADVANTAGES, PROGRESS, AND OPPORTUNITIES

2.1. Abstract

The extracellular matrix (ECM) is a water-swollen, tissue-specific material environment in which biophysiochemical signals are organized and influence cell behaviors. Electrospun nanofibrous substrates have been pursued as platforms for tissue engineering and cell studies that recapitulate features of the native ECM, in particular its fibrous nature. In recent years, progress in the design of electrospun hydrogel systems has demonstrated that molecular design also enables unique studies of cellular behaviors. In comparison to the use of *hydrophobic* polymeric materials, electrospinning *hydrophilic* materials that crosslink to form hydrogels offer the potential to achieve the water-swollen, nanofibrous characteristics of endogenous ECM. Although electrospun hydrogels require an additional crosslinking step to stabilize the fibers (allowing fibers to swell with water instead of dissolving) in comparison to their hydrophobic counterparts, researchers have made significant advances in leveraging hydrogel chemistries to incorporate biochemical and dynamic functionalities within the fibers. Consequently, dynamic biophysical and biochemical properties can be engineered into hydrophilic nanofibers that would be difficult to engineer in hydrophobic systems without strategic and sometimes intensive post-processing techniques. This Review describes common methodologies to control biophysical and biochemical properties of both electrospun hydrophobic and hydrogel nanofibers, with an emphasis on highlighting recent progress using hydrogel nanofibers

with engineered dynamic complexities to develop culture systems for the study of biological function, dysfunction, development, and regeneration.

2.2. Introduction

The extracellular matrix (ECM) is a complex, dynamic, and tissue-specific scaffolding system that presents a myriad of biophysical and biochemical cues that influence cellular behaviors[1–4]. The ECM is typically comprised of varying compositions of fibrous proteins and proteoglycans, coupled with soluble components such as growth factors[5–7]; however, the state of this structure is constantly in flux as it is simultaneously degraded and synthesized by the resident cellular population[4–8]. As the biophysical and biochemical attributes of the ECM at two distinct junctures are never identical, recapitulating tissue-specific milieus *in vitro* is challenging[5–7]. To better understand cellular behaviors and processes occurring in physiologically-relevant systems, *in vitro* culture systems must continue to advance to accurately model the ECM[4,6,9–11].

Progress in developing more sophisticated *in vitro* culture platforms has advanced with new insights into the composition and properties of the ECM coupled with new technical capabilities to recreate its features. The heterogeneous material environment of the ECM is water-rich and nanofibrous in nature[1,4,12], typically comprised of single-fiber diameters on the order of tens to hundreds of nanometers (10-500 nm)[12–16]. Electrospinning is an accessible technique for depositing fibrous substrates with diameters analogous to those comprising native ECM[5–7], and has been established as an effective way to produce nanofibrous materials across many fields of research[17–21], including tissue engineering[22,23]. Within tissue engineering and regenerative medicine, electrospun nanofibers have been applied to wound healing[24] and the engineering of diverse tissue types including models of cardiac[25], vascular[26], neural[27,28], and musculoskeletal[29] environments. In research applications addressing fundamental

biological and physiological questions, electrospun substrates have also been tactically engineered to tease out cellular responses to differing environmental cues and perturbations for *in vitro* studies[2,3,30–32]. For more information, Xue et al.[33] and Rahmati et al.[34] have recently published expansive reviews of the electrospinning process and extensive applications of electrospun materials.

Turning the focus from the process and applications onto the materials themselves, electrospun fibers utilized in tissue engineering applications throughout the years have been primarily comprised of hydrophobic polymers that were solubilized in organic solvents prior to electrospinning (**Figure 2.1**). These materials were prevalent in the early waves of electrospinning due to their favorable performance in the electrospinning process and their ability to form fibrous substrates for cell culture without further stabilization steps, such as interpolymer crosslinking[12,35]. A disadvantage of utilizing many of these hydrophobic polymers is they may lack desired cell-instructive biofunctionality in their fibrous form, and consequently require strategic chemistries to increase the bioactivity prior to seeding cells for culture[36,37]. Furthermore, since these materials are foreign to physiological systems, it may be necessary to engineer them further to mediate biological responses *in vivo* during transplantation and degradation. There are many established methods to modify the surfaces of these hydrophobic nanofibers[36,37]; however, a current shift towards using crosslinked polymers to develop hydrogel networks offers potential to reduce the complexity of post-processing (refer to **Figure 2.1**) by
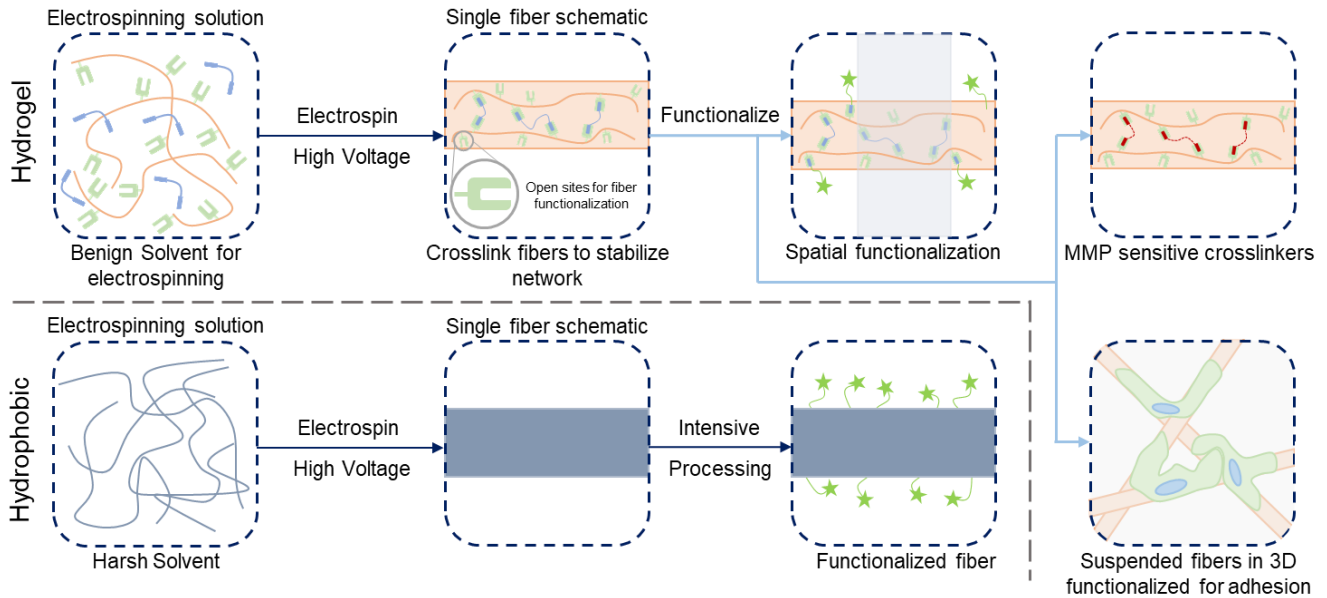
Figure 2.1. Functionalization of hydrogel versus hydrophobic nanofibers. (Top, left to right): electrospinning precursor solution containing a hydrophilic polymer with a crosslinker to stabilize hydrogel nanofibers; solution is electrospun and crosslinked (e.g. with UV irradiation) with leftover sites for further functionalization; three example pathways to functionalize the fibers – spatial control over bioactivity (green stars, shaded area indicates unfunctionalized region)[86], fibers crosslinked with matrix metalloproteinase (MMP) sensitive crosslinkers for tunable degradation[8], suspended hydrogel fibers in a bulk gel for 3D models of the ECM[123]. (Bottom, left to right): electrospinning precursor solution containing hydrophobic polymer (typically in a harsh solvent); solution is electrospun and fibers are ready for processing; intensive chemical processing is typically needed for fiber functionalization.

drawing on the diversity of hydrogel functionalities available for modifying and controlling microenvironmental features and establishing dynamic materials[38].

Another advantage offered by electrospun hydrogel fibers compared to their hydrophobic material analogs is the water-swollen nature of native ECM and of natural fibers within ECM microenvironments[1,4,12]. Furthermore, the plethora of established chemistries used to modify polymeric backbones and engineer crosslinking in hydrogel fiber systems enables the facile development of functionality for controlling the biophysiochemical properties to recapitulate features of the endogenous ECM[1,39–41]. Hydrogel systems for cell culture were originally introduced as advancements from tissue

14

culture polystyrene[1], and as soon as they were developed for cell culture, researchers aimed to advance the technology towards dynamic culture systems[4,38]. Electrospun fibers are mirroring this progression first through the development of hydrogel fibers, and now in trends towards dynamic fibrous environments that allow for modeling and probing of biological processes, while also affording control over the complexity of culture systems to reconstitute natural tissue as closely as possible. Significant progress in the engineering of fibrous culture substrates has been made, with the potential for further developments in materials design to continue to advance towards recapitulating endogenous tissue[42].

This Review focuses on the methods developed to modify the biophysical and biochemical properties of electrospun polymers – both hydrophobic and hydrophilic – with an emphasis on the strengths provided by crosslinkable, hydrophilic polymers that form hydrogels. We further focus on the chemistries developed to modify hydrogel nanofibers to manipulate the complexity of biological systems in space and time, while additionally highlighting the advancements being made by researchers towards the development of dynamic scaffolding that effectively reconstitutes physiologically-relevant ECM. Furthermore, we also provide light commentary highlighting the advantages and associated challenges within these systems to ideally inform the next phase of advancements in nanofibrillar hydrogel design.

2.3. Hydrophobic polymer fibers for cell culture

The use of hydrophobic polymers has been central to the development of fibrous culture systems[43], and materials commonly used include polylactic acid (PLA)[44–47], poly(lactic-co-glycolic acid) (PLGA)[48], polycaprolactone (PCL)[49], polyethylene terephthalate (PET)[50], among many others[51,52]. Since these materials are characteristically hydrophobic, they require nonpolar organic solvents to facilitate the electrospinning process[25,51,53,54]. Therefore – in biomedical applications – water infiltration is limited to spaces between fibers, without substantially absorbing into the polymeric matrices of the fibers themselves[51]. Despite this challenge, these materials are well-suited to the electrospinning process and have seen extensive use in the tissue engineering space. Part of the strength of these materials in electrospinning is that the morphological features of the resulting nanofibers can be readily tailored by simply controlling process parameters[12,54,55], yielding substrates with designed topographical characteristics that contribute to the biophysical properties that cells transduce. Similarly, post-electrospinning techniques have been employed to increase the bioactivity of the fibrous substrates. Since cells are heavily influenced by a combination of both biophysical and biochemical signals in their microenvironment[6,7], techniques have continuously progressed to introduce relevant signals to nanofibers based on these hydrophobic materials in order to influence the cells interacting with them.

2.3.1. Hydrophobic nanofibers enabling control over physical properties

Work aiming to engineer and alter nanofibrous topographies is driven by cellular transduction of biophysical stimuli from their microenvironments to influence signaling

pathways that direct downstream phenotypic fate decisions[56]. Therefore, control over physical properties of culture systems is a critical consideration in biomedical applications including tissue engineering, regenerative medicine, and fundamental investigations into cellular processes and development. The diameters of electrospun fibers can be readily controlled through solution properties and variable parameters of the electrospinning process – in particular solution viscosity, polymer molecular weight, applied voltage, and solution flow rate[55,57,58]. Even with this level of control, careful consideration is needed when developing fibers to match the tissue system of interest. For instance, Young's modulus of electrospun fibers exhibits an inverse relationship with fiber diameter[59]; therefore, a balance is typically needed when engineering models that replicate tissue-specific systems in the body[60].

Treatments for modulating fiber topography. Hydrophobic polymeric fibers are relatively robust, which allows for diverse processing techniques to further control physical and topographical properties. For example, towards engineering topography to influence cell shape and localization through contact guidance, Park and coworkers demonstrated the ability to spatially control the deposition and alignment of PLA nanofibers on polymer surfaces[61]. The hydrophobicity of PLA was leveraged during the electrospinning process and an electrolyte solution of potassium chloride on the collection surface was utilized to focus the electric field during fiber collection – a process that wouldn't be possible with hydrophilic polymers[61]. Moreover, from a post-processing perspective, Szczesny et al. heated poly(L-lactic acid) (PLLA) fibers to 85° C to induce contraction, yielding crimped fibrous substrates that recapitulated the crimped nature of tendinous tissue[62]. Further mechanical testing showed that the crimped fibers provided a

nonlinear stress-strain regime, which mirrors that seen with natural tendon tissue upon initial mechanical loading[62] (refer to **Figure 2.2 Top**). Towards a similar end, Chen et al. leveraged thermally-responsive materials that shrink upon the addition of heat to crimp fibers[63]. The waviness in the resultant fibers improved cellular infiltration into the scaffolds, and also promoted transcriptional growth factor-β (TGF-β) expression from human mesenchymal stromal cells (hMSCs) – an important regulator in the development of connective tissue[63]. While brief, these examples highlight the great potential hydrophobic fibers have to be tailored through modifications to the process, through post-processing, or through leveraging material properties such as thermal-responsiveness, to replicate natural tissue *in vitro*.

2.3.2. Hydrophobic fibers enabling modulation of biochemical properties

Pre-incubation (non-covalent) modifications. In addition to responding to biophysical cues in cell fate decisions, cells also integrate biochemical cues from their local microenvironment[7,39,64–66]. Therefore, chemically modifying hydrophobic fibers that are otherwise inherently bioinert with relevant biomolecules is critical to influencing phenotypic outcomes[36,37]. There is a plethora of studies expanding upon methods for introducing these biochemical cues into fibrous culture systems – many of which include some variation of a chemical coating as a preliminary step. For example, nonspecific adsorption of biomolecules on fibers, such as ECM-derived laminin[27,28] and compounds contained within endothelial cell basal medium-2[49], supported neural and endothelial cell
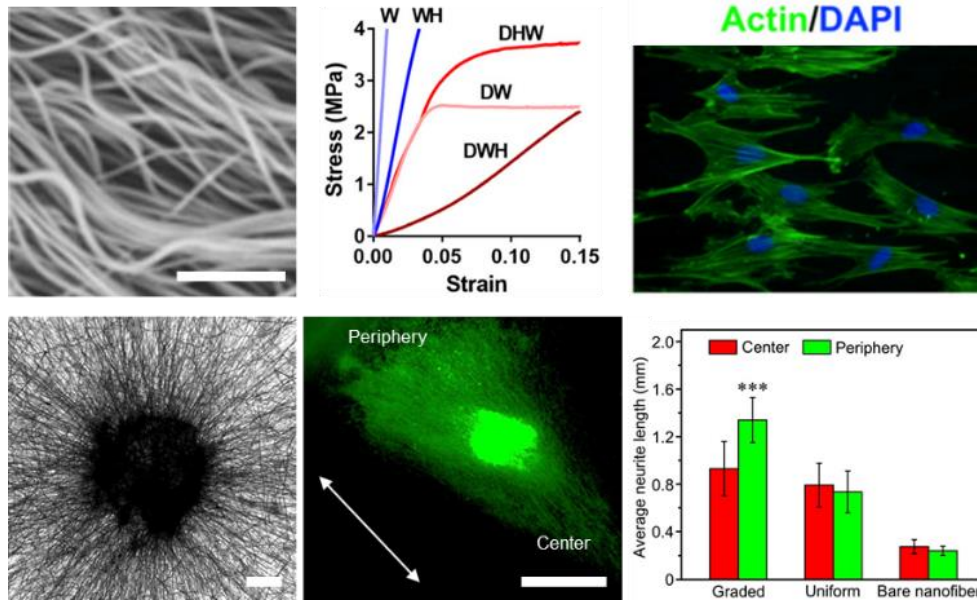
Figure 2.2. Cell culture on modified hydrophobic fibrous scaffolds. (Top, left to right): Crimped PLLA fibers synthesized via heat treatment with sacrificial fibers by Szczesny et al.[62] to develop a tendinous/ligament-like tissue structure; the crimped system (DWH) exhibited a traditional non-linear stress-strain curve similar to that of native tendon/ligament tissue, whereas controls (W, WH, DHW, DW) all were unable to replicate this behavior; actin/DAPI staining of cells seeded on these crimped systems demonstrated less alignment with the fibers and reoriented significantly upon mechanical strain. Scalebar = 1 μm. (Top) Reprinted and adapted with permission from Szczesny et al., copyright 2017 American Chemical Society[62]. (Bottom, left to right): PCL fibers aligned radially due to a novel electrospinning collection setup, scalebar = 200 μm; Tuj-1 staining (green) of dorsal root ganglion cells shows significant neurite extension in the direction of fiber alignment (white arrow) and laminin gradient; quantification displaying average neurite length for the gradient experiments compared to controls of uniform laminin presentation and no laminin presentation. Scalebar = 1mm, ***$p < 0.001$. (Bottom) Reprinted and adapted with permission from Wu et al., copyright 2018 American Chemical Society[76].

adhesion, respectively. Extending this pre-incubation one step further, Kador et al. adsorbed laminin and fibronectin onto PLA scaffolds and covalently bound Netrin-1 protein using carbodiimide (EDC/NHS) crosslinking between the carboxylic acids on laminin/fibronectin and the amines on Netrin-1[67]. Kador and coworkers also demonstrated efficacy in conjugating Netrin-1 to the laminin/fibronectin on fibers utilizing a photo-based succinimidyl-diazirine (SDA) crosslinker[67]. The immobilization of Netrin-1 on these fibrous

scaffolds resulted in increased polarity of retinal ganglion cells when compared to the non-functionalized controls[67].

Polydopamine-based modifications. Other methods aiming to improve the biofunctionality of fibrous substrates include a preliminary step of introducing reactive chemical functionalities to fiber surfaces. Similar to the aforementioned adsorption pathways, polydopamine surface coatings, naturally inspired by the adhesiveness of mussels, allow for the presentation of catechol/quinone groups on fibers[68]. These groups can then freely react with thiols and amines of biomolecules – such as bone morphogenetic protein-2[69], laminin[70], or Arg-Gly-Asp (RGD) peptide motifs[71] – undergoing either Schiff-base reactions or Michael additions[72,73].

High-energy surface treatments. High-energy surface treatments can also be used to introduce bioactivity. For example, Savoji and coworkers utilized plasma-polymerization to introduce a thin coating on PET nanofibers that presented reactive amine groups, which in turn supported the adhesion and subsequent proliferation of human umbilical vein endothelial cells[50]. In addition, Piai et al. treated PLA fibers with UV/ozone to introduce reactive oxygen groups prior to aminolysis via incubation in 1,6-hexamethylenediamine[45]. Chondroitin sulfate was then conjugated to the reactive amines on the PLA fibers by the aforementioned carbodiimide (EDC/NHS) crosslinking[45]. Plasma treatment has also been used in conjunction with the previously discussed polydopamine chemistry to graft another glycosaminoglycan, in this case heparin, onto polycarbonate-urethane grafts to improve bioactivity *in vivo*[74]. Moreover, Tanes et al.[75] and Wu et al.[76] both demonstrated the ability to introduce gradients of nerve growth factor (NGF)[75] and epidermal growth factor (EGF)[76] on PCL nanofibers using bovine serum albumin (BSA)

as a bioinert blocking agent. Both methods utilized oxygen plasma to functionalize the surface, prior to the sequential introduction of BSA to block open sites, then either NGF/EGF was conjugated to fibers to confer bioactivity. In the presence of both an NGF gradient and aligned fibers, dorsal root ganglion cells exhibited a preferential alignment as well as increased average length of extended neurites [75] (refer to **Figure 2.2 Bottom**).

Click chemistries for biochemical modifications. Click chemistries have been explored to functionalize hydrophobic fibers with biochemical cues. Reactions that have been successfully used for controlled presentation of biomolecules include copper-catalyzed azide-alkyne cycloaddition (CuAAC) and sans metal strain-promoted azide-alkyne cycloaddition (SPAAC)[37]. As their names reflect, CuAAC reactions require the presentation of alkynes and azides for conjugation[77], whereas SPAAC reactions require the presentation of strained alkynes and azides for conjugation but proceed in the absence of a copper catalyst[78]. Examples include the functionalization of PLA with an alkyne by Shi et al. to facilitate conjugation of an azide-presenting enzyme onto fibers through CuAAC chemistry[79]. Examples of SPAAC reactions with nanofibers include works by Smith Callahan et al.[80] and Zheng et al.[81] where PLLA and PCL were functionalized with 4-dibenzo-cyclooctynol (DIBO) to provide reactive sites for conjugation of azide-containing molecules. In these works, both cell-adhesive peptides and fluorophores were conjugated to the DIBO-containing nanofibers. We refer to an excellent review by Kalaoglu-Altan et al. regarding 'clickable' electrospun fibers for further information on the use of bioorthogonal chemistries to modify nanofibers[37].

Summary – controlling hydrophobic nanofiber biochemical properties. Nanofibers based on hydrophobic materials have thus far been central to the

development of biomedical electrospun materials and have demonstrated the progress of research in this area – becoming increasingly sophisticated, bioactive platforms with great potential in regenerative medicine. Nonetheless, these systems face certain challenges in biomedical applications that are inherent to the materials used and can be addressed through the use of hydrogel material systems. A minor concern exists in the use of cytotoxic solvents during electrospinning to dissolve hydrophobic polymers[82]. Although the potential to leave behind residual solvent is addressed in work with these materials, water-soluble hydrogel materials that are electrospun from aqueous solutions do not face this challenge. More significant are challenges related to advancing the biomimetic and dynamic features of electrospun fibrous systems. For example, with respect to controlling the biophysical properties of nanofibrous environments, hydrophobic systems largely afford minimal direct control over the stiffness and viscoelasticity of the resultant fibers beyond modifying solution properties prior to electrospinning. Additionally, spatial control over the localization of biomolecules in these hydrophobic nanofibrous systems has been demonstrated through the aforementioned techniques to introduce gradients of growth factors[75,76], but achieving complex spatiotemporal control over biochemical and biophysical features of a fibrous system remains challenging. Progressing towards polymers used in hydrogels offers a library of existent chemistries along with continual research to advance technology and address many of these concerns[38,40,41] (**Figure 2.1**). This offers great potential to expand the possibilities within nanofibrous systems and to combine the strengths of hydrogel materials and nanofibers in engineering biomimetic environments[38,40,41].

2.4. Hydrogel nanofibers

The opportunities for increased control over the biophysical properties and spatiotemporal presentation of biochemical functionality has been a driving factor in the progression towards electrospun *hydrogel* fibers. Hydrogel fibers build on the strengths of hydrogel materials that can be chemically modified with functional moieties – for both crosslinking and introducing biomolecules[1,65]. These strengths allow for the precise tailoring of mechanical and chemical properties to replicate the tissue system of choice[1,38]. Thus, hydrogel nanofibers offer not only the potential for superior control over fiber properties compared to their hydrophobic analogs[83], but the fibers also have the potential to provide a microenvironment that more closely mirrors the water-swollen, fibrous characteristics of natural tissue[13–15].

Fabrication of hydrogel nanofibers. Hydrogel nanofibers are produced via electrospinning similarly to other variants of polymeric nanofibers. Commonly, the solution consists of the hydrophilic polymer of choice (e.g. hyaluronic acid (HA), poly(ethylene glycol) (PEG), or dextran), a crosslinker (for systems that require a linker molecule), a photoinitiator (for photomediated reactions), and water as a solvent[2,84,85]. For lower molecular weight polymers, like HA and PEG, a high molecular weight polymer, typically poly(ethylene oxide), is added to increase solution viscosity and induce chain entanglements[32,84–86]. For higher molecular weight polymers, like dextran, this is not typically needed[2,31,87]. This solution is then typically extruded though a needle at low flow rates, at the point of which an electric field is applied to the solution. This induces a competing interaction between polymer chain entanglements within the solution and electrostatic repulsion from the voltage – which due to solution extrusion, elongates into

a Taylor cone. At the point of the Taylor cone, the solution vaporizes, which causes a polymeric fiber jet to form that whips and accelerates towards the grounded collection surface[12,58]. Following the deposition of the fibers, they must then be stabilized through some variation of crosslinking (to be described in depth-below) in order to facilitate water absorption into the polymeric networks as opposed to fibers solubilizing upon hydration[2,84–86]. Crosslinking also enables control over biophysical properties of hydrogel fibers, with degree of crosslinking directly affecting fiber parameters such as stiffness and diameter – which correlate with capacity for water swelling into the fibers[86,88]. Once crosslinking is complete, facile functionalization of fibers is possible to introduce bioactivity into the fibrous hydrogel system.

Introduction to hydrogel nanofiber crosslinking and stabilization. One specific suite of hydrogel-forming materials represents natural polymers due in part to their innate biocompatibility and presentation of relevant ligands[89,90]. For example, collagen inherently presents bioactive sites for integrin-mediated cell adhesion[12]. However, other polymers can also intrinsically interact with cells – such as hyaluronic acid (HA) (typically produced through fermentation processes[1]) with CD44[91–93]. That being said, cells tend to exhibit low adhesion to HA without chemical modifications to improve bioactivity[86]. Therefore, HA, as well as other polysaccharide materials such as dextran[2], need to be functionalized with bioactive molecules prior to being utilized for cell culture systems. It is also worth including other hydrophilic polymers in this category such as the synthetic polymer poly(ethylene glycol) (PEG)[94]. There are a whole host of established chemistries to modify the backbones of these exemplified hydrophilic polymers with pendant functional moieties, with these moieties doubling as both crosslinking sites and

24

biomolecule conjugation sites. Therefore, strategic modification of these polymers thereby provides significant user control over the resultant biophysical and biochemical characteristics of the nanofibers.

Unlike hydrophobic materials, as discussed previously, polymeric materials used in hydrogels are soluble in water and fibers generated by electrospinning will dissolve upon hydration without stabilization. Thus, hydrogel-based systems must generally be stabilized through some form of intermolecular crosslinking between the polymers that comprise the nanofibers. In many cases, regulation of crosslinking enables control over physical properties, as will be discussed at greater length in the next section. Naturally-derived polymers such as collagen[95] and gelatin[96], for example, can be electrospun; however, though the native materials undergo physical crosslinking, the resultant nanofibers themselves typically are not robust enough for handling without further post-processing[95,96]. To circumvent this, crosslinking agents, like glutaraldehyde, have been utilized with collagen and gelatin to improve resultant mechanical properties[95–99]. Furthermore, Kishan et al. developed a platform for electrospinning gelatin that crosslinks on-the-fly using a diisocyanate crosslinker to retain fiber mechanical properties[100]. Another effective method to stabilize collagen/gelatin-based fibers leverages carbodiimide chemistry, such as EDC/NHS crosslinking, to introduce 'zero-length' crosslinks[101–103]. Chemical crosslinking has also been used to stabilize nanofibers formed from synthetic hydrophilic materials[104], for example using glutaraldehyde to crosslink polyacrylamide (PA)[105] and poly(vinyl alcohol) (PVA)[106–108]. Glutaraldehyde as a crosslinker readily reacts with pendant groups on PA and PVA to form linkages, and offers

the potential to provide user-defined control over the stiffness and swelling of resultant electrospun fibers[105,106].

Chemical modifications for covalent crosslinking of hydrophilic polymers. In many cases, the polymers forming the molecular backbones of these hydrogel materials are chemically modified using various strategies that enable their stabilization after electrospinning for use as fibrous hydrogel systems. Photoinitiated reactions represent a major platform for the stabilization of these hydrogel fibrous networks, and the common methodologies for photoinduced reactions leverage differing versions of the ene-ene scheme – for example through acrylate-based functional groups – and thiol-ene reactions. In the presence of light and a photoinitiator, ene-ene reactions undergo a chain-growth mechanism and form kinetic chains that crosslink the backbone polymers[109]. In the case of the thiol-ene reaction, photoinitiation produces a thiyl radical, which opens and subsequently binds with an adjacent alkene enabling stoichiometric crosslinking[11,110–112]. In addition to the crosslinking type, the degree of substitution on the polymeric backbone itself plays an important role in the regulation of downstream fiber mechanics[113,114] – therefore, careful consideration is needed when designing the specific material system.

Many of these hydrophilic polymers have been modified to present pendant alkenes (using methacrylates and vinyl sulfones, for example) for crosslinking post-electrospinning. Gelatin is commonly modified with methacrylate moieties to create a material (GelMA) that can be stabilized by photoinitiated crosslinking of electrospun fibers[115–117]. Similar chemistry has been used to modify HA[30,118], silk fibroin[119,120], and PEG[32,94]. Dextran, another polysaccharide, can also be modified with methacrylate[2,3,31] or vinyl sulfone[87] functional groups for crosslinking and subsequent reactions that aim at

improving bioactivity. In most cases, alkene groups within nanofibers allow for anhydrous radical-induced polymerization within fibers to stabilize the polymeric networks prior to hydration[121]. One of the strengths of photochemistries is the great potential for spatial control of reactions. Crosslinking, and therefore fiber stability (and ultimately mechanics), can be specified via selective irradiation of electrospun nanofibers through photomasks. Sundararaghavan et al. used this to introduce porosity within thick fibrous substrates that would aid in cell infiltration. By masking regions of fibers during anhydrous crosslinking of methacrylated HA nanofibers, leaving them unexposed to light, regions of fibers could be selectively dissolved during hydration[122] (see **Figure 2.3A**).

      Disadvantages and considerations when electrospinning hydrogels. Although hydrogel materials have stark advantages over their non-hydrogel counterparts, there are some associated disadvantages that need to be considered when designing these material systems for electrospinning. For example, an important consideration when using some lower molecular weight polymers, like HA and PEG, is that a carrier polymer may be required during the electrospinning process to induce chain entanglements in the solution[85,118]. High molecular weight polymers – like poly(ethylene oxide) – may be added to the electrospinning solution to facilitate fiber formation and subsequently be washed away when the scaffolds are hydrated[123]. Furthermore, many biomaterials that form hydrogels are not ready for electrospinning 'out-of-the-box'[1]. Specifically, many of the materials require chemical functionalization to introduce reactive moieties such as methacrylates[2], vinyl sulfones[124], or norbornenes[86] to the polymeric backbones.
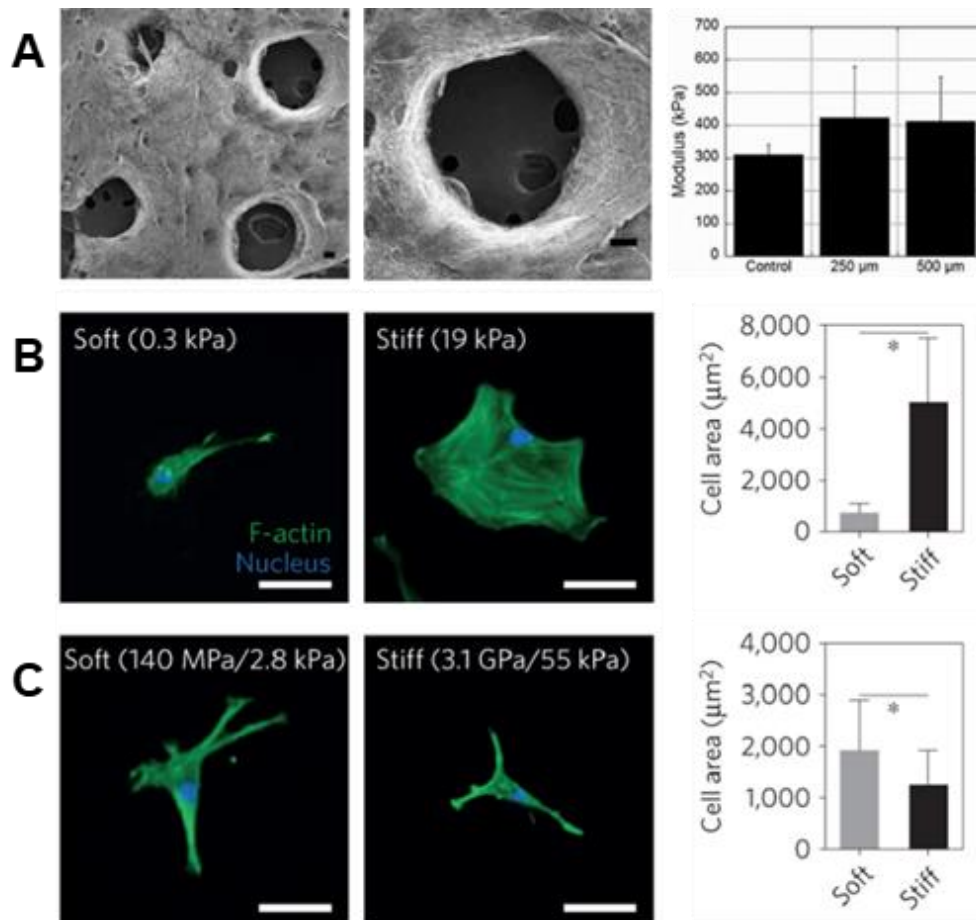
Figure 2.3. Importance of fiber physical properties for cell culture. (A, left to right): SEM micrographs of MeHA fibers with user-specified photopatterned pores, zoomed in micrograph of a photopatterned pore, and a column chart displaying modulus of scaffolds – with no significant difference between scaffolds with pores and scaffolds without pores. (A) Reprinted and adapted with permission from Sundararaghavan et al., copyright 2010 John Wiley and Sons[122]; scalebars = 100 μm. (B, left to right): hMSCs show increased cell spreading on stiff hydrogels as opposed to soft hydrogels – quantified by the column chart illustrating cell area (*p < 0.05). (C, left to right): hMSCs demonstrate increased spreading on soft rather than stiff hydrogel fibers – quantified by the column chart showing cell area (*p < 0.05). These differing results emphasize the need for careful consideration when designing the biophysical properties of fibrous hydrogels for cell culture. (B) and (C) Reprinted and adapted with permission from Baker et al., copyright 2015 Springer Nature[2]; scalebars = 50 μm.

An additional disadvantage of using these functionalized materials is the batch-to-batch variation in their synthesis, which can potentially alter fiber properties[1]. We refer to an excellent review by Caliari and Burdick[1] for further information regarding synthesis and

considerations of common hydrogel biomaterials. Finally, an inherent issue with these hydrophilic materials is the need to crosslink the fibers immediately post-electrospinning, prior to any further functionalization[2,85,86]. Once the material and crosslinking strategy are chosen, however, the resultant biophysical and biochemical properties can be easily modulated – as described in the following sections. Please refer to **Table 2.1** for a representative list of hydrogel biomaterials that have been electrospun, along with a few established methods for crosslinking and modulating the resultant biophysiochemical properties.

2.4.1. Hydrogel nanofibers enabling control over physical properties

As noted, the physical properties of cellular microenvironments exert strong influences over cell behaviors and phenotypes[125,126]. In nanofibrous systems, hydrogel-based materials offer possibilities for engineering these properties, such as the mechanical and viscoelastic environments with which cells interact, within a fiber-based environment to achieve certain outcomes or interrogate biological questions.

Ene-ene mechanism for controlling physical properties. Within systems crosslinked via chain-growth polymerizations, the possibility to propagate kinetic chains after an initial fiber-stabilizing crosslinking allows further light exposures to generate increasingly stiff fibrous networks[113] as well as spatially control mechanical features. This property allows for direct-user control over resultant fiber crosslinking density, and consequently fiber stiffness, via irradiation duration[87].

Following the deposition and stabilization of hydrogel fibers, cell behaviors can be analyzed in *in vitro* tissue models that more closely mirror physiological features and

enable experiments that assess cellular responses to perturbations of these environments. In ene-ene systems, control over mechanical properties, such as Young's modulus, has allowed cellular responses to environments of differing fiber stiffnesses to be assessed[2,3,30,31]. For example, Baker et al. leveraged a methacrylated-dextran system and demonstrated that cell spreading behaviors on 2D stiff fibers (55 kPa, network stiffness) were inhibited in comparison to 2D soft fibers (2.8 kPa, network stiffness) – a phenomenon that is the inverse of what is seen on 2D hydrogels (**Figure 2.3B-C**)[2]. Baker et al. propose that this is due to the cells' superior ability to recruit fibers on soft substrates as opposed to stiff[2], a notion that is corroborated by a computational model presented by Cao et al. that suggests increased focal adhesion size when matrix fibers are recruited by cells[42]. Highlighting the complexity of mechanoresponsive cellular behaviors that can be influenced and interrogated in these systems, modulating fiber stiffness allows for design of 3D environments with high cell infiltration, combating the poor infiltration typically seen through the small pores of electrospun scaffolds[127–129]. Interestingly, Song et al. demonstrated that cellular infiltration can be improved by utilizing stiffer methacrylated-hyaluronic acid (MeHA) fibers[88], a concept that is seemingly contradictory to more cell spreading exhibited on soft fibers. This phenomenon can likely be attributed to the tendency of cells to recruit matrix fibers[88,130], which in turn decreases downstream pore size[88]. In fact, Song et al. demonstrate that on short time scales, cells invade soft fibers quickly, but then are stagnant at longer time scales – whereas cells continually invade stiff fibers across these longer time scales[88]. Furthering this, Heo et al. investigated the effect of nuclear stiffening as a response to matrix mechanics on cellular infiltration into these dense fibrous scaffolds[131]. The result of this work demonstrated that

momentary softening of the nucleus improves infiltration – suggesting that a combination of nuclear softening in conjunction with stiffer fibers can aid in cell migration into thick fibrous matrices[131].

The ene-ene chain-growth polymerization is a common method for developing hydrogel fibers; however, in utilizing a chain-growth polymerization technique for crosslinking fibers and controlling mechanics, one must account for the continued growth and formation of kinetic chains in subsequent exposures to light. This additional exposure can result in increasingly stiff material environments and can cause heterogeneities leading to an inconsistent global network – an issue seen in aqueous chain-growth polymerization[132,133].

Thiol-ene mechanism for controlling physical properties. In comparison, the light-mediated thiol-ene step-growth polymerization offers many of the same strengths of photochemical reactions, but with increased spatiotemporal control over the formation of hydrogel networks[109,112]. Similar to the ene-ene chemistry, hydrophilic polymers have been modified with functional groups for thiol-ene photopolymerization. This reaction relies on a functional alkene that readily reacts with nearby thiyl radicals that are typically induced by a photoinitiator[110]. Commonly, these polymeric backbones for electrospinning include, or are modified with, alkenes such as norbornenes[85,86] and acrylates[134] – among others[135]. To crosslink the fibers, the electrospinning precursor solution must include a crosslinking molecule with multiple thiols, and after electrospinning but before hydration, fibers should be exposed to light to stabilize the fibers, similar to ene-ene chain-growth polymerization. As before, light-initiated chemistry allows spatial control over the reaction, with unexposed regions able to be dissolved upon hydration. As mentioned, the thiol-ene

reaction is advantageous because it can be designed stoichiometrically to directly control crosslinking density via molar ratios of reactive groups within the crosslinker relative to the polymeric backbone, with near ideal networks forming through a step-growth mechanism[132]. The ability to control the level of crosslinking also enables residual alkenes to be preserved after crosslinking for subsequent reaction with molecules containing thiols – for example, in the addition of biomolecules[86,112], which will be discussed in further depth in the next section, or in introducing additional crosslinking molecules to modify mechanics with the spatiotemporal control afforded by photochemistry.

Aiming to utilize thiol-ene chemistries to engineer the mechanical environment cells interacted with, Iglesias-Echevarria et al. designed a coaxial electrospinning method with PCL as the core polymer for structural stability, and PEG-norbornene (PEGNB) as the sheath for tunability[136]. The PEGNB outer layer afforded control over resultant stiffness of the fibers, while also leaving behind residual norbornene groups for subsequent conjugation of thiolated RGD motifs for increased cell adhesion. The stiffness of the PEGNB sheath was modulated to investigate cellular response to differing environments. When bovine pulmonary artery endothelial cells were seeded on fibers of varying stiffnesses, higher cell infiltration and deposition of matrix materials (e.g. collagen, elastin) were seen on fibers with greater Young's moduli[136] – a result in line with those mentioned above by Song et al. utilizing a MeHA fibrous system[88]. Another interesting approach employed by Yang et al. involved electrospun poly((3-mercaptopropyl)methylsiloxane) (PMMS) with triallyl cyanurate (TAC) as the crosslinker[137]. PMMS has pendant thiol groups that can react with any of the alkenes on TAC to form a crosslink that stabilizes the fibers, with residual thiols available for further

modification. In addition to the flexibility in the crosslinking afforded by this system, Yang et al. leveraged the residual thiols on TAC to conjugate a maleimide-modified poly(*N*-isopropylacrylamide) (PNIPAAm) to the fibers – exploiting the thermal-responsiveness of PNIPAAm for user-control over resultant fiber hydrophobicity[137]. In regard to physical properties, the thiol-ene reaction is a facile, powerful platform for the formation of hydrogel fibers for cell culture, providing high levels of control over the resultant fibrous scaffolds.

Summary – controlling hydrogel nanofiber physical properties. The physical properties of hydrogel nanofibers can be particularly well-regulated through photochemistries developed for bulk hydrogels; however, these platforms typically yield static fibers without the inclusion of further processing for dynamic complexity. There exists potential for other chemistries, including *in situ* reactions to be expanded upon below in the section outlining dynamic fiber systems – which can perhaps be used in conjunction with the aforementioned photoinduced chemistries in dual-crosslinking systems. It is worth reiterating that while these hydrogel fiber systems allow strategic control over physical properties that cells experience, regardless of how these fibers are crosslinked, the nanofiber diameters will increase upon fiber hydration – a phenomenon that is directly correlated with polymer hydrophilicity and crosslinking density[88]. Thus, careful balance and consideration are required when designing a hydrogel fiber system that recapitulates the physical properties of the tissue system of choice. However, the physical properties only tell half the story of physiologically-relevant ECM. To design an *in vitro* system that is truly indicative of natural tissue, a synergistic approach that incorporates both the relevant biophysical and biochemical signals is required. Fortunately, the crosslinking methods described above not only provide direct control over

the physical properties, but they can also be used to spatiotemporally incorporate desired biomolecules into the nanofibrillar environment.

2.4.2. Hydrogel fibers enabling modulation of biochemical properties

Within hydrogel materials, modifications such as those described above allow for spatiotemporal modulation not just of the biophysical properties, as there has been considerable progress in utilizing the same chemistries in controlling biochemical properties too. Hydrogels can be designed such that the functional groups used to bind crosslinking molecules might also bind biofunctional molecules, and careful control of the crosslinking process can leave unreacted sites within the hydrogel after crosslinking to couple molecules that increase bioactivity for cellular studies[86,87]. The ene-ene and thiol-ene reaction pathways that have been described above are also commonly utilized to introduce these biochemical signals; however, there are alternative chemistries under development that achieve similar results. We aim to provide an overview of chemistries for incorporating biomolecules into nanofibrous scaffolds based on hydrogel materials, where, in comparison to hydrophobic polymers, aqueous media can be used for all reactions[36,37,86].

Ene-ene mechanism for controlling biochemical properties. Ene-ene chain-growth, though more commonly employed in crosslinking fibers without further functionalization via the mechanism, can be used to introduce biochemical cues. For example, Davidson et al. conjugated methacrylated heparin to free vinyl sulfone groups on dextran fibers through ene-ene photopolymerization to investigate the influence of heparin presentation on resultant cell adhesion and matrix protein sequestration[87]. The

addition of heparin was demonstrated to correlate with improved cell adhesion, as well as improved binding of cell-secreted fibronectin to the dextran fibers[87] (**Figure 2.4A**). Extending the use of heparin to trap biomolecules such as the cell-secreted fibronectin, Mays et al. conjugated methacrylated heparin to hyaluronic acid fibers to facilitate growth factor sequestration in order to promote chick dorsal root ganglia neurite length[138].

An important consideration in methods that functionalize fibers that were crosslinked via photoinitiated chain-growth polymerization through another photoinitiated reaction, is the effect of the subsequent reaction on kinetic chains formed during crosslinking. These kinetic chains can continue to propagate with the continued addition of radicals[87], and this may increase the Young's modulus of the fibers through additional crosslinking. To surmount this challenge, researchers may leverage the Michael-type addition reaction, where thiolated molecules bind to double bonds at slightly elevated pH, to incorporate functional molecules onto the pendant alkenes within these systems, avoiding further polymerization.

Thiol-ene (Michael addition) for controlling biochemical properties. The Michael addition is often used to conjugate thiols to pendant alkenes in hydrogel systems[139–143]. This chemistry allows for facile, homogenous conjugation of thiolated biomolecules to fibrous networks containing alkenes[3,87,118]. This conjugation can be calculated stoichiometrically, allowing for precise control over the level of functionalization. Therefore, this reaction can occur either pre-electrospinning, to modify polymeric materials that will be used in the electrospinning processs[118], or after the crosslinking step that typically follows electrospinning[2]. For example, although HA is a
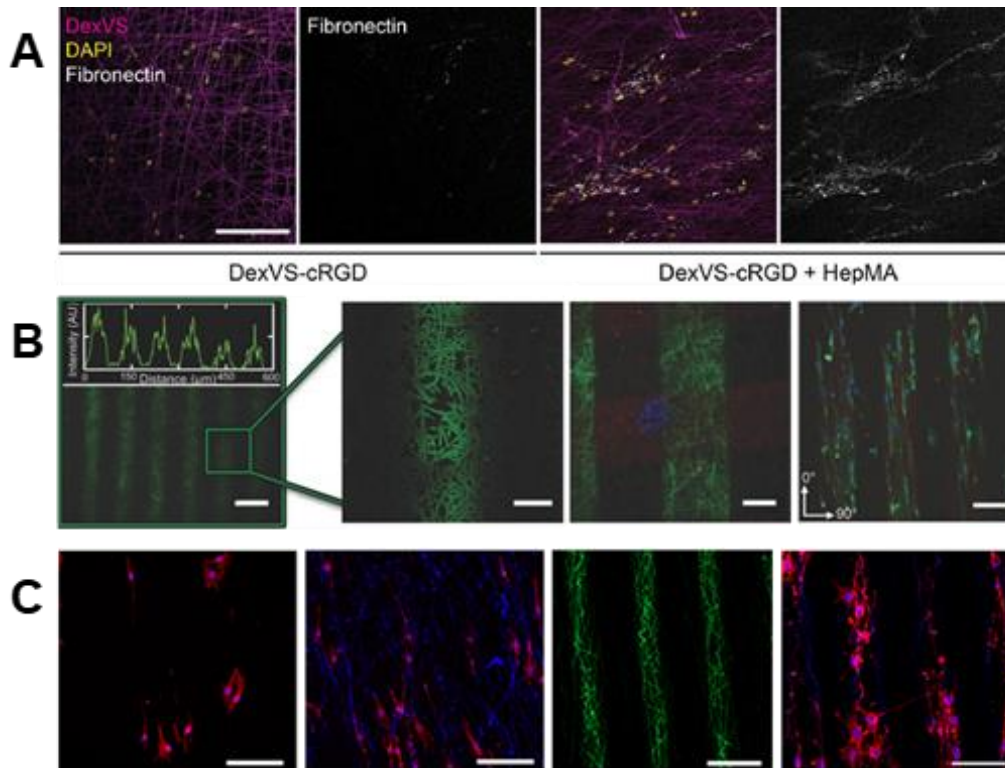
Figure 2.4. Introducing biochemical cues into fibrous hydrogels. (A, left to right): Dextran-vinyl sulfone (DexVS) fibers (magenta) were seeded with human lung fibroblasts (nuclei shown in yellow) in the presence of RGD or RGD + heparin. Conjugation of RGD + heparin to DexVS fibers increased the secretion and subsequent binding of fibronectin (white) onto the fibrous matrix. (A) Reprinted and adapted with permission from Davidson et al., copyright 2020 Elsevier[87]; scalebar = 200 μm. (B, left to right): spatial patterning of thiolated fluorophores onto NorHA fibers via thiol-ene click chemistry. Zoomed in images show high pattern fidelity, and the ability to pattern multiple biomolecules on the same scaffold – indicated by the red, green, and blue fluorophores on the fibers. The ability to pattern adhesive regions, using an RGD motif, allows for preferential cellular localization in RGD+ regions that elongate in the direction of fiber alignment. (B) Reprinted and adapted with permission from Wade et al., copyright 2015 John Wiley and Sons[86]; scalebars (left to right) = 100 μm, 25 μm, 100 μm, and 100 μm. (C, left to right): Patterning of bioactivity on synthetic fibers using UV irradiation. Rat Schwann cells exhibited a less elongated morphology on non-bioactive substrates (far left) when compared to substrates that were activated with UV light (middle left). The use of photomasks allowed for introduction of linear bioactive regions (middle right) which promoted cell attachment over non-bioactive regions (far right). (C) Reprinted and adapted with permission from Girão et al. 2019[145]; scalebars (left to right) = 200 μm, 200 μm, 100 μm, and 100 μm.

naturally-occurring polymer that interacts with cells via the CD44 surface receptor, HA

hydrogel substrates still require modification with ligands that can bind adhesive proteins

on cell surfaces to improve cell adhesion[86]. Kim et al. used the based-catalyzed Michael addition to controllably introduce RGD motifs onto electrospun MeHA fibers and demonstrated that higher presentations of RGD resulted in increased hMSC spreading, proliferation, and formation of focal adhesions[118]. Furthermore, Sundararaghavan and Burdick were able to introduce gradients of RGD in the Z direction into dense fibrous substrates using a novel electrospinning setup that deposited unmodified MeHA and high-RGD-modified MeHA at varying flow rates[144]. The thiol-Michael addition is a powerful and versatile method to introduce controlled densities of biomolecules into fibrous hydrogel systems; however, due to the requirement of a basic pH for the reaction to proceed, there is minimal spatial control over the presentation of these molecules[2,3,30,87,118], as materials that are undergoing modification are often uniformly immersed into a basic buffer containing the thiolated molecule of interest. For spatially controlled addition of bioactivity into fibrous systems, the radical-induced thiol-ene conjugation is preferable.

   Thiol-ene (radical induced) for controlling biochemical properties. Due to the inherent complexity of natural ECM[5–7], as well as the desire – in many experiments – to study cellular responses to differential signals in their microenvironments, the ability to tightly control the heterogeneity of biochemical functionalization of *in vitro* tissue culture scaffolds is desired. The radial-induced coupling of thiolated molecules onto pendant alkenes of hydrogel fibers allows for the precise localization of bioactive molecules that control cellular behaviors, such as adhesion, at high fidelity[86,135]. As discussed previously, this photochemistry allows light exposure to control the positioning of these molecules, so strategically designed photomasks, or carefully focused light, can be employed to control where coupling occurs in XY space. Wade and coworkers demonstrated the

former using aligned electrospun nanofibers created from norbornene-functionalized hyaluronic acid (NorHA)[86]. In this seminal work, Wade et al. showed that through stoichiometric calculations, multiple thiolated peptides (in this case, red/green/blue fluorophores) can be conjugated to fibrous NorHA surfaces – indicating that multiple bioactive molecules can be controllably introduced[86]. Furthermore, using a thiolated RGD motif, Wade et al. demonstrated how 3T3 fibroblasts responded to a combination of microenvironmental cues: a controlled spatial presentation of RGD on an aligned nanofibrous topography[86] (**Figure 2.4B**). Moreover, Sharma and coworkers demonstrated the relative ease in employing this chemistry with PEG-norbornene fibers in a microarray system. This high-throughput platform allowed for investigation of multiple thiolated peptides with a multitude of cell types to probe cellular responses to differing microenvironments[85]. These results, taken together, clearly support the power of this chemistry scheme to control the biochemical cues that are necessary to incorporate into cell culture systems.

UV-irradiation for controlling biochemical properties. In addition to radical-induced coupling, selective UV irradiation has been used to control localization of relevant biomolecules on hydrogel fibers. Similar to the UV functionalization of PLA nanofibers, Girao et al. used the block copolymer poly(ethylene oxide terephthalate)/poly(butylene terephthalate) (PEOT/PBT) to synthesize nanofibers[145]. This block copolymer provides a hydrophilic region (PEOT) and a brittle, hydrophobic region (PBT) – meaning the resultant fibers can absorb high percentages of water. The surfaces of these water-swollen fibers were then subsequently functionalized via selective UV irradiation to spatially control the introduction of reactive groups for biomolecule and cell adhesion. Biomolecules – such

as fluorescein isothiocyanate (FITC)-tagged BSA – were conjugated vertically through the material in the XY plane and rat Schwann cells adhered selectively to functionalized regions[145] (**Figure 2.4C**). The ability to tailor mechanical properties of the resultant fibers by modulating block lengths in the copolymer, in addition to spatial control over presentation of biochemical cues, makes this platform particularly attractive in the use for tissue engineering scaffolds.

Summary – controlling hydrogel nanofiber biochemical properties. Methods like those described above allow for easy and controllable incorporation of relevant biochemical signals into fibrous hydrogel tissue culture systems and demonstrate strengths and potential of hydrogel-based nanofibrous platforms. It is of note that the thiol-ene reaction allows for calculated, stoichiometric crosslinking, leaving residual alkenes available for biomolecule conjugation[86], although similar control might be exerted through careful regulation of other reactions. Light-based mechanisms offer strengths in enabling selective spatial specification of reactions. UV functionalization of fibers has demonstrated the potential to achieve the same end goal, albeit in hydrophobic materials[145], whose properties such as biocompatibility, degradation, and amenability to modification must be carefully considered in material design. Other hydrophilic materials, such as hyaluronic acid and dextran, have strong track records in these areas, but the chemical structure and properties of the backbone polymer are predetermined[1,146]. Regardless of the material selection and chemistry design, hydrogel fibers offer possibilities for high resolution spatial control over the heterogeneity of tissue culture platforms, and materials might easily be combined for next-generation fibrous systems.

2.5. Towards dynamic complexity and mimicking natural tissue

With technologies established to engineer nanofibrous substrates with specific biophysiochemical properties, it is now possible to precisely control the spatial heterogeneity of biophysical and biochemical cues within the scaffolds. Because of this, there is exciting progress in the development of fibrous hydrogel systems that mimic natural tissue, with an emphasis on dynamic complexity – where properties of these systems might be designed to change or be controlled over time.

Engineering degradability into hydrogel nanofibers. Advances in the engineering of bulk hydrogels, both in 2D and 3D, have demonstrated unique strengths in this area – for example in material designs using enzymatically degradable crosslinkers to allow for physiologically-mediated decomposition of the scaffolds[147–149] – and it follows that nanofibers based on hydrogel systems would have similar potential. The potential to engineer materials technologies established in bulk hydrogels into hydrogel-based nanofibers is illustrated by the development of electrospun HA fibers crosslinked with a protease-sensitive crosslinker[8], establishing enzymatic degradability based on materials first used as bulk hydrogels[150]. Wade and coworkers leveraged a maleimide-functionalized HA that was electrospun with a crosslinker peptide that was degradable enzymatically by rhMMP-2 and Type II collagenase[8] (**Figure 2.5A**). The addition of this degradability into fibrous hydrogels allows for dynamic restructuring of the fibrous ECM by resident cells via the secretion of enzymes and subsequent deposition of new matrix proteins. Wade et al. furthered this work by demonstrating efficacy of degradation *in vivo* – highlighting aspects important to translation in a subcutaneous implantation model[8].

Dynamic fibers for selective molecule delivery. Dynamic properties in fibrous

hydrogels are also embodied in applications that load the fibers with bioactive molecules

to create temporal signaling. Temporal control over the release of chemokines or

cytokines represents technologies with great potential for nanofibrous systems to

influence cellular behavior and regeneration. Applications of controlled release from

nanofibrous systems predominantly center on drug delivery applications, and there are

several comprehensive reviews on this topic[55,82,151]; we highlight a few systems here to

illustrate technologies that might be applied in nanofibrous systems designed for tissue

engineering and regenerative medicine.

Non-hydrogel fibers have demonstrated effectiveness in the delivery of molecules

by both coating fibers[152,153] and incorporating bioactive molecules in the precursor

solution[153]. Ahire and coworkers adsorbed HA to the surface of poly(D,L, lactide) fibers

and demonstrated a sustained, linear release of HA over time[152]. Xia et al. also showed

efficacy in the sustained delivery of adsorbed vascular endothelial growth factor (VEGF)

to the surface of poly (L-lactic acid) fibers that included nerve growth factor (NGF) in the

core[153]. This two-step release allowed for sequential addition of biomolecules to the local

environment and can, in theory, be applied to a multitude of growth/soluble factors.

Hydrogel fibers have also demonstrated promising results in the field of drug

delivery. For example, Kishan and coworkers developed a platform that provides a

sustained release of proteins to the local environment using different types of crosslinked

gelatin fibers[154]. Their methacrylated gelatin system relied on traditional mass transfer for

the release of a model protein incorporated within the fibers. On the other hand, gelatin

crosslinked using a diisocyanate molecule was loaded with a model protein that reacted
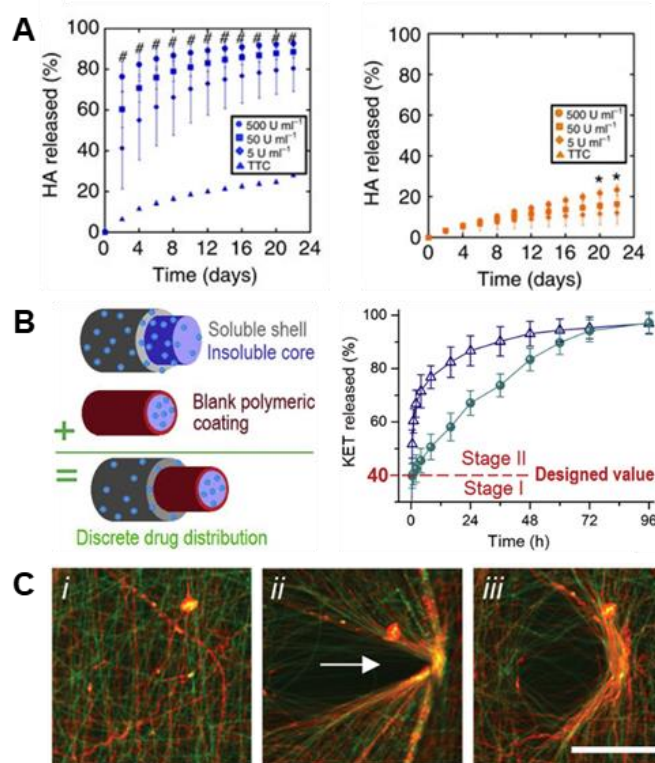
Figure 2.5. Dynamic complexity in electrospun fibers. (A): HA hydrogel fibers were crosslinked with a peptide crosslinker that was susceptible to degradation via matrix metalloproteinases (MMPs). (Left): degradation of MMP-sensitive HA fibers in the presence of differing concentrations of Type II collagenase (# $p < 0.05$, for all test groups versus control), and (right): degradation of HA fibers crosslinked with a peptide that is not sensitive to Type II collagenase (* $p < 0.05$, for 500 U/mL group versus control). There is a clear positive degradation effect when using an MMP-sensitive crosslinker. (A) Reprinted and adapted with permission from Wade et al., copyright 2015 Springer Nature[8]. (B): Triaxial electrospun fibers for sustained drug release. (Left): schematic of the triaxial fibers that include a polymeric coating around the innermost fiber to slow drug release. (Right): Model drug release (KET) from core-shell fibers (blue triangles) and triaxial fibers (green circles). Core-shell and tri-layered fibers both exhibited quick release past stage I (40% of release), but tri-layered fibers slowed the release throughout stage II compared to core-shell fibers – due to the polymeric coating introduced around the core. (B) Reprinted and adapted with permission from Yang et al., copyright 2020 Elsevier[156]. (C, left to right): Hydrazide and aldehyde-functionalized NorHA fibers (i) that react to form hydrazone bonds when in contact (ii) – allowing for permanent, covalent rearrangement of fibrous scaffolds (iii). (C) Reprinted and adapted with permission from Davidson et al., copyright 2019 John Wiley and Sons[167]; scalebars = 100 μm.

with the gelatin backbone, and protein release in this scenario relied on gelatin degradation to free the protein from the fibers[154]. These two gelatin systems can be

employed together to provide a tunable, sustained release of desired proteins from hydrogel fibers to support tissue growth and regeneration.

Core-shell fibers have also proven to be advantageous in the release of bioactive molecules to the adjacent environment. In the spirit of hydrogel fibers, a core-shell fibrous system was developed for the thermally-responsive release of rhodamine B[155]. The shell was comprised of poly-L-lactide-co-caprolactone (PLCL) and the core of poly(*N*-isopropylacrylamide-*co*-*N*-isopropylmethacrylamide) (P(NIPAAm-co-NIPMAAm)) – a thermally responsive polymer. The addition of the thermally-responsive P(NIPAAm-co-NIPMAAm) core allowed for a slower, more sustained release when compared to just a PLCL control[155]. Extending this, Yang and coworkers developed triaxial nanofibers comprised of polyvinylpyrrolidone (PVP) and cellulose acetate (CA), using ketoprofen (KET) as a model drug[156]. Yang et al. assert that the use of a tri-layered electrospun fiber yielded a more beneficial release profile initially, and the use of a CA blocking layer around the core provided a longer, more sustained release than a two layered system[156] (**Figure 2.5B**). While these are select examples of the extensive work in this area[55,82,151], they illustrate the potential to engineer nanofibers to control release profiles and deliver important bioactive molecules relevant in cellular systems. Continuing work in designing dynamic delivery systems has direct implications for engineering temporal complexity into electrospun fibers.

Improving cell infiltration. Incorporating dynamicity into electrospun fibers is an important consideration in developing nanofibrous scaffolds that interface with cells and natural tissue, especially in translation of regenerative materials, as touched on above with respect to controlled release. Efforts to develop dynamic fibrous structures have

sought to overcome a challenge faced by electrospun fibers in implantation: small pore sizes between fibers in larger, dense mats that are of clinically relevant dimensions prevent efficient cell infiltration into the scaffolds[127–129]. One way to surmount this challenge, in addition to the aforementioned intrafiber modifications such as enzymatically degradable crosslinks, is to spin multiple fiber types into a single substrate, where a fiber type might confer dynamic features into the substrate, such as increasing its porosity upon implantation. Specifically, water-soluble poly(ethylene oxide) (PEO) sacrificial fibers that dissolve in water, but take up space during fiber deposition and contribute to the initial structure of a larger electrospun substrate, can be co-spun with a material that is stable and persists over longer timescales[157–159]. This method has shown to improve infiltration, without hindering cellular transduction of microenvironmental cues[158]. This technique has been extended to the development of an engineered intervertebral disc, where an annulus geometry was designed with PCL fibers as the outer shell and hydrogel as the inner core[160]. The addition of PEO sacrificial fibers helped increase cell infiltration into this disc model which yielded superior matrix deposition when compared to the control that did not include sacrificial fibers[160].

Molecular-level dynamic complexities. Dynamic chemistries at the molecular level also offer the potential for engineering dynamic behaviors that emerge at the scales of individual fibers and fibrous systems. Chemical crosslinking approaches that allow for fibers to rearrange in response to outside perturbations—either during assembly of structures or through interactions with cells—have been demonstrated to enable the creation of complex fibrous constructs and to allow cells to modify the physical environment they experience over time. For example, dynamic supramolecular

crosslinking, where non-covalent, reversible interactions occur between complementary molecules on different polymers, can be used to assemble nanofibrous substrates and create structures with biomimetic complexity. Hyaluronic acid functionalized with methacrylates for covalent stabilization of fibers and also β-cyclodextrin (CD) (CD-MeHA) can be used to create nanofibers that form reversible bonds at interfaces with materials similarly functionalized with adamantane through supramolecular host-guest interactions[84]. CD is a cyclic host molecule with a hydrophobic core that hydrophobically interacts with guest molecules, such as adamantane (Ad) in noncovalent bonds that can be dynamically disrupted and restored[161–164]. By designing nanofibers that present complementary functionalities on their surfaces, a nanofibrous substrate presenting CD could be adhered to another presenting Ad, offering capabilities to generate layers of aligned fibers that might be useful in cartilage or cardiac tissue engineering applications, where they might reproduce fibrous tissue structures[84].

Reversible bonds, like the Ad-CD guest-host system, have been demonstrated to introduce viscoelasticity into hydrogel tissue culture systems – allowing for cells to easily deform and remodel the local microenvironment[155,165,166]. Nanofibrous systems with dynamic properties that enable cells to remodel their physical surroundings offer unique capabilities beyond bulk hydrogels, to observe, study, and perturb cellular behaviors through their interaction with fibrous materials. As discussed extensively here, these materials can be designed to offer ECM-like topographies as well as ECM-mimetic biophysical and biochemical features which offer cells more freedom of motion than might be achieved by encapsulating cells within a 3D hydrogel network. Towards establishing nanofibrous systems that allow dynamic, cell-responsive rearrangements of

microenvironmental physical features, Davidson et al. used NorHA that was additionally modified with either hydrazide or aldehyde groups (NorHA-Hyd and NorHA-Ald, respectively) to dual-electrospin a fibrous blend of NorHA-Hyd and NorHA-Ald[167]. At the fiber surfaces, hydrazide and aldehyde functional groups reacted to form hydrazone bonds when the two fiber types were in contact, i.e. an adhesive interaction[150,167,168] (**Figure 2.5C**). The interaction is proposed to allow cells to dynamically remodel the surrounding matrix by recruiting fibers with traction forces – with the recruited fibers subsequently reacting to preserve the structure[167]. Xu et al. also employed this chemical functionality within poly(oligoethylene glycol methacrylate) (POEGMA) fibers. POEGMA was functionalized with hydrazide/aldehyde moieties, which allowed for immediate *in situ* crosslinking following double-barrel electrospinning[168]. Xu et al. found that the hydrazide/aldehyde reaction allowed for the quick formation of crosslinks that were degradable both hydrolytically and enzymatically[168].

   Hydrogel fibers in the third dimension. Towards increasing the dimensionality of fibrous constructs or adding fibrous features to 3D tissue models, electrospun fibers have also been employed in 3D contexts – such as dispersion into bulk hydrogels[124] and shape-shifting 3D scaffolds[169], as highlighted here. The addition of fibrous networks dispersed within amorphous bulk hydrogels allows for recapitulation of the fibrillar nature of endogenous ECM, in a physiologically relevant 3D environment[4]. For example, Matera et al. demonstrated increased human dermal fibroblast spreading in hydrogels with dispersed dextran fibers, as well as cellular morphological changes in a fiber density-dependent manner[124] (**Figure 2.6 Top**). This example reinforces the stark influence of the
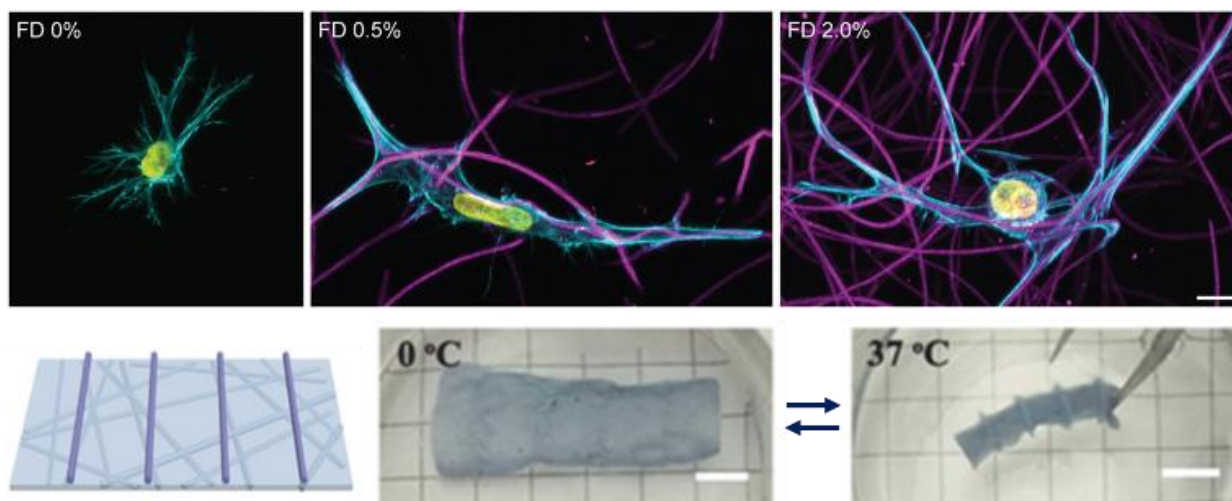
Figure 2.6. Electrospun fibers in 3D. (Top): Dispersion of DexVS fibers in 3D GelMA hydrogels. Increasing concentrations of suspended fibers (from left to right) demonstrates stark influence of fiber density on cell morphology – 0% and 2% show high levels of spread, whereas 0.5% shows a uniaxial morphology. (Top) Reprinted and adapted with permission from Matera et al., copyright 2019 American Chemical Society[124]; scalebar = 10 μm. (Bottom): P(NIPAAm-ABP) electrospun fibers with 3D printed supports. (from left to right): schematic of 3D printed supports atop of the nanofibrous P(NIPAAm-ABP) substrate; scaffold is suspended in water and adopts a relaxed conformation since the temperature is below the LCST (0° C); scaffold rolls and deforms when suspended in water with a temperature above the LCST (37° C) – thus acting as a shape-shifting hydrogel nanofiber system. (Bottom) Reprinted and adapted with permission from Chen et al., copyright 2018 John Wiley and Sons[170]; scalebars = 5 mm.

biophysical signals that fibers provide within 3D cell culture systems as researchers progress towards perfecting models of ECM *in vitro*.

From a biofabrication-specific standpoint, Chen and coworkers demonstrated the ability to electrospin poly(N-isopropylacrylamide) (P(NIPAAm)) hydrogel nanofibrous scaffolds that were secondarily crosslinked via UV light with acryloylbenzophenone (P(NIPAAm-ABP)) to form thermo-responsive mats[169]. Photocrosslinkable P(NIPAAm) solutions were also 3D printed onto these electrospun mats to provide rigid structure (i.e. trusses) to the mats. Due to P(NIPAAm)'s conformational changes above and below its lower critical solution temperature (LCST), the electrospun mats with supports exhibit

shape changes upon temperature transition around the LCST due to the amount of water that is contained within the fibrous network. Below the LCST (0° C), P(NIPAAm-ABP) scaffolds demonstrated a relaxed structure; however, once the temperature was increased to above the LCST (37° C), the scaffolds rolled into shapes that were dictated by the structures 3D printed atop of the mats – hence shape-shifting nanofibrous hydrogel scaffolds (**Figure 2.6 Bottom**)[169]. This system demonstrates efficacy in controlling the topography of nanofibrous hydrogel culture systems and can be extended to virtually any tissue system where 3D geometric structure is of interest.

Summary – dynamic complexity and mimicking natural tissue. Work in the field continues to advance dynamic features in fibrous cell culture systems that will be central to mimicking natural tissue systems, probing fundamental biological questions, and successfully designing systems for regenerative medicine. The inclusion of protease degradable crosslinkers, dynamic remodeling, sacrificial fibers for increased cellular infiltration, and the extension towards 3D scaffolds are key progressions in the development of fiber systems. However, the field of electrospun fibers – namely hydrogel fibers – is still trending behind the progress seen with 2D/3D bulk hydrogel systems, and there exists clear potential for hydrogel-based nanofibers to continue to be engineered to better recapitulate native physiology and control cell behaviors.

2.6. Next generation hydrogel fibers

As the field continues to progress towards fibrous hydrogel systems that recapture the salient features of a tissue system of interest, technology developed for engineering 2D/3D bulk hydrogels offers considerable opportunities for application in electrospun

hydrogel systems. For example, expanding upon chemistries enabling dynamic degradation via the usage of a protease-sensitive crosslinker, chemical functionalities exist that allow directed degradation, such as photocleavable crosslinking through nitrobenzyl ether groups developed and demonstrated by the Anseth group[170,171]. These have allowed for user-defined degradation at extremely short timescales relative to protease degradation.

Technologies that allow reversible biochemical cues to be incorporated into bulk hydrogels offer the potential for dynamic spatiotemporal control over microenvironmental features. The presentation of relevant biomolecules within the ECM is constantly in flux[4–7], and the ability to replicate this signaling complexity within an engineered microenvironment is critical to studying and replicating biological processes. Work that has reversibly, and repeatedly, introduced bioactive molecules into culture systems has utilized both covalent and supramolecular chemistries. Light-based approaches include nitrobenzyl ether techniques to photocleave the molecules from the scaffolds[10,172], while the Anseth group designed an allyl-sulfide that mediates multiple thiol-ene click reactions for incorporation and subsequent removal of desired molecules[11,111]. These studies were conducted with bulk PEG hydrogels but can conceivably be applied to PEG electrospun fibers or other hydrogel fibers that are modified to support these chemistries.

Groups have also employed supramolecular chemistries to reversibly incorporate bioactive molecules in hydrogel materials. Guest-host interactions allow for self-assembly of molecules but can be easily disrupted via the addition of a competing molecule[173]. For example, Boekhoven et al. utilized β-cyclodextrin as a host molecule and took advantage of differing affinities of naphthyl and adamantane to reversibly incorporate

biomolecules[173]. To develop technology enabling greater control over these reversible interactions, oligonucleotides with toeholds have been employed for their ability to provide bioactive domains on hydrogel surfaces[174]. Bioactivity was removed via the addition of complementary oligonucleotides that took advantage of the toehold region – providing a system with defined bioactivity by cyclical addition of these oligonucleotides[174]. Both of these examples demonstrated the ability to control cell morphology and spreading based on the presentation of these bioactive ligands on alginate surfaces[173,174]. Extending technologies such as these onto established hydrogel fibers would broaden opportunities to dynamically modulate complexity in water-swollen fibrous networks.

With continued progress and innovation in the materials design of fibrous hydrogel systems – and building upon exciting observations enabled by these platforms – we believe that it is inevitable that the technologies mentioned above will pave the way for platforms that truly recapitulate the endogenous ECM. With the growing understanding of the hydrated, fibrillar structure and function of the extracellular matrix, this progress is needed before we can truly probe fundamental physiological processes *in vitro*. As we progress forward, the growing ability to precisely define the biophysiochemical properties of an *in vitro* system offers the unique capability of engineering biomimetic environments for controlled perturbations to homeostasis in order to understand fundamental physiological function, dysfunction, development, and regeneration. Moreover, in addition to this fundamental experimentation, the ability to replicate natural tissue would be a significant stride towards the seamless integration of engineered therapeutics for successful tissue regeneration. With applications ranging the full scale of tissue engineering – from fundamental studies to clinical translation – the development of

dynamic, fibrillar hydrogels offers seemingly limitless potential as the field continues to develop.

In this regard, this thesis aims to offer novel biofabrication platforms to engineer dynamic complexities into electrospun hydrogels – specifically to increase the dimensionality of the resultant fibers in both time and space. Particular focus is placed on (1) incorporating user-defined, temporal control over the presentation of biomolecules within fibrous hydrogel scaffolds (time dimension) and (2) developing 3D, ECM-mimetic hydrogel environments using electrospun hydrogel fiber building blocks (space dimension). The biofabrication platforms described herein aim to offer generalizable materials approaches that are accessible to the general scientist, thereby providing the tools necessary to design models of virtually any tissue system *in vitro*.

Table 2.1. Representative list of hydrophilic materials used to form hydrogel fibers with post-processing techniques.

Material	Example crosslinking method(s)	Modulation of biophysiochemical properties
Fully-Synthetic Materials		
Polyacrylamide (PA)	**Chemical:** • Glutaraldehyde crosslinker[105]	**Biochemical:** • Likely adsorption-based modifications **Biophysical:** • Degree (extent) of crosslinking[105]
Poly(vinyl alcohol) (PVA)	**Chemical:** • Glutaraldehyde crosslinker[106] • PVA composites for crosslinking[107] **Physical:** • Controlling hydrophobicity through PVA modifications[108]	**Biochemical:** • Likely adsorption-based modifications **Biophysical:** • Degree (extent) of crosslinking[106] or PVA modification[108] • Degree of hydrolysis (i.e. quantity of pendant reactive groups)[107]
Poly(ethylene glycol) (PEG)	**Chemical:** • Pendant norbornenes (step-growth polymerization)[85,136] • Pendant methacrylates (chain-growth polymerization)[32]	**Biochemical** • Adsorption-based modifications[32] • Pendant norbornenes provide sites for addition of biomolecules ○ Light-mediated thiol-ene conjugation[85] **Biophysical:** • Stiffness controlled via irradiation and crosslinker– for example: norbornenes[136] and methacrylates[32]
Naturally-Derived Materials		
Collagen	**Chemical:** • Glutaraldehyde crosslinker[95,97,99] • Carbodiimide crosslinking (EDC/NHS)[102]	**Biochemical:** • Collagen provides natural bioactive sites for cell adhesion and interaction[95] **Biophysical:** • Degree (extent) of chemical crosslinking[97]
Gelatin	**Chemical:** • Glutaraldehyde[98] and diisocyanate crosslinkers[100] • Carbodiimide crosslinking (EDC/NHS)[101,103] • Pendant methacrylates (chain-growth polymerization)[115–117] **Physical:** • Dehydrothermal crosslinking (generally weaker fibers)[96]	**Biochemical:** • Gelatin provides natural bioactive sites for cell adhesion and interaction[96] **Biophysical:** • Degree (extent) of chemical crosslinking[96] • Degree of chain-growth polymerization (e.g. with methacrylates)[115,116]

Hyaluronic Acid (HA)	**Chemical:**
	• Pendant norbornenes (step-growth polymerization)[86]
	• Pendant methacrylates (chain-growth polymerization)[30,88,118,126,144]
	• Pendant maleimides (chain-growth polymerization)[8]
	• Hydrazide/aldehyde proximity reactions to crosslink adjacent fibers[145]
		Biochemical:
		• Pendant molecules provide sites for addition of biomolecules
		   ○ Michael addition: thiolated biomolecules react with pendant alkenes in basic conditions[8,118]
		   ○ Light-mediated thiol-ene conjugation[86]
		Biophysical:
		• Stiffness also controlled via irradiation time – for example: methacrylates[88,122]
		• Stiffness within norbornene modified systems can conceivably be controlled via crosslinker added, following from Gramlich et al.[112]

Dextran	**Chemical:**
	• Pendant methacrylates (chain-growth polymerization)[2,3,31]
	• Pendant vinyl sulfones (chain-growth polymerization)[87,124,146]
		Biochemical:
		• Pendant molecules provide sites for addition of biomolecules
		   ○ Methacrylated heparin conjugated to free methacrylates within methacrylated-dextran fibers[87]
		   ○ Michael addition: thiolated biomolecules react with pendant alkenes in basic conditions[2,3,31,87,124,146]
		Biophysical:
		• Stiffness also controlled via irradiation time – for example: chain-growth polymerization[2]

2.7. References

(1)   Caliari, S. R.; Burdick, J. A. A Practical Guide to Hydrogels for Cell Culture. *Nat. Methods* 2016, *13* (5), 405–414. https://doi.org/10.1038/nmeth.3839.

(2)   Baker, B. M.; Trappmann, B.; Wang, W. Y.; Sakar, M. S.; Kim, I. L.; Shenoy, V. B.; Burdick, J. A.; Chen, C. S. Cell-Mediated Fibre Recruitment Drives Extracellular Matrix Mechanosensing in Engineered Fibrillar Microenvironments. *Nat. Mater.* 2015, *14*, 1262–1268. https://doi.org/https://doi.org/10.1038/nmat4444.

(3)   Davidson, C. D.; Wang, W. Y.; Zaimi, I.; Jayco, D. K. P.; Baker, B. M. Cell Force-Mediated Matrix Reorganization Underlies Multicellular Network Assembly. *Sci. Rep.* 2019, *9*, 1–13. https://doi.org/https://doi.org/10.1038/s41598-018-37044-1.

(4)   Baker, B. M.; Chen, C. S. Deconstructing the Third Dimension – How 3D Culture Microenvironments Alter Cellular Cues. *J. Cell Sci.* 2012, *125* (13), 3015–3024. https://doi.org/https://doi.org/10.1242/jcs.079509.

(5)   Frantz, C.; Stewart, K. M.; Weaver, V. M. The Extracellular Matrix at a Glance. *J. Cell Sci.* 2010, *123* (24), 4195–4200. https://doi.org/https://doi.org/10.1242/jcs.023820.

(6)   Wade, R. J.; Burdick, J. A. Engineering ECM Signals into Biomaterials. *Mater. Today* 2012, *15* (10), 454–459. https://doi.org/https://doi.org/10.1016/S1369-7021(12)70197-9.

(7)   Lutolf, M. P.; Hubbell, J. A. Synthetic Biomaterials as Instructive Extracellular Microenvironments for Morphogenesis in Tissue Engineering. *Nat. Biotechnol.* 2005, *23*, 47–55. https://doi.org/https://doi.org/10.1038/nbt1055.

(8)   Wade, R. J.; Bassin, E. J.; Rodell, C. B.; Burdick, J. A. Protease-Degradable Electrospun Fibrous Hydrogels. *Nat. Commun.* 2015, *6*, 1–10. https://doi.org/https://doi.org/10.1038/ncomms7639.

(9)   Velasco-Hogan, A.; Xu, J.; Meyers, M. A. Additive Manufacturing as a Method to Design and Optimize Bioinspired Structures. *Adv. Mater.* 2018, *30* (1800940), 1–26. https://doi.org/https://doi.org/10.1002/adma.201800940.

(10)   Deforest, C. A.; Anseth, K. S. Photoreversible Patterning of Biomolecules within Click-Based Hydrogels. *Angew. Chemie Int. Ed.* 2012, *51* (8), 1816–1819. https://doi.org/https://doi.org/10.1002/anie.201106463.

(11)   Grim, J. C.; Brown, T. E.; Aguado, B. A.; Chapnick, D. A.; Viert, A. L.; Liu, X.; Anseth, K. S. A Reversible and Repeatable Thiol–Ene Bioconjugation for Dynamic

Patterning of Signaling Proteins in Hydrogels. *ACS Cent. Sci.* 2018, *4*, 909–916. https://doi.org/https://doi.org/10.1021/acscentsci.8b00325.

(12)   Wade, R. J.; Burdick, J. A. Advances in Nanofibrous Scaffolds for Biomedical Applications: From Electrospinning to Self-Assembly. *Nano Today* 2014, *9* (6), 722–742. https://doi.org/10.1016/j.nantod.2014.10.002.

(13)   Shoulders, M. D.; Raines, R. T. Collagen Structure and Stability. *Annu. Rev. Biochem.* 2009, *78*, 929–958. https://doi.org/https://doi.org/10.1146/annurev.biochem.77.032207.120833.

(14)   Hynes, R. O. The Extracellular Matrix: Not Just Pretty Fibrils. *Science (80-.).* 2009, *326* (5957), 1216–1219. https://doi.org/10.1126/science.1176009.

(15)   Griffith, L. G.; Swartz, M. A. Capturing Complex 3D Tissue Physiology in Vitro. *Mol. Cell Biol.* 2006, *7*, 211–224. https://doi.org/https://doi.org/10.1038/nrm1858.

(16)   Stevens, M. M.; George, J. H. Exploring and Engineering the Cell Surface Interface. *Science (80-.).* 2005, *310* (5751), 1135–1138. https://doi.org/10.1126/science.1106587.

(17)   Liu, C.; Hsu, P.-C.; Lee, H.-W.; Ye, M.; Zheng, G.; Liu, N.; Li, W.; Cui, Y. Transparent Air Filter for High-Efficiency PM 2.5 Capture. *Nat. Commun.* 2015, *6*, 1–9. https://doi.org/https://doi.org/10.1038/ncomms7205.

(18)   Wang, Y.; Li, W.; Xia, Y.; Jiao, X.; Chen, D. Electrospun Flexible Self-Standing γ-Alumina Fibrous Membranes and Their Potential as High-Efficiency Fine Particulate Filtration Media. *J. Mater. Chem. A* 2014, *2* (36), 15124–15131. https://doi.org/https://doi.org/10.1039/C4TA01770F.

(19)   Herricks, T. E.; Kim, S.-H.; Kim, J.; Li, D.; Kwak, J. H.; Grate, J. W.; Kim, S. H.; Xia, Y. Direct Fabrication of Enzyme-Carrying Polymer Nanofibers by Electrospinning. *J. Mater. Chem.* 2005, *15* (31), 3241–3245. https://doi.org/https://doi.org/10.1039/B503660G.

(20)   Ji, X.; Wang, P.; Su, Z.; Ma, G.; Zhang, S. Enabling Multi-Enzyme Biocatalysis Using Coaxial-Electrospun Hollow Nanofibers: Redesign of Artificial Cells. *J. Mater. Chem. B* 2014, *2* (2), 181–190. https://doi.org/https://doi.org/10.1039/C3TB21232G.

(21)   Islam, M. S.; Ang, B. C.; Andriyana, A.; Afifi, A. M. A Review on Fabrication of Nanofibers via Electrospinning and Their Applications. *SN Appl. Sci.* 2019, *1*, 1248. https://doi.org/https://doi.org/10.1007/s42452-019-1288-4.

(22)	Liu, H.; Ding, X.; Zhou, G.; Li, P.; Wei, X.; Fan, Y. Electrospinning of Nanofibers for Tissue Engineering Applications. *J. Nanomater.* 2013, *2013*, 1–11. https://doi.org/https://doi.org/10.1155/2013/495708.

(23)	Kishan, A. P.; Cosgriff-Hernandez, E. M. Recent Advancements in Electrospinning Design for Tissue Engineering Applications: A Review. *J. Biomed. Mater. Res. A* 2017, *105* (10), 2892–2905. https://doi.org/10.1002/jbm.a.36124.

(24)	Sun, L.; Gao, W.; Fu, X.; Shi, M.; Xie, W.; Zhang, W.; Zhao, F.; Chen, X. Enhanced Wound Healing in Diabetic Rats by Nanofibrous Scaffolds Mimicking the Basketweave Pattern of Collagen Fibrils in Native Skin. *Biomater. Sci.* 2018, *6* (2), 340–349. https://doi.org/10.1039/c7bm00545h.

(25)	Schoen, B.; Avrahami, R.; Baruch, L.; Efraim, Y.; Goldfracht, I.; Elul, O.; Davidov, T.; Gepstein, L.; Zussman, E.; Machluf, M. Electrospun Extracellular Matrix: Paving the Way to Tailor-Made Natural Scaffolds for Cardiac Tissue Regeneration. *Adv. Funct. Mater.* 2017, *27*, 1–9. https://doi.org/https://doi.org/10.1002/adfm.201700427.

(26)	De Valence, S.; Tille, J. C.; Giliberto, J. P.; Mrowczynski, W.; Gurny, R.; Walpoth, B. H.; Möller, M. Advantages of Bilayered Vascular Grafts for Surgical Applicability and Tissue Regeneration. *Acta Biomater.* 2012, *8* (11), 3914–3920. https://doi.org/10.1016/j.actbio.2012.06.035.

(27)	Christopherson, G. T.; Song, H.; Mao, H. The Influence of Fiber Diameter of Electrospun Substrates on Neural Stem Cell Differentiation and Proliferation. *Biomaterials* 2009, *30* (4), 556–564. https://doi.org/https://doi.org/10.1016/j.biomaterials.2008.10.004.

(28)	Lim, S. H.; Liu, X. Y.; Song, H.; Yarema, K. J.; Mao, H. The Effect of Nanofiber-Guided Cell Alignment on the Preferential Differentiation of Neural Stem Cells. *Biomaterials* 2010, *31* (34), 9031–9039. https://doi.org/10.1016/j.biomaterials.2010.08.021.

(29)	Chamundeswari, V. N.; Yuan Siang, L.; Jin Chuah, Y.; Shi Tan, J.; Wang, D.-A.; Loo, S. C. J. Sustained Releasing Sponge-like 3D Scaffolds for Bone Tissue Engineering Applications. *Biomed. Mater.* 2017, *13*, 1–11. https://doi.org/10.1088/1748-605X/aa8bcd.

(30)	Davidson, M. D.; Song, K. H.; Lee, M. H.; Llewellyn, J.; Du, Y.; Baker, B. M.; Wells, R. G.; Burdick, J. A. Engineered Fibrous Networks to Investigate the Influence of Fiber Mechanics on Myofibroblast Differentiation. *ACS Biomater. Sci. Eng.* 2019, *5* (8), 3899–3908. https://doi.org/https://doi.org/10.1021/acsbiomaterials.8b01276.

(31)   Wang, W. Y.; Davidson, C. D.; Lin, D.; Baker, B. M. Actomyosin Contractility-Dependent Matrix Stretch and Recoil Induces Rapid Cell Migration. *Nat. Commun.* 2019, *10*, 1–12. https://doi.org/10.1038/s41467-019-09121-0.

(32)   Wingate, K.; Bonani, W.; Tan, Y.; Bryant, S. J.; Tan, W. Compressive Elasticity of Three-Dimensional Nanofiber Matrix Directs Mesenchymal Stem Cell Differentiation to Vascular Cells with Endothelial or Smooth Muscle Cell Markers. *Acta Biomater.* 2012, *8* (4), 1440–1449. https://doi.org/10.1016/j.actbio.2011.12.032.

(33)   Xue, J.; Wu, T.; Dai, Y.; Xia, Y. Electrospinning and Electrospun Nanofibers: Methods, Materials, and Applications. *Chem. Rev.* 2019, *119* (8), 5298–5415. https://doi.org/10.1021/acs.chemrev.8b00593.

(34)   Rahmati, M.; Mills, D. K.; Urbanska, A. M.; Saeb, M. R.; Venugopal, J. R.; Ramakrishna, S.; Mozafari, M. Electrospinning for Tissue Engineering Applications. *Prog. Mater. Sci.* 2021, *117*, 1–41. https://doi.org/10.1016/j.pmatsci.2020.100721.

(35)   Schiffman, J. D.; Schauer, C. L. A Review: Electrospinning of Biopolymer Nanofibers and Their Applications. *Polym. Rev.* 2008, *48* (2), 317–352. https://doi.org/10.1080/15583720802022182.

(36)   Jordan, A. M.; Viswanath, V.; Kim, S.; Pokorski, J. K.; Korley, L. T. J. Processing and Surface Modification of Polymer Nanofibers for Biological Scaffolds: A Review. *J. Mater. Chem. B* 2016, *4*, 5958–5974. https://doi.org/10.1039/c6tb01303a.

(37)   Kalaoglu-Altan, O. I.; Sanyal, R.; Sanyal, A. Reactive and "clickable" Electrospun Polymeric Nanofibers. *Polym. Chem.* 2015, *6* (18), 3372–3381. https://doi.org/10.1039/c5py00098j.

(38)   Burdick, J. A.; Murphy, W. L. Moving from Static to Dynamic Complexity in Hydrogel Design. *Nat. Commun.* 2012, *3*, 1–8. https://doi.org/10.1038/ncomms2271.

(39)   Tibbitt, M. W.; Anseth, K. S. Hydrogels as Extracellular Matrix Mimics for 3D Cell Culture. *Biotechnol. Bioeng.* 2009, *103* (4), 655–663. https://doi.org/https://doi.org/10.1002/bit.22361.

(40)   Highley, C. B.; Prestwich, G. D.; Burdick, J. A. Recent Advances in Hyaluronic Acid Hydrogels for Biomedical Applications. *Curr. Opin. Biotechnol.* 2016, *40*, 35–40. https://doi.org/10.1016/j.copbio.2016.02.008.

(41)   Burdick, J. A.; Prestwich, G. D. Hyaluronic Acid Hydrogels for Biomedical Applications. *Adv. Healthc. Mater.* 2011, *23* (12), H41–H56. https://doi.org/10.1002/adma.201003963.

(42)   Cao, X.; Ban, E.; Baker, B. M.; Lin, Y.; Burdick, J. A.; Chen, C. S.; Shenoy, V. B. Multiscale Model Predicts Increasing Focal Adhesion Size with Decreasing Stiffness in Fibrous Matrices. *Proc. Natl. Acad. Sci. U. S. A.* 2017, *114* (23), E4549–E4555. https://doi.org/10.1073/pnas.1620486114.

(43)   Li, W.-J.; Laurencin, C. T.; Caterson, E. J.; Tuan, R. S.; Ko, F. K. Electrospun Nanofibrous Structure: A Novel Scaffold for Tissue Engineering. *J. Biomed. Mater. Res.* 2002, *60* (4), 613–621. https://doi.org/10.1002/jbm.10167.

(44)   Lee, B. L.-P.; Jeon, H.; Wang, A.; Yan, Z.; Yu, J.; Grigoropoulos, C.; Li, S. Femtosecond Laser Ablation Enhances Cell Infiltration into Three-Dimensional Electrospun Scaffolds. *Acta Biomater.* 2012, *8* (7), 2648–2658. https://doi.org/10.1016/j.actbio.2012.04.023.

(45)   Piai, J. F.; da Silva, M. A.; Martins, A.; Torres, A. B.; Faria, S.; Reis, R. L.; Muniz, E. C.; Neves, N. M. Chondroitin Sulfate Immobilization at the Surface of Electrospun Nanofiber Meshes for Cartilage Tissue Regeneration Approaches. *Appl. Surf. Sci.* 2017, *403*, 112–125. https://doi.org/https://doi.org/10.1016/j.apsusc.2016.12.135.

(46)   Shabani, I.; Haddadi-Asl, V.; Seyedjafari, E.; Soleimani, M. Cellular Infiltration on Nanofibrous Scaffolds Using a Modified Electrospinning Technique. *Biochem. Biophys. Res. Commun.* 2012, *423* (1), 50–54. https://doi.org/https://doi.org/10.1016/j.bbrc.2012.05.069.

(47)   He, L.; Tang, S.; Prabhakaran, M. P.; Liao, S.; Tian, L.; Zhang, Y.; Xue, W.; Ramakrishna, S. Surface Modification of PLLA Nano-Scaffolds with Laminin Multilayer by Lbl Assembly for Enhancing Neurite Outgrowth. *Macromol. Biosci.* 2013, *13* (11), 1601–1609. https://doi.org/10.1002/mabi.201300177.

(48)   Ko, Y.-G.; Kwon, O. H. Reinforced Gelatin-Methacrylate Hydrogels Containing Poly(Lactic-Co-Glycolic Acid) Nanofiber Fragments for 3D Bioprinting. *J. Ind. Eng. Chem.* 2020, *89*, 147–155. https://doi.org/https://doi.org/10.1016/j.jiec.2020.04.021.

(49)   Soliman, S.; Sant, S.; Nichol, J. W.; Khabiry, M.; Traversa, E.; Khademhosseini, A. Controlling the Porosity of Fibrous Scaffolds by Modulating the Fiber Diameter and Packing Density. *J. Biomed. Mater. Res. A* 2011, *96* (3), 566–574. https://doi.org/10.1002/jbm.a.33010.

(50)   Savoji, H.; Hadjizadeh, A.; Maire, M.; Ajji, A.; Wertheimer, M. R.; Lerouge, S. Electrospun Nanofiber Scaffolds and Plasma Polymerization: A Promising Combination towards Complete, Stable Endothelial Lining for Vascular Grafts. *Macromol. Biosci.* 2014, *14* (8), 1084–1095. https://doi.org/https://doi.org/10.1002/mabi.201300545.

(51)   Hu, X.; Liu, S.; Zhou, G.; Huang, Y.; Xie, Z.; Jing, X. Electrospinning of Polymeric Nanofibers for Drug Delivery Applications. *J. Control. Release* 2014, *185*, 12–21. https://doi.org/https://doi.org/10.1016/j.jconrel.2014.04.018.

(52)   Bashur, C. A.; Shaffer, R. D.; Dahlgren, L. A.; Guelcher, S. A.; Goldstein, A. S. Effect of Fiber Diameter and Alignment of Electrospun Polyurethane Meshes on Mesenchymal Progenitor Cells. *Tissue Eng. Part A* 2009, *15* (9), 2435–2445. https://doi.org/10.1089/ten.tea.2008.0295.

(53)   Haider, A.; Haider, S.; Kang, I. K. A Comprehensive Review Summarizing the Effect of Electrospinning Parameters and Potential Applications of Nanofibers in Biomedical and Biotechnology. *Arab. J. Chem.* 2018, *11* (8), 1165–1188. https://doi.org/https://doi.org/10.1016/j.arabjc.2015.11.015.

(54)   Agarwal, S.; Wendorff, J. H.; Greiner, A. Use of Electrospinning Technique for Biomedical Applications. *Polymer (Guildf).* 2008, *49* (26), 5603–5621. https://doi.org/https://doi.org/10.1016/j.polymer.2008.09.014.

(55)   Chakraborty, S.; Liao, I.-C.; Adler, A.; Leong, K. W. Electrohydrodynamics: A Facile Technique to Fabricate Drug Delivery Systems. *Adv. Drug Deliv. Rev.* 2009, *61* (12), 1043–1054. https://doi.org/10.1016/j.addr.2009.07.013.

(56)   Miller, A. E.; Hu, P.; Barker, T. H. Feeling Things Out: Bidirectional Signaling of the Cell–ECM Interface, Implications in the Mechanobiology of Cell Spreading, Migration, Proliferation, and Differentiation. *Adv. Healthc. Mater.* 2020, *9* (1901445), 1–24. https://doi.org/10.1002/adhm.201901445.

(57)   Peijs, T. Electrospun Polymer Nanofibers and Their Composites. In *Comprehensive Composite Materials II*; 2018; pp 162–200. https://doi.org/10.1016/B978-0-12-803581-8.10025-6.

(58)   Pham, Q. P.; Sharma, U.; Mikos, A. G. Electrospinning of Polymeric Nanofibers for Tissue Engineering Applications: A Review. *Tissue Eng.* 2006, *12* (5), 1197–1211. https://doi.org/10.1089/ten.2006.12.1197.

(59)   Ojha, S. S. Structure-Property Relationship of Electrospun Fibers. In *Electospun Nanofibers*; 2017; pp 239–253. https://doi.org/10.1016/B978-0-08-100907-9.00010-6.

(60)   Nezarati, R. M.; Eifert, M. B.; Dempsey, D. K.; Cosgriff-Hernandez, E. Electrospun Vascular Grafts with Improved Compliance Matching to Native Vessels. *J. Biomed. Mater. Res. B Appl. Biomater.* 2015, *103B* (2), 313–323. https://doi.org/10.1002/jbm.b.33201.

(61)   Park, S. M.; Eom, S.; Choi, D.; Han, S. J.; Park, S. J.; Kim, D. S. Direct Fabrication of Spatially Patterned or Aligned Electrospun Nano Fiber Mats on Dielectric Polymer Surfaces. *Chem. Eng. J.* 2018, *335*, 712–719. https://doi.org/10.1016/j.cej.2017.11.018.

(62)   Szczesny, S. E.; Driscoll, T. P.; Tseng, H.-Y.; Liu, P.-C.; Heo, S.-J.; Mauck, R. L.; Chao, P.-H. G. Crimped Nanofibrous Biomaterials Mimic Microstructure and Mechanics of Native Tissue and Alter Strain Transfer to Cells. *ACS Biomater. Sci. Eng.* 2017, *3* (11), 2869–2876. https://doi.org/https://doi.org/10.1021/acsbiomaterials.6b00646.

(63)   Chen, H.; Baptista, D. F.; Criscenti, G.; Crispim, J.; Fernandes, H.; van Blitterswijk, C.; Truckenmüller, R.; Moroni, L. From Fiber Curls to Mesh Waves: A Platform for the Fabrication of Hierarchically Structured Nanofibers Mimicking Natural Tissue Formation. *Nanoscale* 2019, *11* (30), 14312–14321. https://doi.org/10.1039/c8nr10108f.

(64)   Seliktar, D. Designing Cell-Compatible Hydrogels for Biomedical Applications. *Science (80-.).* 2012, *336* (6085), 1124–1129. https://doi.org/10.1126/science.1214804.

(65)   Murphy, W. L.; McDevitt, T. C.; Engler, A. J. Materials as Stem Cell Regulators. *Nat. Mater.* 2014, *13*, 547–557. https://doi.org/https://doi.org/10.1038/nmat3937.

(66)   Griffith, L. G.; Naughton, G. Tissue Engineering — Current Challenges and Expanding Opportunities. *Science (80-.).* 2002, *295* (5557), 1009–1014. https://doi.org/10.1126/science.1069210.

(67)   Kador, K. E.; Alsehli, H. S.; Zindell, A. N.; Lau, L. W.; Andreopoulos, F. M.; Watson, B. D.; Goldberg, J. L. Retinal Ganglion Cell Polarization Using Immobilized Guidance Cues on a Tissue-Engineered Scaffold. *Acta Biomater.* 2014, *10* (12), 4939–4946. https://doi.org/10.1016/j.actbio.2014.08.032.

(68)   Lee, H.; Rho, J.; Messersmith, P. B. Facile Conjugation of Biomolecules onto Surfaces via Mussel Adhesive Protein Inspired Coatings. *Adv. Mater.* 2009, *21* (4), 431–434. https://doi.org/https://doi.org/10.1002/adma.200801222.

(69)   Cho, H.; Madhurakkat Perikamana, S. K.; Lee, J.; Lee, J.; Lee, K.-M.; Shin, C. S.; Shin, H. Effective Immobilization of BMP-2 Mediated by Polydopamine Coating on Biodegradable Nanofibers for Enhanced in Vivo Bone Formation. *ACS Appl. Mater. Interfaces* 2014, *6* (14), 11225–11235. https://doi.org/10.1021/am501391z.

(70)   Nazeri, N.; Karimi, R.; Ghanbari, H. The Effect of Surface Modification of PLGA/CNT Nanofibrous Scaffolds by Laminin Protein on Nerve Tissue Engineering. *J.*

Biomed. Mater. Res. A 2021, *109*, 159–169.
https://doi.org/https://doi.org/10.1002/jbm.a.37013.

(71)   Shin, Y. M.; Jun, I.; Lim, Y.-M.; Rhim, T.; Shin, H. Bio-Inspired Immobilization of Cell-Adhesive Ligands on Electrospun Nanofibrous Patches for Cell Delivery. *Macromol. Mater. Eng.* 2013, *298* (5), 555–564.
https://doi.org/https://doi.org/10.1002/mame.201200217.

(72)   Lynge, M. E.; van der Westen, R.; Postma, A.; Städler, B. Polydopamine—a Nature-Inspired Polymer Coating for Biomedical Science. *Nanoscale* 2011, *3* (12), 4916–4928. https://doi.org/10.1039/c1nr10969c.

(73)   Ryu, J. H.; Messersmith, P. B.; Lee, H. Polydopamine Surface Chemistry: A Decade of Discovery. *ACS Appl. Mater. Interfaces* 2018, *10* (9), 7523–7540.
https://doi.org/10.1021/acsami.7b19865.

(74)   Qiu, X.; Lee, B. L.-P.; Ning, X.; Murthy, N.; Dong, N.; Li, S. End-Point Immobilization of Heparin on Plasma-Treated Surface of Electrospun Polycarbonate-Urethane Vascular Graft. *Acta Biomater.* 2017, *51*, 138–147.
https://doi.org/10.1016/j.actbio.2017.01.012.

(75)   Tanes, M. L.; Xue, J.; Xia, Y. A General Strategy for Generating Gradients of Bioactive Proteins on Electrospun Nanofiber Mats by Masking with Bovine Serum Albumin. *J. Mater. Chem. B* 2017, *5* (28), 5580–5587.
https://doi.org/10.1039/C7TB00974G.

(76)   Wu, T.; Xue, J.; Li, H.; Zhu, C.; Mo, X.; Xia, Y. General Method for Generating Circular Gradients of Active Proteins on Nanofiber Scaffolds Sought for Wound Closure and Related Applications. *ACS Appl. Mater. Interfaces* 2018, *10* (10), 8536–8545.
https://doi.org/https://doi.org/10.1021/acsami.8b00129.

(77)   Haldón, E.; Nicasio, M. C.; Pérez, P. J. Copper-Catalysed Azide-Alkyne Cycloadditions (CuAAC): An Update. *Org. Biomol. Chem.* 2015, *13* (37), 9528–9550.
https://doi.org/10.1039/c5ob01457c.

(78)   Mbua, N. E.; Guo, J.; Wolfert, M. A.; Steet, R.; Boons, G.-J. Strain-Promoted Alkyne-Azide Cycloadditions (SPAAC) Reveal New Features of Glycoconjugate Biosynthesis. *ChemBioChem* 2011, *12* (12), 1912–1921.
https://doi.org/10.1002/cbic.201100117.

(79)   Shi, Q.; Chen, X.; Lu, T.; Jing, X. The Immobilization of Proteins on Biodegradable Polymer Fibers via Click Chemistry. *Biomaterials* 2008, *29* (8), 1118–1126. https://doi.org/https://doi.org/10.1016/j.biomaterials.2007.11.008.

(80)   Smith Callahan, L. A.; Xie, S.; Barker, I. A.; Zheng, J.; Reneker, D. H.; Dove, A. P.; Becker, M. L. Directed Differentiation and Neurite Extension of Mouse Embryonic Stem Cell on Aligned Poly(Lactide) Nanofibers Functionalized with YIGSR Peptide. *Biomaterials* 2013, *34* (36), 9089–9095. https://doi.org/https://doi.org/10.1016/j.biomaterials.2013.08.028.

(81)   Zheng, J.; Xie, S.; Lin, F.; Hua, G.; Yu, T.; Reneker, D. H.; Becker, M. L. 4-Dibenzocyclooctynol (DIBO) as an Initiator for Poly(ε-Caprolactone): Copper-Free Clickable Polymer and Nanofiber-Based Scaffolds. *Polym. Chem.* 2013, *4* (7), 2215–2218. https://doi.org/10.1039/c3py00153a.

(82)   Pillay, V.; Dott, C.; Choonara, Y. E.; Tyagi, C.; Tomar, L.; Kumar, P.; du Toit, L. C.; Ndesendo, V. M. K. A Review of the Effect of Processing Variables on the Fabrication of Electrospun Nanofibers for Drug Delivery Applications. *J. Nanomater.* 2013, *2013*, 1–22. https://doi.org/https://doi.org/10.1155/2013/789289.

(83)   de Lima, G. G.; Lyons, S.; Devine, D. M.; Nugent, M. J. D. Electrospinning of Hydrogels for Biomedical Applications. In *Hydrogels*; Springer Singapore, 2018; pp 219–258. https://doi.org/https://doi.org/10.1007/978-981-10-6077-9_9.

(84)   Highley, C. B.; Rodell, C. B.; Kim, I. L.; Wade, R. J.; Burdick, J. A. Ordered, Adherent Layers of Nanofibers Enabled by Supramolecular Interactions. *J. Mater. Chem. B* 2015, *2* (46), 8110–8115. https://doi.org/https://doi.org/10.1039/C4TB00724G.

(85)   Sharma, S.; Floren, M.; Ding, Y.; Stenmark, K. R.; Tan, W.; Bryant, S. J. A Photoclickable Peptide Microarray Platform for Facile and Rapid Screening of 3-D Tissue Microenvironments. *Biomaterials* 2017, *143*, 17–28. https://doi.org/10.1016/j.biomaterials.2017.07.025.

(86)   Wade, R. J.; Bassin, E. J.; Gramlich, W. M.; Burdick, J. A. Nanofibrous Hydrogels with Spatially Patterned Biochemical Signals to Control Cell Behavior. *Adv. Mater.* 2015, *27* (8), 1356–1362. https://doi.org/https://doi.org/10.1002/adma.201404993.

(87)   Davidson, C. D.; Jayco, D. K. P.; Matera, D. L.; DePalma, S. J.; Hiraki, H. L.; Wang, W. Y.; Baker, B. M. Myofibroblast Activation in Synthetic Fibrous Matrices Composed of Dextran Vinyl Sulfone. *Acta Biomater.* 2020, *105*, 78–86. https://doi.org/https://doi.org/10.1016/j.actbio.2020.01.009.

(88)   Song, K. H.; Heo, S.-J.; Peredo, A. P.; Davidson, M. D.; Mauck, R. L.; Burdick, J. A. Influence of Fiber Stiffness on Meniscal Cell Migration into Dense Fibrous Networks. *Adv. Healthc. Mater.* 2019, *9* (1901228), 1–10. https://doi.org/https://doi.org/10.1002/adhm.201901228.

(89)   Moroni, L.; Burdick, J. A.; Highley, C.; Lee, S. J.; Morimoto, Y.; Takeuchi, S.; Yoo, J. J. Biofabrication Strategies for 3D in Vitro Models and Regenerative Medicine. *Nat. Rev. Mater.* 2018, *3*, 21–37. https://doi.org/https://doi.org/10.1038/s41578-018-0006-y.

(90)   Li, M.; Mondrinos, M. J.; Gandhi, M. R.; Ko, F. K.; Weiss, A. S.; Lelkes, P. I. Electrospun Protein Fibers as Matrices for Tissue Engineering. *Biomaterials* 2005, *26* (30), 5999–6008. https://doi.org/10.1016/j.biomaterials.2005.03.030.

(91)   Kwon, M. Y.; Wang, C.; Galarraga, J. H.; Puré, E.; Han, L.; Burdick, J. A. Influence of Hyaluronic Acid Modification on CD44 Binding towards the Design of Hydrogel Biomaterials. *Biomaterials* 2019, *222* (119451), 1–9. https://doi.org/https://doi.org/10.1016/j.biomaterials.2019.119451.

(92)   Misra, S.; Hascall, V. C.; Markwald, R. R.; Ghatak, S. Interactions between Hyaluronan and Its Receptors (CD44, RHAMM) Regulate the Activities of Inflammation and Cancer. *Front. Immunol.* 2015, *6* (201), 1–31. https://doi.org/https://doi.org/10.3389/fimmu.2015.00201.

(93)   Chung, C.; Beecham, M.; Mauck, R. L.; Burdick, J. A. The Influence of Degradation Characteristics of Hyaluronic Acid Hydrogels on in Vitro Neocartilage Formation by Mesenchymal Stem Cells. *Biomaterials* 2009, *30* (26), 4287–4296. https://doi.org/10.1016/j.biomaterials.2009.04.040.

(94)   Roberts, J. J.; Bryant, S. J. Comparison of Photopolymerizable Thiol-Ene PEG and Acrylate-Based PEG Hydrogels for Cartilage Development. *Biomaterials* 2013, *34* (38), 9969–9979. https://doi.org/10.1016/j.biomaterials.2013.09.020.

(95)   Castilla-Casadiego, D. A.; Ramos-Avilez, H. V.; Herrera-Posada, S.; Calcagno, B.; Loyo, L.; Shipmon, J.; Acevedo, A.; Quintana, A.; Almodovar, J. Engineering of a Stable Collagen Nanofibrous Scaffold with Tunable Fiber Diameter, Alignment, and Mechanical Properties. *Macromol. Mater. Eng.* 2016, *301* (9), 1064–1075. https://doi.org/https://doi.org/10.1002/mame.201600156.

(96)   Campiglio, C. E.; Negrini, N. C.; Farè, S.; Draghi, L. Cross-Linking Strategies for Electrospun Gelatin Scaffolds. *Materials (Basel).* 2019, *12* (2476), 1–23. https://doi.org/https://doi.org/10.3390/ma12152476.

(97)   Jha, B. S.; Ayres, C. E.; Bowman, J. R.; Telemeco, T. A.; Sell, S. A.; Bowlin, G. L.; Simpson, D. G. Electrospun Collagen: A Tissue Engineering Scaffold with Unique Functional Properties in a Wide Variety of Applications. *J. Nanomater.* 2011, *2011* (348268), 1–15. https://doi.org/https://doi.org/10.1155/2011/348268.

(98)   Aoki, H.; Miyoshi, H.; Yamagata, Y. Electrospinning of Gelatin Nanofiber Scaffolds with Mild Neutral Cosolvents for Use in Tissue Engineering. *Polym. J.* 2015, *47*, 267–277. https://doi.org/https://doi.org/10.1038/pj.2014.94.

(99)   Zhang, X.; Tang, K.; Zheng, X. Electrospinning and Crosslinking of COL/PVA Nanofiber-Microsphere Containing Salicylic Acid for Drug Delivery. *J. Bionic Eng.* 2016, *13* (1), 143–149. https://doi.org/https://doi.org/10.1016/S1672-6529(14)60168-2.

(100) Kishan, A. P.; Nezarati, R. M.; Radzicki, C. M.; Renfro, A. L.; Robinson, J. L.; Whitely, M. E.; Cosgriff-Hernandez, E. M. In Situ Crosslinking of Electrospun Gelatin for Improved Fiber Morphology Retention and Tunable Degradation. *J. Mater. Chem. B* 2015, *3*, 7930–7938. https://doi.org/10.1039/c5tb00937e.

(101) Liu, L.; Kamei, K.; Yoshioka, M.; Nakajima, M.; Li, J.; Fujimoto, N.; Terada, S.; Tokunaga, Y.; Koyama, Y.; Sato, H.; et al. Nano-on-Micro Fibrous Extracellular Matrices for Scalable Expansion of Human ES/IPS Cells. *Biomaterials* 2017, *124*, 47–54. https://doi.org/https://doi.org/10.1016/j.biomaterials.2017.01.039.

(102) Fischer, R. L.; McCoy, M. G.; Grant, S. A. Electrospinning Collagen and Hyaluronic Acid Nanofiber Meshes. *J. Mater. Sci. Mater. Med.* 2012, *23*, 1645–1654. https://doi.org/10.1007/s10856-012-4641-3.

(103) Ghassemi, Z.; Slaughter, G. Cross-Linked Electrospun Gelatin Nanofibers for Cell-Based Assays. *Conf. Proc. IEEE Eng. Med. Biol. Soc.* 2018, *2018* (July), 6088–6091. https://doi.org/10.1109/EMBC.2018.8513549.

(104) Young, R. E.; Graf, J.; Miserocchi, I.; Van Horn, R. M.; Gordon, M. B.; Anderson, C. R.; Sefcik, L. S. Optimizing the Alignment of Thermoresponsive Poly(N-Isopropyl Acrylamide) Electrospun Nanofibers for Tissue Engineering Applications: A Factorial Design of Experiments Approach. *PLoS One* 2019, *14* (7), 1–15. https://doi.org/10.1371/journal.pone.0219254.

(105) Lu, P.; Hsieh, Y.-L. Organic Compatible Polyacrylamide Hydrogel Fibers. *Polymer (Guildf).* 2009, *50* (15), 3670–3679. https://doi.org/https://doi.org/10.1016/j.polymer.2009.05.040.

(106) Destaye, A. G.; Lin, C. K.; Lee, C. K. Glutaraldehyde Vapor Cross-Linked Nanofibrous PVA Mat with in Situ Formed Silver Nanoparticles. *ACS Appl. Mater. Interfaces* 2013, *5* (11), 4745–4752. https://doi.org/10.1021/am401730x.

(107) Park, J. C.; Ito, T.; Kim, K. O.; Kim, K. W.; Kim, B. S.; Khil, M. S.; Kim, H. Y.; Kim, I. S. Electrospun Poly(Vinyl Alcohol) Nanofibers: Effects of Degree of Hydrolysis and

Enhanced Water Stability. *Polym. J.* 2010, *42* (3), 273–276. https://doi.org/10.1038/pj.2009.340.

(108) Kim, C. K.; Kim, B. S.; Sheikh, F. A.; Lee, U. S.; Khil, M. S.; Kim, H. Y. Amphiphilic Polyvinyl Alcohol Hybrids and Electrospun Nanofibers Incorporating Polyhedral Oligosilsesquioxane. *Macromolecules* 2007, *40* (14), 4823–4828. https://doi.org/10.1021/ma070056e.

(109) Hui, E.; Gimeno, K. I.; Guan, G.; Caliari, S. R. Spatiotemporal Control of Viscoelasticity in Phototunable Hyaluronic Acid Hydrogels. *Biomacromolecules* 2019, *20* (11), 4126–4134. https://doi.org/https://doi.org/10.1021/acs.biomac.9b00965.

(110) Hoyle, C. E.; Bowman, C. N. Thiol – Ene Click Chemistry. *Angew. Chemie* 2010, *49*, 1540–1573. https://doi.org/https://doi.org/10.1002/anie.200903924.

(111) Grim, J. C.; Marozas, I. A.; Anseth, K. S. Thiol-Ene and Photo-Cleavage Chemistry for Controlled Presentation of Biomolecules in Hydrogels. *J. Control. Release* 2015, *219*, 95–106. https://doi.org/10.1016/j.jconrel.2015.08.040.

(112) Gramlich, W. M.; Kim, I. L.; Burdick, J. A. Synthesis and Orthogonal Photopatterning of Hyaluronic Acid Hydrogels with Thiol-Norbornene Chemistry. *Biomaterials* 2013, *34* (38), 9803–9811. https://doi.org/10.1016/j.biomaterials.2013.08.089.

(113) Ifkovits, J. L.; Burdick, J. A. Review: Photopolymerizable and Degradable Biomaterials for Tissue Engineering Applications. *Tissue Eng.* 2007, *13* (10), 2369–2385. https://doi.org/10.1089/ten.2007.0093.

(114) Van Den Bulcke, A. I.; Bogdanov, B.; De Rooze, N.; Schacht, E. H.; Cornelissen, M.; Berghmans, H. Structural and Rheological Properties of Methacrylamide Modified Gelatin Hydrogels. *Biomacromolecules* 2000, *1* (1), 31–38. https://doi.org/https://doi.org/10.1021/bm990017d.

(115) Aldana, A. A.; Malatto, L.; Rehman, M. A. U.; Boccaccini, A. R.; Abraham, G. A. Fabrication of Gelatin Methacrylate (GelMA) Scaffolds with Nano- and Micro-Topographical and Morphological Features. *Nanomaterials* 2019, *9* (120), 1–12. https://doi.org/https://doi.org/10.3390/nano9010120.

(116) Zhao, X.; Sun, X.; Yildirimer, L.; Lang, Q.; Lin, Z. Y. (William); Zheng, R.; Zhang, Y.; Cui, W.; Annabi, N.; Khademhosseini, A. Cell Infiltrative Hydrogel Fibrous Scaffolds for Accelerated Wound Healing. *Acta Biomater.* 2017, *49*, 66–77. https://doi.org/https://doi.org/10.1016/j.actbio.2016.11.017.

(117) Lobo, A. O.; Afewerki, S.; de Paula, M. M. M.; Ghannadian, P.; Marciano, F. R.; Zhang, Y. S.; Webster, T. J.; Khademhosseini, A. Electrospun Nanofiber Blend with Improved Mechanical and Biological Performance. *Int. J. Nanomedicine* 2018, *13*, 7891–7903. https://doi.org/10.2147/IJN.S175619.

(118) Kim, I. L.; Khetan, S.; Baker, B. M.; Chen, C. S.; Burdick, J. A. Fibrous Hyaluronic Acid Hydrogels That Direct MSC Chondrogenesis through Mechanical and Adhesive Cues. *Biomaterials* 2013, *34* (22), 5571–5580. https://doi.org/10.1016/j.biomaterials.2013.04.004.

(119) Bessonov, I. V.; Rochev, Y. A.; Arkhipova, A. Y.; Kopitsyna, M. N.; Bagrov, D. V.; Karpushkin, E. A.; Bibikova, T. N.; Moysenovich, A. M.; Soldatenko, A. S.; Nikishin, I. I.; et al. Fabrication of Hydrogel Scaffolds via Photocrosslinking of Methacrylated Silk Fibroin. *Biomed. Mater.* 2019, *14* (034102), 1–15. https://doi.org/10.1088/1748-605X/ab04e0.

(120) Bae, S. Bin; Kim, M. H.; Park, W. H. Electrospinning and Dual Crosslinking of Water-Soluble Silk Fibroin Modified with Glycidyl Methacrylate. *Polym. Degrad. Stab.* 2020, *179* (109304), 1–9. https://doi.org/10.1016/j.polymdegradstab.2020.109304.

(121) Tan, A. R.; Ifkovits, J. L.; Baker, B. M.; Brey, D. M.; Mauck, R. L.; Burdick, J. A. Electrospinning of Photocrosslinked and Degradable Fibrous Scaffolds. *J. Biomed. Mater. Res. A* 2008, *87* (4), 1034–1043. https://doi.org/10.1002/jbm.a.31853.

(122) Sundararaghavan, H. G.; Metter, R. B.; Burdick, J. A. Electrospun Fibrous Scaffolds with Multiscale and Photopatterned Porosity. *Macromol. Biosci.* 2010, *10* (3), 265–270. https://doi.org/10.1002/mabi.200900363.

(123) Dong, B.; Arnoult, O.; Smith, M. E.; Wnek, G. E. Electrospinning of Collagen Nanofiber Scaffolds from Benign Solvents. *Macromol. Rapid Commun.* 2009, *30* (7), 539–542. https://doi.org/10.1002/marc.200800634.

(124) Matera, D. L.; Wang, W. Y.; Smith, M. R.; Shikanov, A.; Baker, B. M. Fiber Density Modulates Cell Spreading in 3D Interstitial Matrix Mimetics. *ACS Biomater. Sci. Eng.* 2019, *5*, 2965–2975. https://doi.org/https://doi.org/10.1021/acsbiomaterials.9b00141.

(125) Hall, M. S.; Alisafaei, F.; Ban, E.; Feng, X.; Hui, C. Y.; Shenoy, V. B.; Wu, M. Fibrous Nonlinear Elasticity Enables Positive Mechanical Feedback between Cells and ECMs. *Proc. Natl. Acad. Sci. U. S. A.* 2016, *113* (49), 14043–14048. https://doi.org/10.1073/pnas.1613058113.

(126) Sundararaghavan, H. G.; Saunders, R. L.; Hammer, D. A.; Burdick, J. A. Fiber Alignment Directs Cell Motility over Chemotactic Gradients. *Biotechnol. Bioeng.* 2013, *110* (4), 1249–1254. https://doi.org/10.1002/bit.24788.

(127) Qu, F.; Guilak, F.; Mauck, R. L. Cell Migration: Implications for Repair and Regeneration in Joint Disease. *Nat. Rev. Rheumatol.* 2019, *15*, 167–179. https://doi.org/https://doi.org/10.1038/s41584-018-0151-0.

(128) Baker, B. M.; Mauck, R. L. The Effect of Nanofiber Alignment on the Maturation of Engineered Meniscus Constructs. *Biomaterials* 2007, *28* (11), 1967–1977. https://doi.org/10.1016/j.biomaterials.2007.01.004.

(129) Baker, B. M.; Nathan, A. S.; Huffman, G. R.; Mauck, R. L. Tissue Engineering With Meniscus Cells Derived From Surgical Debris. *Osteoarthr. Cartil.* 2009, *17* (3), 336–345. https://doi.org/10.1016/j.joca.2008.08.001.

(130) Abhilash, A. S.; Baker, B. M.; Trappmann, B.; Chen, C. S.; Shenoy, V. B. Remodeling of Fibrous Extracellular Matrices by Contractile Cells: Predictions from Discrete Fiber Network Simulations. *Biophys. J.* 2014, *107* (8), 1829–1840. https://doi.org/10.1016/j.bpj.2014.08.029.

(131) Heo, S. J.; Song, K. H.; Thakur, S.; Miller, L. M.; Cao, X.; Peredo, A. P.; Seiber, B. N.; Qu, F.; Driscoll, T. P.; Shenoy, V. B.; et al. Nuclear Softening Expedites Interstitial Cell Migration in Fibrous Networks and Dense Connective Tissues. *Sci. Adv.* 2020, *6* (25), 1–13. https://doi.org/10.1126/sciadv.aax5083.

(132) Kloxin, A. M.; Kloxin, C. J.; Bowman, C. N.; Anseth, K. S. Mechanical Properties of Cellularly Responsive Hydrogels and Their Experimental Determination. *Adv. Mater.* 2010, *22* (31), 3484–3494. https://doi.org/10.1002/adma.200904179.

(133) Lin-Gibson, S.; Jones, R. L.; Washburn, N. R.; Horkay, F. Structure-Property Relationships of Photopolymerizable Poly(Ethylene Glycol) Dimethacrylate Hydrogels. *Macromolecules* 2005, *38* (7), 2897–2902. https://doi.org/https://doi.org/10.1021/ma0487002.

(134) Shanmuganathan, K.; Sankhagowit, R. K.; Iyer, P.; Ellison, C. J. Thiol-Ene Chemistry: A Greener Approach to Making Chemically and Thermally Stable Fibers. *Chem. Mater.* 2011, *23* (21), 4726–4732. https://doi.org/https://doi.org/10.1021/cm2015093.

(135) Kalaoglu-Altan, O. I.; Verbraeken, B.; Lava, K.; Gevrek, T. N.; Sanyal, R.; Dargaville, T.; De Clerck, K.; Hoogenboom, R.; Sanyal, A. Multireactive Poly(2-

Oxazoline) Nanofibers through Electrospinning with Crosslinking on the Fly. *ACS Macro Lett.* 2016, *5* (6), 676–681. https://doi.org/https://doi.org/10.1021/acsmacrolett.6b00188.

(136) Iglesias-Echevarria, M.; Durante, L.; Johnson, R.; Rafuse, M.; Ding, Y.; Bonani, W.; Maniglio, D.; Tan, W. Coaxial PCL/PEG-Thiol-Ene Microfiber with Tunable Physico-Chemical Properties for Regenerative Scaffolds. *Biomater. Sci.* 2019, *7* (9), 3640–3651. https://doi.org/10.1039/c9bm00388f.

(137) Yang, H.; Zhang, Q.; Lin, B.; Fu, G.; Zhang, X.; Guo, L. Thermo-Sensitive Electrospun Fibers Prepared by a Sequential Thiol-Ene Click Chemistry Approach. *J. Polym. Sci. A Polym. Chem.* 2012, *50* (20), 4182–4190. https://doi.org/https://doi.org/10.1002/pola.26244.

(138) Mays, E. A.; Kallakuri, S. S.; Sundararaghavan, H. G. Heparin-Hyaluronic Acid Nanofibers for Growth Factor Sequestration in Spinal Cord Repair. *J. Biomed. Mater. Res. A* 2020, *2020* (March), 1–9. https://doi.org/10.1002/jbm.a.36962.

(139) Nair, D. P.; Podgórski, M.; Chatani, S.; Gong, T.; Xi, W.; Fenoli, C. R.; Bowman, C. N. The Thiol-Michael Addition Click Reaction: A Powerful and Widely Used Tool in Materials Chemistry. *Chem. Mater.* 2014, *26* (1), 724–744. https://doi.org/https://doi.org/10.1021/cm402180t.

(140) Petrou, C. L.; D'Ovidio, T. J.; Bolukbas, D. A.; Tas, S.; Brown, R. D.; Allawzi, A.; Lindstedt, S.; Nozik-Grayck, E.; Stenmark, K. R.; Wagner, D. E.; et al. Clickable, Decellularized Extracellular Matrix as a New Tool for Building Dynamic, Hybrid Hydrogels to Model Chronic Fibrotic Diseases in Vitro. *J. Mater. Chem. B* 2020, *8* (31), 6814–6826. https://doi.org/https://doi.org/10.1039/D0TB00613K.

(141) Trappmann, B.; Baker, B. M.; Polacheck, W. J.; Choi, C. K.; Burdick, J. A.; Chen, C. S. Matrix Degradability Controls Multicellularity of 3D Cell Migration. *Nat. Commun.* 2017, *8* (371), 1–8. https://doi.org/https://doi.org/10.1038/s41467-017-00418-6.

(142) Zustiak, S. P.; Boukari, H.; Leach, J. B. Solute Diffusion and Interactions in Cross-Linked Poly(Ethylene Glycol) Hydrogels Studied by Fluorescence Correlation Spectroscopy. *Soft Matter* 2010, *6* (15), 3609–3618. https://doi.org/10.1039/C0SM00111B.

(143) Han, K.; Yin, W.-N.; Fan, J.-X.; Cao, F.-Y.; Zhang, X.-Z. Photo-Activatable Substrates for Site-Specific Differentiation of Stem Cells. *ACS Appl. Mater. Interfaces* 2015, *7* (42), 23679–23684. https://doi.org/https://doi.org/10.1021/acsami.5b07455.

(144) Sundararaghavan, H. G.; Burdick, J. A. Gradients with Depth in Electrospun Fibrous Scaffolds for Directed Cell Behavior. *Biomacromolecules* 2011, *12* (6), 2344–2350. https://doi.org/10.1021/bm200415g.

(145) Girão, A. F.; Wieringa, P.; Pinto, S. C.; Marques, P. A. A. P.; Micera, S.; van Wezel, R.; Ahmed, M.; Truckenmueller, R.; Moroni, L. Ultraviolet Functionalization of Electrospun Scaffolds to Activate Fibrous Runways for Targeting Cell Adhesion. *Front. Bioeng. Biotechnol.* 2019, *7* (159), 1–10. https://doi.org/https://doi.org/10.3389/fbioe.2019.00159.

(146) Saha, K.; Pollock, J. F.; Schaffer, D. V.; Healy, K. E. Designing Synthetic Materials to Control Stem Cell Phenotype. *Curr. Opin. Chem. Biol.* 2007, *11* (4), 381–387. https://doi.org/10.1016/j.cbpa.2007.05.030.

(147) Nih, L. R.; Moshayedi, P.; Llorente, I. L.; Berg, A. R.; Cinkornpumin, J.; Lowry, W. E.; Segura, T.; Carmichael, S. T. Engineered HA Hydrogel for Stem Cell Transplantation in the Brain: Biocompatibility Data Using a Design of Experiment Approach. *Data Br.* 2017, *10*, 202–209. https://doi.org/10.1016/j.dib.2016.11.069.

(148) Nih, L. R.; Sideris, E.; Carmichael, S. T.; Segura, T. Injection of Microporous Annealing Particle (MAP) Hydrogels in the Stroke Cavity Reduces Gliosis and Inflammation and Promotes NPC Migration to the Lesion. *Adv. Mater.* 2017, *29* (1606471), 1–8. https://doi.org/10.1002/adma.201606471.

(149) Holloway, J. L.; Ma, H.; Rai, R.; Burdick, J. A. Modulating Hydrogel Crosslink Density and Degradation to Control Bone Morphogenetic Protein Delivery and in Vivo Bone Formation. *J. Control. Release* 2014, *191*, 63–70. https://doi.org/https://doi.org/10.1016/j.jconrel.2014.05.053.

(150) Purcell, B. P.; Lobb, D.; Charati, M. B.; Dorsey, S. M.; Wade, R. J.; Zellars, K. N.; Doviak, H.; Pettaway, S.; Logdon, C. B.; Shuman, J. A.; et al. Injectable and Bioresponsive Hydrogels for On-Demand Matrix Metalloproteinase Inhibition. *Nat. Mater.* 2014, *13*, 653–661. https://doi.org/https://doi.org/10.1038/nmat3922.

(151) Bhattarai, R. S.; Bachu, R. D.; Boddu, S. H. S.; Bhaduri, S. Biomedical Applications of Electrospun Nanofibers: Drug and Nanoparticle Delivery. *Pharmaceutics* 2019, *11* (5), 1–30. https://doi.org/10.3390/pharmaceutics11010005.

(152) Ahire, J. J.; Robertson, D.; Neveling, D. P.; Van Reenen, A. J.; Dicks, L. M. T. Hyaluronic Acid-Coated Poly(d,l-Lactide) (PDLLA) Nanofibers Prepared by Electrospinning and Coating. *RSC Adv.* 2016, *6* (41), 34791–34796. https://doi.org/10.1039/c6ra01996j.

(153)   Xia, B.; Lv, Y. Dual-Delivery of VEGF and NGF by Emulsion Electrospun Nano Fibrous Scaffold for Peripheral Nerve Regeneration. *Mater. Sci. Eng. C* 2018, *82*, 253–264. https://doi.org/10.1016/j.msec.2017.08.030.

(154)   Kishan, A.; Walker, T.; Sears, N.; Wilems, T.; Cosgriff-Hernandez, E. Development of a Bimodal, in Situ Crosslinking Method to Achieve Multifactor Release from Electrospun Gelatin. *J. Biomed. Mater. Res. A* 2018, *106* (5), 1155–1164. https://doi.org/10.1002/jbm.a.36342.

(155)   Pawłowska, S.; Rinoldi, C.; Nakielski, P.; Ziai, Y.; Urbanek, O.; Li, X.; Kowalewski, T. A.; Ding, B.; Pierini, F. Ultraviolet Light-Assisted Electrospinning of Core–Shell Fully Cross-Linked P(NIPAAm-Co-NIPMAAm) Hydrogel-Based Nanofibers for Thermally Induced Drug Delivery Self-Regulation. *Adv. Mater. Interfaces* 2020, *7* (12), 1–13. https://doi.org/https://doi.org/10.1002/admi.202000247.

(156)   Yang, Y.; Chang, S.; Bai, Y.; Du, Y.; Yu, D.-G. Electrospun Triaxial Nanofibers with Middle Blank Cellulose Acetate Layers for Accurate Dual-Stage Drug Release. *Carbohydr. Polym.* 2020, *243* (116477), 1–9. https://doi.org/https://doi.org/10.1016/j.carbpol.2020.116477.

(157)   Phipps, M. C.; Clem, W. C.; Grunda, J. M.; Clines, G. A.; Bellis, S. L. Increasing the Pore Sizes of Bone-Mimetic Electrospun Scaffolds Comprised of Polycaprolactone, Collagen I and Hydroxyapatite to Enhance Cell Infiltration. *Biomaterials* 2012, *33* (2), 524–534. https://doi.org/10.1016/j.biomaterials.2011.09.080.

(158)   Baker, B. M.; Shah, R. P.; Silverstein, A. M.; Esterhai, J. L.; Burdick, J. A.; Mauck, R. L. Sacrificial Nanofibrous Composites Provide Instruction without Impediment and Enable Functional Tissue Formation. *Proc. Natl. Acad. Sci. U. S. A.* 2012, *109* (35), 14176–14181. https://doi.org/10.1073/pnas.1206962109.

(159)   Baker, B. M.; Gee, A. O.; Metter, R. B.; Nathan, A. S.; Marklein, R. A.; Burdick, J. A.; Mauck, R. L. The Potential to Improve Cell Infiltration in Composite Fiber-Aligned Electrospun Scaffolds by the Selective Removal of Sacrificial Fibers. *Biomaterials* 2008, *29* (15), 2348–2358. https://doi.org/10.1016/j.biomaterials.2008.01.032.

(160)   Ashinsky, B. G.; Gullbrand, S. E.; Bonnevie, E. D.; Wang, C.; Kim, D. H.; Han, L.; Mauck, R. L.; Smith, H. E. Sacrificial Fibers Improve Matrix Distribution and Mechanical Properties in a Tissue-Engineered Intervertebral Disc. *Acta Biomater.* 2020, *111*, 232–241. https://doi.org/https://doi.org/10.1016/j.actbio.2020.05.019.

(161)   Gomes, M. E.; Domingues, R. M. A.; Reis, R. L. Tissue Engineering and Regenerative Medicine : New Trends and Directions — A Year in Review. *Tissue Eng. Part B* 2017, *23* (3), 211–224. https://doi.org/10.1089/ten.TEB.2017.0081.

(162) Highley, C. B.; Rodell, C. B.; Burdick, J. A. Direct 3D Printing of Shear-Thinning Hydrogels into Self-Healing Hydrogels. *Adv. Mater.* 2015, *27* (34), 5075–5079. https://doi.org/10.1002/adma.201501234.

(163) Sinawang, G.; Osaki, M.; Takashima, Y.; Yamaguchi, H.; Harada, A. Biofunctional Hydrogels Based on Host–Guest Interactions. *Polym. J.* 2020, *52*, 839–859. https://doi.org/https://doi.org/10.1038/s41428-020-0352-7.

(164) Tanaka, M.; Nakahata, M.; Linke, P.; Kaufmann, S. Stimuli-Responsive Hydrogels as a Model of the Dynamic Cellular Microenvironment. *Polym. J.* 2020, *52*, 861–870. https://doi.org/https://doi.org/10.1038/s41428-020-0353-6.

(165) Loebel, C.; Mauck, R. L.; Burdick, J. A. Local Nascent Protein Deposition and Remodelling Guide Mesenchymal Stromal Cell Mechanosensing and Fate in Three-Dimensional Hydrogels. *Nat. Mater.* 2019, *18*, 883–891. https://doi.org/https://doi.org/10.1038/s41563-019-0307-6.

(166) Vining, K. H.; Stafford, A.; Mooney, D. J. Sequential Modes of Crosslinking Tune Viscoelasticity of Cell-Instructive Hydrogels. *Biomaterials* 2019, *188*, 187–197. https://doi.org/https://doi.org/10.1016/j.biomaterials.2018.10.013.

(167) Davidson, M. D.; Ban, E.; Schoonen, A. C. M.; Lee, M.-H.; D'Este, M.; Shenoy, V. B.; Burdick, J. A. Mechanochemical Adhesion and Plasticity in Multifiber Hydrogel Networks. *Adv. Mater.* 2019, *32* (1905719), 1–8. https://doi.org/https://doi.org/10.1002/adma.201905719.

(168) Xu, F.; Sheardown, H.; Hoare, T. Reactive Electrospinning of Degradable Poly(Oligoethylene Glycol Methacrylate)-Based Nanofibrous Hydrogel Networks. *Chem. Commun.* 2016, *52*, 1451–1454. https://doi.org/https://doi.org/10.1039/C5CC08053C.

(169) Chen, T.; Bakhshi, H.; Liu, L.; Ji, J.; Agarwal, S. Combining 3D Printing with Electrospinning for Rapid Response and Enhanced Designability of Hydrogel Actuators. *Adv. Funct. Mater.* 2018, *28* (19), 3–9. https://doi.org/10.1002/adfm.201800514.

(170) Kloxin, A. M.; Kasko, A. M.; Salinas, C. N.; Anseth, K. S. Photodegradable Hydrogels for Dynamic Tuning of Physical and Chemical Properties. *Science (80-.).* 2009, *324* (5923), 59–63.

(171) DeForest, C. A.; Anseth, K. S. Cytocompatible Click-Based Hydrogels with Dynamically Tunable Properties through Orthogonal Photoconjugation and Photocleavage Reactions. *Nat. Chem.* 2011, *3*, 925–931. https://doi.org/https://doi.org/10.1038/nchem.1174.

(172) Deforest, C. A.; Tirrell, D. A. A Photoreversible Protein-Patterning Approach for Guiding Stem Cell Fate in Three-Dimensional Gels. *Nat. Mater.* 2015, *14*, 523–531. https://doi.org/https://doi.org/10.1038/nmat4219.

(173) Boekhoven, J.; Rubert Pérez, C. M.; Sur, S.; Worthy, A.; Stupp, S. I. Dynamic Display of Bioactivity through Host-Guest Chemistry. *Angew. Chemie - Int. Ed.* 2013, *52* (46), 12077–12080. https://doi.org/https://doi.org/10.1002/anie.201306278.

(174) Freeman, R.; Stephanopoulos, N.; Álvarez, Z.; Lewis, J. A.; Sur, S.; Serrano, C. M.; Boekhoven, J.; Lee, S. S.; Stupp, S. I. Instructing Cells with Programmable Peptide DNA Hybrids. *Nat. Commun.* 2017, *8*, 15982. https://doi.org/https://doi.org/10.1038/ncomms15982.

CHAPTER 3: USER-DEFINED, TEMPORAL PRESENTATION OF BIOACTIVE MOLECULES ON HYDROGEL SUBSTRATES USING SUPRAMOLECULAR COILED COIL COMPLEXES

3.1. Abstract

The ability to spatiotemporally control the presentation of relevant biomolecules in synthetic culture systems has gained significant attention as researchers strive to recapitulate the endogenous extracellular matrix (ECM) *in vitro*. With the biochemical composition of the ECM constantly in flux, the development of platforms that allow for user-defined control of bioactivity is desired. Here, we reversibly conjugate bioactive molecules to hydrogel-based substrates through supramolecular coiled coil complexes that form between complementary peptides. Our system employs a thiolated peptide for tethering hydrogel surfaces (T-peptide) through a spatially-controlled photomediated click reaction. The complementary association peptide (A-peptide), containing the bioactive domain, forms a heterodimeric coiled coil complex with the T-peptide. Addition of a disruptor peptide (D-peptide) engineered specifically to target the A-peptide outcompetes the T-peptide for binding and removes the A-peptide and the attached bioactive motif from the scaffold. We use this platform to demonstrate spatiotemporal control of biomolecule presentation within hydrogel systems in a repeatable process that can be extended to adhesive motifs for cell culture. NIH 3T3 fibroblasts seeded on hyaluronic acid hydrogels and polyethylene glycol-based fibrous substrates supramolecularly functionalized with an RGD motif demonstrated significant cell spreading over their nonfunctionalized counterparts. Upon displacement of the RGD motif, fibroblasts occupied less area and

clustered on the substrates. Taken together, this platform enables facile user-defined incorporation and removal of biomolecules in a repeatable process for controlled presentation of bioactivity in engineered culture systems.

3.2. Introduction

The extracellular matrix (ECM) is intricate scaffolding that plays a central role in regulating cellular fates through multifaceted biophysical and biochemical processes[1–4]. In efforts to recapitulate microenvironmental features of the ECM *in vitro*[5–7], the dynamic nature of the ECM must be considered, with the presentation of cell fate cues in flux during continual restructuring[4,8–10]. To develop culture systems that influence cell migration, proliferation, and differentiation, approaches are needed to engineer the presentation of molecules involved in cell fate decisions[11–13]. Hydrogel biomaterials are advantageous *in vitro* platforms as they can replicate tissue-specific mechanics and be modified with biomolecules through numerous established strategies[14–17].

The immobilization of biomolecules onto or within tissue culture substrates is important when engineering environments that mimic the ECM[18–21]. One successful approach for incorporating bioactive molecules into scaffolds is photo-mediated thiol-ene click conjugation[22–26]. Modifying hydrogel-forming polymers with norbornene groups enables spatial control over biomolecule presentation via photo-mediated thiol-ene click conjugation when used in conjunction with photomasks that selectively shield light[1,18,19,27]. Controlling the localization of molecules on tissue culture scaffolds affords the ability to establish a spatial distribution of bioactive cues and gradients of signaling molecules to better recapitulate physiological environments and potentiate downstream cellular fates[22].

While providing spatial control, a drawback of these covalent methods for conjugation of biomolecules to hydrogels is that the resulting materials do not capture the dynamic nature of *in vivo* cellular niches[11,12,28,29]. Cells continually transduce signals provided by biochemical and biophysical cues in their microenvironment[30], and to achieve

the dynamic characteristics of natural tissue in a biomaterial system, the ability to define the presentation of relevant signals, both spatially and temporally, is necessary[20]. To this end, researchers have made significant strides developing techniques to dynamically introduce bioactive cues into hydrogel systems[31,32]. For example, photo-mediated thiol-ene conjugation with subsequent photocleavage by means of *o*-nitrobenzyl-based ether linkers enabled reversible incorporation of bioactive compounds into hydrogel networks[11,28,33]. Additionally, Grim et al. developed a method for repeatable biomolecule presentation via a reversible, light-mediated thiol-ene conjugation in conjunction with an engineered allyl-sulfide as a chain transfer agent[12,29]. In a biologically inspired example, 3,4-dihydroxy-L-phenylalanine (DOPA), a catechol-containing amino acid present in mussels, facilitated reversible incorporation of biomolecules through dynamic-covalent esters formed between DOPA and phenylboronic acid[34]. These methods demonstrate efficacy in reversible incorporation of biomolecules; however, they primarily leverage covalent bonds when immobilizing bioactive molecules – thus motivating exploration into reversibility driven by noncovalent interactions.

Supramolecular interactions offer approaches for dynamic incorporation of biomolecules into hydrogel scaffolds to capture the dynamic biochemical and biophysical features of cellular microenvironments[35–39]. For example, host-guest pairs within hydrogels rapidly assemble, but can dissociate under externally applied forces[37,40,41]. Boekhoven et al. achieved temporally controlled presentation of adhesive peptides within a hydrogel by appending the peptides to a napthyl group for interaction with a *β*-cyclodextrin host immobilized to alginate[41]. Subsequent addition of a bio-inert peptide attached to a higher affinity adamantane guest displaced the adhesive peptide and

resulted in smaller 3T3 fibroblast cell areas[41]. Additionally, oligonucleotides can be designed for reversible pairing through a process known as toehold-mediated strand displacement[42–44]. Two complementary oligonucleotides pair, with one of the oligonucleotides designed with a longer 'toehold' region that can remain unpaired prior to introduction of a third, longer oligonucleotide designed to be fully complementary with the toehold-containing sequence. Adding the longer complementary strand displaces the shorter oligonucleotide due to the higher affinity interaction between the two longer oligonucleotides. This non-covalent interaction facilitates reversible and repeatable addition of biomolecules under short timescales through differences in association affinities on hydrogel scaffolds[42–44].

We sought here to adopt concepts from each platform to develop a new method that affords reversible, dynamic incorporation of bioactive molecules into hydrogel networks with spatiotemporal control. We employ coiled coil-forming peptides that supramolecularly assemble in a specific manner in solution[45–47]. Similar to toehold-mediated strand displacement with DNA, Gröger et al. showed coiled coil peptides can undergo a similar process[45]. Introduction of a longer, higher affinity peptide to a lower affinity, toehold-containing coiled coil complex (dissociation constant, $K_D \sim 10^{-8}$ M) displaced the shorter, lower affinity component and yielded a high affinity coiled coil ($K_D \sim 10^{-9}$ M)[45]. These associations are similar in nature to other specific supramolecular assemblies, such as cyclodextrin-adamantane ($K_D \sim 10^{-5}$ M)[41] and cucurbituril host-guest systems ($K_D \sim 10^{-11}$-10^{-12} M)[36]. We considered that the comparatively moderate affinities in the coiled coil system ($K_D \sim 10^{-8}$-10^{-9} M)[45] would allow for stable presentation of biomolecules over extended periods of time, with facile release potentiated via the

addition of specific competitive molecules. Furthermore, while cyclodextrin and cucurbituril-based assemblies are reversible, the relatively straightforward synthesis and potential to reversibly trigger binding and release over multiple cycles under physiological conditions render coiled coil peptide platforms highly attractive for dynamic modulation of synthetic cellular microenvironments.

We hypothesized that coiled coil-forming peptides could be strategically designed to allow for both spatially-controlled conjugation via photo-mediated thiol-ene reactions and temporal control of biomolecule presentation via toehold-mediated strand displacement of coiled coil complexes. The ability to disrupt these associations and remove the biomolecules provides the desired constitutive "on/off" functionality – enabling facile reversible functionalization of *in vitro* culture systems. Herein, we describe the design, structural and thermodynamic characterization, and patterning of biomolecules using a coiled coil peptide-based system on both hyaluronic acid (HA) and fibrous polyethylene glycol (PEG) hydrogel surfaces. Using the patterned substrates, we demonstrate temporal attachment and release of biomolecules. To showcase the potential of this system in modulating bioactivity in engineered microenvironments, we build on previous work studying supramolecular assemblies in reversible modulation of cell adhesion and morphology *in vitro*[41,43]. The reversible presentation of an adhesive sequence enables visual confirmation of changes occurring at the cellular level of *in vitro* models and may be of use in studies perturbing microenvironmental adhesion to ECM-derived peptide binding sequences to understand cell fate decisions.

Taken together, this coiled coil-forming peptide system represents a compelling platform for reversible, spatiotemporally controlled presentation of bioactive molecules.

We note that this user-defined release process can be repeated over multiple cycles, lending itself to applications that require spatiotemporally controlled presentation of biomolecules that can be modulated through external cues as well as be reloaded for subsequent multi-stage release. In addition to the examples discussed here, this platform may be broadly applicable to understanding and controlling biomolecular composition in cellular microenvironments, for example to dynamically present growth factors and cytokines to modulate bioactivity *in vitro*.

3.3. Materials and Methods

3.3.1. Synthesis of norbornene-functionalized hyaluronic acid

NorHA was synthesized as previously described[18]. Briefly, sodium hyaluronate (HA, Lifecore, 62 kDa) was dissolved in deionized (DI) water with Dowex 50W x 8 ion-exchange resin (3 g resin per 1 g HA) for 2 h, and subsequently filtered, titrated to pH 7.02-7.05 with tert-butylammonium hydroxide (TBA, FisherSci) to yield HA-tert-butylammonium salt (HA-TBA). The final product was frozen at -80 °C, lyophilized, and stored under nitrogen. HA-TBA was then dissolved in anhydrous dimethyl sulfoxide (DMSO) and allowed to react with benzotriazole-1-yl-oxy-tris-(dimethylamino)-phosphonium hexafluorophosphate coupling reagent (BOP, Sigma, 0.3 mol equivalents relative to carboxylic acids on HA), and 5-norbornene-2-methylamine (nor-amine, Sigma, 1 mol equivalent relative to carboxylic acids on HA) to functionalize HA with norbornene groups. After ~2 h, the reaction was quenched with cold DI water, and the solution was transferred to a membrane (molecular weight cutoff: 6-8 kDa) and dialyzed against DI water for 5 d. Precipitate was removed by filtration, and the solution was re-dialyzed against DI water for 5 d prior to freezing at -80 °C, lyophilizing, purging with nitrogen, and storing at -20 °C until ready for use. The degree of modification was determined to be ~25% by ^{1}H nuclear magnetic resonance spectroscopy (^{1}H NMR, 500 MHz Varian Inova 500).

3.3.2. Peptide Synthesis

All peptides used in this study, unless otherwise stated, were synthesized using a Liberty Blue (CEM) automated, microwave-assisted solid phase peptide synthesizer via

Fmoc methods. Briefly, Rink amide resin (Advanced Chemtech, Rink Resin SS, 100-200 mesh, 1% DVB) was swollen with dimethylformamide (DMF, Aldrich, ACS reagent grade), and the immobilized Fmoc group removed with 20% (v/v) piperidine in dimethylformamide. Fmoc-protected amino acids (Advanced ChemTech, 0.2 M in DMF, 5 equivalents relative to theoretical available sites on the resin) and the coupling agents diisopropylcarbodiimide (DIC, Aldrich, 99%, 1 M in DMF) and Oxyma Pure (Advanced ChemTech, 1 M in DMF) were added to the reaction vessel and heated to 90 °C for 4 min. The Fmoc deprotection and coupling steps were repeated to build the peptide from the C-terminus to the N-terminus. For fluorescent peptides, 5(6)-carboxyfluorescein (Sigma Aldrich, ≥95%) was added last onto the N-terminus. The resultant peptides were cleaved from the resin with a cocktail of 92.5% trifluoroacetic acid (TFA, Aldrich, 99%), 2.5% triisopropylsilane (TIPS, Aldrich, 99%), 2.5% 2,2'-(ethylenedioxy) diethanethiol (DODT, Aldrich, 95%), and 2.5% DI water, and then isolated by precipitation into cold diethyl ether (Aldrich, ACS reagent, contains butylated hydroxytoluene as inhibitor) and centrifugation. After removal of ether under vacuum, the peptides were resuspended in DI water, frozen in liquid nitrogen, lyophilized, and stored at -20 °C as powders until ready for use. High performance liquid chromatography (HPLC) was used to determine peptide purity; since we noted no appreciable byproduct species, the peptides were used without further purification (**Figure S3.4**). Peptide primary structure was confirmed via electrospray ionization mass spectrometry (ESI MS, **Figures S3.2 & S3.3** and **Table S3.1**). Secondary structures were determined by circular dichroism (CD) spectroscopy (**Figure S3.5**).

3.3.3. Isothermal titration calorimetry

Experiments were performed using a standard volume affinity isothermal titration calorimeter (TA Instruments, New Castle, DE) with peptide solutions prepared in either 1X phosphate buffered saline (PBS) or NIH 3T3 fibroblast culture medium at indicated concentrations. Peptide solutions were adjusted to pH 7.4 using NaOH or HCl and then degassed for 10 min at 25 °C. Titrations consisted of an initial 2 µL injection, followed by 24 or 49 injections (10 µL each) of one peptide solution (150-200 µM) into 1.3 mL of a second peptide solution (10-20 µM). Following an initial delay of 200 s, injections were separated by 200 s. Experiments were performed at 25 °C with the stirring speed set to 125 rpm and the cooling rate set to medium. The reference cell was filled with 1.3 mL of degassed, deionized water. The thermograms were analyzed using NanoAnalyze software (TA Instruments) and heats of binding (in kJ/mol) were obtained by integrating the area under each injection peak in the baseline-subtracted thermograms, then dividing by moles of each injected volume. When possible, the resultant curves were then fit to either the independent (one site) or multiple sites binding models to obtain K_D values. Heats of dilution from blank injections – either peptide (150-200 µM) into 1X PBS/fibroblast medium or 1X PBS/fibroblast medium into peptide (10-20 µM) – were subtracted from experimental heats to yield the blank-corrected data[48]. In all analyses, we neglected the heats from the initial 2 µL injection.

3.3.4. Fabrication of NorHA hydrogels

Prior to formation of NorHA hydrogels, glass coverslips (22x22 mm) were functionalized with 3-(mercaptopropyl) trimethoxysilane (MTS, Sigma Aldrich, 95%) to

present pendant sulfhydryl groups as follows. Briefly, glass coverslips were plasma treated (Harrick Plasma) for 3 min, and MTS was added dropwise to plasma treated surface prior to being baked at 100 °C for 1 h, and 120 ºC for 10 min in an exhausted oven. The coverslips were washed sequentially in dichloromethane (DCM), 70% ethanol in water, and DI water, then stored under inert atmosphere until ready for use. NorHA hydrogels were synthesized from a solution consisting of 5% (w/v) NorHA, 1 mM lithium phenyl-2,4,6-trimethyl benzoylphosphinate (LAP) photoinitiator to induce thiyl radicals, and dithiothreitol (DTT) for crosslinking ([thiol]:[norbornene] = 0.6) in PBS. For each hydrogel, 50 µL of the NorHA solution was pipetted onto a thiol-functionalized glass coverslip (22x22 mm), sandwiched with an 18x18 mm coverslip, and crosslinked by irradiation for 2 min at 365 nm (10 mW/cm^2, Omnicure) to covalently stabilize the gel network. NorHA hydrogels to be used in spatial patterning experiments were incubated in a 1% (w/v) bovine serum albumin (BSA) solution in PBS for 30 min to limit nonspecific binding prior to subsequent experiments; NorHA hydrogels to be uniformly patterned were incubated solely in PBS prior to use in experiments.

3.3.5. Preparation of norbornene-functionalized polyethylene glycol (PEGNB) electrospun fibers

The electrospinning protocol was adapted from Sharma and coworkers[24] and all fibers were collected on thiolated coverslips – identical to those used for preparing the 2D NorHA hydrogels. Solutions consisting of 8-arm PEGNB (10% w/v, ~20 kDa, JenKem Technology USA), polyethylene oxide (5% w/v, ~400 kDa, carrier polymer), DTT ([thiol]:[norbornene] = 0.6), and 2-hydroxy-4'-(2-hydroxyethoxy)-2-methylpropiophenone

(I2959, 0.05% w/v) were mixed for at least 24 h in PBS. Electrospinning was conducted on a custom setup with the following parameters: 16-gauge needle; ~15 cm between the needle and collection surface; 0.8 mL/h flow rate; 10-14 kV positive voltage applied to the needle; and 6 kV negative voltage applied to the collection surface. Fibers were collected for at least 10 min and crosslinked for 15 min (365 nm, 10 mW/cm^2, Omnicure) under nitrogen. Fibers were then incubated in a 1% (w/v) BSA/PBS solution if they were to be spatially patterned or in PBS alone if they were to be uniformly patterned prior to subsequent experimentation.

3.3.6. Photoligation of peptides to hydrogels and fibers

NorHA hydrogels and PEGNB fibers were fabricated with a 0.6 thiol:norbornene ratio to avail norbornene groups for photo-patterned attachment of thiolated peptides after crosslinking. For fluorescent-based experiments (**Figures 3.2 & 3.3**), solutions of thiolated peptides (20 µM, T-peptide or thiolated fluorophore), BSA (1% w/v), and LAP (1 mM) in PBS were added dropwise to the surface of the hydrogels/fibers, covered with photomasks (CAD/Art Services), and irradiated (365 nm, 10 mW/cm^2) for 2 min. For cell-based experiments (**Figures 3.4 & 3.5**), a 100 μM solution of the T-peptide with 1 mM LAP in PBS was added dropwise to the surface of the hydrogels/fibers and irradiated with light (365 nm, 10 mW/cm^2) for 2 min. Following radical-induced thiol-ene coupling of the peptides to the hydrogel/fiber surfaces, samples were washed 3x in PBS for at least 30 min per wash to remove unreacted peptide and stored at room temperature until further use. Hydrogels/fibers with covalently tethered fluorophores were imaged directly after the wash steps, while other samples were used in coiled coil experiments as described below.

3.3.7. Formation of coiled coil complexes and subsequent peptide release

To induce coiled coil peptide complex formation on NorHA hydrogels and PEGNB fibers, the scaffolds with tethered T-peptide were swollen with a 20 μM solution of the complementary A-peptide (2 mL per well) for 3 min prior to washing 3x with PBS for at least 30 min per wash to remove unbound peptide. To release the A-peptide, D-peptide was introduced into the system (3 mL per well, 20 μM for fluorescence experiments) at multiple time points. During the disruption process, the higher affinity D-peptide binds A-peptides, disrupting the A-peptide:T-peptide coiled coil and removing the A-peptides from the surface. Solution (1 mL) was removed at predetermined timepoints and the remaining 2 mL were aspirated off and replaced with fresh D-peptide solution. Aliquots collected at each time point were stored at 4 °C until analysis.

To introduce an Arg-Gly-Asp (RGD) cell adhesion motif into hydrogels and fibers for cell culture, 100 μM of the T-peptide was tethered to the substrates by the radical-induced thiol-ene click reaction as described above. Subsequently, following the same protocol as above, solutions of either 0 μM, 10 μM, or 100 μM of a complementary A-peptide containing an RGD sequence (GYG<u>RGD</u>SPG(KIAALKE)$_4$) were added to supramolecularly attach the adhesion motif to the surface. For disruption of this complex and removal of RGD from the system, 100 μM solutions of the D-peptide were used. For covalent RGD immobilization, a thiolated version of the RGD peptide (GCGYG<u>RGD</u>SPG, Genscript) was added to the surface at the designated RGD concentrations for photo-mediated thiol-ene attachment.

3.3.8. Determination of peptide release

Kinetics of peptide release from NorHA hydrogels were indirectly assessed using plate reader measurements of fluorophore intensity in the supernatant at time points during disruption. Briefly, the A-peptide was synthesized as described above with 5(6)-carboxyfluorescein (FAM) included on the N-terminus during peptide synthesis, and the fluorescence of the disruption solution at each time point was determined via a BioTek Synergy 4 fluorescence spectrophotometer (excitation: 495 nm; emission: 518 nm). Three hydrogels were assessed for each experimental group.

Peptide release was further assessed visually using fluorescence microscopy (Leica DMi8 Widefield) during disruption. At each time point, fluorescent images (20x, dry) were taken of each NorHA hydrogel and the average intensity of photopatterned stripes was determined via ImageJ pixel intensity analysis. Three stripes per hydrogel were measured across three hydrogels for each experimental group.

3.3.9. Cell Culture

NIH 3T3 fibroblasts (kindly provided by Dr. Steven Caliari at the University of Virginia) were used for all cell experiments (passages 4-8). Cells were cultured in Dulbecco's modified Eagle's medium (DMEM) fortified with 10% (v/v) calf bovine serum (ATCC) and 1X antibiotic-antimycotic (Gibco). Prior to seeding cells on 2D NorHA hydrogels or PEGNB fibers, hydrogels and fibers were sterilized with germicidal light for 2 h and swelled with culture medium for at least 30 min. Cells suspended in culture medium were seeded at a density of 5×10^4 cells per hydrogel or fiber sample and allowed

24 h to adhere to the surface. Cells were then fixed for subsequent analysis, as described below.

For release experiments, hydrogel/fibrous scaffolds were similarly seeded at a density of 5×10^4 cells per scaffold, and cells were allowed to adhere for 24 h. Following the 24 h window, the medium was removed and replaced with culture medium containing D-peptide (2 mL, supplemented with 100 μM of the D-peptide) to induce release of the A-peptide. The D-peptide-containing medium was exchanged a total of two times, with exchanges at 1 h intervals, to facilitate displacement of coiled-RGD peptide. An incubation time of 1 h was allowed after the second treatment for a cumulative 3 h window. Following this release cycle, cells were fixed and treated for subsequent analysis.

3.3.10. Cell staining

For analysis of cell experiments, fibroblasts were fixed in a 10% (v/v) solution of neutral buffered formalin for 15 min before permeabilization with a 0.1% (v/v) Triton X-100/PBS solution for 10 min. Samples were then blocked by incubation in a 3% (w/v) BSA solution for at least 1 h to prevent nonspecific binding. F-actin was visualized by staining with Alexa Fluor-488-phalloidin (Thermofisher, 1:600 dilution) for at least 1 h and nuclei were visualized by staining with DAPI (ThermoFisher, $1:1\times10^4$ dilution) for 1 min. Samples were washed once with PBS, once with 0.1% (v/v) TWEEN-20 in PBS, and again in PBS after the staining steps to remove unbound fluorophore. All samples were protected from light and stored at 4 °C until imaging.

3.3.11. Imaging and image analysis

All imaging was conducted on a Leica DMi8 Widefield microscope. Coverslips with NorHA hydrogels or PEGNB fibers were placed on microscope slides, sandwiched with a 25x25 mm coverslip, and inverted for imaging. Imaging settings (exposure time and light intensity) were held constant for all imaging where fluorescence intensities were compared across multiple samples. For imaging of hydrogels containing fluorescent peptides, three distinct photopatterned stripes per scaffold from three scaffolds were imaged for analysis. Images acquired with the 20x dry objective were used for intensity comparisons. To evaluate pattern fidelity, we plotted the normalized intensity line profiles across 3 stripes on each sample; all intensity profiles were normalized to the lowest intensity value corresponding to each representative image.

For cellular experiments, at least three distinct areas per scaffold for three hydrogel and three fibrous scaffolds were imaged for cell spread area analyses. A 40x dry objective was used for cell area measurements, while a 100x oil immersion objective was used to visualize F-actin formation.

3.3.12. Statistical analyses

For quantitative comparisons between two experimental groups, independent t-tests were used; for comparisons with more than two experimental groups, a one-way ANOVA was leveraged in conjunction with a Tukey HSD post-hoc test with an α value of 0.95 indicating statistical significance.

3.4. Results and Discussion

Hydrogels are advantageous for use in synthetic ECM-mimetic materials due to their high water content – similar to natural tissue – and tailorability to specific applications[4,14]. Moreover, many tissue-specific ECMs have fibrous components, and fibers are thus attractive *in vitro* models of physiological milieus[4,14,49,50]. Towards introducing spatiotemporally controlled signals within these model environments, we investigated the ability of supramolecular coiled coil complexes to facilitate dynamic presentation of molecular adhesion motifs on or within both 2D NorHA hydrogels and fibrous PEGNB hydrogels.

Hyaluronic acid is a hydrophilic, non-sulfated glycosaminoglycan that is ubiquitous in natural ECM, and thus intrinsically biocompatible[16,17]. PEG is a hydrophilic, biocompatible synthetic polymer used widely for biomedical applications, including for solubilization of therapeutics and as components of ECM-mimetic hydrogels[14,29]. Both HA and PEG are amenable to chemical modification either on the side chains or at the chain ends[14]. We installed norbornene moieties on both HA and PEG (NorHA and PEGNB, respectively) to enable efficient, spatially controlled photo-mediated thiol-ene click reactions for addition of thiolated cross-linkers and biomolecules[18,24,51,52]. The resulting NorHA hydrogels and PEGNB fibers were crosslinked using dithiothreitol (DTT) as a crosslinker, adjusting the stoichiometry to leave residual norbornene groups available for post-crosslinking addition of thiolated peptides[1,18,24].

Coiled coil-forming peptides were designed as shown in **Scheme 3.1** based on a previously described complementary glutamic acid/lysine (E/K)-rich peptide pairs that form heterodimeric coiled coils[45,47,53] and undergo toehold-mediated strand

displacement[45]. We sought to modify the sequences with cysteine residues to facilitate thiol-ene conjugation to NorHA and PEGNB and demonstrate transfer of fluorophore or adhesive motif-tagged complementary peptides. For immobilization to the hydrogel surfaces, a tethered peptide (T-peptide) was designed with a cysteine for conjugation[54], a glycine spacer, and three repeating heptads of EIAALEK as the glutamic acid (E)-rich coiled coil-forming motif (I = isoleucine, A = alanine, L = leucine)[45,47]. The complementary association peptide (A-peptide) was designed with four repeating, lysine (K)-rich complementary KIAALKE heptads[45,47]. The extra heptad repeat provides a toehold motif for triggered removal of the A peptide in the presence of the higher affinity disruptor peptide (D-peptide) having four complementary repeating E-rich EIAALEK heptads[45]. We hypothesized that this difference in affinities would facilitate removal of A-peptides from the hydrogels by disrupting the A-peptide:T-peptide coiled coils upon introduction of the D-peptide in solution. We further extend this platform for dynamic incorporation of adhesive ligands (here, the fibronectin-derived RGD motif) for use in cell culture systems. To accomplish this, we modified the A-peptide with an RGD sequence ("coiled-RGD") at the N-terminus.
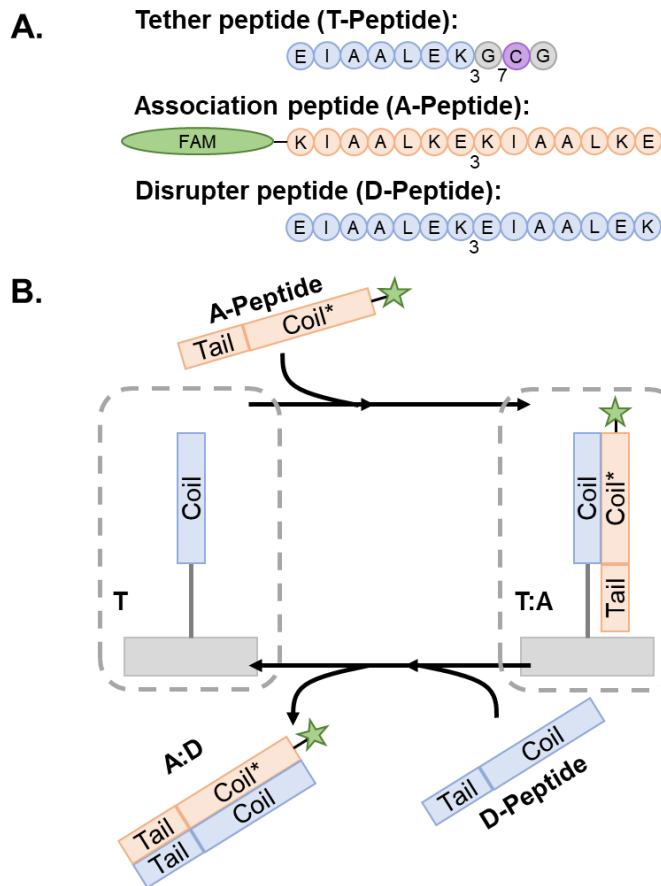
Scheme 3.1. Coiled coil peptides and process schematic of peptide association and subsequent removal via toehold-mediated strand displacement. A) Representative peptides used in this study. Blue regions indicate E-rich coiled coil-forming heptads and orange regions indicate complementary K-rich heptads, with toehold motifs indicated where applicable. B) Tethered peptides are covalently conjugated to NorHA/PEGNB surfaces prior to incubation with A-peptide to form T:A coiled-coil complex. The system is then incubated with D-peptide to interrupt the complex and form the A:D coiled-coil – thus removing the FAM-tagged A-peptide from the hydrogel and leaving behind a vacant T-peptide. Scheme inspired by Gröger et al.[45]

3.4.1. Thermodynamic characterization of coiled coil peptide interactions using isothermal titration calorimetry (ITC)

Prior to applying these peptides to NorHA hydrogels and PEGNB fibers for reversible biomolecule attachment, their interactions when forming complexes were characterized using ITC. ITC is capable of assessing thermodynamic properties of associations in solution[48,55]. The coiled coil forming peptide pairs shown in **Scheme 3.1** were analyzed in either NIH 3T3 fibroblast medium, PBS, or both, and representative baseline-subtracted thermograms and integrated data are shown in **Figure 3.1** for the complexes used in the cell culture studies – namely T-Peptide:Coiled-RGD Peptide and Coiled-RGD Peptide:D-Peptide, as well as a control experiment showing no interactions between non-complementary T-Peptide and D-Peptide pairs. Other replicates in medium, as well as PBS trials, are included in the supplemental information (**Figures S3.6-3.8** for medium and **Figures S3.9-3.13** for PBS).

Analysis of the ITC data in culture medium indicates that the T-Peptide:Coiled-RGD peptide forms two distinct, independent sites of interaction with strong affinities ($K_{D,1}$ ~ 10^{-7}-10^{-9} M, $K_{D,2}$ ~ 10^{-6}-10^{-7} M, represented in **Figure 3.1**). This result is consistent with two-stage binding processes reported for coiled coils formed from peptides with mismatched lengths[45,56]. Conversely, ITC of the same two peptides without the RGD moiety (i.e., T-Peptide:A-peptide association) showed only one binding site (K_D ~ 10^{-6}, **Figure S3.9**). Therefore, the multiple binding sites are likely encouraged due to the presence of RGD causing a greater mismatch in peptide lengths. As noted by the K_D
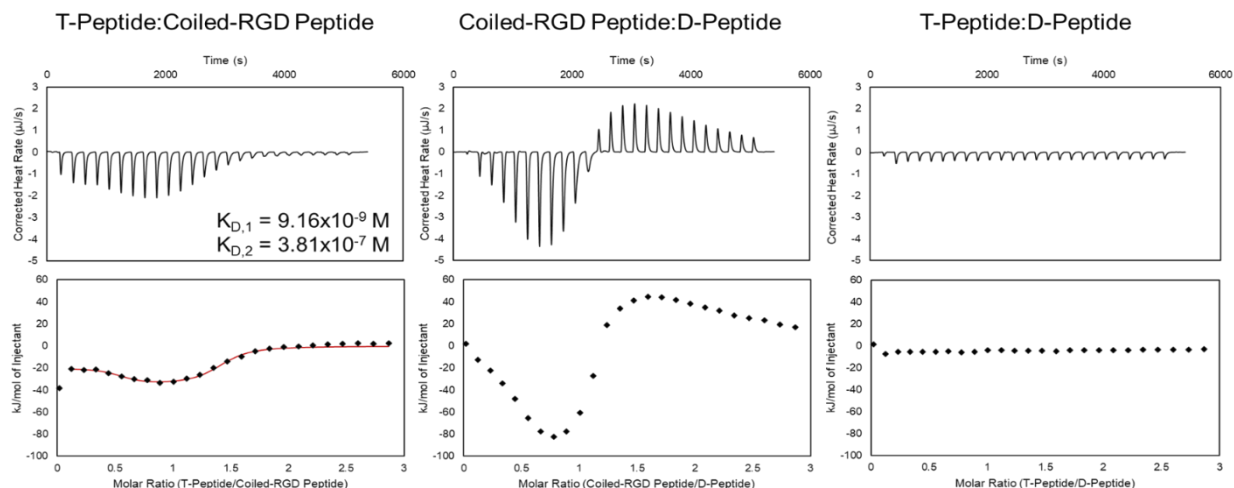
Figure 3.1. Isothermal titration calorimetry of T-Peptide:Coiled-RGD Peptide, Coiled-RGD Peptide:D-Peptide, and T-Peptide:D-Peptide interactions in NIH 3T3 fibroblast medium. (top) Baseline-subtracted ITC thermograms, integrated to yield the heats of interaction in kJ/mol (bottom plots). If possible, the integrated plots were fit to models (shown as a red line) that provide parameters for the interaction in solution. The T-Peptide:Coiled-RGD Peptide complex exhibits high affinities, as evidenced by the K_D values on the order of 10^{-7}-10^{-9} M. The larger exothermic heats of interaction measured for the Coiled-RGD Peptide:D-Peptide complex as compared to the T-Peptide:Coiled-RGD Peptide complex demonstrate the greater strength of these interactions. No appreciable heats of interaction were observed for non-complementary T-peptide:D-peptide pairs.

values, both sites of the T-Peptide:Coiled-RGD Peptide complex exhibit strong binding affinities, which is advantageous for stable presentation of biomolecules.

Interestingly, the Coiled-RGD Peptide:D-Peptide trace also seems to exhibit two-stage binding; however, the presence of both exothermic and endothermic heats of interaction prevents a model from fitting the data. This two-stage binding is intriguing as the coiled-RGD peptide and D-Peptide both contain 4 coiled coil-forming heptad repeats. Therefore, the additional RGD residues yield mismatched lengths which may explain the multi-stage model. Moreover, these endothermic peaks may be indicative of higher order structures forming in solution, as has been reported for peptides that undergo self-complementary assembly[57]. Nevertheless, the larger magnitude of the heats of

interaction from the Coiled-RGD Peptide:D-Peptide interaction (~-80 kJ/mol, **Figure 3.1**) compared to those of the T-Peptide:Coiled-RGD Peptide (~-30 kJ/mol, **Figure 3.1**) indicate that the Coiled-RGD Peptide:D-Peptide complex is thermodynamically favored over the T-Peptide:Coiled-RGD Peptide complex. Therefore, we conclude that the coiled-RGD peptide will preferentially interact with the D-peptide in the presence of the T-peptide – facilitating reversibility in our system.

The T-Peptide:D-Peptide analysis indicates no discernible interactions between the two peptides in solution, with heats of interaction of essentially 0 kJ/mol after correcting for the heats of dilution of T peptide into media and media into D-peptide. These results indicate that, as expected, the D-Peptide does not interact with the T-peptide, and the D-Peptide should displace the coiled-RGD peptide from the T-Peptide:Coiled-RGD Peptide coiled coil due to the differences in their strengths of interaction – comparable to the results presented by Gröger et al.[45] using similar peptides to form coiled coils in solution.

These ITC experiments were also conducted in the presence of PBS to investigate how the absence of serum affects peptide complex affinities. The resultant ITC thermograms and integrated analyses (**Figures S3.9-3.13**) indicate only marginally different heats of interaction when PBS is used rather than cell culture medium.

3.4.2. Spatial patterning of FAM-tagged peptides onto NorHA hydrogels and PEGNB

fibers

First, we tested the hypothesis that supramolecular coiled coil-mediated immobilization would yield similar patterns as covalent immobilization of fluorophores onto hydrogels. In these experiments, 100 µm-wide stripes were generated using a photomask and standard lithographic techniques[1,10,18]. Covalently bound fluorophores were introduced by patterning a thiolated FAM onto NorHA/PEGNB surfaces (see **Figure 3.2A**). For supramolecular patterning, unlabeled, thiolated T-peptide was first photopatterned onto NorHA and PEGNB substrates, followed by incubation with a solution of the FAM-tagged complementary A-peptide. NorHA and PEGNB scaffolds were washed with PBS to remove any unbound fluorophore prior to imaging (refer to **Figure 3.2B** for a schematic of the process, and **Figure 3.2C** for representative images). The resulting micrographs (**Figure 3.2**) demonstrate that the NorHA and PEGNB systems can be modified with fluorophore to generate stripe patterns either by covalent or supramolecular methods. The covalent systems typically yielded more uniform intensity profiles with higher peaks when compared to their coiled coil counterparts (**Figure 3.2A & 3.2C**). Qualitatively, this can be visualized by the non-patterned regions of the coiled coil systems exhibiting more fluorescent signal than the covalent non-patterned regions. It is possible that steric hindrance near the surface limited uniform conjugation of FAM in the coiled coil system and/or that non-specific interactions between the hydrogel and peptides were greater when using coiled structures compared to the shorter peptides used in covalent conjugation.
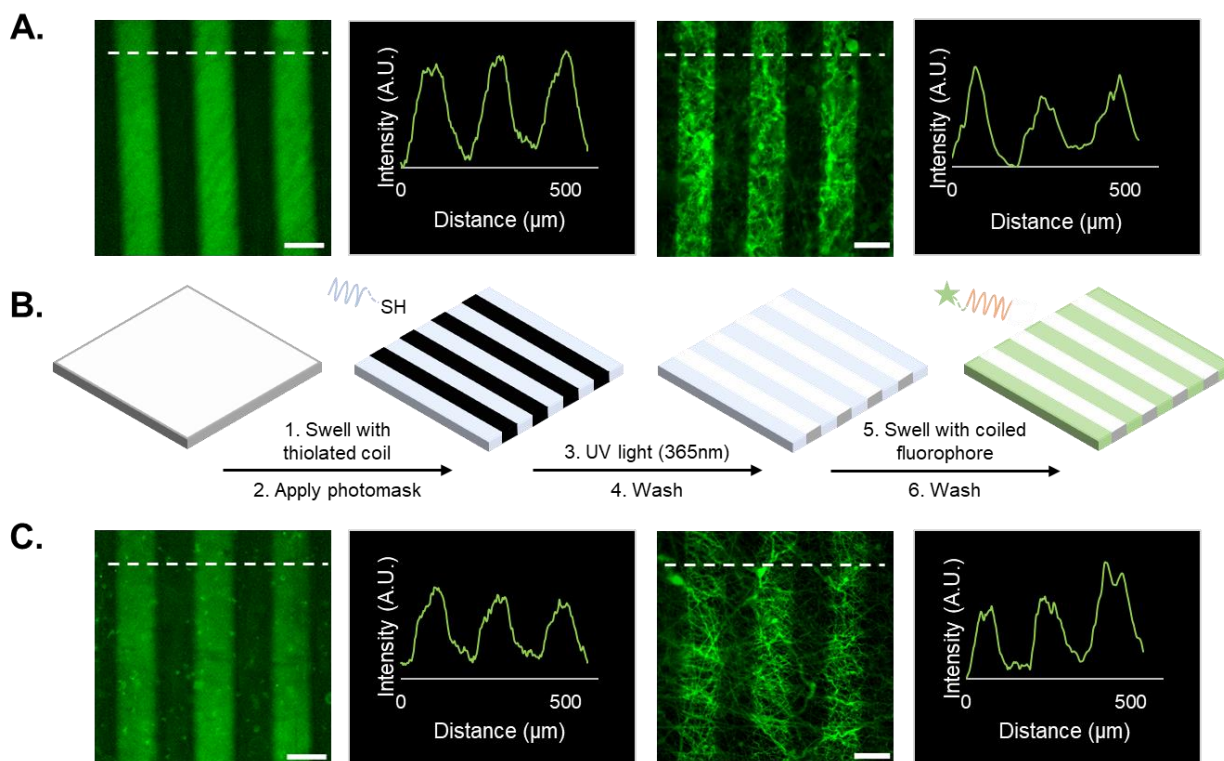
Figure 3.2. Supramolecular vs. covalent immobilization of FAM on NorHA hydrogels and PEGNB fibers. A) Covalent system (from left to right): representative micrographs of covalently photopatterned FAM on a NorHA hydrogel; representative intensity line profile; representative micrograph of covalently bound FAM on PEGNB fibers; representative intensity profile. B) Schematic of the supramolecular patterning process for FAM utilizing our coiled-coil system: swelling of substrate – either 2D hydrogel or fibers –with thiolated T-peptide, application of photomask and irradiation with 365 nm light; substrate is then washed and swelled with the complementary FAM-tagged A-peptide; finally, substrate is then washed again to remove unbound peptide. C) Coiled system (from left to right): representative micrograph of FAM bound by coiled-coil system on a NorHA hydrogel; representative intensity profile; representative micrograph of FAM bound by coiled-coil system on PEGNB fibers; representative intensity profile. Scale bars = 100 μm. Dashed white lines indicate sample location of intensity profiles plotted for each micrograph.

Prior to the release studies, we compared the stripe intensities of the covalent and coiled coil systems to determine the system's net intensity under identical light conditions – analogous to a 'loading capacity' of prospective biomolecules. Analysis of stripe intensities from fluorescent micrographs indicated that although the average intensity of the coiled coil system was marginally lower than the covalent system, an independent t-

95

test suggests there is no statistical significance (**Figure 3.3B**). Therefore, our platform for supramolecular addition of biomolecules generates patterned stripes similarly to its covalent ligation analog at the experimental (20 μM) concentrations, allowing equivalent conjugation of fluorophore based on our semi-quantitative analysis.

3.4.3. Supramolecular immobilization of FAM via coiled coil peptide complexes is reversible and repeatable

Following experiments demonstrating spatially controlled supramolecular addition of FAM-tagged peptides to hydrogels using the coiled coil system, we sought to evaluate its efficacy as a reversible, repeatable process towards temporally controlled presentation of biomolecules on and in cell culture substrates.

We measured FAM concentration in solution as a function of time to determine the stability of the supramolecular coiled coil structure in buffer over time and monitor the toehold-mediated disruption of the complexes by adding the disrupter peptide (**Figure 3.3A**). All release studies were performed on NorHA hydrogels due to the ability to form substrates precisely and reproducibly with consistent surface area across samples, enabling a closer comparison across all groups. First, we examined the release of the FAM-tagged A-peptide in the presence of the D-peptide (hereafter "(+) D-peptide"). Plate reader fluorescence measurements of supernatant samples indicated a large cumulative release in the (+) D-peptide test group, suggesting that release is dependent on the addition of the D-peptide to disrupt the T:A coiled coil. To support this conclusion, we compared the (+) D-peptide test group to various controls. These controls consisted of a
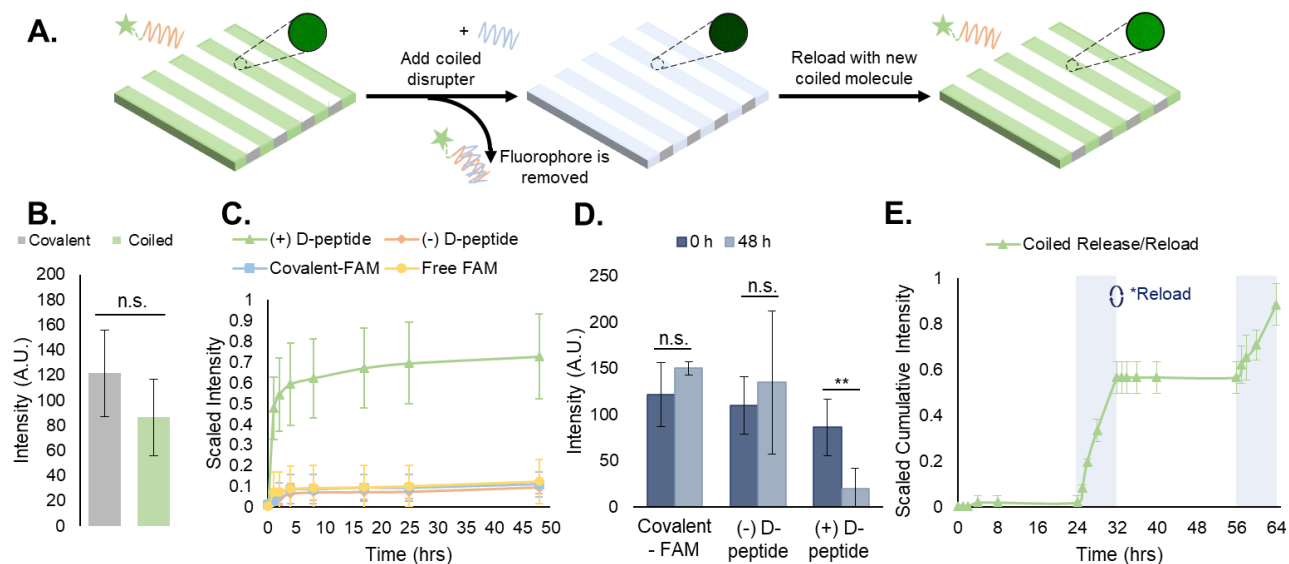
Figure 3.3. Reversible, repeatable addition of biomolecules to peptide-functionalized hydrogels. A) Schematic of FAM-tagged A-peptide release from substrates via toehold-mediated strand displacement upon addition of the complementary D-peptide, with inset images showing intensity- and exposure-controlled resultant changes in stripe fluorescence, with the ability to reload the vacant T-peptide sites in order to repeat the process. B) Quantitative comparison of the average intensities of FAM by covalent and coiled-coil conjugations indicates no significant difference in stripe intensity between both platforms. C) Cumulative release curves of the coiled coil disruption compared to the various controls. This indicates a coiled coil complex forming that is stable, with reversibility being disrupter-dependent. D) Average stripe intensity at 0 h and 48 h time points, based on fluorescent micrographs, indicating a statistically significant difference (** $p < 0.01$) stripe intensity at 48 h for only the '(+) D-peptide' test group. E) Repeated loading and release of FAM-tagged peptides from hydrogels shown by holding the hydrogels in PBS for 24 hours prior to inducing a D-peptide-dependent release for 8 h. Gels were then reloaded with A-peptide and the process was repeated. Profile shown is cumulative release from both disruption cycles. This further reinforces the notion that the system is stable over time in buffer and disruption can occur more than once via a release and reload protocol. Error bars represent standard deviation.

coiled coil system that was not subjected to D-peptide treatment (hereafter "(-) D-peptide"), a covalently bound FAM (hereafter "covalent-FAM"), and the FAM molecule in solution ("free-FAM"). The (-) D-peptide group was designed to evaluate supramolecular complex stability in buffer for extended periods of time (~48 h), and the free-FAM control was designed to determine the extent of non-specific interactions between the

fluorophore in solution with the T-peptide-modified substrates. Using standard plate reader fluorescence measurements of supernatant samples, we measured FAM release profiles. The results indicated large cumulative release from the coiled coil group in comparison to controls that exhibited minimal, if any, release of fluorescent molecules (**Figure 3.3C**). Furthermore, the supramolecular coiled coils persist over days in the absence of the D-peptide, indicating that this system can stably, but reversibly, incorporate biomolecules onto norbornene-modified hydrogels. The free-FAM control contained no stripes to quantify in subsequent analysis, suggesting no discernable interactions between the free molecule and the T-peptide surface.

To further quantify the release of the FAM-tagged A-peptide via addition of the disrupter, we looked at the average stripe intensities of the '(+) D-peptide' test group compared to the (-) D-peptide and 'covalent-FAM' controls at the first and last time points to compare the decrease in intensity upon FAM release. There were no significant differences between the stripe intensities at the first and last timepoints (0 h and 48 h) for the controls (**Figure 3.3D**). However, the (+) D-peptide test group showed a statistically significant reduction in intensity after D-peptide treatment (** $p < 0.01$). Together, these data confirm the hypotheses that: (1) coiled coil peptides enable supramolecular immobilization on hydrogels; and (2) introduction of the D-peptide facilitates removal of supramolecularly immobilized molecules by toehold-mediated strand displacement.

We further investigated how different concentrations of D-peptide affected removal of the FAM-tagged A-peptide (**Figure S3.14**). Increasing concentrations of D-peptide generally enhanced and accelerated removal of the FAM-tagged A-peptide from the hydrogel surfaces; however, we began to observe diminishing increases in removal at

higher concentrations of D-peptide. We postulate that at these higher concentrations, kinetics of peptide displacement might limit reversibility in the system over availability of D-peptide, with steric hindrances imposed by NorHA surfaces possibly limiting reversibility as well. Thus, increasing the concentration of D-peptide has the most significant effects on increasing A-peptide removal at lower concentrations of D-peptide, with only marginal improvement at higher concentrations of the competitive disrupter. Additionally, removal of A-peptide from T:A coiled coils in the presence of 3T3 fibroblast medium was investigated as a precedent for subsequent cell studies. Shown in **Figure S3.14**, removal in culture medium is similar to removal in PBS. Combining this observation with ITC measurements (**Figures S3.6-3.8**), we conclude that the specific and dynamic properties of the coiled-coil system extend to protein-rich environments, such as cell media.

Toehold-mediated removal of the A-peptide by addition of the complementary, higher affinity D-peptide leaves T-peptide sites vacant on the surface of NorHA hydrogels for binding other bioactive molecules. As a proof-of-concept, after release of the initially bound FAM-tagged A-peptide, we incubated the same scaffolds with a fresh solution of FAM-tagged A-peptide and rinsed the substrates with PBS to remove unbound peptide. After a 24 h incubation in PBS, D-peptide was reintroduced to cue a second removal of FAM-tagged peptide to demonstrate the repeatability of the process (**Figure 3.3E**). The second release profile (t = 56-64 h) resembled the first (t = 24-32 h), albeit with a slightly smaller magnitude of cumulative release. These results suggest that this is a reversible and repeatable process, but we can also postulate that the D-peptide does not completely remove the A-peptide (**Figure 3.3D**, where the '(+) D-peptide' group does not return to a

0-intensity value following disruption). This may be due to interactions with the NorHA surface that sterically interfere with removal, interactions with material in the gels that prevent reaching 100% removal, or equilibrium of toehold-mediated strand displacement.

3.4.4. Supramolecular, coiled coil-mediated immobilization of RGD confers bioactivity that supports 3T3 fibroblast adhesion to NorHA hydrogels and PEGNB fibers with comparable morphologies to covalent ligation

After using FAM-tagged A-peptides as a proof-of-concept to establish the viability of coiled coils for immobilization of biomolecules onto NorHA hydrogels and PEGNB fibers, we next incorporated the cell-adhesive RGD-containing peptide sequence GYG<u>RGD</u>SPG into the A-peptide at the N-terminus to impart cell adhesive properties[1]. Here, photopatterned T-peptide hydrogels bound RGD-functionalized A-peptide ("coiled-RGD"). A thiolated version of the RGD peptide (G<u>C</u>GYG<u>RGD</u>SPG) was also covalently bound to NorHA and PEGNB substrates for comparisons against our coiled coil system. To test cell behavior on scaffolds displaying the RGD motif, we cultured NIH 3T3 fibroblasts on NorHA hydrogels and PEGNB fibers previously modified with different RGD concentrations (0, 10, 100 μM RGD via coiled coil or covalent conjugation). After incubation for 24 h, the samples were fixed and stained for fluorescent visualization of F-actin and cell nuclei, and cell area quantified. See **Figure 3.4A** for cell area quantification and 3B/C for fluorescent micrographs of NorHA gels and PEGNB fibers, respectively.

3.4.4.1. 3T3 fibroblast behavior on covalent and coiled coil presentation of RGD on NorHA hydrogels

As expected, images of 3T3 fibroblasts cultured on RGD-presenting substrates showed larger cell area, indicative of cell spreading. Increasing covalent RGD presentation from 0 μM to 10 μM and 100 μM increased cell spreading, with the 100 μM groups exhibiting statistically significant differences in cell area compared to substrates exposed to 0 μM covalent RGD (**Figure 3.4A**, ** p < 0.01). In our supramolecular system, the 10 μM coiled coil presentation of RGD significantly increases cell area (** p < 0.01) compared to the 0 μM control, as does the 100 μM treatment (** p < 0.01). Indeed, at low concentrations of ligand presentation, it is known that fibroblast cell area responds positively with increased ligand concentration[58]. Yet, we observe a marginally smaller average area with the 100 μM group compared to the 10 μM group (**Figure 3.4A**). Similar results in the literature attribute this phenomenon to integrin inhibition due to free RGD in solution[41,59]. However, owing to the strong interactions between the T-peptide and the coiled-RGD in this system (K_D ~ 10^{-7}-10^{-9} in culture medium), it is likely that the observed differences in cell areas between the 10 μM and 100 μM groups are due to a combination of RGD density and gel mechanics. Oria et al.[60] demonstrate a bimodal relationship between the spacing of ECM ligands, which are controlled here by the concentration of the coiled-RGD, and substrate mechanics – with their interplay affecting focal adhesion formation. At the hydrogel mechanics used within this study, distance between the RGD ligands in the 10 μM groups may promote spreading and focal adhesion formation, and distances between ligands in the 100 μM groups may inhibit cell spreading and focal adhesion formation due to their proximity to one another[60]. Cell spreading and highly
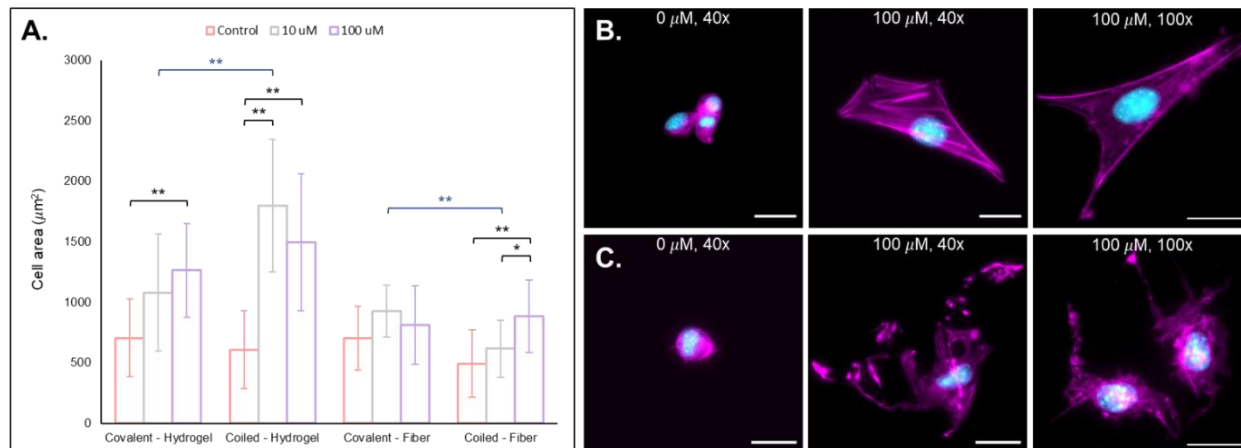
Figure 3.4. 3T3 fibroblast behavior on substrates with presentation of RGD through the coiled coil platform. (A) Quantifications of cell area for each of the groups with comparisons to their covalently conjugated analogs. (B) NorHA 2D hydrogel. (from left to right): 0 μM RGD, 100 μM RGD, and 100 μM RGD hydrogel zoomed in to better visualize cell structure. (C) PEGNB hydrogel fibers. (from left to right): 0 μM RGD, 100 μM RGD, and 100 μM RGD fibers zoomed in to better view cell structure. It is clear qualitatively from the images, and quantitively from the cell area comparisons, that generally the addition of the coiled RGD peptide to the substrates improves bioactivity, and thus cell area increases. Furthermore, it is important to note that the F-actin stress fibers are more organized for cells on NorHA scaffolds than those on PEGNB fibers. Scalebars = 25 μm, ** $p < 0.01$, * $p < 0.05$. Error bars represent standard deviation.

organized F-actin stress fibers within the RGD-presenting coiled coil system can be seen in representative images of the 0 μM and 100 μM groups (**Figure 3.4B**) – likely a function of the high surface concentration of RGD allowing filopodia attachment during spreading and migration[61].

We also observe generally larger cell areas for the 10 μM and 100 μM RGD groups with our coiled coil system compared to the covalent groups, with a statistically significant difference between the 10 μM supramolecular and covalent groups (** $p < 0.01$). We hypothesize that this is likely due to the non-covalent, supramolecular characteristics of our coiled coil system that potentially allows cellular remodeling of RGD ligands within its environment. A covalent conjugation permanently immobilizes a pendant ligand on a substrate, allowing cells to exert traction forces[62,63]. These traction forces are ubiquitous

and implicated in dynamic tissue processes (e.g. contraction)[62–64], and they may induce remodeling of the supramolecular coiled coil system. Since the conjugated T-peptide provides open and dynamic sites for coiled coil complexes to form, we postulate that cells may be able to reorganize the physical locations of the A-peptide motifs on the NorHA hydrogel surface through traction forces – thus providing a dynamic surface that leads to increased cell area. Dynamic interactions with 2D surfaces and 3D hydrogel matrices are known to play important roles in cell fate processes[65–67], and supramolecular functionalization of materials may allow for ongoing, cell-mediated changes in surface properties.

3.4.4.2. 3T3 behavior on covalent and coiled coil presentation of RGD on PEGNB fibers

Like NorHA hydrogel groups, we also observed increased cell spreading on PEGNB fibers that present RGD covalently and supramolecularly (after application of 10 and 100 μM RGD) compared to the 0 μM RGD controls (**Figure 3.4**). Interestingly, cell spreading on PEGNB fibers to which RGD was covalently conjugated was not significantly greater than spreading on the control fibers, although there appeared to be a slight increase in cell area for both groups compared to the 0 μM control (**Figure 3.4A**). Like the covalently bound RGD on PEGNB fibers, the supramolecular immobilization of RGD on fibers exhibited modest differences in cell areas between the 0 μM and 10 μM groups but demonstrated statistically larger cell areas in the 100 μM group compared to the unfunctionalized control (** $p < 0.01$). Furthermore, coiled coil complexes on fibers induced cells to spread significantly more in the 100 μM group compared to the 10 μM

group (* p < 0.05). Cell area also decreased in moving from the experimental group of 10 μM RGD (in solution) covalently bound to fibers to the group of 10 μM RGD reversibly bound to fibers via coiled coil conjugation (** p < 0.01). Representative fluorescent micrographs of cell spreading and F-actin formation on PEGNB fibers are shown in **Figure 3.4C**.

In considering both materials systems, we observe that the supramolecular addition of the coiled RGD ligand promotes 3T3 fibroblast adhesion and spreading on both NorHA hydrogels and PEGNB fibers, and it presents a generalizable method for temporally-controlled functionalization of hydrogel substrates for cell adhesion in further studies.

3.4.5. The addition of the D-peptide induces removal of the coiled adhesive motif which actuates changes in cell morphology

After demonstrating that cells can adhere and spread on substrates supramolecularly functionalized with coiled-RGD, we sought to investigate the effects of its removal via the addition of the competing D-peptide on cell adherence and morphology. Both the NorHA hydrogel and PEGNB hydrogel fiber systems exhibited changes in cell adherence that could be observed qualitatively upon the addition of the D-peptide (**Figure 3.5A-B**). Quantitatively, we saw significant changes in cell areas in both systems, with cell areas on the NorHA hydrogels decreasing by roughly 50% and cell areas on the PEGNB fibers decreasing to the same sizes as seen on unmodified PEGNB fibers (**Figure 3.5C**).
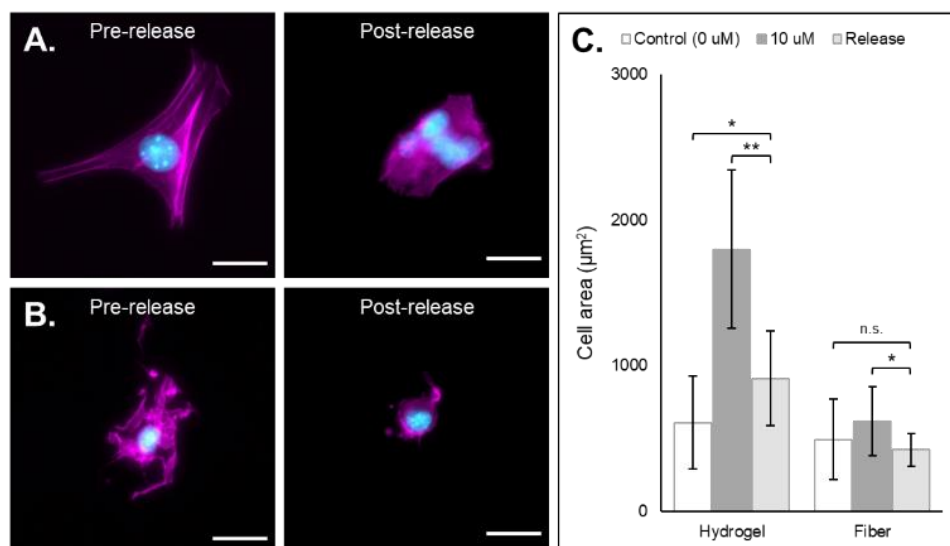
Figure 3.5. 3T3 morphology changes following removal of coiled-RGD peptide via the addition of the competing D-peptide. (A) NorHA hydrogel (from left to right): Representative fluorescent micrograph of a fibroblast seeded on a NorHA hydrogel functionalized with 10 μM of the coiled-RGD motif; representative fluorescent micrograph of fibroblasts on a NorHA hydrogel originally functionalized with 10 μM of the coiled-RGD motif and treated with 100 μM of the D-peptide. Cells exhibited fewer extensions and appeared to aggregate. (B) PEGNB fibers. (left to right): Representative fluorescent micrograph of a fibroblast seeded on PEGNB fibers functionalized with 10 μM of the coiled-RGD motif; representative fluorescent micrograph of a fibroblast on PEGNB fibers originally functionalized with 10 μM of the coiled-RGD motif and treated with 100 μM of the D-peptide. Cells exhibited fewer extensions and covered less surface area. (C) Quantification of cell area across groups in release experimentation. Statistics solely compared cell area after treatment with D-peptide to the control and 10 μM coiled-RGD groups prior to treatment with D-peptide. Scalebars = 25 μm, n.s. = no significance, * p < 0.05, ** p < 0.01, error bars represent standard deviation.

3.4.5.1. Removal of coiled-RGD peptide from NorHA hydrogels

We saw statistically significant decreases in fibroblast area on the NorHA hydrogel substrates modified with 10 μM RGD after incubation with D-peptide (** p < 0.01, **Figure 3.5C**). There was a significant reduction of cell area from an average of 1800 $\pm$ 550 μm^2 on the 10 μM scaffolds prior to release to an average of 910 $\pm$ 330 μm^2 afterwards. Average cell area after RGD release was still significantly larger than average area

observed in the control groups of 610 ± 320 μm^2 (0 μM RGD, * p < 0.05, **Figure 3.5C**). Based on observations discussed previously, we attribute this to steric hindrance and molecular interactions in the hydrogel that may inhibit D-peptide from fully displacing and removing the coiled-RGD motifs from the T-peptide, and also to thermodynamic equilibrium of toehold-mediated strand displacement, by which some A-peptide would be expected to remain associated with T-peptide even in the presence of D-peptide. Moreover, it is possible that due to the 24 h culture period prior to addition of the D-peptide, fibroblasts developed interactions with the NorHA gels that were difficult to disrupt – possibly through extended cellular interactions across the gel surface and into the gel itself – as well as nascent matrix deposition from the fibroblasts that might become integrated with the hydrogel surface[68]. Interestingly, there were also noticeably more cell clusters following removal of the coiled-RGD ligands – suggesting that cells aggregate and adhere to other cells when concentrations of available RGD decrease. This observation correlates to cell clusters seen here with 0 μM RGD (refer to representative micrograph in **Figure 3.4B**) and to work by Dumbleton and coworkers who demonstrated multiple cell types clustering on unfunctionalized hydrogels[69]. Furthermore, the behavior is analogous to work by Freeman et al., who demonstrated the ability to remove adhesive laminin-derived IKVAV-peptide ligands from hydrogel surfaces and showed that neural stem cells tended to cluster in neurospheres once these ligands were removed from the culture surface[43].

3.4.5.2. Removal of coiled-RGD peptide from PEGNB fibers

We also observed a statistically significant decrease in fibroblast area on PEGNB fibers after incubation with D-peptide compared to cells on the 10 μM scaffolds prior to incubation with D-peptide (* $p < 0.05$, **Figure 3.5C**). Interestingly, there was no statistical significance in cell area between the scaffolds after removal of the coiled RGD from the 10 μM scaffolds and the 0 μM control scaffolds, indicating that the introduction of the D-peptide to the systems removed enough of the coiled-RGD peptide to return cell morphology to a state similar to the unfunctionalized control. Just as we observed in the NorHA hydrogel system, treatment with the D-peptide reversed adhesion of cells to the culture substrate through disrupting coiled coil interactions between the T- and RGD-containing A-peptides. We also note that differences in trends between the NorHA hydrogel and electrospun PEGNB fibers, for example, the relative extent to which cell spreading was reversed. This might be attributed to factors including differences in the polymer backbone chemistries, differences in molecular concentration after processing a hydrogel by electrospinning, cellular responses to different topographies, or changes in viscoelastic properties or ligand densities between systems.

Nonetheless, overall changes in cell adhesion and morphology were temporally controlled via the addition of the D-peptide to displace the coiled-RGD in both NorHA and PEGNB systems. This demonstrates the potential for user-controlled perturbation of cellular microenvironments. Taken together with previous results, this coiled coil system offers both spatial and temporal control over patterning of ligands that can affect cell behaviors.

3.5. Conclusions and Outlook

Coiled coil peptides offer a versatile system for engineering spatial and temporal signals into hydrogel environments. Biofunctionality of a peptide can readily be altered through standard peptide synthesis techniques, and thiol groups in cysteine residues allow their incorporation via light-controlled reactions amenable to spatial patterning, as well as by other bioconjugation reactions, such as Michael additions. The supramolecular coiled coil interaction also presents a reversible platform that allows for the repeated introduction and removal of bioactivity within *in vitro* hydrogel and hydrogel fiber culture systems. Proof-of-concept experiments showing reversible immobilization of FAM demonstrated comparable efficacy in functionalizing photoreactive biomaterials with high spatial control using coiled coil complexes compared to covalent photoligations. We confirmed the stability of the supramolecular coiled coil association over time, with release being dependent on toehold-mediated strand displacement by the D-peptide – a process that can be repeated after subsequent reloading with A-peptide. We then developed an extension of the A-peptide that included a cell-adhesive RGD motif on the N-terminus. Using this coiled-RGD for cell studies illustrated the ability to culture fibroblasts on materials functionalized with RGD via this coiled coil system. The concentration of the coiled-RGD peptide bound to the T-peptide affected the cell spread area on both NorHA hydrogels and PEGNB fibers. Finally, removal of the coiled-RGD via introduction of the D-peptide caused a statistically significant decrease in cell spread area – on both hydrogels and fibers – indicating that the reversal of RGD presentation has a direct impact on fibroblast morphology.

Based on these observations, future work should allow for the investigation of how dynamism in cell culture environments affects downstream cell behaviors. User-defined perturbations to these culture environments will allow for incremental advancements based on discrete changes to the microenvironment. Future work will also consider differences in cell behaviors on hydrogels and hydrogel-based fibers, as well as differences between hydrogel backbone materials in this system. We believe this platform might be applied to many other areas of research that desire user-controlled addition and subsequent temporal release of bioactive compounds that can be reloaded for multiple release cycles.

3.6. Acknowledgements

3.7. Supplementary Figures

Figure S3.1. Norbornene-functionalized hyaluronic acid (NorHA) ^{1}H NMR spectrum. Spectrum is normalized to a value of 3.00 based on the methyl groups highlighted in pink, and degree of functionalization was determined based on the integral values associated with the norbornene groups (endo- and exo-) highlighted in blue. Degree of HA modification with norbornene groups was determined to be ~25%.

Table S3.1. Mass spectrometry of peptides used in this study. Peptide sequences, with corresponding text nomenclature, along with their calculated and observed m/z values as determined by electrospray ionization (ESI) mass spectroscopy. Refer to **Figures S3.2 & S3.3** for spectra.

Sequence	Peptide Title	Calculated m/z	Observed m/z
H_2N-(EIAALEK)$_3$G$_7$CG-NH$_2$	T-peptide	2839.47	2840.47
H_2N-FAM-(KIAALKE)$_4$-NH$_2$	A-peptide	3389.24	3390.96
H_2N-GYGRGDSPG-(KIAALKE)$_4$-NH$_2$	Coiled RGD	3877.29	3879.28
H_2N-(EIAALEK)$_4$-NH$_2$	D-Peptide	3034.71	3035.71
H_2N-FAM-(EIAALEK)$_3$-G$_3$-CG-NH$_2$	Covalent	2969.70	2970.43
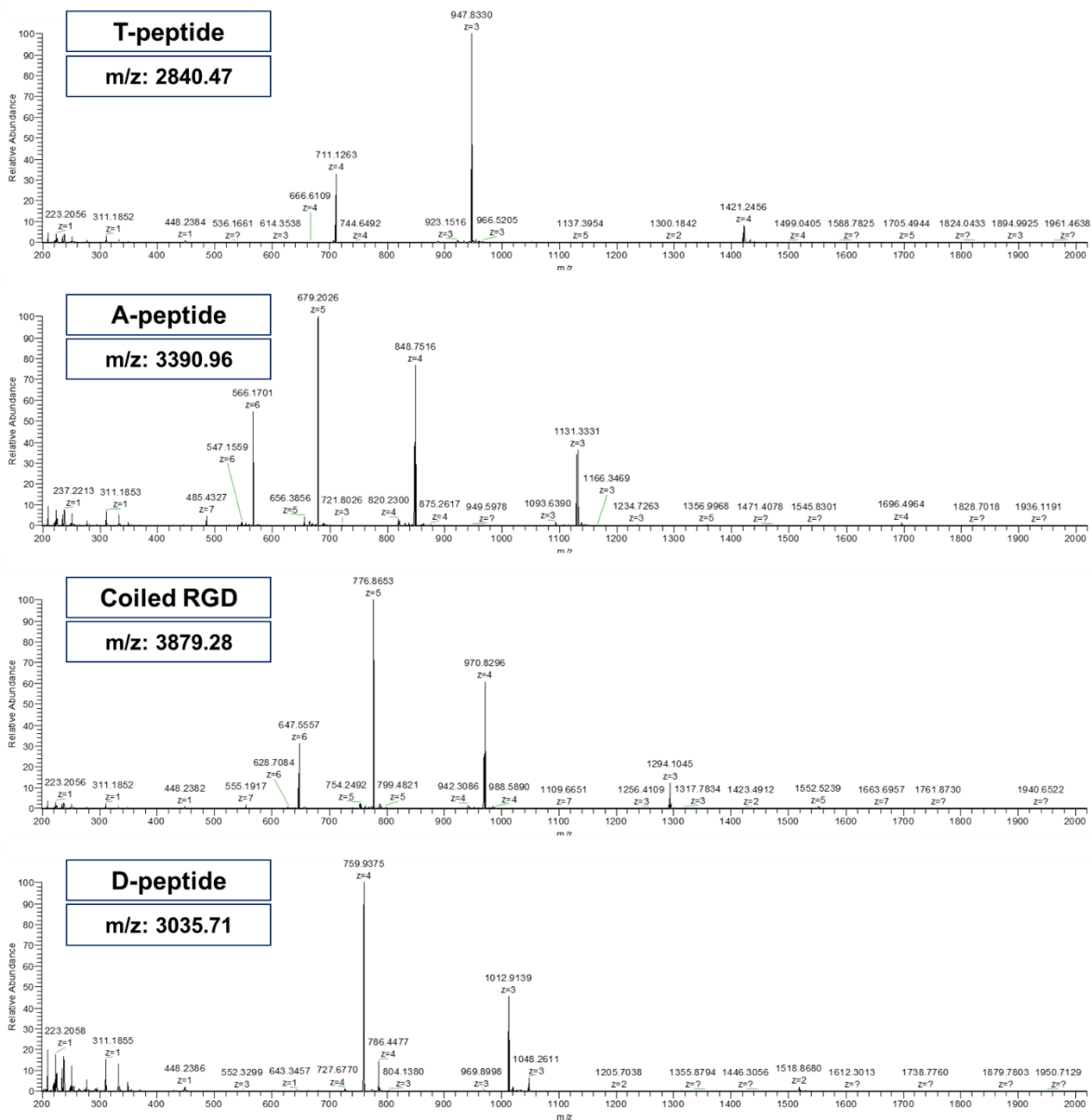
Figure S3.2. Electrospray ionization (ESI) mass spectra for coiled coil-forming peptides. Refer to **Table S3.1** for calculated and observed m/z.
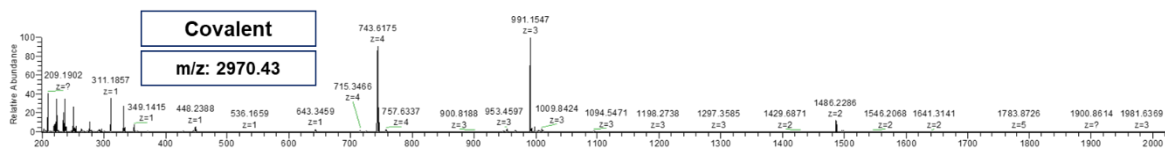
Figure S3.3. ESI spectrum for thiolated fluorophore peptide used for covalent controls in this study. Refer to **Table S3.1** for calculated and observed m/z. It is important to note that although this was the observed m/z value, there were non-negligible amounts of other molecular weights in this peptide – likely partially from N-termini without conjugated FAM and disulfide bridges forming.

111
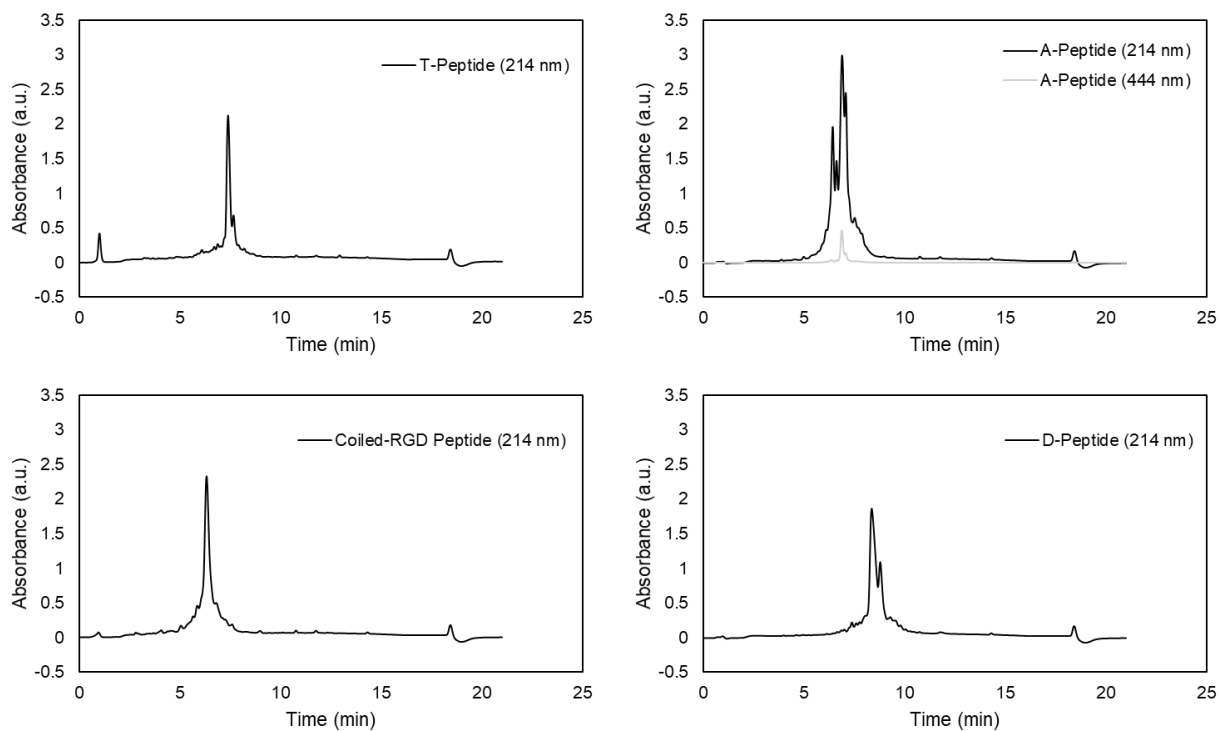
Figure S3.4. Analytical HPLC traces for peptides used in this study. Synthetic peptides were detected at 214 nm, while FAM absorbance on the A-peptide was detected at 444 nm. The 444 nm trace for the A-peptide confirms that one peak in the chromatograph corresponds to labeled peptide, suggesting that the other corresponds to unlabeled peptide. Peptides were eluted using an AB linear gradient of 6.2% CH_3CN/min from 5 to 95% CH_3CN, where eluent A was 0.1% aqueous trifluoracetic acid (v/v) and eluent B was 0.1% trifluoroacetic acid in CH_3CN.
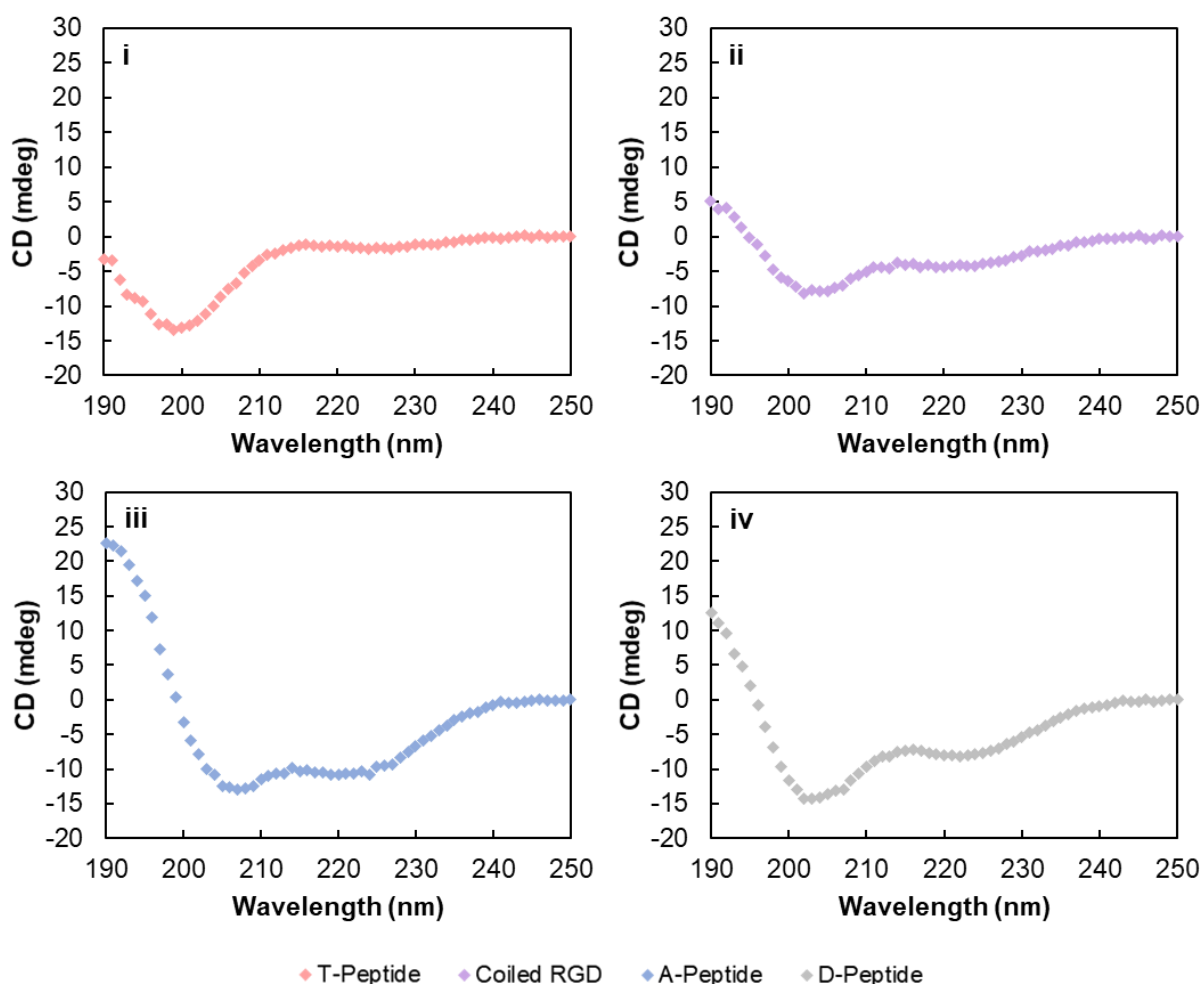
Figure S3.5. Circular dichroism (CD) spectra of coiled coil-forming peptides used in this study. CD spectra of (i) T-peptide, (ii) Coiled RGD, (iii) A-peptide, and (iv) D-peptide in 10 mM PBS (pH 7.4) at 0.1 mg/mL. CD measurements were taken at 25 °C, with a data pitch of 0.1 nm and scanning speed of 50 nm/min. The spectra are shown as the average of 3 scans per sample.

Table S3.2. α-helix percentage for peptides used in this study. Helicity calculations were performed based on a previously described method.[70]

Peptide Title	Percent Helicity
T-peptide	4.6%
Coiled RGD	10.8%
A-peptide	29.1%
D-Peptide	22.6%

The spectrum of the T-peptide (EIAALEK)$_3$G$_7$CG (S4-i) shows the peptide adopts a random coil structure (overall α-helicity of 4.6%). As the T-peptide behaved how we expected it to in forming coiled-coil complexes with release being dependent on the addition of the competing D-peptide (see publication **Figure 3.2**), we postulate that the 7-

glycine spacer added to provide physical space between the hydrogel/fiber substrates and the coiled domains might also consequently limit the overall α-helical nature of the peptide. That said, it still allowed for stable coiled-coil complexes to form on hydrogel/hydrogel fiber substrates that could easily be disrupted via the user-defined addition of the complementary D-peptide. This was unsurprising as randomly coiled peptides have been previously shown to adopt the helical secondary structure as they assemble into coiled-coil complexes – specifically when the sequence contains the necessary amino acid motifs to complex with the complementary strand as they do here (E/K complementary heptads)[53].

The spectrum of the Coiled RGD peptide GYG<u>RGD</u>SPG-(KIAALKE)$_4$ (S4-ii) shows a modest helical structure based on the CD spectrum (overall α-helicity of 10.8%), with the addition of the bioactive RGD domain likely limiting the formation of the α-helix – as (KIAALKE)$_4$ itself has been previously shown to be α-helical[47].

The A-peptide (S4-iii) – FAM-(KIAALKE)$_4$ – and the D-peptide (S4-iv) – (EIAALEK)$_4$ – have the highest α-helical content among the peptides in this study (overall α-helicity of 29.1% and 22.6%, respectively), as indicated by the CD spectra. Overall, despite the peptides exhibiting varying degrees of α-helicity, they demonstrated the ability to form coiled-coil complexes with their complements, thus enabling user-defined, temporal presentation of bioactive molecules on NorHA hydrogels and PEGNB fibers as shown in **Figures 3.1 & 3.2** (fluorophore experiments), as well as **Figures 3.3 & 3.4** (fibroblast experiments).
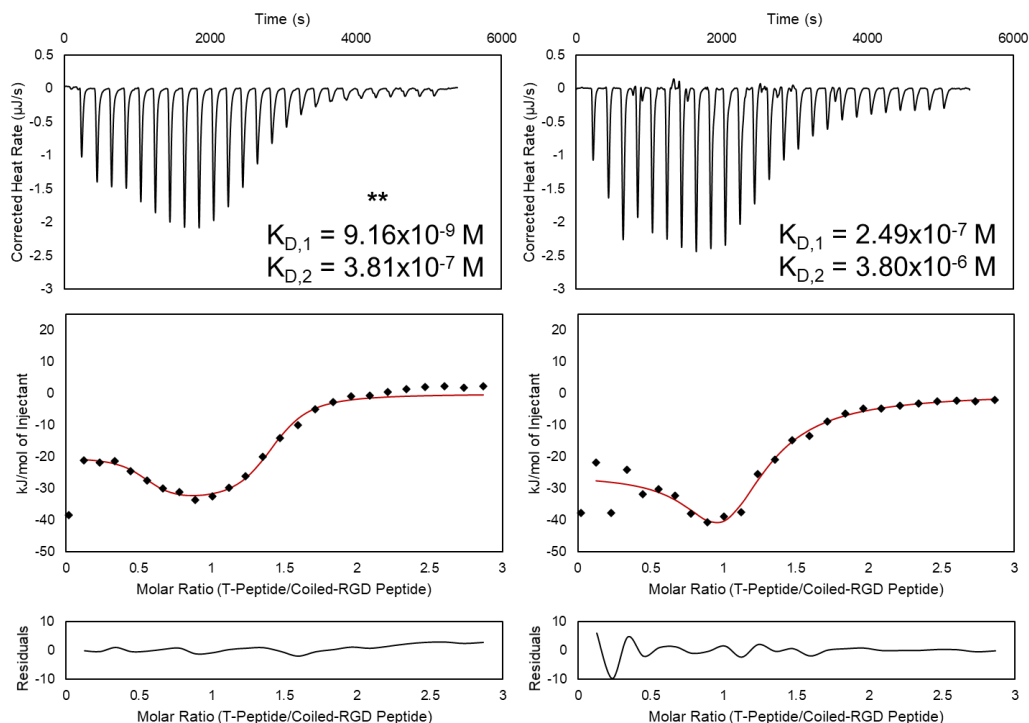
Figure S3.6. ITC trials for T-Peptide:Coiled-RGD Peptide associations in NIH 3T3 fibroblast medium. Experiments were performed with injections of 200 μM T-Peptide into 20 μM Coiled-RGD Peptide at pH 7.4. Integrated plots were fit to a multiple-site model that yielded affinity parameters for these complexes. T-Peptide:Coiled-RGD Peptide dissociation constant values from the model are on the order of 10^{-7}-10^{-9} M for the first site and 10^{-6}-10^{-7} M for the second site. ** *Indicates plot series included in main text* **Figure 3.1***.*
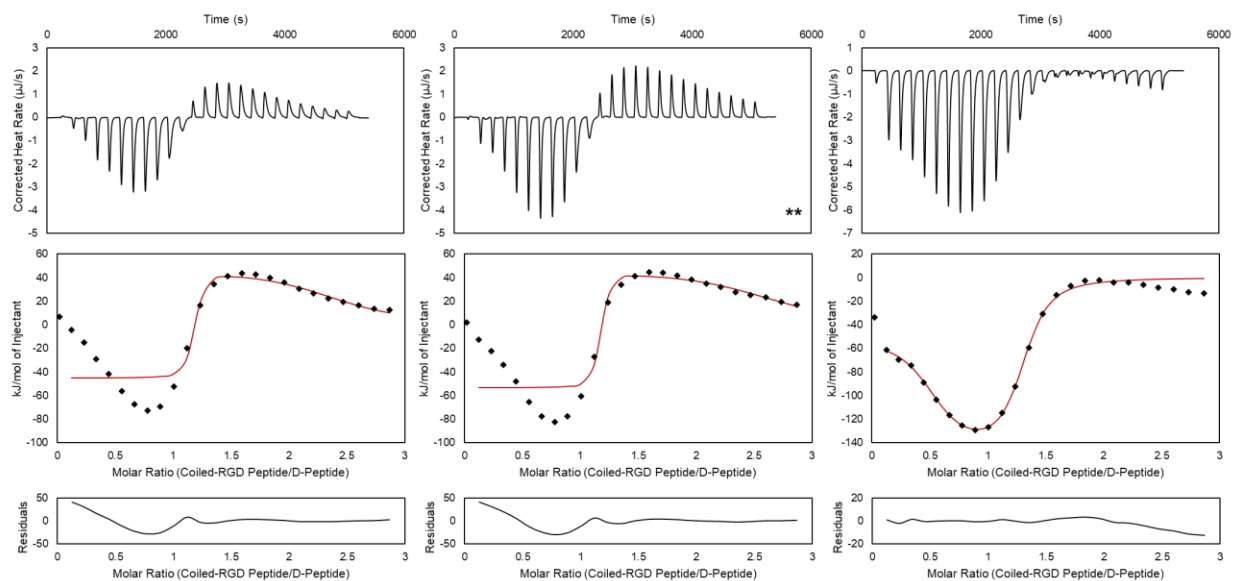
Figure S3.7. ITC trials for Coiled-RGD Peptide:D-Peptide associations in NIH 3T3 fibroblast medium. Experiments were performed with injections of 200 μM Coiled-RGD Peptide into 20 μM D-Peptide at pH 7.4. Integrated plots were fit to a multiple-site model

that yielded affinity information for these complexes; however, the plots (notably left and middle) demonstrated high residuals for the fits at low molar ratios, indicating that the models may not reliably represent the data. Therefore, K_D values from the model would not accurately represent the system. Nevertheless, the magnitudes of the exothermic peaks (refer to y-axes on integrated plots) are considerably greater than those seen for T-Petide:Coiled RGD Peptide (**Figure S3.6**), indicating that the Coiled-RGD:D-Peptide complex is thermodynamically favored compared to the T-Peptide:Coiled-RGD Peptide complex in culture medium. This favorability likely facilitates the removal of Coiled-RGD peptide from T-Peptide via the introduction of D-peptide into the system. Notably, the ITC traces exhibit endothermic peaks (left and middle), which are potentially indicative of higher-order structures forming in solution[57]. Interestingly, the last plot series (right) does not exhibit the endothermic peaks seen in the other two traces, and we are currently investigating the cause of the endothermic peaks as a separate study. ** *Indicates plot series included in main text* **Figure 3.1**.

Figure S3.8. ITC trials for T-Peptide:D-Peptide associations in NIH 3T3 fibroblast medium. Experiments were performed with injections of 200 μM T-Peptide into 20 μM D-Peptide at pH 7.4. Integrated plots were unable to be fit to an association model and subtracting integrated heats of dilution yield heats of interaction of essentially 0 kJ/mol. Therefore, the T-Peptide and D-peptide do not appreciably associate when in fibroblast culture medium. ** *Indicates plot series included in main text* **Figure 3.1**.

Figure S3.9. ITC trials for T-Peptide:A-Peptide associations in PBS. Experiments were performed with injections of 200 μM T-Peptide into 20 μM A-Peptide at pH 7.4, with the exception of the final trace (bottom right), which was performed with injections of 200 μM T-Peptide into 10 μM A-Peptide at pH 7.4. The first trace (top left) was performed with 50 injections, whereas the remaining traces were performed with 25 injections. Integrated plots were fit to an independent-site model that yielded affinity parameters for these complexes. T-Peptide:A-Peptide dissociation constant values are on the order of 10^{-6}-10^{-7} M.
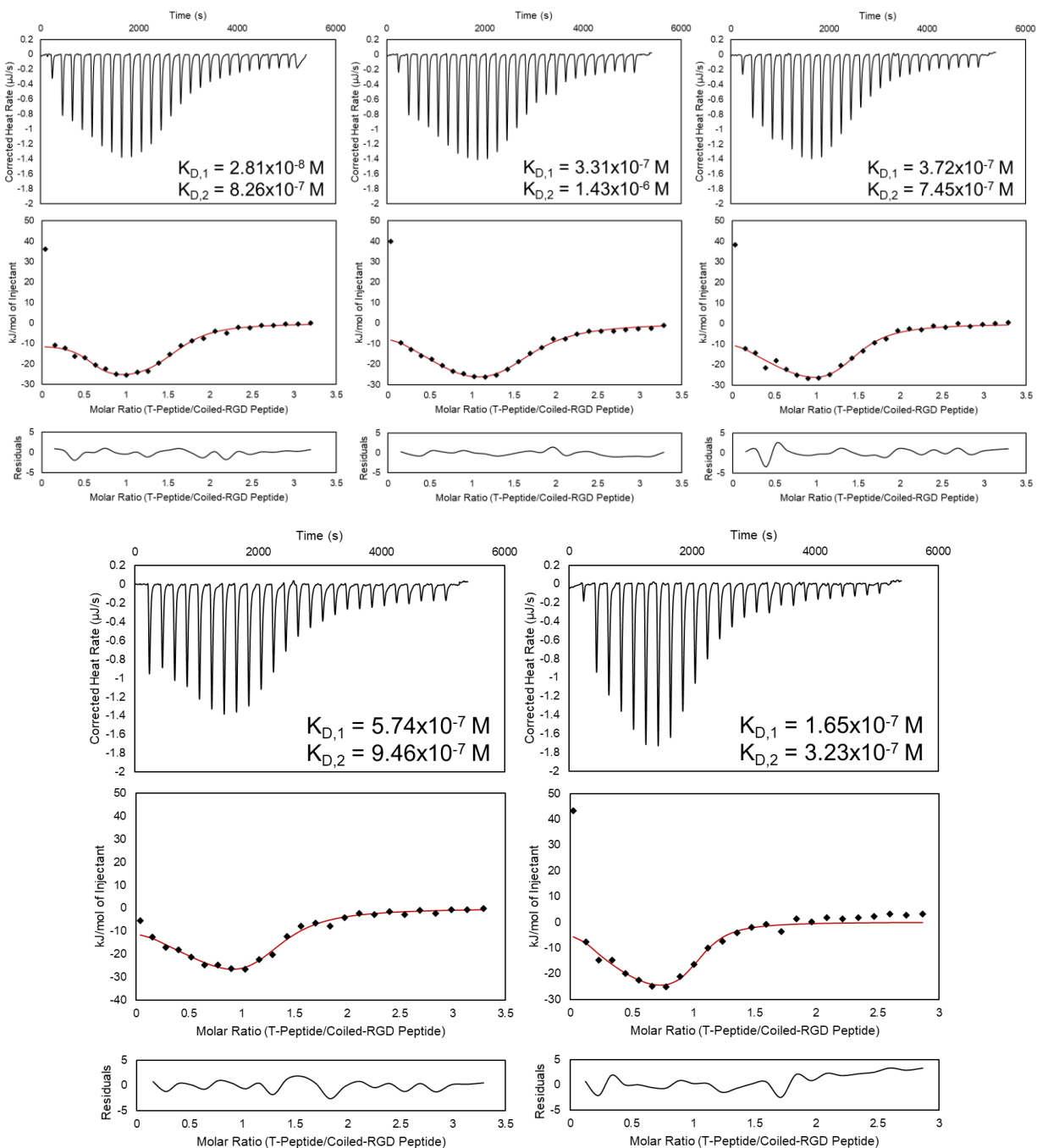
Figure S3.10. ITC trials for T-Peptide:Coiled-RGD Peptide associations in PBS. Experiments were performed with injections of 172 μM T-Peptide into 16 μM Coiled-RGD Peptide at pH 7.4, with the exception of the final trace (bottom right), which was performed with injections of 200 μM T-Peptide into 20 μM Coiled-RGD Peptide at pH 7.4. Integrated plots were fit to a multiple-site model that yielded affinity parameters for these complexes. T-Peptide:Coiled-RGD Peptide dissociation constant values are on the order of 10^{-7}-10^{-8} M for the first site and 10^{-6}-10^{-7} M for the second site.
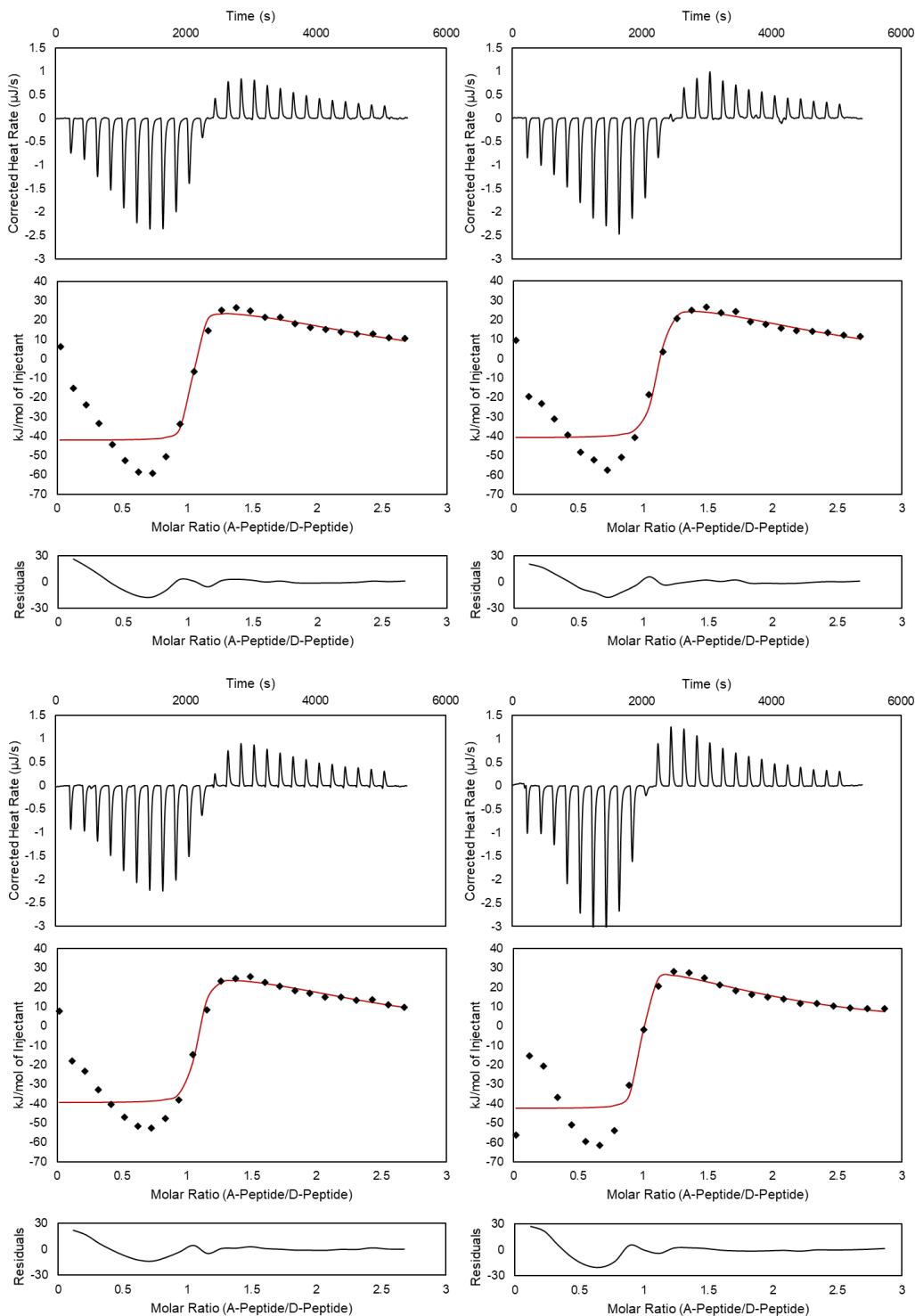
Figure S3.11. ITC trials for A-Peptide:D-Peptide associations in PBS. Experiments were performed with injections of 155 μM A-Peptide into 17 μM D-Peptide at pH 7.4, with the exception of the final trace (bottom right), which was performed with injections of 200 μM A-Peptide into 20 μM D-Peptide at pH 7.4. Integrated plots were fit to a multiple-site model that yielded affinity information for these complexes; however, the plots all demonstrated high residuals for the fits at low molar ratios, indicating that the models may

not reliably represent the data. Therefore, K_D values from the model would not accurately represent the system. Nevertheless, the magnitudes of the exothermic peaks (refer to y-axes on integrated plots) are considerably greater than those seen for T-Peptide:A-Peptide (**Figure S3.9**), indicating that the A-Peptide:D-Peptide complex is thermodynamically favorable compared to the T-Peptide:A-Peptide in PBS. This favorability likely facilitates the removal of A-peptide from T-Peptide via the introduction of D-peptide into the system. Notably, the ITC traces exhibit endothermic peaks, which are potentially indicative of higher-order structures forming in solution[57].
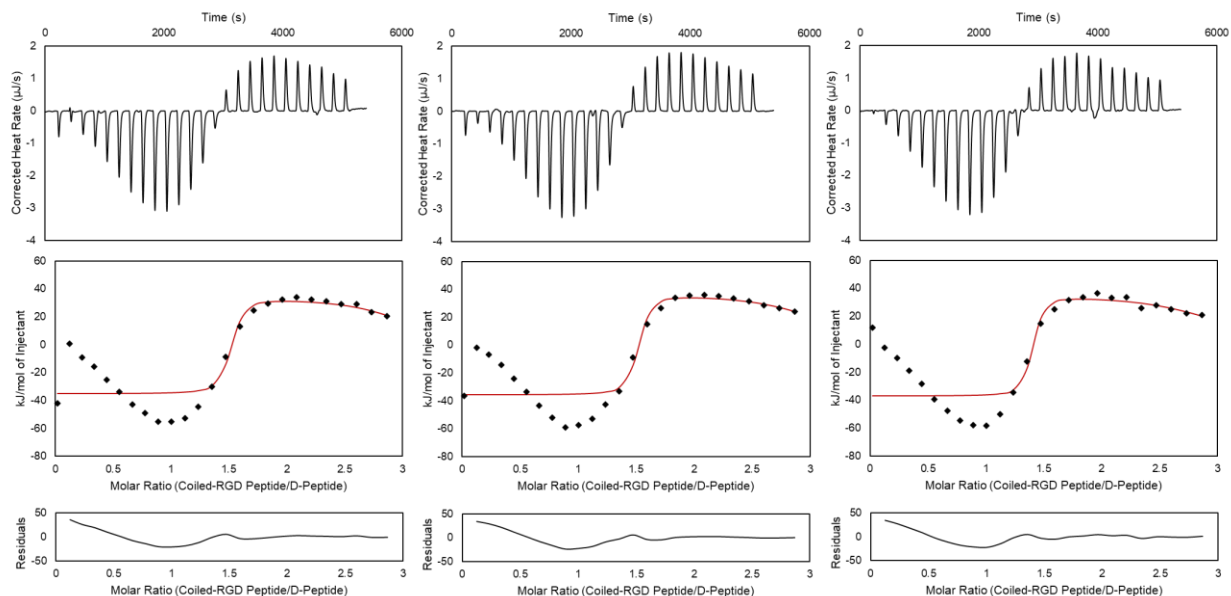
Figure S3.12. ITC trials for Coiled-RGD Peptide:D-Peptide associations in PBS. Experiments were performed with injections of 200 μM Coiled-RGD Peptide into 20 μM D-Peptide at pH 7.4. Integrated plots were fit to a multiple-site model that yielded affinity information for these complexes; however, the plots all demonstrated high residuals for the fits, indicating that the models may not reliably represent the data. Therefore, K_D values from the model would not accurately represent the system. Nevertheless, the magnitudes of the exothermic peaks (refer to y-axes on integrated plots) are considerably greater than those seen for T-Peptide:Coiled-RGD Peptide (**Figure S3.10**), indicating that the Coiled-RGD Peptide:D-Peptide complex is thermodynamically favorable compared to the T-Peptide:Coiled-RGD Peptide in PBS. This favorability likely facilitates the removal of Coiled-RGD peptide from T-Peptide via the introduction of D-peptide into the system. Notably, the ITC traces exhibit endothermic peaks, which are potentially indicative of higher-order structures forming in solution[57].
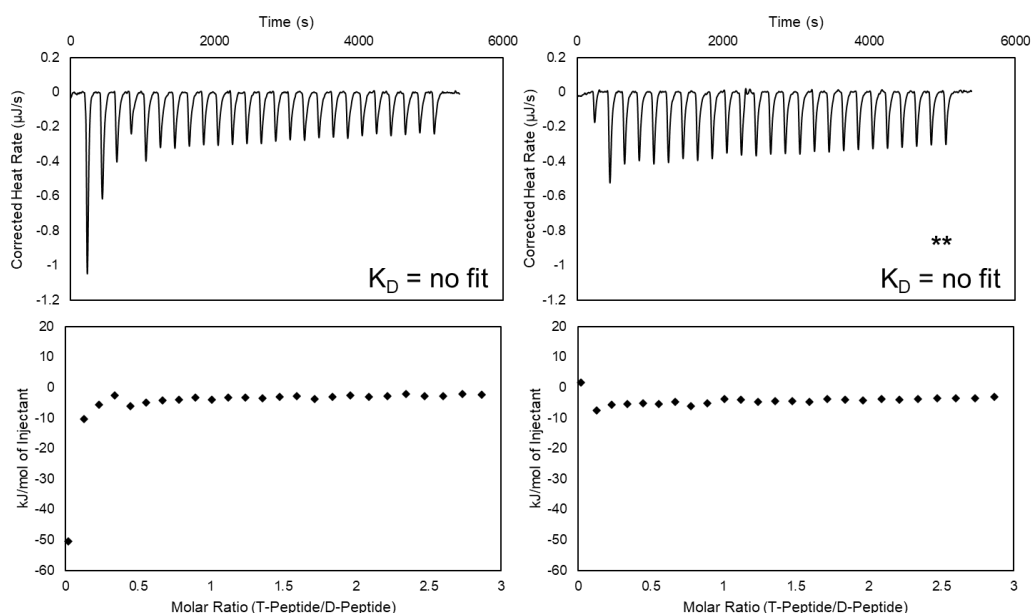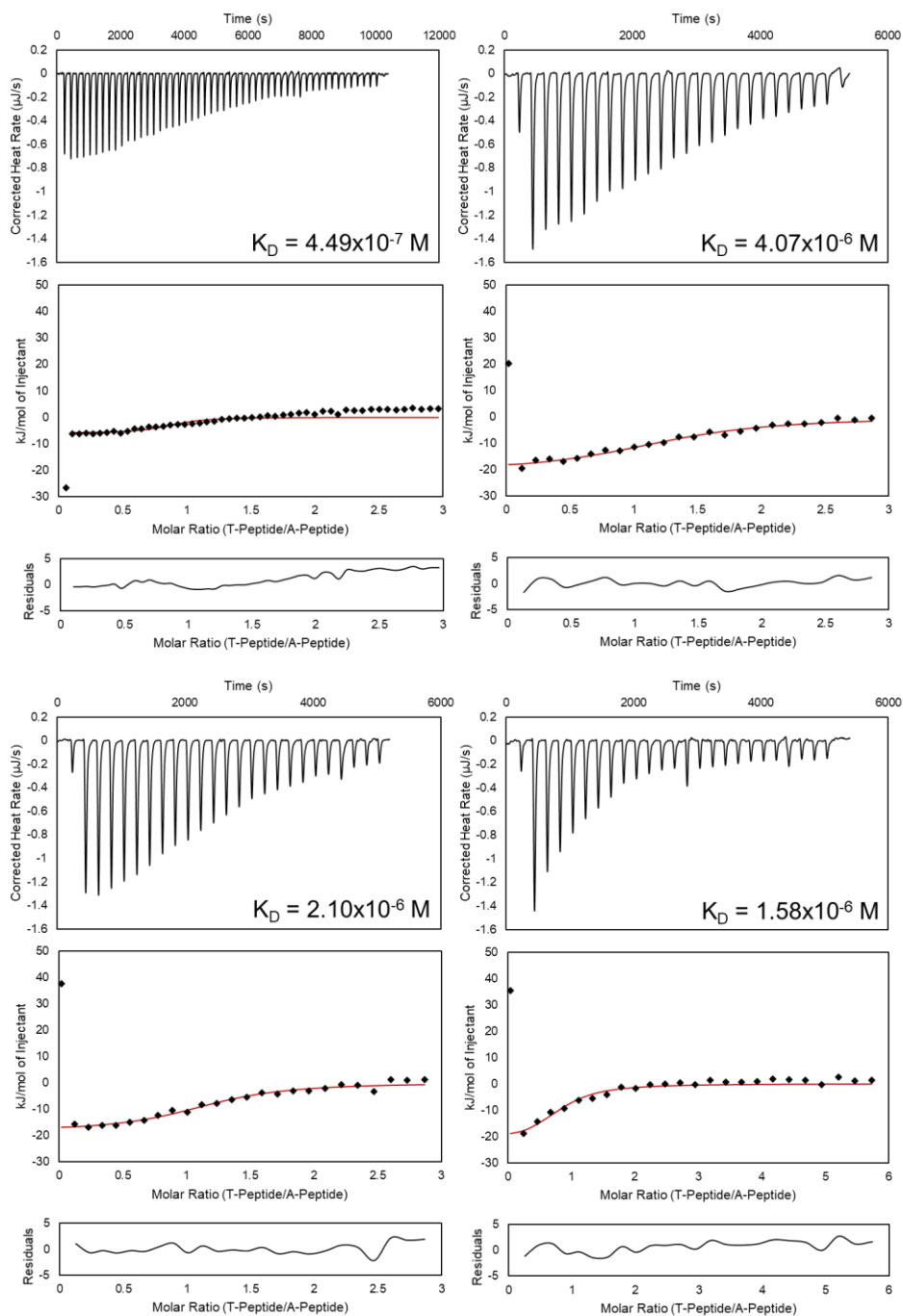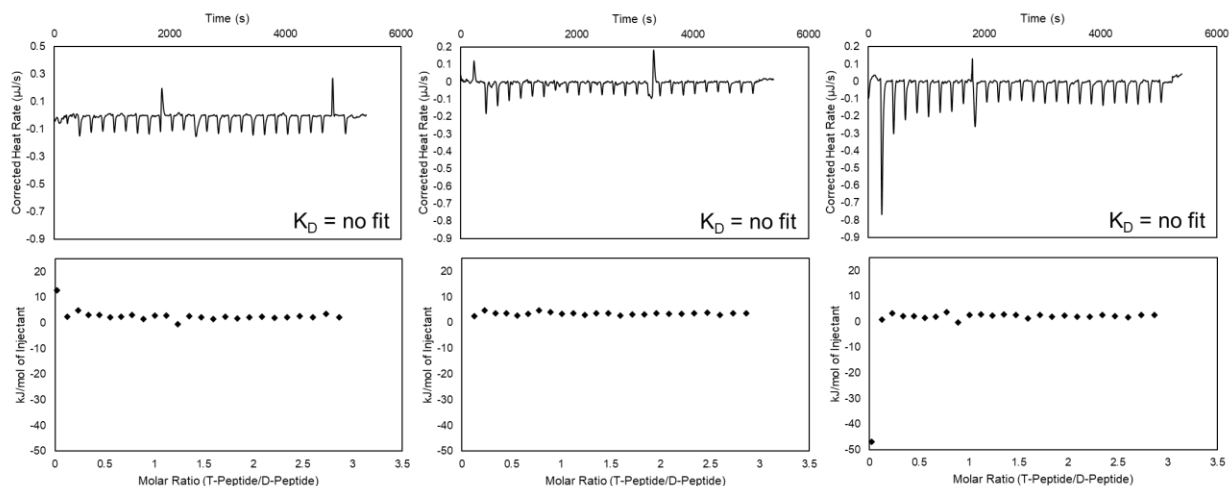
Figure S3.13. ITC trials for T-Peptide:D-Peptide associations in PBS. Experiments were performed with injections of 200 μM T-Peptide into 20 μM D-Peptide at pH 7.4. Integrated plots were unable to be fit to an association model and subtracting integrated heats of dilution yield heats of interaction of essentially 0 kJ/mol. Therefore, the T-Peptide and D-peptide do not appreciably associate in PBS.
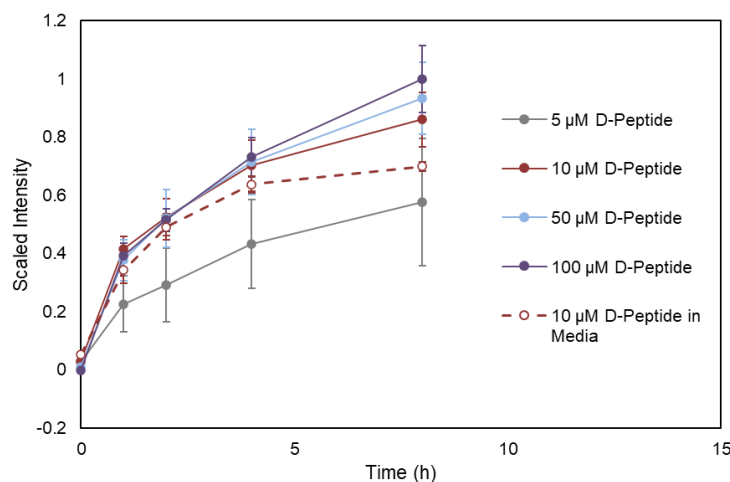
Figure S3.14. Concentration dependency of D-peptide on release of A-peptide with comparison to release in cell media. Release of A-Peptide with 5, 10, 50, and 100 μM D-Peptide solutions *in PBS* illustrates that increasing concentration of D-Peptide increases removal of A-peptide from the system. However, at higher concentrations, only marginal improvement is observed in A-peptide removal – suggesting that kinetics of peptide displacement govern removal rather than D-Peptide availability at higher concentrations.

10 μM D-peptide *in 3T3 fibroblast media* generally follows the same trend with marginally lower removal compared to 10 μM D-Peptide in PBS. This could be due to interactions with the serum in media, but it is more likely that differences in FAM concentration in cell media are more difficult to track with the plate reader protocol. We refer to the ITC data (**Figures S3.6-3.13**) that indicate similar affinities in both PBS and cell media.

122

3.8. References

(1)   Wade, R. J.; Bassin, E. J.; Gramlich, W. M.; Burdick, J. A. Nanofibrous Hydrogels with Spatially Patterned Biochemical Signals to Control Cell Behavior. *Adv. Mater.* 2015, *27* (8), 1356–1362. https://doi.org/https://doi.org/10.1002/adma.201404993.

(2)   Baker, B. M.; Trappmann, B.; Wang, W. Y.; Sakar, M. S.; Kim, I. L.; Shenoy, V. B.; Burdick, J. A.; Chen, C. S. Cell-Mediated Fibre Recruitment Drives Extracellular Matrix Mechanosensing in Engineered Fibrillar Microenvironments. *Nat. Mater.* 2015, *14*, 1262–1268. https://doi.org/https://doi.org/10.1038/nmat4444.

(3)   Davidson, C. D.; Wang, W. Y.; Zaimi, I.; Jayco, D. K. P.; Baker, B. M. Cell Force-Mediated Matrix Reorganization Underlies Multicellular Network Assembly. *Sci. Rep.* 2019, *9*, 1–13. https://doi.org/https://doi.org/10.1038/s41598-018-37044-1.

(4)   Baker, B. M.; Chen, C. S. Deconstructing the Third Dimension – How 3D Culture Microenvironments Alter Cellular Cues. *J. Cell Sci.* 2012, *125* (13), 3015–3024. https://doi.org/https://doi.org/10.1242/jcs.079509.

(5)   Wade, R. J.; Burdick, J. A. Engineering ECM Signals into Biomaterials. *Mater. Today* 2012, *15* (10), 454–459. https://doi.org/https://doi.org/10.1016/S1369-7021(12)70197-9.

(6)   Velasco-Hogan, A.; Xu, J.; Meyers, M. A. Additive Manufacturing as a Method to Design and Optimize Bioinspired Structures. *Adv. Mater.* 2018, *30* (1800940), 1–26. https://doi.org/https://doi.org/10.1002/adma.201800940.

(7)   Grigoryan, B.; Paulsen, S. J.; Corbett, D. C.; Sazer, D. W.; Fortin, C. L.; Zaita, A. J.; Greenfield, P. T.; Calafat, N. J.; Gounley, J. P.; Ta, A. H.; et al. Multivascular Networks and Functional Intravascular Topologies within Biocompatible Hydrogels. *Science (80-.).* 2019, *364*, 458–464.

(8)   Frantz, C.; Stewart, K. M.; Weaver, V. M. The Extracellular Matrix at a Glance. *J. Cell Sci.* 2010, *123* (24), 4195–4200. https://doi.org/https://doi.org/10.1242/jcs.023820.

(9)   Lutolf, M. P.; Hubbell, J. A. Synthetic Biomaterials as Instructive Extracellular Microenvironments for Morphogenesis in Tissue Engineering. *Nat. Biotechnol.* 2005, *23*, 47–55. https://doi.org/https://doi.org/10.1038/nbt1055.

(10)   Wade, R. J.; Bassin, E. J.; Rodell, C. B.; Burdick, J. A. Protease-Degradable Electrospun Fibrous Hydrogels. *Nat. Commun.* 2015, *6*, 1–10. https://doi.org/https://doi.org/10.1038/ncomms7639.

(11)	Deforest, C. A.; Anseth, K. S. Photoreversible Patterning of Biomolecules within Click-Based Hydrogels. *Angew. Chemie Int. Ed.* 2012, *51* (8), 1816–1819. https://doi.org/https://doi.org/10.1002/anie.201106463.

(12)	Grim, J. C.; Marozas, I. A.; Anseth, K. S. Thiol-Ene and Photo-Cleavage Chemistry for Controlled Presentation of Biomolecules in Hydrogels. *J. Control. Release* 2015, *219*, 95–106. https://doi.org/10.1016/j.jconrel.2015.08.040.

(13)	Stevens, M. M.; George, J. H. Exploring and Engineering the Cell Surface Interface. *Science (80-.).* 2005, *310* (5751), 1135–1138. https://doi.org/10.1126/science.1106587.

(14)	Caliari, S. R.; Burdick, J. A. A Practical Guide to Hydrogels for Cell Culture. *Nat. Methods* 2016, *13* (5), 405–414. https://doi.org/10.1038/nmeth.3839.

(15)	Tibbitt, M. W.; Anseth, K. S. Hydrogels as Extracellular Matrix Mimics for 3D Cell Culture. *Biotechnol. Bioeng.* 2009, *103* (4), 655–663. https://doi.org/https://doi.org/10.1002/bit.22361.

(16)	Highley, C. B.; Prestwich, G. D.; Burdick, J. A. Recent Advances in Hyaluronic Acid Hydrogels for Biomedical Applications. *Curr. Opin. Biotechnol.* 2016, *40*, 35–40. https://doi.org/10.1016/j.copbio.2016.02.008.

(17)	Burdick, J. A.; Prestwich, G. D. Hyaluronic Acid Hydrogels for Biomedical Applications. *Adv. Healthc. Mater.* 2011, *23* (12), H41–H56. https://doi.org/10.1002/adma.201003963.

(18)	Gramlich, W. M.; Kim, I. L.; Burdick, J. A. Synthesis and Orthogonal Photopatterning of Hyaluronic Acid Hydrogels with Thiol-Norbornene Chemistry. *Biomaterials* 2013, *34* (38), 9803–9811. https://doi.org/10.1016/j.biomaterials.2013.08.089.

(19)	Hui, E.; Gimeno, K. I.; Guan, G.; Caliari, S. R. Spatiotemporal Control of Viscoelasticity in Phototunable Hyaluronic Acid Hydrogels. *Biomacromolecules* 2019, *20* (11), 4126–4134. https://doi.org/https://doi.org/10.1021/acs.biomac.9b00965.

(20)	Burdick, J. A.; Murphy, W. L. Moving from Static to Dynamic Complexity in Hydrogel Design. *Nat. Commun.* 2012, *3*, 1–8. https://doi.org/10.1038/ncomms2271.

(21)	Davidson, C. D.; Jayco, D. K. P.; Matera, D. L.; DePalma, S. J.; Hiraki, H. L.; Wang, W. Y.; Baker, B. M. Myofibroblast Activation in Synthetic Fibrous Matrices Composed of Dextran Vinyl Sulfone. *Acta Biomater.* 2020, *105*, 78–86. https://doi.org/https://doi.org/10.1016/j.actbio.2020.01.009.

(22) Fisher, S. A.; Tam, R. Y.; Fokina, A.; Mahmoodi, M. M.; Distefano, M. D.; Shoichet, M. S. Photo-Immobilized EGF Chemical Gradients Differentially Impact Breast Cancer Cell Invasion and Drug Response in Defined 3D Hydrogels. *Biomaterials* 2018, *178*, 751–766. https://doi.org/10.1016/j.biomaterials.2018.01.032.

(23) Tam, R. Y.; Smith, L. J.; Shoichet, M. S. Engineering Cellular Microenvironments with Photo- and Enzymatically Responsive Hydrogels: Toward Biomimetic 3D Cell Culture Models. *Acc. Chem. Res.* 2017, *50* (4), 703–713. https://doi.org/10.1021/acs.accounts.6b00543.

(24) Sharma, S.; Floren, M.; Ding, Y.; Stenmark, K. R.; Tan, W.; Bryant, S. J. A Photoclickable Peptide Microarray Platform for Facile and Rapid Screening of 3-D Tissue Microenvironments. *Biomaterials* 2017, *143*, 17–28. https://doi.org/10.1016/j.biomaterials.2017.07.025.

(25) Roberts, J. J.; Bryant, S. J. Comparison of Photopolymerizable Thiol-Ene PEG and Acrylate-Based PEG Hydrogels for Cartilage Development. *Biomaterials* 2013, *34* (38), 9969–9979. https://doi.org/10.1016/j.biomaterials.2013.09.020.

(26) Hoyle, C. E.; Bowman, C. N. Thiol – Ene Click Chemistry. *Angew. Chemie* 2010, *49*, 1540–1573. https://doi.org/https://doi.org/10.1002/anie.200903924.

(27) Kalaoglu-Altan, O. I.; Verbraeken, B.; Lava, K.; Gevrek, T. N.; Sanyal, R.; Dargaville, T.; De Clerck, K.; Hoogenboom, R.; Sanyal, A. Multireactive Poly(2-Oxazoline) Nanofibers through Electrospinning with Crosslinking on the Fly. *ACS Macro Lett.* 2016, *5* (6), 676–681. https://doi.org/https://doi.org/10.1021/acsmacrolett.6b00188.

(28) Deforest, C. A.; Tirrell, D. A. A Photoreversible Protein-Patterning Approach for Guiding Stem Cell Fate in Three-Dimensional Gels. *Nat. Mater.* 2015, *14*, 523–531. https://doi.org/https://doi.org/10.1038/nmat4219.

(29) Grim, J. C.; Brown, T. E.; Aguado, B. A.; Chapnick, D. A.; Viert, A. L.; Liu, X.; Anseth, K. S. A Reversible and Repeatable Thiol–Ene Bioconjugation for Dynamic Patterning of Signaling Proteins in Hydrogels. *ACS Cent. Sci.* 2018, *4*, 909–916. https://doi.org/https://doi.org/10.1021/acscentsci.8b00325.

(30) Weng, G.; Bhalla, U. S.; Iyengar, R. Complexity in Biological Signaling Systems. *Science (80-.).* 1999, *284* (April), 92–97.

(31) Xie, C.; Sun, W.; Lu, H.; Kretzschmann, A.; Liu, J.; Wagner, M.; Butt, H. J.; Deng, X.; Wu, S. Reconfiguring Surface Functions Using Visible-Light-Controlled Metal-Ligand Coordination. *Nat. Commun.* 2018, *9* (1), 1–9. https://doi.org/10.1038/s41467-018-06180-7.

(32)   Fumasi, F. M.; Stephanopoulos, N.; Holloway, J. L. Reversible Control of Biomaterial Properties for Dynamically Tuning Cell Behavior. *J. Appl. Polym. Sci.* 2020, *137* (25), 1–16. https://doi.org/10.1002/app.49058.

(33)   Kloxin, A. M.; Kasko, A. M.; Salinas, C. N.; Anseth, K. S. Photodegradable Hydrogels for Dynamic Tuning of Physical and Chemical Properties. *Science (80-.).* 2009, *324* (5923), 59–63.

(34)   Liu, L.; Tian, X.; Ma, Y.; Duan, Y.; Zhao, X.; Pan, G. A Versatile Dynamic Mussel-Inspired Biointerface: From Specific Cell Behavior Modulation to Selective Cell Isolation. *Angew. Chemie - Int. Ed.* 2018, *57* (26), 7878–7882. https://doi.org/10.1002/anie.201804802.

(35)   Mann, J. L.; Yu, A. C.; Agmon, G.; Appel, E. A. Supramolecular Polymeric Biomaterials. *Biomater. Sci.* 2018, *6* (1), 10–37. https://doi.org/10.1039/c7bm00780a.

(36)   Appel, E. A.; Biedermann, F.; Rauwald, U.; Jones, S. T.; Zayed, J. M.; Scherman, O. A. Supramolecular Cross-Linked Networks via Host - Guest Complexation with Cucurbit[8]Uril. *J. Am. Chem. Soc.* 2010, *132* (40), 14251–14260. https://doi.org/https://doi.org/10.1021/ja106362w.

(37)   Highley, C. B.; Rodell, C. B.; Burdick, J. A. Direct 3D Printing of Shear-Thinning Hydrogels into Self-Healing Hydrogels. *Adv. Mater.* 2015, *27* (34), 5075–5079. https://doi.org/10.1002/adma.201501234.

(38)   Appel, E. A.; Loh, X. J.; Jones, S. T.; Biedermann, F.; Dreiss, C. A.; Scherman, O. A. Ultrahigh-Water-Content Supramolecular Hydrogels Exhibiting Multistimuli Responsiveness. *J. Am. Chem. Soc.* 2012, *134*, 11767–11773. https://doi.org/10.1021/ja3044568.

(39)   Tang, J. D.; Mura, C.; Lampe, K. J. Stimuli-Responsive, Pentapeptide, Nanofiber Hydrogel for Tissue Engineering. *J. Am. Chem. Soc.* 2019, *141* (12), 4886–4899. https://doi.org/10.1021/jacs.8b13363.

(40)   Highley, C. B.; Rodell, C. B.; Kim, I. L.; Wade, R. J.; Burdick, J. A. Ordered, Adherent Layers of Nanofibers Enabled by Supramolecular Interactions. *J. Mater. Chem. B* 2015, *2* (46), 8110–8115. https://doi.org/https://doi.org/10.1039/C4TB00724G.

(41)   Boekhoven, J.; Rubert Pérez, C. M.; Sur, S.; Worthy, A.; Stupp, S. I. Dynamic Display of Bioactivity through Host-Guest Chemistry. *Angew. Chemie - Int. Ed.* 2013, *52* (46), 12077–12080. https://doi.org/https://doi.org/10.1002/anie.201306278.

(42)   McNamara, S. L.; Brudno, Y.; Miller, A. B.; Ham, H. O.; Aizenberg, M.; Chaikof, E. L.; Mooney, D. J. Regenerating Antithrombotic Surfaces through Nucleic Acid Displacement. *ACS Biomater. Sci. Eng.* 2020, *6*, 2159–2166. https://doi.org/10.1021/acsbiomaterials.0c00038.

(43)   Freeman, R.; Stephanopoulos, N.; Álvarez, Z.; Lewis, J. A.; Sur, S.; Serrano, C. M.; Boekhoven, J.; Lee, S. S.; Stupp, S. I. Instructing Cells with Programmable Peptide DNA Hybrids. *Nat. Commun.* 2017, *8*, 15982. https://doi.org/https://doi.org/10.1038/ncomms15982.

(44)   Freeman, R.; Han, M.; Alvarez, Z.; Lewis, J. A.; Wester, J. R.; Stephanopoulos, N.; McClendon, M. T.; Lynsky, C.; Godbe, J. M.; Sangji, H.; et al. Reversible Self-Assembly of Superstructured Networks. *Science (80-.).* 2018, *813* (November), 808–813.

(45)   Grçger, K.; Gavins, G.; Seitz, O. Molecular Recognition Strand Displacement in Coiled-Coil Structures: Controlled Induction and Reversal of Proximity. *Angew. Chemie - Int. Ed.* 2017, *56*, 14217–14221. https://doi.org/10.1002/anie.201705339.

(46)   Lupas, A. N.; Gruber, M. The Structure of Alpha-Helical Coiled Coils. *Adv. Protein Chem.* 2005, *70* (04), 37–78. https://doi.org/10.1016/S0065-3233(04)70003-0.

(47)   Litowski, J. R.; Hodges, R. S. Designing Heterodimeric Two-Stranded α-Helical Coiled-Coils. Effects of Hydrophobicity and α-Helical Propensity on Protein Folding, Stability, and Specificity. *J. Biol. Chem.* 2002, *277* (40), 37272–37279. https://doi.org/10.1074/jbc.M204257200.

(48)   Archer, W. R.; Schulz, M. D. Isothermal Titration Calorimetry: Practical Approaches and Current Applications in Soft Matter. *Soft Matter* 2020, *16* (38), 8760–8774. https://doi.org/10.1039/d0sm01345e.

(49)   Wade, R. J.; Burdick, J. A. Advances in Nanofibrous Scaffolds for Biomedical Applications: From Electrospinning to Self-Assembly. *Nano Today* 2014, *9* (6), 722–742. https://doi.org/10.1016/j.nantod.2014.10.002.

(50)   Davidson, C. D.; Jayco, D. K. P.; Wang, W. Y.; Shikanov, A.; Baker, B. M. Fiber Crimp Confers Matrix Mechanical Nonlinearity, Regulates Endothelial Cell Mechanosensing, and Promotes Microvascular Network Formation. *J. Biomech. Eng.* 2020, *142* (11), 1–9. https://doi.org/10.1115/1.4048191.

(51)   Iglesias-Echevarria, M.; Durante, L.; Johnson, R.; Rafuse, M.; Ding, Y.; Bonani, W.; Maniglio, D.; Tan, W. Coaxial PCL/PEG-Thiol-Ene Microfiber with Tunable Physico-

Chemical Properties for Regenerative Scaffolds. *Biomater. Sci.* 2019, *7* (9), 3640–3651. https://doi.org/10.1039/c9bm00388f.

(52)   Kloxin, A. M.; Kloxin, C. J.; Bowman, C. N.; Anseth, K. S. Mechanical Properties of Cellularly Responsive Hydrogels and Their Experimental Determination. *Adv. Mater.* 2010, *22* (31), 3484–3494. https://doi.org/10.1002/adma.200904179.

(53)   Apostolovic, B.; Klok, H. A. PH-Sensitivity of the E3/K3 Heterodimeric Coiled Coil. *Biomacromolecules* 2008, *9* (11), 3173–3180. https://doi.org/10.1021/bm800746e.

(54)   Nair, D. P.; Podgórski, M.; Chatani, S.; Gong, T.; Xi, W.; Fenoli, C. R.; Bowman, C. N. The Thiol-Michael Addition Click Reaction: A Powerful and Widely Used Tool in Materials Chemistry. *Chem. Mater.* 2014, *26* (1), 724–744. https://doi.org/https://doi.org/10.1021/cm402180t.

(55)   Kabiri, M.; Unsworth, L. D. Application of Isothermal Titration Calorimetry for Characterizing Thermodynamic Parameters of Biomolecular Interactions: Peptide Self-Assembly and Protein Adsorption Case Studies. *Biomacromolecules* 2014, *15* (10), 3463–3473. https://doi.org/10.1021/bm5004515.

(56)   De Crescenzo, G.; Litowski, J. R.; Hodges, R. S.; O'Connor-McCourt, M. D. Real-Time Monitoring of the Interactions of Two-Stranded de Novo Designed Coiled-Coils: Effect of Chain Length on the Kinetic and Thermodynamic Constants of Binding. *Biochemistry* 2003, *42* (6), 1754–1763. https://doi.org/10.1021/bi0268450.

(57)   Kabiri, M.; Bushnak, I.; McDermot, M. T.; Unsworth, L. D. Toward a Mechanistic Understanding of Ionic Self-Complementary Peptide Self-Assembly: Role of Water Molecules and Ions. *Biomacromolecules* 2013, *14* (11), 3943–3950. https://doi.org/10.1021/bm401077b.

(58)   Gaudet, C.; Marganski, W. A.; Kim, S.; Brown, C. T.; Gunderia, V.; Dembo, M.; Wong, J. Y. Influence of Type I Collagen Surface Density on Fibroblast Spreading, Motility, and Contractility. *Biophys. J.* 2003, *85* (5), 3329–3335. https://doi.org/10.1016/S0006-3495(03)74752-3.

(59)   Rowley, J. A.; Mooney, D. J. Alginate Type and RGD Density Control Myoblast Phenotype. *J. Biomed. Mater. Res.* 2002, *60* (2), 217–223. https://doi.org/10.1002/jbm.1287.

(60)   Oria, R.; Wiegand, T.; Escribano, J.; Elosegui-artola, A.; Uriarte, J. J.; Moreno-pulido, C.; Platzman, I.; Delcanale, P.; Albertazzi, L.; Navajas, D.; et al. Force Loading Explains Spatial Sensing of Ligands by Cells. *Nature* 2017, *552*, 219–224. https://doi.org/10.1038/nature24662.

(61)   Ekerdt, B. L.; Segalman, R. A.; Schaffer, D. V. Spatial Organization of Cell-Adhesive Ligands for Advanced Cell Culture. *Biotechnol. J.* 2013, *8*, 1411–1423. https://doi.org/10.1002/biot.201300302.

(62)   Legant, W. R.; Miller, J. S.; Blakely, B. L.; Cohen, D. M.; Genin, G. M.; Chen, C. S. Measurement of Mechanical Tractions Exerted by Cells in Three-Dimensional Matrices. *Nat. Methods* 2010, *7* (12), 969–971. https://doi.org/10.1038/NMETH.1531.

(63)   Legant, W. R.; Pathak, A.; Yang, M. T.; Deshpande, V. S.; McMeeking, R. M.; Chen, C. S. Microfabricated Tissue Gauges to Measure and Manipulate Forces from 3D Microtissues. *Proc. Natl. Acad. Sci. U. S. A.* 2009, *106* (25), 10097–10102. https://doi.org/10.1073/pnas.0900174106.

(64)   Viola, J. M.; Porter, C. M.; Gupta, A.; Alibekova, M.; Prahl, L. S.; Hughes, A. J. Guiding Cell Network Assembly Using Shape-Morphing Hydrogels. *Adv. Mater.* 2020, *2002195*, e2002195. https://doi.org/10.1002/adma.202002195.

(65)   Khetan, S.; Guvendiren, M.; Legant, W. R.; Cohen, D. M.; Chen, C. S.; Burdick, J. A. Degradation-Mediated Cellular Traction Directs Stem Cell Fate in Covalently Crosslinked Three-Dimensional Hydrogels. *Nat. Mater.* 2013, *12*, 458–465. https://doi.org/10.1038/nmat3586.

(66)   Roberts, J. N.; Sahoo, J. K.; McNamara, L. E.; Burgess, K. V; Yang, J.; Alakpa, E. V; Anderson, H. J.; Hay, J.; Turner, L.-A.; Yarwood, S. J.; et al. Dynamic Surfaces for the Study of Mesenchymal Stem Cell Growth through Adhesion Regulation. *ACS Nano* 2016, *10*, 6667–6679. https://doi.org/10.1021/acsnano.6b01765.

(67)   Li, W.; Yan, Z.; Ren, J.; Qu, X. Manipulating Cell Fate: Dynamic Control of Cell Behaviors on Functional Platforms. *Chem. Soc. Rev.* 2018, *47*, 8639–8684. https://doi.org/10.1039/c8cs00053k.

(68)   Loebel, C.; Mauck, R. L.; Burdick, J. A. Local Nascent Protein Deposition and Remodelling Guide Mesenchymal Stromal Cell Mechanosensing and Fate in Three-Dimensional Hydrogels. *Nat. Mater.* 2019, *18*, 883–891. https://doi.org/https://doi.org/10.1038/s41563-019-0307-6.

(69)   Dumbleton, J.; Agarwal, P.; Huang, H.; Hogrebe, N.; Han, R.; Gooch, K. J.; He, X. The Effect of RGD Peptide on 2D and Miniaturized 3D Culture of HEPM Cells, MSCs, and ADSCs with Alginate Hydrogel. *Cell. Mol. Bioeng.* 2016, *9* (2), 277–288. https://doi.org/10.1007/s12195-016-0428-9.

(70)   Forood, B.; Feliciano, E. J.; Nambiar, K. P. Stabilization of A-Helical Structures in Short Peptides via End Capping. *Proc. Natl. Acad. Sci.* 1993, *90*, 838–842.

CHAPTER 4: ELECTROSPUN FIBERS ADD ECM-MIMETIC CONTEXT TO TRADITIONAL HYDROGEL CULTURE PLATFORMS

4.1. Abstract

There is a growing appreciation for engineering more dynamic biophysical and biochemical attributes of the extracellular matrix (ECM) into *in vitro* tissue models. More recently, fibrous proteins (e.g., collagen, etc.) have received considerable focus due to their contribution to the structural properties and mechanical profile of natural tissue. Accordingly, researchers have sought to develop biofabrication platforms that incorporate these desired fibrous components into synthetically engineered ECM-mimetics (e.g., hydrogels). Electrospinning is an accessible platform that has seen extensive use in the tissue engineering space due to its ability to fabricate polymeric nano-to-microfibers that are able to mimic some of the fibrous context provided by matrix proteins in endogenous tissue. Previous research has primarily focused on increasing the biochemical complexity of these fibers; however, traditional electrospun meshes are complicated by the dense, stochastic deposition of fibers that presents as mostly two-dimensional to cells when utilized as culture substrates. This challenge has motivated the advancement of biofabrication platforms to utilize polymeric fibers in a 3D environment to recapitulate the architecture of natural tissue systems more effectively. In this review, we briefly describe the design considerations associated with electrospinning fibers, then focus extensively on the demonstrated strategies that leverage them to provide ECM-mimetic context to traditional 3D hydrogel culture platforms.

4.2. Introduction

Over the last few decades, strategies to engineer synthetic models of tissue systems *in vitro* have continually evolved to enable more physiologically relevant studies of the structure function relationships between cells and their local extracellular matrix (ECM)[1–4]. This increased sophistication is in response to the growing appreciation of the complex heterogeneity of the native ECM and the dynamic biophysical and biochemical stimuli it imparts to the local milieu for cells to transduce[5–9]. The ECM in healthy tissues is in perfect balance and responds accordingly to external perturbations to conserve a homeostatic environment[6–8]; however, engineering these features into synthetic models *in vitro* remains a challenge with currently available biofabrication technologies[2]. The ECM naturally exists in 4D (i.e., 3D space and time)[6,8,10,11], and early iterations of ECM-mimetics aimed to simplify this via reducing that dimensionality – in time, space, or both – to enable isolation of specific variables to investigate[2,12]. While these studies are successful in determining how singular variables affect cell processes, the dimensional reduction prevents the ability to discern how the interplay between different matrix properties affects cell behaviors.

Hydrogel-forming biomaterials are mainstays in the tissue engineering space due to their ability to form water-swollen networks that are easily tailored to recapitulate various tissue systems *in vitro*[12–14]. While some hydrogel-forming polymers are naturally derived, such as hyaluronic acid[15,16], early iterations of hydrogel scaffolds were often viewed as "blank slate" materials and used as inert environments to support cells or protect them for delivery *in vivo*[2,12,17]. More recently, there has been considerable interest in leveraging the flexibility of hydrogels to recapitulate the complex and dynamic

131

heterogeneity of the ECM more effectively such that their utility extends far past serving as an inert scaffolding system[18,19].

Crosslinking chemistry and crosslinker molecule are well studied pathways to engineer dynamic complexity into hydrogel systems[20]. For example, through the thiol-ene click reaction, spatiotemporal control is afforded by dictating where and when the material is crosslinked or modified chemically[21,22]. There are also myriad chemistries that enable reversible crosslinks[23–26] or triggered degradation via external stimuli[20,27]. Crosslinker molecules can be designed with specific sequences that are recognized by cell-secreted enzymes for degradation[28–30], thereby enhancing potential integration with *in vivo* systems. Utilizing noncovalent crosslinking mechanisms is another common avenue for creating a dynamic environment for tissue engineering[31]. For example, self-assembling peptide amphiphiles are capable of forming nanoscale fibrils that coalesce into a global hydrogel scaffold suitable for cell culture[32–35]. Additionally, guest-host interactions are another class of supramolecular crosslinking mechanisms to create a dynamic hydrogel environment[36–41]. We refer the reader to the following excellent reviews for further information on including dynamic complexity into hydrogels for tissue engineering applications[2,14,31,42].

While hydrogels continue to see widespread use in modeling the ECM, they are often inherently limited by the nanoscale porosity and topography dictated by the continuous polymer network[32,43,44]. Moreover, capturing more complex matrix mechanics like nonlinear elasticity and viscoelasticity is difficult in many bulk hydrogel platforms. In the native ECM, fibers comprised of proteins like collagen, laminin, and fibronectin present a dynamic environment that can be remodeled by cellular activity with microscale

topographical cues that cells transduce[45–47]. This fibrous component also contributes to the tensile strength of the interstitial hydrogel in the tissue and provides adhesion sites for cells to engage[48]. Through integrin-mediated anchoring to the ECM fibers, cells are able to exert traction forces and recruit these matrix proteins to locally increase the fiber content, and thus, increase the local stiffness of the environment[49–52]. These contractility processes are heavily implicated in common physiological functions like the folding of tissues during development or the closure of wounds in the natural healing cascade[43]. The abundant evidence of the importance of these native ECM fibers *in* vivo has sparked a rising interest in incorporating fibrous topography into synthetic 3D culture platforms that aim to replicate the ECM *in vitro*.

There are numerous established platforms for incorporating a fibrous component into hydrogels for recapitulating the ECM[32]. Perhaps the simplest is through the use of naturally derived proteins like collagen[53], or ECM-derived protein mixtures like Matrigel[17]. These examples are well-demonstrated to self-assemble into bulk hydrogels that contain protein fibrils – the precursor to ECM fibers. At the molecular level, they innately possess cell-adhesive ligands to promote cell-matrix interactions, as well as sites naturally susceptible to proteolytic degradation for dynamic restructuring of the matrix[54]. While these offer simple implementation, they share some of the shortcomings of other self-assembling materials such as the aforementioned peptide amphiphiles, where minimal tunability is afforded over scaffold mechanics and topography[32]. This has inspired the use of other biofabrication platforms that enable the design of nano-to-microscale fibers to mimic the fibrous proteins in endogenous tissue with increased control over scaffold biophysical properties.

These platforms include solution deposition techniques like wet-spinning and melt-blowing, which are both accessible methods to produce fibers at the nano- and microscale[55]. For wet-spinning, a polymer is dissolved in a suitable solvent and is then extruded into a nonsolvent bath where polymeric fibers form[56–58]. Melt-blowing is a scalable technique originally designed for the textile industry in which a polymer melt is extruded through nozzles and blown by hot gas to form polymer fibers[55,59–61]. Drawing on concepts from electrohydrodynamics, melt-electrowriting and electrospinning are two of the most common platforms to engineer polymer fibers[55]. Melt-electrowriting is a form of additive manufacturing where an electrical voltage is applied to a polymer melt flowing through a nozzle. Upon deposition onto a cooled collection plate, the polymer solidifies in fiber form with high degrees of spatial control over fiber localization[62–65]. Electrospinning is another prevalent electrohydrodynamic process that enables the design of fibers useful for tissue engineering. Here, an electrical field is applied to a polymer solution which, though electrostatic repulsion, forces solvent evaporation and a polymer fiber to form on the collection surface[45]. While all of these techniques are able to deposit fibers that range the nano-to-microscale, they can be limited by their flexibility in application[55,66]. For instance, wet-spinning commonly requires a strategic solvent/nonsolvent system[56] or aqueous two-phase system[58] that can be difficult to design and in turn offers minimal control over resultant fiber properties. Additionally, melt-blowing and melt-electrowriting require polymer melts[55], which is not accessible for some polymer choices – namely naturally-inspired polysaccharides like hyaluronic acid.

In comparison, electrospinning is a dry spinning method, where the solvents used are evaporated during the processing, yielding fibrous scaffolds ready for use or further

modifications[45,67]. Therefore, electrospinning is a widely adaptable technique for a wide range of polymer choices for tissue engineering. Hydrophobic versus hydrophilic base polymers require a strategic choice for the solvent used when creating the electrospinning precursor solution, where hydrophobic polymers commonly require organic solvents and hydrophilic polymers are typically electrospun aqueously[45]. Electrospinning process parameters (e.g., solution viscosity, applied voltage, etc.) dictate the mechanical properties of hydrophobic materials[68–70], with often intensive post-processing parameters required for modulating the biochemical profile. Conversely, electrospinning hydrophilic materials that crosslink into hydrogel fibers enable all of the flexibilities that are associated with dynamic hydrogels, just in a fibrillar format – such as crosslinking density, crosslinker type, and tethering biomolecules[12,45]. We refer the readers to the following review on creating dynamic hydrogel fibers for further information on modulating the biochemical and biophysical profile of electrospun hydrogel fibers[45]. While electrospinning is a promising technique to create fibrous scaffolds for tissue engineering, there is increasing interest in its utility for 3D models of the ECM. Therefore, in this review, we focus on the design considerations of electrospun fibers, methods to extend them to 3D applications, and their function in hydrogel-fiber composites to provide the fibrous context to traditional 3D hydrogel culture systems.

4.3. Design considerations for electrospun fibers

The resultant product of traditional electrospinning is a dense, continuous fiber mesh that is stochastically deposited on the grounded collection surface. Historically, this fibrous scaffold was considered three-dimensional given the nano-to-microscale

topography dictated by the discrete fibers that comprise the mesh. However, the dimensions are primarily in XY space at the meso-to-macroscale as scaffolds are treated as substrates for cell culture and cells experience minimal influence in the Z direction. Nevertheless, electrospun fibers as substrates for cell culture have helped identify critical design parameters and fiber properties that might be useful in 3D. Some of these properties include fiber diameter and density, fiber anisotropy, and fiber stiffness, as well as the incorporation of dynamic complexities, which all are consequential in influencing cell behaviors[45,46] (**Figure 4.1**).

4.3.1. Fiber diameter

Fiber diameter plays a large role in the dimensionality of the fibers as a substrate[71–73] (**Figure 4.1a**). When designing the fiber diameter for a scaffold, a scaling argument is useful to conceptualize how cells will perceive the topography on the resultant fibrous substrate. For example, decreasing fiber diameter (100-300nm) to the same order of magnitude of cells' filopodia (100-200nm)[74] allows for cells to transduce single fiber topography. This concept was demonstrated in notable work by Christopherson et al.[72] where neural stem cells preferentially differentiated into oligodendrocytes on fibers 283nm in diameter because dendrites were able to extend along the fibers. In this same work, fibers 1452nm in diameter potentiated neuronal differentiation due to cells extending along a single fiber longitudinal axis[72]. Bashur and coworkers[75] illustrated a similar result where increasing fiber diameter resulted in increased spindle-shaped morphologies. Interestingly, work from Whited and Rylander[73] showed that fibers with diameters of 1200nm introduced a level of topography that possibly influenced cells to reside within the space between fibers and not extend along fiber axes. Therefore, larger

fiber diameters have the potential to introduce a degree of topography that prevents cells from navigating the substrate during culture.

4.3.2. Fiber density

Another important design criterion in electrospun substrates is the fiber density (**Figure 4.1b**). Electrospun scaffolds are inherently dense networks due to the stochastic deposition of the fibers during the electrospinning process. These dense networks are known to limit cell infiltration and there are numerous strategies to improve porosity of electrospun scaffolds[76]. One notable strategy includes the use of sacrificial fibers – essentially a second electrospinning setup that uses a water-soluble polymer to take up space during scaffold production but washes away upon swelling in aqueous media[77–79]. Other techniques include patterned porosity through fiber crosslinking methods[80], laser ablation[81], and salt leaching[82]. These techniques are well-demonstrated to assist cell infiltration into dense scaffolds to increase the dimensionality of an electrospun substrate. The density of the fiber network has also been shown to be implicated in disease progression. For example, a recent study from Devarasou et al. showed that decreasing the fiber density of the scaffold was correlated with an increased cancer-associated fibroblast activation[83]. Another interesting study demonstrated that cells cultured on less dense scaffolds exhibited a higher propensity for infection with wildtype SARS-CoV-2 than cells on dense scaffolds, suggesting that the biomechanics of the lung (i.e., correlating with lung age) might not be a driving factor behind the higher infection rates of geriatric populations with the virus[84].
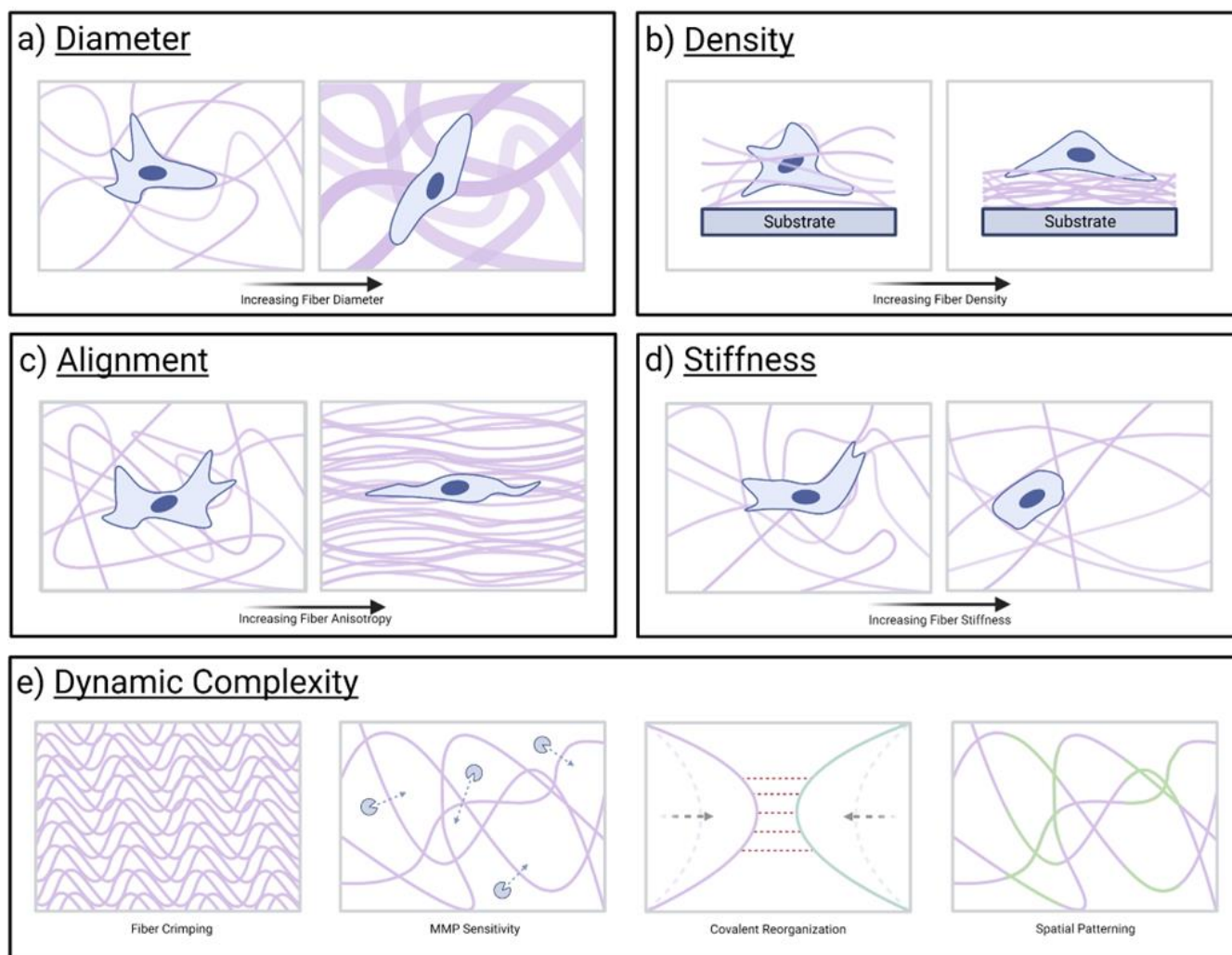
Figure 4.1. Design considerations implicated in the fabrication of electrospun fibers. Overview of the different properties of electrospun fibers that can influence the biophysical and biochemical environment of a cell culture scaffold. (a-d) Properties that are directly related to the precursor solution properties (e.g., concentration, solvent, polymer type, etc.) and electrospinning process parameters (e.g., flow rate, needle gauge, applied voltage, collector type, etc.). Schematics indicate how cells might respond to different presentations of these fiber characteristics. (e) Dynamic properties of electrospun fibers are often added during post-electrospinning processing (except covalent reorganization, which is commonly achieved through reactive groups on the polymer backbone that are presented on fiber surfaces). Schematics inspired by: (a) refs. [71–73,75], (b) refs. [76–79], (c) refs. [85–89], (d) refs. [91–93], and (e) refs. [97–101]. Figure created using BioRender.com.

4.3.3. Fiber alignment

Controlling the alignment of the electrospun fibers has also been shown to influence cell behaviors and morphologies (**Figure 4.1c**). There are a number of

established techniques to align electrospun fibers, but perhaps the most commonly utilized method is to collect the resultant fibers on a rotating surface that is moving at a sufficient linear velocity to induce a parallel orientation. Through the contact guidance conferred by the aligned fibers, cells generally adopt a spindle-like morphology in the direction of fiber anisotropy[85]. These contact guidance signals are also known to assist in potentiating stem cell differentiation[86]. For example, Lim et al.[87] and de Sousa et al.[88] both reported increased beta III tubulin expression (Tuj1) in neural stem cells cultured on aligned electrospun fibers compared to randomized fibers. These physical cues are also established to be a driving factor in cell motility. In one particular study, Sundararaghavan and coworkers[89] demonstrated that fiber alignment had a greater effect on endothelial cell migration than a chemotactic gradient of VEGF, suggesting that topography might be a more powerful driver of migration than growth factor signals. Therefore, the topographical signals and contact guidance conferred by a cell culture system are important considerations when designing an *in vitro* system.

4.3.4. Fiber stiffness

Fiber stiffness is the last intrinsic fiber property that needs to be considered when designing a 2D electrospun substrate (**Figure 4.1d**). Importantly, there is an important distinction between single-fiber mechanics and bulk scaffold mechanics. Due to the nature of the electrospinning process, when a fiber forms due to solvent vaporization, the fiber is considerably more polymer-dense than traditional bulk hydrogels. These fibers overlap to create a network that has different bulk properties compared to single fibers, where single fibers have the potential to be orders of magnitude stiffer than the bulk

fibrous scaffold[90]. A simple way to control fiber stiffness is during the electrospinning process, which is commonly done when electrospinning hydrophobic polymers that offer minimal downstream control over the biophysical properties of the fibers[45]. Leveraging hydrogel-forming biomaterials circumvents this challenge and provides enhanced flexibility in the stiffness of resultant electrospun fibers. It is well established that soft fibers in the scaffold allows for cells to recruit discrete fibers and reorganize the network[91]. Indeed, early work from Baker and coworkers[92] reported a contradictory relationship between fiber stiffness and cell spreading when compared to soft and stiff 2D hydrogels. In a soft fibrous environment, cells were able to recruit fibers locally and increase their spreading and focal adhesion formation – a phenomenon that is the opposite on soft 2D hydrogels, where higher stiffness is generally required to promote cell spreading. This ability to recruit and reorganize fibers has since been demonstrated to enhance cell migration[93], activation of fibroblasts and expression of α-smooth muscle actin in fibrosis models[43,94], vascuologenesis[95], and migration of cells into the depth of thicker electrospun scaffolds[96].

4.3.5. Dynamic complexity in electrospun fibers

Towards utilizing 2D electrospun fibers as more cell-instructive, ECM-mimetic structures, there has been an increased focus on incorporating dynamic complexity into the resultant fibrous scaffolds (**Figure 4.1e**). For example, introducing nonlinear matrix mechanics to 2D electrospun scaffolds is achievable through "crimping" the fibers in the scaffold, which was done through heat treatment of polyester fibers[97] or through the selective conjugation of a hydrophilic peptide to hydrogel fibers[98]. Cell-responsive

sources of dynamic complexity have also been introduced through advanced crosslinking strategies. To this end, protease-sensitive hydrogel fibers have been developed using a matrix metalloproteinase-cleavable crosslinker molecule to allow for cell-mediated degradation of individual fibers[99]. Additionally, Davidson and coworkers[100] utilized hydrogel fibers that presented hydrazone-forming moieties to allow cells to recruit those fibers and covalently remodel the network. Another source of complexity is through the spatiotemporal presentation of biomolecules to the environment[101]. Perhaps the most common technique for achieving this is through spatially-controlled thiol-ene coupling chemistries[102–104], and these biomolecules are tunable to allow for user-defined temporal release[104]. Localizing the presentation of cell-instructive molecules, like adhesive ligands, enables precise specification of the cellular microenvironment. These spatiotemporal control mechanisms are designed to provide flexibility when engineering electrospun fibers that permit dynamic complexity in the resultant scaffold.

4.3.6. Electrospun fiber design summary

While the discussed examples are nowhere near exhaustive, they highlight the flexibility involved when designing electrospun fibers for use in 2D culture scaffolds. However, endogenous ECM exists in 3D, with considerable dynamic complexities that influence cell behaviors in the milieu, thereby motivating the desire to translate electrospun fibers into 3D. Here, we group the current methods that utilize electrospun fibers in 3D within 3 groups: (1) thick electrospun scaffolds via increased fiber density or multiple layered meshes, (2) fiber:hydrogel composite macrostructures, and (3) electrospun fibers within hydrogel microparticle systems. Hereafter, we aim to provide an

overview of the seminal works in these groups to inform the next stage of electrospun fibers in 3D.

4.4. Thick electrospun scaffolds via increased fiber density or layered constructs

4.4.1. Thick fibrous scaffolds via increased fiber deposition

It was previously discussed that a traditional electrospun scaffold has minimal dimensionality as the deposited scaffolds are 2D at the meso- and macroscale. Perhaps the simplest strategy to introduce the third dimension to these scaffolds is to develop thicker meshes through either increasing fiber density by electrospinning for longer periods of time or layering multiple meshes to build a 3D scaffold from the bottom up. Increasing the duration of the electrospinning process will inherently allow for more fibers to deposit on the collection surface, thereby building out the scaffold in 3D space where thickness is dictated by process time (**Figure 4.2a**). There are numerous studies that leverage thicker electrospun scaffolds for cell culture applications[76,96,105–107]. Interestingly, when the thickness of the scaffold is increased, it provides the opportunity to modulate the composition of the resultant fibers. For example, haptotactic gradients can be introduced throughout the thickness of electrospun meshes to enhance cellular infiltration into the scaffold[106]. This increased complexity demonstrates a possible avenue to control the biochemical profile of thick electrospun meshes. It is important to note, however, that the degree of porosity is a pervasive challenge in thick electrospun scaffolds. Strategies to surmount this challenge include modulating the fiber diameter and packing density[76], selective protease degradation and sacrificial fibers[107], and selective crosslinking to incorporate macroscale porosity[80]. While these thick, 3D scaffolds aim to increase the

dimensionality of traditional 2D electrospun fibers, they are still commonly utilized as substrates where cells are seeded on top of the scaffold and metrics like cell invasion are investigated.
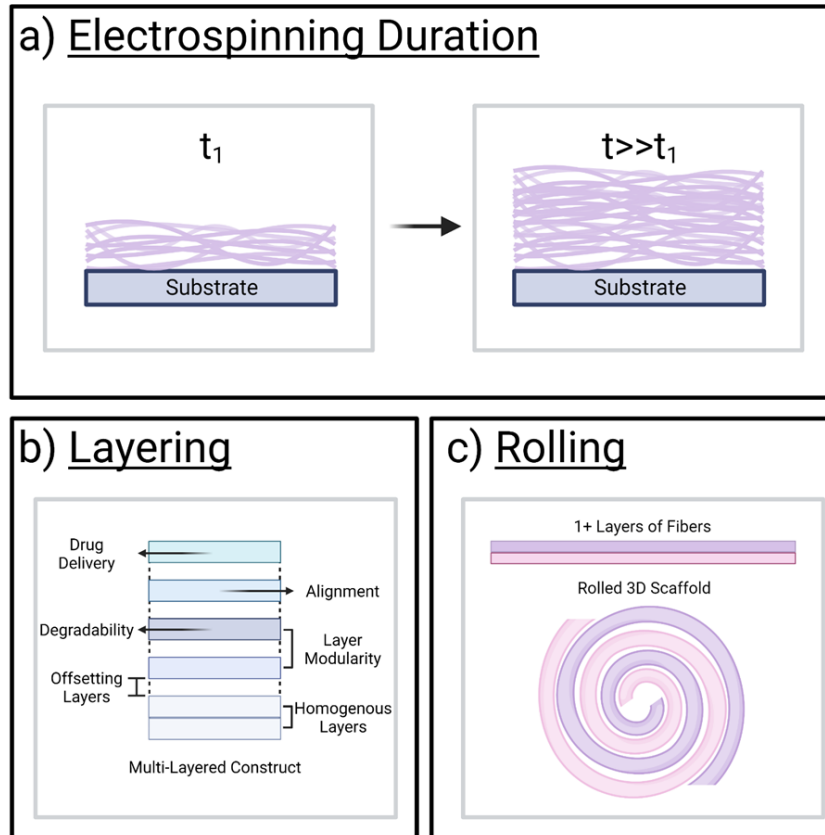
Figure 4.2. Thick electrospun scaffolds via increasing fiber deposition or layering of multiple scaffolds. Early iterations of 3D electrospun fibers leveraged thicker scaffolds to increase the dimensionality of the traditional 2D scaffolds. (a) Perhaps the simplest strategy to fabricate a thick electrospun mesh is to increase the duration of the electrospinning process, and thus the fiber deposition onto the collection surface. (b) Layer-by-layer addition of electrospun scaffolds enables a modular design approach to thick electrospun scaffolds, where each layer can present different biophysical cues (e.g., alignment, etc.) and biochemical cues (e.g., drug delivery, degradability, etc.). (c) Rolling a scaffold with 1+ layers enables a 3D construct that might be useful for a variety of different tissue engineering applications. A cylindrical scaffold comprised of different layers still affords the modularity associated with other layer-by-layer strategies, but also provides an additional level of biomimicry by recapitulating the structural features of cylindrical systems (e.g., vasculature). Schematics inspired by: (a) refs. [76], (b) refs. [121,125–127,130], (c) refs. [115,116,123]. Figure created using BioRender.com.

4.4.2. Thick electrospun scaffolds via layering multiple discrete meshes

Stacking of multiple individual electrospun scaffolds is an extension of thick fibrous meshes that allows for additional control by designing each layer within the thick scaffold. This is most commonly achieved through layering multiple individual scaffolds together[108–114] or rolling a singular scaffold to form circular layers[115,116] (**Figure 4.2b-c**). These layers can be self-supported or held together via supramolecular interactions that support adhesion between layers[117]. In one example, Orr and coworkers demonstrated that layering multiple aligned PCL meshes increased the tensile strength of the scaffold while also promoting the deposition of collagen I from human adipose-derived stem cells. This strategy suggests better clinical translation by engineering physiologically-relevant sizing of the constructs that are designed to supplement tendon tissue engineering[118], thereby exemplifying the advantages of a layer-by layer approach with electrospun meshes.

Perhaps the most intriguing and powerful strength of the layer-by-layer approach is the capacity for modular design. Each layer has the capability to be individually designed to contribute a unique aspect to the overall 3D scaffold. In the simplest form, this can be achieved by controlling the types of fibers within each layer and the cell types seeded on each layer[114], with the ability to create cell-dense constructs throughout Z-space via layers of confluent cells on fibers[119]. However, the aforementioned design parameters for electrospun fibers are all implicated when constructing a 3D matrix via layer-by-layer assembly. For example, the contact guidance cues that cells transduce within their local microenvironment can be directly specified by the fiber diameter[120] and fiber alignment[121,122] used for that specific layer of the overall scaffold. Inspired by this,

144

Yang et al.[121] demonstrated the ability to dictate cell directionality by solely changing the angle of aligned fibers within each layer of a scaffold. Additionally, Kim and coworkers[123] developed a novel nerve-guide conduit via rolling an electrospun mesh with spatially-controlled alignment. In this example, the inside of the conduit presented aligned fibers to promote directional cell growth, with outer layers comprised of randomized fibers to increase the mechanical fidelity of the overall structure[123].

The capacity for modular design also enables the specification of dynamic complexities into the overall scaffold. A common platform for introducing dynamic complexity is via controlling the degradation profile of the fibers to enhance integration *in vivo*[124]. Yu et al. implemented this concept via rolling five different layers of PLGA fibers where the ratio of PLA:PGA was modulated to tune the degradation time scale within each layer[125]. This rolled structure was designed as a nerve guide conduit that would enable degradation from inside-out to prevent collapse of the conduit during nerve regeneration. Another notable avenue for dynamic complexity in layered electrospun scaffolds is incorporating controlled release profiles for delivery of bioactive molecules. For example, a layer of fibers can be electrospun containing bioactive cargo that will release over time due to diffusion into aqueous media when the scaffold is hydrated. Interestingly, Kamath et al.[126] and Yu et al.[127] demonstrated increased control over the initial burst and long-term cumulative release profiles of biomolecules via protection of the cargo-containing fibers with layers of hydrophobic PCL fibers to slow diffusion. Other examples of dynamic complexity in layered scaffolds include the use of stimuli-responsive layers. To this end, Cho and coworkers[128] reported a modular design of tri-layered

scaffolds where each layer could individually respond to changes in temperature and pH to engineer smart soft actuators for a variety of applications.

Utilizing layered electrospun fibers to form 3D scaffolds allows for considerable control over the biophysical and biochemical compositions of the resultant constructs. While only briefly outlined here, strategies to build a layer-by-layer *in vitro* model are widely applicable. Through careful design of the individual fibers that comprise each layer (i.e., polymer choice, fiber stiffness, alignment, dynamic complexities, etc.), a tissue-specific *in vitro* construct can be easily engineered. Although, it is important to note that the porosity of the overall construct remains a pervasive challenge. Similar to electrospinning 2D scaffolds or thick 3D scaffolds, the density of the deposited fibers often yields sub-cell scale porosity, thereby limiting cell infiltration and migration[129]. Strategies to circumvent this include offsetting layers of fibers to provide space between layers for cells to navigate[130] or utilizing mesh collectors to modulate fiber density within each layer[131]; however, simple methods to directly control porosity in layered electrospun scaffolds remains challenging.

4.4.3. Thick electrospun scaffolds summary

There is considerable demonstrated utility of thick electrospun scaffolds fabricated via extended electrospinning times or multiple layers of 2D scaffolds, but they neglect to recapture many of the important features of the ECM. Notably, these scaffolds are comprised completely of fibrous polymers, which is not necessarily representative of tissue composition *in vivo*. Most tissue types contain a fibrous reticular network with a water-swollen hydrogel component dispersed between the fibrous proteins[6,48]. Therefore,

146

to faithfully recapitulate the ECM microenvironment *in vitro*, a combination of hydrogel and fibrous components are needed. In line with this, there are many demonstrated platforms to incorporate electrospun fibers in 3D in combination with hydrogel components.

4.5. Electrospun fiber:hydrogel composite structures for 3D tissue models

4.5.1. Encapsulating continuous fibrous scaffolds in 3D hydrogels

Electrospun fiber:hydrogel composite structures are an emerging platform to engineer 3D tissue models due to their ability to more closely recapitulate the microarchitecture of the ECM. Early iterations of these composite structures utilized traditional 2D electrospun scaffolds and encapsulated them within a hydrogel matrix to form a 3D construct (**Figure 4.3a**) strategies that successfully incorporate electrospun fibers within a fibrous matrix. Examples of these methods in practice include encapsulating rolled electrospun meshes within a hydrogel for coronary artery bypass grafts[132], multilayered scaffolds bound together using a crosslinked hydrogel[133], and homogeneous distribution of sectioned fibrous scaffolds within a hydrogel[134]. These approaches leverage the innate topography of electrospun fibers along with the contribution of fibers to the tensile strength and complex mechanics of the 3D hydrogel[132]; however, the dimensionality of the overall construct is typically dictated by the hydrogel with the fibers contributing in a quasi-2D role.

To address this, modified encapsulation techniques have been employed to enable the fibers to contribute throughout the entire hydrogel in 3D. For example, Ekaputra and coworkers[135] leveraged a dual-deposition process where PCL/collagen fibers were

electrospun onto a rotating mandrel along with simultaneous electrospraying of a hyaluronic acid hydrogel derivative. The electrosprayed hyaluronic acid introduced space between the fibers while also enabled the creation of a 3D construct that enabled increased cellularization[135]. Other techniques include utilizing core-shell electrospun fibers where a gelatin shell would enable *in situ* hydrogel encapsulation of the core fibers through gelatin network formation[136], as well as leveraging modified electrospinning setups to enable uniform distribution of fibers in a hydrogel network[137]. Importantly, a uniform distribution of fibers within a hydrogel, regardless of the encapsulation technique, introduces ECM-mimetic structural and interstitial hydrogel characteristics to the engineered environment, with fibers reinforcing the mechanical properties of the resultant construct[137].
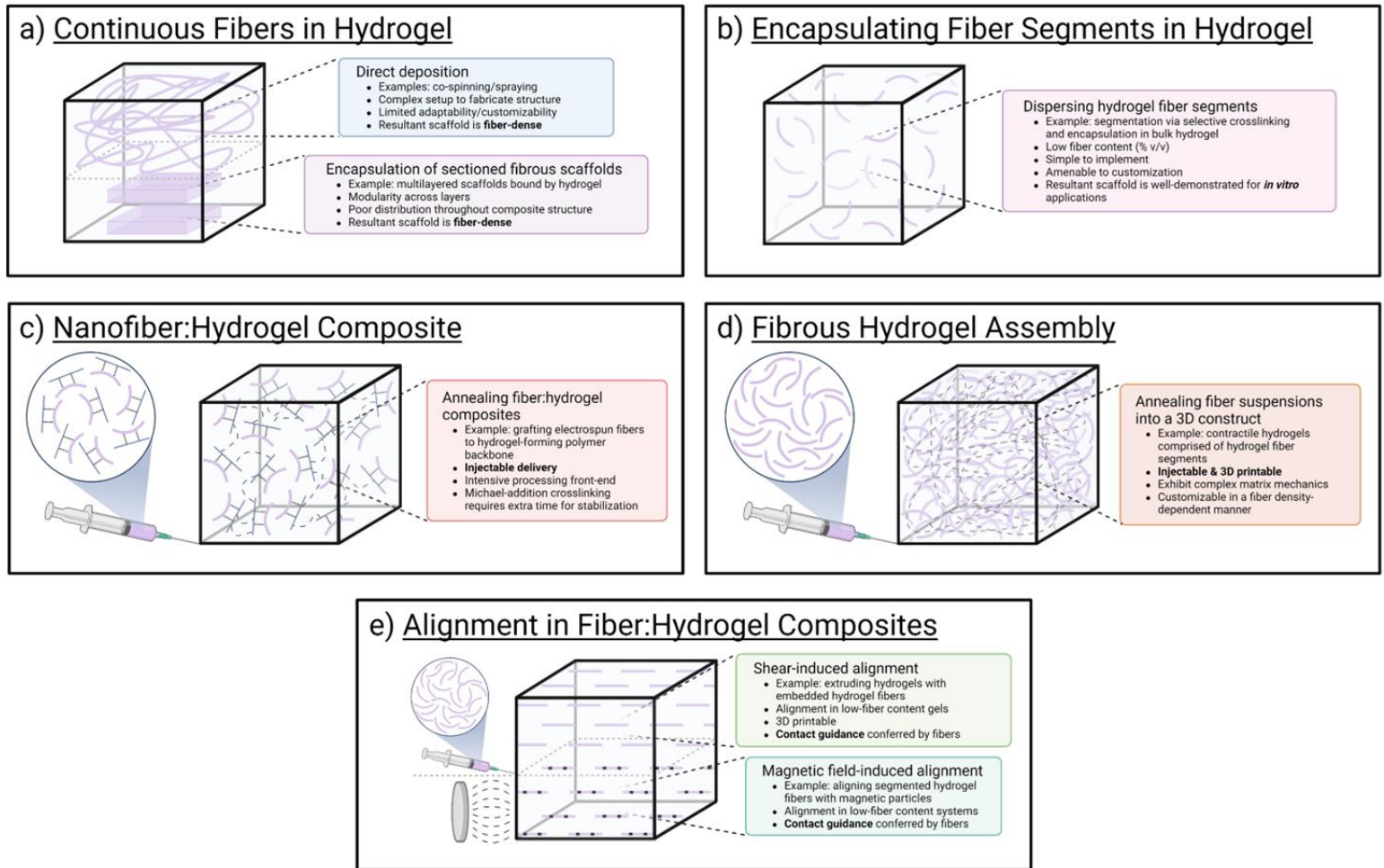
Figure 4.3. Electrospun fiber:hydrogel composite structures for 3D tissue models. (a) The simplest strategy to incorporate electrospun fibers into a 3D bulk hydrogel is to utilize continuous fiber meshes and encapsulate them in hydrogel. This can also be done on-the-fly during the electrospinning process where a second polymer is electrosprayed, yielding droplets of hydrogel that encompass the fibers – thereby simultaneously building out the fiber and hydrogel components of the construct over time. (b) Encapsulating fiber segments in hydrogel is perhaps a more biomimetic strategy to utilize electrospun fibers in 3D. These fiber segments are incorporated at low volume and used to study how cells respond to fibrous cues in bulk hydrogel (e.g., *in vitro* modeling of fibrosis). (c) Nanofiber:hydrogel composites are similar to the previous strategy of encapsulating fiber segments, except this platform grafts fibers to a hydrogel-forming polymer's backbone, which directly incorporates the fibers into the crosslinking process. A significant advantage of this platform is that it adds segmented fibers to an injectable hydrogel system, thereby providing a minimally-invasive delivery mechanism for *in vivo* studies. (d) Fibrous hydrogel assemblies illustrate a flipped version of the previous strategies, where the electrospun fibers comprise the majority of the scaffold, with a crosslinking molecule in between fibers to covalently immobilize the network. This system is similarly injectable, which enables 3D printing for complex *in vitro* structures, and the potential for *in vivo* delivery. Notably, the high-fiber content of these scaffolds enables contractile cell types

to recruit individual fibers and locally reorganize their microenvironment. (e) There are also demonstrated biofabrication platforms to align fibers within 3D bulk hydrogels to confer anisotropy to cells cultured in the environment. For example, 3D printing of fiber-hydrogel solutions enables shear-induced alignment of the fibers in the hydrogel following crosslinking. This same anisotropy can be achieved through magnetic alignment of fibers if the electrospun fibers were designed to contain magnetic particles during the fabrication step. Schematics inspired by: (a) refs. [133–135,138], (b) refs. [139–141], (c) refs. [142–144], (d) refs. [145], and (e) refs. [146–148]. Figure created using BioRender.com.

4.5.2. Encapsulating fiber segments in 3D hydrogels

Leveraging encapsulated electrospun fibers indeed recapitulates ECM-mimetic structural context in engineered *in vitro* constructs; however, the presence of fibrous proteins within the native ECM can be more complex and not necessarily analogous to directly incorporated continuous electrospun networks. For example, the collagen protein fibers within endogenous ECM environments are ~3-22 μm in length[149] and ~300-900 nm in diameter[32]. In response, to mimic the fibrous microarchitecture of natural tissue more accurately, researchers have shifted towards utilizing segmented electrospun fibers that are uniformly encapsulated in 3D bulk hydrogels. Strategies for this include embedding small quantities of electrospun fiber segments into traditional bulk hydrogels, grafting hydrogel backbones to fiber segments, and annealing individual fibers together to form a 3D bulk construct.

4.5.3. Embedding electrospun fiber segments into 3D bulk hydrogels

An emerging strategy to incorporate a fibrous component to ECM models is to utilize short electrospun fiber segments that are embedded within a bulk hydrogel (**Figure 4.3b**). When utilized in small quantities, embedded fiber segments add a fibrous component to traditional hydrogels while conserving the interstitial hydrogel matrix between fibers. Importantly, similar to rebar in concrete, the addition of these electrospun fiber segments can bolster the mechanical properties of the hydrogel when compared to its purely continuous analog[150,151]. From a physiological perspective, these fibers mimic the architecture of natural tissues at low fiber content and can model a pathogenic environment simply by increasing fiber content within the matrix[139]. Indeed, embedded

fiber segments have been shown to affect cell spreading in 3D environments in a fiber density-dependent manner that is statistically significant compared to a bulk hydrogel without embedded fibers[140,141]. These engineered constructs are able to model a pro-fibrotic environment where upregulation of yes-associated protein (YAP) expression – a marker associated with fibrosis progression – is casually related to increased fiber content within the construct[139,140]. While these constructs are well demonstrated as models of fibrosis, their utility extends far past this pathology. Indeed, recent work has shown that embedded fibers can mediate cell spreading in the wound healing space through Rho GTPase activity[152], and can also model the peritumoral environment to study epithelial-mesenchymal transition and cellular migration[153]. In addition to the examples provided, this established strategy to model the 3D ECM is generalizable and can be leveraged to recapitulate virtually any tissue system of interest due to the direct control over fiber content and interstitial hydrogel mechanical and chemical properties.

4.5.4. Grafting hydrogel-forming polymers to electrospun fiber segments

Another promising technology platform to incorporate fibrous topography within 3D hydrogels is to covalently bond segmented fibers to the hydrogel-forming polymer backbone (**Figure 4.3c**). Similar to previous strategies where fiber segments are embedded in the bulk hydrogel, grafting electrospun fibers to the hydrogel backbone significantly increases the storage moduli of the resultant constructs[142] – a result that is consistent with the known mechanical contributions that fibers add to native tissue. Perhaps the most intriguing aspect of this platform is its injectability, which enables a targeted and minimally-invasive delivery mechanism[142]. Critically, fibers that are not

grafted to the polymer backbone were observed to phase separate out of the bulk hydrogel, thereby highlighting the importance of chemical conjugation between the fibers and the interstitial hydrogel matrix[142]. In this example, Li et al. utilized carboxyl-modified PCL fibers to introduce a maleimide to the fiber surface that would react with a HA-SH/PEGDA hydrogel system to covalently graft fibers within the hydrogel[142]. However, it is worth noting that this is likely attainable through many other chemistries. Conceivably, electrospun hydrogels that possess reactive moieties on their surface could covalently interact with bulk hydrogel solutions to achieve a similar suspension of fibers grafted to the bulk 3D hydrogel construct.

These injectable, nanofiber-laden constructs have a wide array of established applications. They were originally investigated as scaffolds to augment soft tissue regeneration, with demonstrated ability to promote pro-regenerative macrophage phenotypes and functional angiogenesis in a rat model[142]. Since, there has been considerable work extending the utility of these composite structures to other tissue systems. One particularly interesting example is the application of this platform to promote regeneration in a spinal cord contusion model. In this study, the injectable electrospun fiber:hydrogel composite was introduced to a spinal cord injury to assess its ability to promote neural tissue regeneration[143]. Similar to previous reports, the injected scaffold promoted a pro-regenerative macrophage polarization, which in turn yielded increased angiogenesis and axon and neuron presence compared to controls. While this fiber:hydrogel composite structure provided mechanical support to the injury area and promoted a pro-regenerative environment, it did not result in any measurable functional recovery, suggesting that improvements are still needed to provide both structure and

function to spinal cord injuries[143]. This study was extended to also deliver MSCs along with the fiber:hydrogel composite to investigate their ability to augment repair of spinal cord injuries[144]. The inclusion of MSCs indeed resulted in increased presence of axons and astrocytes compared to just the fiber:hydrogel composite; however, MSCs were still unable to improve functional recovery, continuing to suggest that advances are still needed when using these composites as injectable therapeutics[144]. In addition to these examples, this particular suite of fiber:hydrogel composites has also seen use in the treatment of Crohn's disease-related fistulas[154] and has also been enhanced with fractionated fat to further promote a pro-regenerative environment upon delivery[155].

4.5.5. Crosslinking discrete electrospun fiber segments into a bulk construct

The previously described fiber:hydrogel composites relied on the hydrogel contribution as the main component of the overall 3D construct. Conversely, an emerging fiber:hydrogel composite platform utilizes electrospun hydrogel fibers as the backbone of the 3D scaffold with annealing achieved via incorporation of a crosslinking molecule[145] (**Figure 4.3d**). In this design, the hydrogel fibers are crosslinked together to form a 3D construct that is amenable to contracting under cell-relevant forces. Davidson et al.[145] demonstrated that different fiber densities within the hydrogel assembly dictated the ability for cells to contract the overall scaffold. This contraction behavior was due to the ability of cells to exert traction forces and recruit fibers, thereby locally stiffening the matrix – characteristics that are advantageous for modeling the ECM during development and pathogenic progression (e.g., fibrosis)[145]. These fiber:hydrogel composites represent

154

another platform to introduce dimensionality to electrospun fibers where high fiber contents are desired in the resultant construct, with many potential biological applications.

4.5.6. Alignment within electrospun fiber:hydrogel composites

Fiber:hydrogel composites are a versatile suite of biofabrication platforms that enable modeling the ECM *in vitro* with physiologically-relevant fiber content and complex matrix mechanics. Advances in these technologies have enabled alignment of the fiber component of the hydrogel to mimic the anisotropic nature of many tissue types (e.g., muscle tissue) (**Figure 4.3e**). Previously described work has demonstrated that fibers within fiber:hydrogel composite assemblies can undergo alignment when strains are introduced to the system[145]. There has been some additional work aiming to provide user-defined control over alignment of the fibrous component directly through the biofabrication process. Prendergast and coworkers have demonstrated a 3D printable bioink that contains short fiber segments that undergo shear-induced alignment during the printing process[146]. This platform was further extended to culture meniscal constructs where the contact guidance from anisotropic fibers within the printed material yielded increased cell and collagen alignment[147]. Hiraki et al. developed another interesting strategy to align fibers within a fiber:hydrogel composite structure[148]. Here, magnetic particles were incorporated into electrospun fibers that were segmented and encapsulated within a bulk hydrogel. These fibers were observed to undergo alignment within the hydrogel upon introduction of a magnetic field[148]. These strategies are advantageous as they are accessible methods to introduce alignment within fiber:hydrogel composite structures that aim to model tissues where anisotropy is a critical attribute.

4.5.7. Electrospun fiber:hydrogel composite summary

Electrospun fiber:hydrogel composite structures are a continuously evolving class of biofabrication platforms that offer many advantages when engineering ECM-mimetics. The fibers within the hydrogel contribute to the overall mechanics and provide adhesion sites for cells to engage – analogous to fibrous proteins in native tissue. Embedded fibers within bulk hydrogels offer an attractive method for modeling both healthy tissue and disease progression through both randomized and aligned orientations, with injectable composites providing an interesting platform for wound regeneration. While these technologies offer great advantages to traditional hydrogel culture, they are still in their relative infancy, and there is room for enhancements as the platforms are adapted to model additional tissue systems *in vitro* or applied to support functional regeneration to new injury models *in vivo*.

4.6. Electrospun fiber-based granular hydrogel systems

4.6.1. Layered electrospun fibers within hydrogel microparticles

Granular hydrogels are an attractive class of biomaterials due to their vast array of applications in the tissue engineering and regenerative medicine spaces – serving as platforms for extrusion printing and injecting, as well as permissive environments for 3D cell culture[156–158]. These hydrogel systems offer many advantages over traditional 3D bulk hydrogels, including more direct control over porosity and scaffold mechanics which are tunable through individual hydrogel microparticle (HMP) design[159]. Recent works with HMPs have begun to incorporate electrospun fibers to increase the dynamic complexities of granular hydrogel scaffolds. For example, an interesting study utilized a layer-by-layer

approach of electrospun fibers and hydrogel to introduce modularity within individual HMPs[160]. Importantly, traditional HMPs are advantageous due to their capacity for modular design by mixing different types of HMPs within a single system[161,162]; however, Cho and coworkers were able to leverage the different layers of electrospun fibers to introduce modularity within each HMP and this strategy was applied to deliver two different growth factors simultaneously[160] (**Figure 4.4a**).
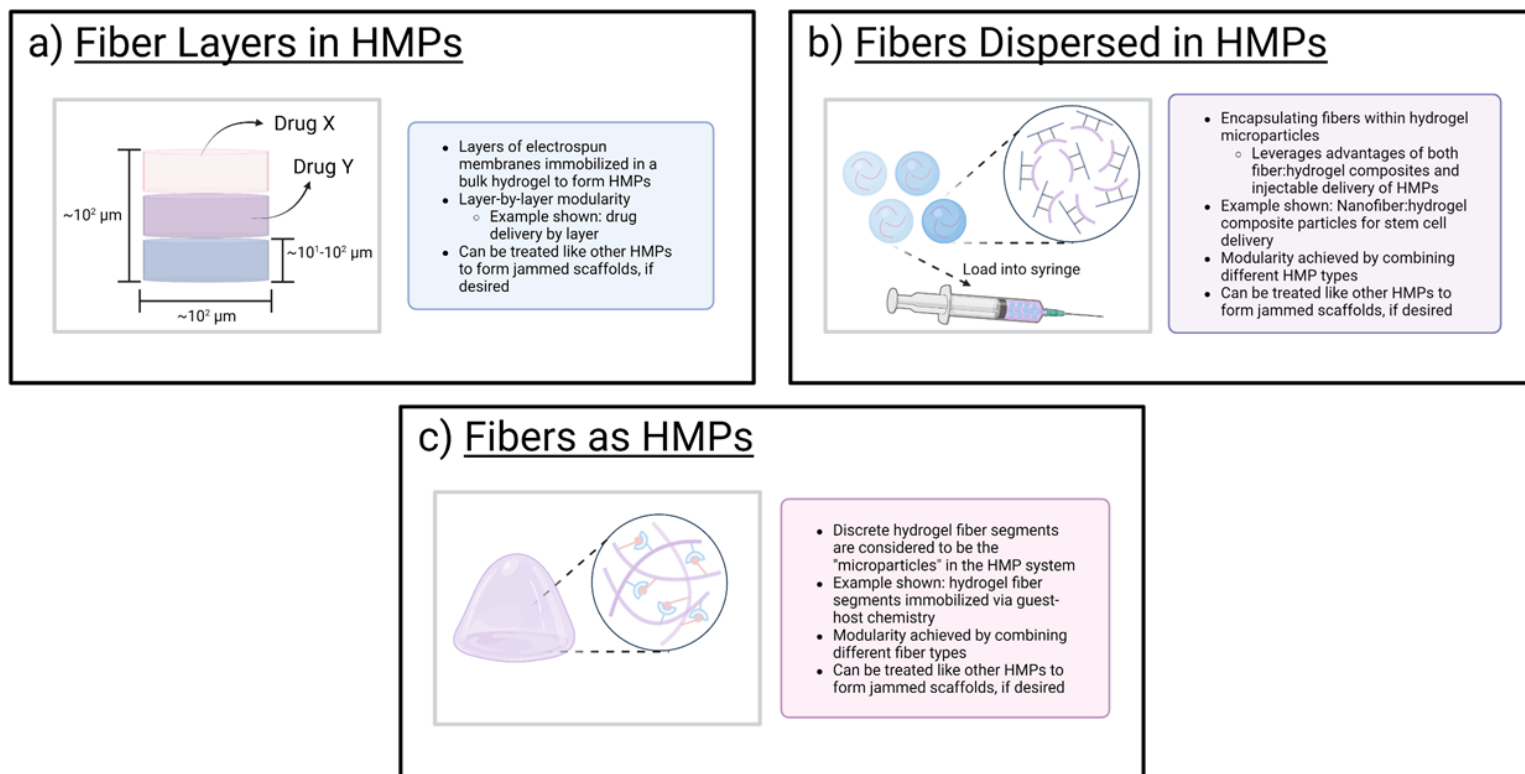
Figure 4.4. Electrospun fiber-based granular hydrogel systems. (a) HMPs constructed of different layers of electrospun fibers enable the same modularity as layer-by-layer 3D electrospun meshes, just in the context of HMPs. These layers can be used to toggle different drug delivery profiles within each HMP, and resultant particles can theoretically be utilized like other HMPs (e.g., injectable slurry, jamming, etc.). (b) Fibers dispersed in HMPs achieve the same advantages of the nanofiber:hydrogel composite previously described, with better injection properties due to the fragmented nature of the hydrogel when compared to the previous iteration of the composite hydrogel. (c) Segmented hydrogel fibers as the "particles" in HMP systems demonstrate favorable injectability as tissue culture scaffolds as well as unique properties when utilized as granular hydrogel scaffolds. Schematics inspired by: (a) refs. [160], (b) refs. [163], and (c) refs. [167,168]. Figure created using BioRender.com.

4.6.2. Hydrogel microparticles with dispersed electrospun fibers

HMPs have also been designed to encapsulate dispersed fiber segments, where the advantages of fibers embedded within a bulk hydrogel are combined with the advantages associated with HMPs. Important work from Yao et al.[163] demonstrated that mechanically fragmented HMPs comprised of PCL fibers grafted to a hyaluronic acid hydrogel backbone show enhanced injectability while promoting a pro-regenerative environment when delivered with MSCs *in vivo*. This study illustrates the ability to adapt the previously described fiber:hydrogel composites[142] as a granular hydrogel media via mechanical fragmentation into individual microparticles. Electrospraying is another accessible biofabrication platform that, when combined with segmented electrospun fibers, can yield HMPs with encapsulated fibers. This class of fiber-containing HMPs has shown considerable promise as a stem cell delivery mechanism[164], a platform for directing cell behavior via presentation of bioactive peptide motifs[165], and a scaffold that promotes cell infiltration and tissue integration when applied *in vivo*[166].

4.6.3. Segmented electrospun hydrogel fibers as the "grains" in granular hydrogel systems

The last major class of electrospun fibers applied in granular hydrogel systems is when the individual "grain" of the granular hydrogel is a segmented fiber. Analogous to spherical microparticles, segmented electrospun fiber lengths are packed together to form a 3D bulk hydrogel construct. Miller et al. demonstrated the utility of a fiber-based granular hydrogel stabilized via supramolecular interactions where adamantane-modified fibers were mixed with β-cyclodextrin- modified fibers to form a robust 3D hydrogel network that

promoted MSC spreading and elongation[167]. This platform was extended *in vivo* and encapsulated in a degradable interstitial hydrogel prior to injection into a pelvic organ prolapse injury model to augment tissue repair[168]. Additional work from our lab has shown that segmented electrospun fibers entangle when packed together via centrifugation and behave like a robust 3D hydrogel at rest but exhibit interesting mechanical properties when the scaffold is perturbed – such as injectability and extensibility of the material, with shear-induced alignment of fibers occurring during extrusion printing that confers contact guidance cues to cells seeded on printed filaments[169]. This work was furthered to demonstrate the utility of packed electrospun microfibers as a permissive granular hydrogel for 3D cell culture. Indeed, these systems are tailorable to model the viscoelasticity of native tissue and recapitulate complex matrix mechanics like stress dissipation properties characteristic to many tissue types *in vivo*[169].

4.6.4. Electrospun fiber-based granular hydrogel systems summary

Applying electrospun fibers to granular hydrogel systems offers considerable advantages to engineering ECM-mimetic biomaterials scaffolds. The modularity offered by layer-by-layer assembly of HMPs[160] and the topography provided when incorporating dispersed fiber segments within HMPs[163–166] enable a more ECM-like context when utilizing granular hydrogels to model tissues *in vitro*. However, perhaps the most interesting use of electrospun fibers in granular hydrogels is when segmented hydrogel fibers are treated as "grains" and packed together to form 3D hydrogel environment[167–169]. These scaffolds are shown to be easily modified to model various tissue mechanics with controlled topography, thereby illustrating their wide range of utility when modeling

the ECM *in vitro*. While this platform is still rapidly evolving, preliminary demonstrations suggest their efficacy in tissue-mimetic scaffolds *in vitro*.

4.7. Moving forward in 3D electrospun fiber design

Applying electrospun fibers in 3D contexts is a growing field that has major implications in tissue engineering and regenerative medicine spaces. While early iterations focused on "thick" scaffolds via extended electrospinning durations and layering of multiple scaffolds, they often contain supraphysiological fiber densities and nanoscale porosities that frustrate the ability to utilize these scaffolds both *in vitro* and *in vivo*. Bulk fiber:hydrogel composites are promising biofabrication platforms to model both healthy and pathogenic ECM *in vitro* or support tissue regeneration *in vivo*. Similarly, electrospun fibers within granular hydrogel systems have demonstrated utility in both modeling tissue *in vitro* and supporting tissue regeneration *in vivo*. However, these biofabrication techniques are still in their infancy and further studies are needed to extend their applicability to other tissue models.

In the future, fiber:hydrogel composites and fiber-based granular hydrogel assemblies can be applied to new tissue systems in addition to the already established *in vitro* and *in vivo* applications. Virtually all tissue types contain some form of fiber content with varying levels of anisotropy, suggesting the utility of these techniques to study both healthy and diseased tissue models. Additionally, when applied *in vivo* to augment tissue repair, further advancements are needed to provide both structure and function, with functional regeneration currently remaining elusive. Perhaps more studies into modifying the biochemical and biophysical profiles, along with the dynamic complexities of the fiber-

containing scaffolds based on different fiber/hydrogel design considerations can further enhance the endogenous regeneration cascade and reestablish function to different damaged tissue models – a hurdle that must be cleared prior to clinical translation.

Overall, while we continuously improve fiber:hydrogel composites and fiber-based granular hydrogel scaffolds, we must also surmount the critical step forward of simplifying the accessibility of electrospinning and hydrogel formation. This will allow for the biofabrication platforms described herein to be readily adopted by both tissue engineers and non-tissue engineers alike.

4.8. References

(1)   Khademhosseini, A.; Langer, R. A Decade of Progress in Tissue Engineering. *Nat. Protoc.* **2016**, *11* (10). https://doi.org/10.1038/nprot.2016.123.

(2)   Burdick, J. A.; Murphy, W. L. Moving from Static to Dynamic Complexity in Hydrogel Design. *Nat. Commun.* **2012**, *3*, 1–8. https://doi.org/10.1038/ncomms2271.

(3)   Kim, Y.; Ko, H.; Kwon, I. K.; Shin, K. Extracellular Matrix Revisited: Roles in Tissue Engineering. *Int. Neurourol. J.* **2016**, *20*, 23–29.

(4)   Moroni, L.; Burdick, J. A.; Highley, C.; Lee, S. J.; Morimoto, Y.; Takeuchi, S.; Yoo, J. J. Biofabrication Strategies for 3D in Vitro Models and Regenerative Medicine. *Nat. Rev. Mater.* **2018**, *3*, 21–37. https://doi.org/https://doi.org/10.1038/s41578-018-0006-y.

(5)   Saraswathibhatla, A.; Indana, D.; Chaudhuri, O. Cell – Extracellular Matrix Mechanotransduction in 3D. *Nat. Rev. Mol. Cell Biol.* **2023**, *24*, 495–516. https://doi.org/10.1038/s41580-023-00583-1.

(6)   Frantz, C.; Stewart, K. M.; Weaver, V. M. The Extracellular Matrix at a Glance. *J. Cell Sci.* **2010**, *123* (24), 4195–4200. https://doi.org/https://doi.org/10.1242/jcs.023820.

(7)   Hynes, R. O. The Extracellular Matrix: Not Just Pretty Fibrils. *Science (80-.).* **2009**, *326* (5957), 1216–1219. https://doi.org/10.1126/science.1176009.

(8)   Geckil, H.; Xu, F.; Zhang, X.; Moon, S.; Demirci, U. Engineering Hydrogels as Extracellular Matrix Mimics. *Nanomedicine (Lond)* **2011**, *5* (3), 469–484. https://doi.org/10.2217/nnm.10.12.Engineering.

(9)   Miller, A. E.; Hu, P.; Barker, T. H. Feeling Things Out: Bidirectional Signaling of the Cell–ECM Interface, Implications in the Mechanobiology of Cell Spreading, Migration, Proliferation, and Differentiation. *Adv. Healthc. Mater.* **2020**, *9* (1901445), 1–24. https://doi.org/10.1002/adhm.201901445.

(10)   Baker, B. M.; Chen, C. S. Deconstructing the Third Dimension – How 3D Culture Microenvironments Alter Cellular Cues. *J. Cell Sci.* **2012**, *125* (13), 3015–3024. https://doi.org/https://doi.org/10.1242/jcs.079509.

(11)   Lutolf, M. P.; Hubbell, J. A. Synthetic Biomaterials as Instructive Extracellular Microenvironments for Morphogenesis in Tissue Engineering. *Nat. Biotechnol.*

2005, *23*, 47–55. https://doi.org/https://doi.org/10.1038/nbt1055.

(12) Caliari, S. R.; Burdick, J. A. A Practical Guide to Hydrogels for Cell Culture. *Nat. Methods* **2016**, *13* (5), 405–414. https://doi.org/10.1038/nmeth.3839.

(13) Tibbitt, M. W.; Anseth, K. S. Hydrogels as Extracellular Matrix Mimics for 3D Cell Culture. *Biotechnol. Bioeng.* **2009**, *103* (4), 655–663. https://doi.org/https://doi.org/10.1002/bit.22361.

(14) Correa, S.; Grosskopf, A. K.; Hernandez, H. L.; Chan, D.; Yu, A. C.; Stapleton, L. M.; Appel, E. A. Translational Applications of Hydrogels. *Chem. Rev.* **2020**. https://doi.org/10.1021/acs.chemrev.0c01177.

(15) Burdick, J. A.; Prestwich, G. D. Hyaluronic Acid Hydrogels for Biomedical Applications. *Adv. Healthc. Mater.* **2011**, *23* (12), H41–H56. https://doi.org/10.1002/adma.201003963.

(16) Highley, C. B.; Prestwich, G. D.; Burdick, J. A. Recent Advances in Hyaluronic Acid Hydrogels for Biomedical Applications. *Curr. Opin. Biotechnol.* **2016**, *40*, 35–40. https://doi.org/10.1016/j.copbio.2016.02.008.

(17) Aisenbrey, E. A.; Murphy, W. L. Synthetic Alternatives to Matrigel. *Nat. Rev. Mater.* **2020**, *5* (7), 539–551. https://doi.org/10.1038/s41578-020-0199-8.Synthetic.

(18) Sands, R. W.; Mooney, D. J. Polymers to Direct Cell Fate by Controlling the Microenvironment. *Curr. Opin. Biotechnol.* **2007**, *18* (5), 448–453.

(19) Zhang, K.; Feng, Q.; Fang, Z.; Gu, L.; Bian, L. Structurally Dynamic Hydrogels for Biomedical Applications : Pursuing a Fine Balance between Macroscopic Stability and Microscopic Dynamics. *ACS Chem. Rev.* **2021**. https://doi.org/10.1021/acs.chemrev.1c00071.

(20) Hu, W.; Wang, Z.; Xiao, Y.; Zhang, S.; Wang, J. Advances in Crosslinking Strategies of Biomedical Hydrogels. *Biomater. Sci.* **2019**, *7* (3), 843–855. https://doi.org/10.1039/c8bm01246f.

(21) Hoyle, C. E.; Bowman, C. N. Thiol – Ene Click Chemistry. *Angew. Chemie* **2010**, *49*, 1540–1573. https://doi.org/https://doi.org/10.1002/anie.200903924.

(22) Gramlich, W. M.; Kim, I. L.; Burdick, J. A. Synthesis and Orthogonal Photopatterning of Hyaluronic Acid Hydrogels with Thiol-Norbornene Chemistry.

Biomaterials **2013**, *34* (38), 9803–9811.
https://doi.org/10.1016/j.biomaterials.2013.08.089.

(23) Grim, J. C.; Brown, T. E.; Aguado, B. A.; Chapnick, D. A.; Viert, A. L.; Liu, X.;
Anseth, K. S. A Reversible and Repeatable Thiol–Ene Bioconjugation for
Dynamic Patterning of Signaling Proteins in Hydrogels. *ACS Cent. Sci.* **2018**, *4*,
909–916. https://doi.org/https://doi.org/10.1021/acscentsci.8b00325.

(24) Grim, J. C.; Marozas, I. A.; Anseth, K. S. Thiol-Ene and Photo-Cleavage
Chemistry for Controlled Presentation of Biomolecules in Hydrogels. *J. Control.
Release* **2015**, *219*, 95–106. https://doi.org/10.1016/j.jconrel.2015.08.040.

(25) Deforest, C. A.; Tirrell, D. A. A Photoreversible Protein-Patterning Approach for
Guiding Stem Cell Fate in Three-Dimensional Gels. *Nat. Mater.* **2015**, *14*, 523–
531. https://doi.org/https://doi.org/10.1038/nmat4219.

(26) Deforest, C. A.; Anseth, K. S. Photoreversible Patterning of Biomolecules within
Click-Based Hydrogels. *Angew. Chemie Int. Ed.* **2012**, *51* (8), 1816–1819.
https://doi.org/https://doi.org/10.1002/anie.201106463.

(27) DeForest, C. A.; Anseth, K. S. Cytocompatible Click-Based Hydrogels with
Dynamically Tunable Properties through Orthogonal Photoconjugation and
Photocleavage Reactions. *Nat. Chem.* **2011**, *3*, 925–931.
https://doi.org/https://doi.org/10.1038/nchem.1174.

(28) Rodell, C. B.; Wade, R. J.; Purcell, B. P.; Dusaj, N. N.; Burdick, J. A. Selective
Proteolytic Degradation of Guest − Host Assembled, Injectable Hyaluronic Acid
Hydrogels. *ACS Biomater. Sci. Eng.* **2015**, *1*, 277–286.
https://doi.org/10.1021/ab5001673.

(29) Ifkovits, J. L.; Burdick, J. A. Review: Photopolymerizable and Degradable
Biomaterials for Tissue Engineering Applications. *Tissue Eng.* **2007**, *13* (10),
2369–2385. https://doi.org/10.1089/ten.2007.0093.

(30) Khetan, S.; Guvendiren, M.; Legant, W. R.; Cohen, D. M.; Chen, C. S.; Burdick, J.
A. Degradation-Mediated Cellular Traction Directs Stem Cell Fate in Covalently
Crosslinked Three-Dimensional Hydrogels. *Nat. Mater.* **2013**, *12*, 458–465.
https://doi.org/10.1038/nmat3586.

(31) Feliciano, A. J.; Blitterswijk, C. Van; Moroni, L.; Baker, M. B. Realizing Tissue
Integration with Supramolecular Hydrogels. **2021**, *124*, 1–14.
https://doi.org/10.1016/j.actbio.2021.01.034.

(32) Prince, E.; Kumacheva, E. Design and Applications of Man-Made Biomimetic Fibrillar Hydrogels. *Nat. Rev. Mater.* **2019**, *4*, 99–115.

(33) Newcomb, C. J.; Sur, S.; Lee, S. S.; Yu, J. M.; Zhou, Y.; Snead, M. L.; Stupp, S. I. Supramolecular Nanofibers Enhance Growth Factor Signaling by Increasing Lipid Raft Mobility. *Nano Lett.* **2016**, *16*, 3042–3050. https://doi.org/10.1021/acs.nanolett.6b00054.

(34) Stupp, S. I. Self-Assembly and Biomaterials. *Nano Lett.* **2010**, *10*, 4783–4786. https://doi.org/10.1021/nl103567y.

(35) Sather, N. A.; Sai, H.; Sasselli, I. R.; Sato, K.; Ji, W.; Synatschke, C. V; Zambrotta, R. T.; Edelbrock, J. F.; Kohlmeyer, R. R.; Hardin, J. O.; et al. 3D Printing of Supramolecular Polymer Hydrogels with Hierarchical Structure. *Small* **2021**, *17*, 1–14. https://doi.org/10.1002/smll.202005743.

(36) Sinawang, G.; Osaki, M.; Takashima, Y.; Yamaguchi, H.; Harada, A. Biofunctional Hydrogels Based on Host–Guest Interactions. *Polym. J.* **2020**, *52*, 839–859. https://doi.org/https://doi.org/10.1038/s41428-020-0352-7.

(37) Boekhoven, J.; Rubert Pérez, C. M.; Sur, S.; Worthy, A.; Stupp, S. I. Dynamic Display of Bioactivity through Host-Guest Chemistry. *Angew. Chemie - Int. Ed.* **2013**, *52* (46), 12077–12080. https://doi.org/https://doi.org/10.1002/anie.201306278.

(38) Highley, C. B.; Rodell, C. B.; Burdick, J. A. Direct 3D Printing of Shear-Thinning Hydrogels into Self-Healing Hydrogels. *Adv. Mater.* **2015**, *27* (34), 5075–5079. https://doi.org/10.1002/adma.201501234.

(39) Uman, S.; Dhand, A.; Burdick, J. A. Recent Advances in Shear-Thinning and Self-Healing Hydrogels for Biomedical Applications. *J. Appl. Polym. Sci.* **2020**, *48668*, 1–20. https://doi.org/10.1002/app.48668.

(40) Sankaran, S.; Jaatinen, L.; Brinkmann, J.; Zambelli, T.; Voros, J.; Jonkheijm, P. Cell Adhesion on Dynamic Supramolecular Surfaces Probed by Fluid Force Microscopy- Based Single-Cell Force Spectroscopy. *ACS Nano* **2017**, *11*, 3867–3874. https://doi.org/10.1021/acsnano.7b00161.

(41) Appel, E. A.; Biedermann, F.; Rauwald, U.; Jones, S. T.; Zayed, J. M.; Scherman, O. A. Supramolecular Cross-Linked Networks via Host - Guest Complexation with Cucurbit[8]Uril. *J. Am. Chem. Soc.* **2010**, *132* (40), 14251–14260. https://doi.org/https://doi.org/10.1021/ja106362w.

(42) Zhang, Y. S.; Khademhosseini, A. Advances in Engineering Hydrogels. *Science (80-.).* **2017**, *356* (6337), 1–27. https://doi.org/10.1126/science.aaf3627.

(43) Davidson, M. D.; Song, K. H.; Lee, M. H.; Llewellyn, J.; Du, Y.; Baker, B. M.; Wells, R. G.; Burdick, J. A. Engineered Fibrous Networks to Investigate the Influence of Fiber Mechanics on Myofibroblast Differentiation. *ACS Biomater. Sci. Eng.* **2019**, *5* (8), 3899–3908. https://doi.org/https://doi.org/10.1021/acsbiomaterials.8b01276.

(44) Stevens, M. M.; George, J. H. Exploring and Engineering the Cell Surface Interface. *Science (80-.).* **2005**, *310* (5751), 1135–1138. https://doi.org/10.1126/science.1106587.

(45) Grewal, M. G.; Highley, C. B. Electrospun Hydrogels for Dynamic Culture Systems: Advantages, Progress, and Opportunities. *Biomater. Sci.* **2021**, *9*, 4228–4245. https://doi.org/10.1039/d0bm01588a.

(46) Wade, R. J.; Burdick, J. A. Advances in Nanofibrous Scaffolds for Biomedical Applications: From Electrospinning to Self-Assembly. *Nano Today* **2014**, *9* (6), 722–742. https://doi.org/10.1016/j.nantod.2014.10.002.

(47) Dean, D.; Nain, A. S.; Genin, G. M. The Mechanobiology of Cells, Fibers, and Their Interactions. *Acta Biomater.* **2023**, *163*, 1–6. https://doi.org/10.1016/j.actbio.2023.04.045.

(48) Rozario, T.; Desimone, D. W. The Extracellular Matrix in Development and Morphogenesis : A Dynamic View. *Dev. Biol.* **2010**, *341* (1), 126–140. https://doi.org/10.1016/j.ydbio.2009.10.026.

(49) Hall, M. S.; Alisafaei, F.; Ban, E.; Feng, X.; Hui, C. Y.; Shenoy, V. B.; Wu, M. Fibrous Nonlinear Elasticity Enables Positive Mechanical Feedback between Cells and ECMs. *Proc. Natl. Acad. Sci. U. S. A.* **2016**, *113* (49), 14043–14048. https://doi.org/10.1073/pnas.1613058113.

(50) Wang, H.; Abhilash, A. S.; Chen, C. S.; Wells, R. G.; Shenoy, V. B. Long-Range Force Transmission in Fibrous Matrices Enabled by Tension-Driven Alignment of Fibers. *Biophysj* **2014**, *107* (11), 2592–2603. https://doi.org/10.1016/j.bpj.2014.09.044.

(51) Storm, C.; Pastore, J. J.; MacKintosh, F. C.; Lubensky, T. C.; Janmey, P. A. Nonlinear Elasticity in Biological Gels. *Nature* **2005**, *435*, 191–194. https://doi.org/10.1038/nature03497.1.

(52) Pamonag, M.; Hinson, A.; Burton, E. J.; Jafari, N.; Id, D. S.; Babcock, S.; Basha, R.; Hu, X.; Id, K. E. K. Individual Cells Generate Their Own Self- Reinforcing Contact Guidance Cues through Local Matrix Fiber Remodeling. *PLoS One* **2022**, 1–20. https://doi.org/10.1371/journal.pone.0265403.

(53) Xie, J.; Bao, M.; Bruekers, M. C.; Huck, W. T. S. Collagen Gels with Different Fibrillar Microarchitectures Elicit Different Cellular Responses. *Appl. Mater. Interfaces* **2017**, *9*, 19630–19637. https://doi.org/10.1021/acsami.7b03883.

(54) Ariz, M.; Esparza, M.; Amaveda, H.; Ederra, C.; Garcı, M.; Mora, M.; Movilla, N.; Id, C. O. The Use of Mixed Collagen-Matrigel Matrices of Increasing Complexity Recapitulates the Biphasic Role of Cell Adhesion in Cancer Cell Migration: ECM Sensing, Remodeling and Forces at the Leading Edge of Cancer Invasion. *PLoS One* **2020**, 1–29. https://doi.org/10.21227/va80-yf12.

(55) Jenkins, T. L.; Little, D. Synthetic Scaffolds for Musculoskeletal Tissue Engineering: Cellular Responses to Fiber Parameters. *Regen. Med.* **2019**, 1–14. https://doi.org/10.1038/s41536-019-0076-5.

(56) Han, L.; Yu, S.; Wang, T.; Behn, A. W.; Yang, F. Microribbon-Like Elastomers for Fabricating Macroporous and Highly Flexible Scaffolds That Support Cell Proliferation in 3D. *Adv. Funct. Mater.* **2013**, *23*, 346–358. https://doi.org/10.1002/adfm.201201212.

(57) Pan, Z.; Nunes, J. K.; Duprat, C.; Shum, H. C.; Stone, H. A. Controlling Extrudate Volume Fraction through Poroelastic Extrusion of Entangled Looped Fibers. *Nat. Commun.* **2023**, *14* (1242), 1–9. https://doi.org/10.1038/s41467-023-36860-y.

(58) Shen, Y.; Liu, Y.; Nunes, J. K.; Wang, C.; Xu, M.; To, M. K.; Stone, H. A.; Shum, H. C. Fibro-Gel: An All-Aqueous Hydrogel Consisting of Microfibers with Tunable Release Profile and Its Application in Wound Healing. *Adv. Mater.* **2023**, *35* (19), 1–13. https://doi.org/10.1002/adma.202211637.

(59) Jenkins, T. L.; Meehan, S. Meltblown Polymer Fabrics as Candidate Scaffolds for Rotator Cuff Tendon Tissue Engineering. *Tissue Eng. Part A* **2017**, *23* (4), 958–967. https://doi.org/10.1089/ten.tea.2016.0470.

(60) Tuin, S. A.; Pourdeyhimi, B.; Loboa, E. G. Creating Tissues from Textiles: Scalable Nonwoven Manufacturing Techniques for Fabrication of Tissue Engineering Scaffolds. *Biomed. Mater.* **2016**, *11*. https://doi.org/10.1088/1748-6041/11/1/015017.

(61) Gattazzo, F.; Maria, C. De; Whulanza, Y.; Taverni, G.; Ahluwalia, A.; Vozzi, G.

Realisation and Characterization of Conductive Hollow Fibers for Neuronal Tissue Engineering. *J. Biomed. Mater. Res. Part B* **2015**, *103B*, 1107–1119. https://doi.org/10.1002/jbm.b.33297.

(62)   Dalton, P. D. Melt Electrowriting with Additive Manufacturing Principles. *Curr. Opin. Biomed. Eng.* **2017**, *2*, 49–57. https://doi.org/10.1016/j.cobme.2017.05.007.

(63)   Shahverdi, M.; Seifi, S.; Akbari, A.; Mohammadi, K. Melt Electrowriting of PLA , PCL , and Composite PLA / PCL Scaffolds for Tissue Engineering Application. *Sci. Rep.* **2022**, 1–16. https://doi.org/10.1038/s41598-022-24275-6.

(64)   Galarraga, J. H.; Locke, R. C.; Witherel, C. E.; Stoeckl, B. D.; Castilho, M. Fabrication of MSC-Laden Composites of Hyaluronic Acid Hydrogels Reinforced with MEW Scaffolds for Cartilage Repair. *Biofabrication* **2022**, *14* (014106).

(65)   Loewner, S.; Heene, S.; Baroth, T.; Heymann, H.; Cholewa, F.; Blume, H.; Blume, C. Recent Advances in Melt Electro Writing for Tissue Engineering for 3D Printing of Microporous Scaffolds for Tissue Engineering. *Front. Bioeng. Biotechnol.* **2022**. https://doi.org/10.3389/fbioe.2022.896719.

(66)   Greiner, A.; Wendorff, J. H. Electrospinning: A Fascinating Method for the Preparation of Ultrathin Fibers. *Angew. Chemie - Int. Ed.* **2007**, *46*, 5670–5703. https://doi.org/10.1002/anie.200604646.

(67)   Kalaoglu-Altan, O. I.; Sanyal, R.; Sanyal, A. Reactive and "clickable" Electrospun Polymeric Nanofibers. *Polym. Chem.* **2015**, *6* (18), 3372–3381. https://doi.org/10.1039/c5py00098j.

(68)   Chakraborty, S.; Liao, I.-C.; Adler, A.; Leong, K. W. Electrohydrodynamics: A Facile Technique to Fabricate Drug Delivery Systems. *Adv. Drug Deliv. Rev.* **2009**, *61* (12), 1043–1054. https://doi.org/10.1016/j.addr.2009.07.013.

(69)   Peijs, T. Electrospun Polymer Nanofibers and Their Composites. In *Comprehensive Composite Materials II*; 2018; pp 162–200. https://doi.org/10.1016/B978-0-12-803581-8.10025-6.

(70)   Pham, Q. P.; Sharma, U.; Mikos, A. G. Electrospinning of Polymeric Nanofibers for Tissue Engineering Applications: A Review. *Tissue Eng.* **2006**, *12* (5), 1197–1211. https://doi.org/10.1089/ten.2006.12.1197.

(71)   Noriega, S. E.; Hasanova, G. I.; Schneider, M. J.; Larsen, G. F.; Subramanian, A. Effect of Fiber Diameter on the Spreading, Proliferation and Differentiation of Chondrocytes on Electrospun Chitosan Matrices. *Cells Tissues Organs* **2012**, *195*

(3), 207–221. https://doi.org/10.1159/000325144.

(72)   Christopherson, G. T.; Song, H.; Mao, H. The Influence of Fiber Diameter of
       Electrospun Substrates on Neural Stem Cell Differentiation and Proliferation.
       Biomaterials **2009**, *30* (4), 556–564.
       https://doi.org/https://doi.org/10.1016/j.biomaterials.2008.10.004.

(73)   Whited, B. M.; Rylander, M. N. The Influence of Electrospun Scaffold Topography
       on Endothelial Cell Morphology, Alignment, and Adhesion in Response to Fluid
       Flow. *Biotechnol. Bioeng.* **2014**, *111* (1), 184–195.
       https://doi.org/10.1002/bit.24995.

(74)   Innocenti, M. New Insights into the Formation and the Function of Lamellipodia
       and Ruf Fl Es in Mesenchymal Cell Migration. *Cell Adh. Migr.* **2018**, *12* (5), 401–
       416.

(75)   Bashur, C. A.; Shaffer, R. D.; Dahlgren, L. A.; Guelcher, S. A.; Goldstein, A. S.
       Effect of Fiber Diameter and Alignment of Electrospun Polyurethane Meshes on
       Mesenchymal Progenitor Cells. *Tissue Eng. Part A* **2009**, *15* (9), 2435–2445.
       https://doi.org/10.1089/ten.tea.2008.0295.

(76)   Soliman, S.; Sant, S.; Nichol, J. W.; Khabiry, M.; Traversa, E.; Khademhosseini,
       A. Controlling the Porosity of Fibrous Scaffolds by Modulating the Fiber Diameter
       and Packing Density. *J. Biomed. Mater. Res. A* **2011**, *96* (3), 566–574.
       https://doi.org/10.1002/jbm.a.33010.

(77)   Baker, B. M.; Gee, A. O.; Metter, R. B.; Nathan, A. S.; Marklein, R. A.; Burdick, J.
       A.; Mauck, R. L. The Potential to Improve Cell Infiltration in Composite Fiber-
       Aligned Electrospun Scaffolds by the Selective Removal of Sacrificial Fibers.
       Biomaterials **2008**, *29* (15), 2348–2358.
       https://doi.org/10.1016/j.biomaterials.2008.01.032.

(78)   Baker, B. M.; Shah, R. P.; Silverstein, A. M.; Esterhai, J. L.; Burdick, J. A.; Mauck,
       R. L. Sacrificial Nanofibrous Composites Provide Instruction without Impediment
       and Enable Functional Tissue Formation. *Proc. Natl. Acad. Sci. U. S. A.* **2012**,
       109 (35), 14176–14181. https://doi.org/10.1073/pnas.1206962109.

(79)   Ashinsky, B. G.; Gullbrand, S. E.; Bonnevie, E. D.; Wang, C.; Kim, D. H.; Han, L.;
       Mauck, R. L.; Smith, H. E. Sacrificial Fibers Improve Matrix Distribution and
       Mechanical Properties in a Tissue-Engineered Intervertebral Disc. *Acta Biomater.*
       2020, *111*, 232–241. https://doi.org/https://doi.org/10.1016/j.actbio.2020.05.019.

(80)   Sundararaghavan, H. G.; Metter, R. B.; Burdick, J. A. Electrospun Fibrous

Scaffolds with Multiscale and Photopatterned Porosity. *Macromol. Biosci.* **2010**, *10* (3), 265–270. https://doi.org/10.1002/mabi.200900363.

(81)   Joshi, V. S.; Lei, Y.; Walthers, C. M.; Wu, B.; Dunn, J. C. Y. Macroporosity Enhances Vascularization of Electrospun Scaffolds. *J. Surg. Res.* **2013**, *183* (1), 18–26. https://doi.org/10.1016/j.jss.2013.01.005.

(82)   Ameer, J. M.; Kumar PR, A.; Kasoju, N. Strategies to Tune Electrospun Sca Ff Old Porosity for Effective Cell Response in Tissue Engineering. *J. Funct. Biomater.* **2019**, *10* (30).

(83)   Devarasou, S.; Kang, M.; Kwon, T. Y.; Cho, Y.; Shin, J. H. Fibrous Matrix Architecture-Dependent Activation of Fibroblasts with a Cancer-Associated Fibroblast-like Phenotype. *ACS Biomater. Sci. Eng.* **2023**, *9*, 280–291. https://doi.org/10.1021/acsbiomaterials.2c00694.

(84)   Paul, A.; Kumar, S.; Kaoud, T. S.; Pickett, M. R.; Bohanon, A. L.; Zoldan, J.; Dalby, K. N.; Parekh, S. H. Biomechanical Dependence of SARS-CoV-2 Infections. *ACS Appl. Bio Mater.* **2022**, *5*, 2307–2315. https://doi.org/10.1021/acsabm.2c00143.

(85)   Baker, B. M.; Mauck, R. L. The Effect of Nanofiber Alignment on the Maturation of Engineered Meniscus Constructs. *Biomaterials* **2007**, *28* (11), 1967–1977. https://doi.org/10.1016/j.biomaterials.2007.01.004.

(86)   DePalma, S. J.; Davidson, C. D.; Stis, A. E.; Helms, A. S.; Baker, B. M. Microenvironmental Determinants of Organized IPSC-Cardiomyocyte Tissues on Synthetic Fibrous Matrices. *Biomater. Sci.* **2021**, *9*, 93–107. https://doi.org/10.1039/d0bm01247e.

(87)   Lim, S. H.; Liu, X. Y.; Song, H.; Yarema, K. J.; Mao, H. The Effect of Nanofiber-Guided Cell Alignment on the Preferential Differentiation of Neural Stem Cells. *Biomaterials* **2010**, *31* (34), 9031–9039. https://doi.org/10.1016/j.biomaterials.2010.08.021.

(88)   Sousa, M. C. A. De; Rodrigues, C. A. V; Ferreira, I. A. F.; Ferreira, F. C. Functionalization of Electrospun Nanofibers and Fiber Alignment Enhance Neural Stem Cell Proliferation and Neuronal Differentiation. *Front. Bioeng. Biotechnol.* **2020**, *8* (October). https://doi.org/10.3389/fbioe.2020.580135.

(89)   Sundararaghavan, H. G.; Saunders, R. L.; Hammer, D. A.; Burdick, J. A. Fiber Alignment Directs Cell Motility over Chemotactic Gradients. *Biotechnol. Bioeng.* **2013**, *110* (4), 1249–1254. https://doi.org/10.1002/bit.24788.

(90) Kim, I. L.; Khetan, S.; Baker, B. M.; Chen, C. S.; Burdick, J. A. Fibrous Hyaluronic Acid Hydrogels That Direct MSC Chondrogenesis through Mechanical and Adhesive Cues. *Biomaterials* **2013**, *34* (22), 5571–5580. https://doi.org/10.1016/j.biomaterials.2013.04.004.

(91) Abhilash, A. S.; Baker, B. M.; Trappmann, B.; Chen, C. S.; Shenoy, V. B. Remodeling of Fibrous Extracellular Matrices by Contractile Cells: Predictions from Discrete Fiber Network Simulations. *Biophys. J.* **2014**, *107* (8), 1829–1840. https://doi.org/10.1016/j.bpj.2014.08.029.

(92) Baker, B. M.; Trappmann, B.; Wang, W. Y.; Sakar, M. S.; Kim, I. L.; Shenoy, V. B.; Burdick, J. A.; Chen, C. S. Cell-Mediated Fibre Recruitment Drives Extracellular Matrix Mechanosensing in Engineered Fibrillar Microenvironments. *Nat. Mater.* **2015**, *14*, 1262–1268. https://doi.org/https://doi.org/10.1038/nmat4444.

(93) Wang, W. Y.; Davidson, C. D.; Lin, D.; Baker, B. M. Actomyosin Contractility-Dependent Matrix Stretch and Recoil Induces Rapid Cell Migration. *Nat. Commun.* **2019**, *10*, 1–12. https://doi.org/10.1038/s41467-019-09121-0.

(94) Davidson, C. D.; Jayco, D. K. P.; Matera, D. L.; DePalma, S. J.; Hiraki, H. L.; Wang, W. Y.; Baker, B. M. Myofibroblast Activation in Synthetic Fibrous Matrices Composed of Dextran Vinyl Sulfone. *Acta Biomater.* **2020**, *105*, 78–86. https://doi.org/https://doi.org/10.1016/j.actbio.2020.01.009.

(95) Davidson, C. D.; Wang, W. Y.; Zaimi, I.; Jayco, D. K. P.; Baker, B. M. Cell Force-Mediated Matrix Reorganization Underlies Multicellular Network Assembly. *Sci. Rep.* **2019**, *9*, 1–13. https://doi.org/https://doi.org/10.1038/s41598-018-37044-1.

(96) Song, K. H.; Heo, S.-J.; Peredo, A. P.; Davidson, M. D.; Mauck, R. L.; Burdick, J. A. Influence of Fiber Stiffness on Meniscal Cell Migration into Dense Fibrous Networks. *Adv. Healthc. Mater.* **2019**, *9* (1901228), 1–10. https://doi.org/https://doi.org/10.1002/adhm.201901228.

(97) Szczesny, S. E.; Driscoll, T. P.; Tseng, H.-Y.; Liu, P.-C.; Heo, S.-J.; Mauck, R. L.; Chao, P.-H. G. Crimped Nanofibrous Biomaterials Mimic Microstructure and Mechanics of Native Tissue and Alter Strain Transfer to Cells. *ACS Biomater. Sci. Eng.* **2017**, *3* (11), 2869–2876. https://doi.org/https://doi.org/10.1021/acsbiomaterials.6b00646.

(98) Davidson, C. D.; Jayco, D. K. P.; Wang, W. Y.; Shikanov, A.; Baker, B. M. Fiber Crimp Confers Matrix Mechanical Nonlinearity, Regulates Endothelial Cell Mechanosensing, and Promotes Microvascular Network Formation. *J. Biomech.*

Eng. **2020**, *142* (11), 1–9. https://doi.org/10.1115/1.4048191.

(99) Wade, R. J.; Bassin, E. J.; Rodell, C. B.; Burdick, J. A. Protease-Degradable Electrospun Fibrous Hydrogels. *Nat. Commun.* **2015**, *6*, 1–10. https://doi.org/https://doi.org/10.1038/ncomms7639.

(100) Davidson, M. D.; Ban, E.; Schoonen, A. C. M.; Lee, M.-H.; D'Este, M.; Shenoy, V. B.; Burdick, J. A. Mechanochemical Adhesion and Plasticity in Multifiber Hydrogel Networks. *Adv. Mater.* **2019**, *32* (1905719), 1–8. https://doi.org/https://doi.org/10.1002/adma.201905719.

(101) Girão, A. F.; Wieringa, P.; Pinto, S. C.; Marques, P. A. A. P.; Micera, S.; van Wezel, R.; Ahmed, M.; Truckenmueller, R.; Moroni, L. Ultraviolet Functionalization of Electrospun Scaffolds to Activate Fibrous Runways for Targeting Cell Adhesion. *Front. Bioeng. Biotechnol.* **2019**, *7* (159), 1–10. https://doi.org/https://doi.org/10.3389/fbioe.2019.00159.

(102) Wade, R. J.; Bassin, E. J.; Gramlich, W. M.; Burdick, J. A. Nanofibrous Hydrogels with Spatially Patterned Biochemical Signals to Control Cell Behavior. *Adv. Mater.* **2015**, *27* (8), 1356–1362. https://doi.org/https://doi.org/10.1002/adma.201404993.

(103) Sharma, S.; Floren, M.; Ding, Y.; Stenmark, K. R.; Tan, W.; Bryant, S. J. A Photoclickable Peptide Microarray Platform for Facile and Rapid Screening of 3-D Tissue Microenvironments. *Biomaterials* **2017**, *143*, 17–28. https://doi.org/10.1016/j.biomaterials.2017.07.025.

(104) Grewal, M. G.; Gray, V. P.; Letteri, R. A.; Highley, C. B. User-Defined, Temporal Presentation of Bioactive Molecules on Hydrogel Substrates Using Supramolecular Coiled Coil Complexes. *Biomater. Sci.* **2021**, *9* (12), 4374–4387. https://doi.org/10.1039/d1bm00016k.

(105) Zhao, X.; Sun, X.; Yildirimer, L.; Lang, Q.; Lin, Z. Y. (William); Zheng, R.; Zhang, Y.; Cui, W.; Annabi, N.; Khademhosseini, A. Cell Infiltrative Hydrogel Fibrous Scaffolds for Accelerated Wound Healing. *Acta Biomater.* **2017**, *49*, 66–77. https://doi.org/https://doi.org/10.1016/j.actbio.2016.11.017.

(106) Sundararaghavan, H. G.; Burdick, J. A. Gradients with Depth in Electrospun Fibrous Scaffolds for Directed Cell Behavior. *Biomacromolecules* **2011**, *12* (6), 2344–2350. https://doi.org/10.1021/bm200415g.

(107) Phipps, M. C.; Clem, W. C.; Grunda, J. M.; Clines, G. A.; Bellis, S. L. Increasing the Pore Sizes of Bone-Mimetic Electrospun Scaffolds Comprised of Polycaprolactone, Collagen I and Hydroxyapatite to Enhance Cell Infiltration.

Biomaterials **2012**, *33* (2), 524–534.
https://doi.org/10.1016/j.biomaterials.2011.09.080.

(108) Merrilees, M.; Buunk, N.; Zuo, N.; Larsen, N.; Karimi, S.; Tucker, N. Use of Stacked Layers of Electrospun L-Lactide/Glycolide Co-Polymer Fibers for Rapid Construction of Skin Sheets. *Bioengineering* **2021**, *8* (7), 1–11.

(109) Noh, J.; Lin, S.; Xue, Y.; Chang, G.; Han, Q.; Chen, L.; Jia, Y. Layer-by-Layer 3-Dimensional Nanofiber Tissue Scaffold with Controlled Gap by Electrospinning. *Mater. Res. Express* **2018**, *5* (025401).

(110) Chainani, A.; Hippensteel, K. J.; Kishan, A.; Garrigues, N. W.; Ruch, D. S.; Guilak, F.; Little, D. Multilayered Electrospun Scaffolds for Tendon Tissue Engineering. *Tissue Eng. Regen. Med.* **2013**, *19*, 2594–2604. https://doi.org/10.1089/ten.tea.2013.0165.

(111) Huang, C.; Hu, R.; Yin, M. Electrospun Gelatin Polycaprolactone Nanofibrous Membranes Combined with a Coculture of Bone Marrow Stromal Cells and Chondrocytes for Cartilage Engineering. *Int. J. Nanomedicine* **2015**, *10*, 2089–2099.

(112) Inanc, B.; Arslan, Y. E.; Seker, S.; Elcin, A. E.; Elcin, Y. M. Periodontal Ligament Cellular Structures Engineered with Electrospun Poly (DL -Lactide- Co -Glycolide) Nanofibrous Membrane Scaffolds. *J. Biomed. Mater. Res. Part A* **2008**, 186–195. https://doi.org/10.1002/jbm.a.32066.

(113) Srouji, S.; Kizhner, T.; Suss-Tobi, E.; Livne, E.; Zussman, E. 3-D Nanofibrous Electrospun Multilayered Construct Is an Alternative ECM Mimicking Scaffold. *J. Mater. Sci. Mater. Med.* **2008**, *19*, 1249–1255. https://doi.org/10.1007/s10856-007-3218-z.

(114) Yang, X.; Shah, J. D.; Wang, H. Nanofiber Enabled Layer-by-Layer Approach Toward Three-Dimensional Tissue Formation. *Tissue Eng. Part A* **2009**, *15* (4), 945–956.

(115) Deng, M.; Kumbar, S. G.; Nair, L. S.; Weikel, A. L.; Allcock, H. R.; Laurencin, C. T. Biomimetic Structures: Biological Implications of Dipeptide-Substituted Polyphosphazene – Polyester Blend Nanofiber Matrices for Load-Bearing Bone Regeneration. *Adv. Funct. Mater.* **2011**, *21*, 2641–2651. https://doi.org/10.1002/adfm.201100275.

(116) Kosowska, K.; Domalik-Pyzik, P.; Krok-Borkowicz, M.; Chlopek, J. Polylactide/Hydroxyapatite Nonwovens Incorporated into Chitosan/Graphene

Materials Hydrogels to Form Novel Hierarchical Scaffolds. *Int. J. Mol. Sci.* **2020**, *21* (2330).

(117) Highley, C. B.; Rodell, C. B.; Kim, I. L.; Wade, R. J.; Burdick, J. A. Ordered, Adherent Layers of Nanofibers Enabled by Supramolecular Interactions. *J. Mater. Chem. B* **2015**, *2* (46), 8110–8115. https://doi.org/https://doi.org/10.1039/C4TB00724G.

(118) Orr, S. B.; Chainani, A.; Hippensteel, K. J.; Kishan, A.; Gilchrist, C.; Garrigues, N. W.; Ruch, D. S.; Guilak, F.; Little, D. Aligned Multilayered Electrospun Scaffolds for Rotator Cuff Tendon Tissue Engineering. *Acta Biomater.* **2015**, *24*, 117–126. https://doi.org/10.1016/j.actbio.2015.06.010.

(119) Beachley, V.; Hepfer, R. G.; Katsanevakis, E.; Zhang, N.; Wen, X. Precisely Assembled Nanofiber Arrays as a Platform to Engineer Aligned Cell Sheets for Biofabrication. *Bioengineering* **2014**, *1*, 114–133. https://doi.org/10.3390/bioengineering1030114.

(120) Pham, Q. P.; Sharma, U.; Mikos, A. G. Electrospun Poly (E -Caprolactone) Microfiber and Multilayer Nanofiber/Microfiber Scaffolds: Characterization of Scaffolds and Measurement of Cellular Infiltration. *Biomacromolecules* **2006**, *7*, 2796–2805.

(121) Yang, Y.; Wimpenny, I.; Ahearne, M. Portable Nanofiber Meshes Dictate Cell Orientation throughout Three-Dimensional Hydrogels. *Nanomedicine Nanotechnology, Biol. Med.* **2011**, *7*, 131–136. https://doi.org/10.1016/j.nano.2010.12.011.

(122) Cai, Y.; Zhang, G.; Wang, L.; Jiang, Y.; Ouyang, H.; Zou, X. Novel Biodegradable Three-Dimensional Macroporous Scaffold Using Aligned Electrospun Nanofibrous Yarns for Bone Tissue Engineering. *J. Biomed. Mater. Res. Part A* **2012**, *100A*, 1187–1194. https://doi.org/10.1002/jbm.a.34063.

(123) Kim, J. I.; Hwang, T. I.; Aguilar, L. E.; Park, C. H.; Kim, C. S. A Controlled Design of Aligned and Random Nanofibers for 3D Bi-Functionalized Nerve Conduits Fabricated via a Novel Electrospinning Set-Up. *Sci. Rep.* **2016**, *6*. https://doi.org/10.1038/srep23761.

(124) Arabpour, Z.; Nasrin, A. B.; Jafar, L. B.; Hossein, S. E.; Malekabadi, E.; Nazeri, N.; Vaez, A.; Salehi, M.; Sefat, F.; Ostad, S. N. Design and Characterization of Biodegradable Multi Layered Electrospun Nanofibers for Corneal Tissue Engineering Applications. *J. Biomed. Mater. Res.* **2019**, *107A*, 2340–2349. https://doi.org/10.1002/jbm.a.36742.

(125) Yu, L.; Zhang, W.; Jiang, Y.; Guo, C. Gradient Degradable Nerve Guidance Conduit with Multilayer Structure Prepared by Electrospinning. *Mater. Lett.* **2020**. https://doi.org/10.1016/j.matlet.2020.128238.

(126) Kamath, S. M.; Sridhar, K.; Jaison, D.; Gopinath, V.; Ibrahim, B. K. M. Fabrication of Tri-layered Electrospun Polycaprolactone Mats with Improved Sustained Drug Release Profile. *Sci. Rep.* **2020**, *10*, 1–13. https://doi.org/10.1038/s41598-020-74885-1.

(127) Yu, D.; Huang, C.; Jiang, C.; Zhu, H. Features of a Simvastatin-loaded Multi-layered Co-electrospun Barrier Membrane for Guided Bone Regeneration. *Exp. Ther. Med.* **2021**, *22*, 1–13. https://doi.org/10.3892/etm.2021.10145.

(128) Cho, K.; Kang, D.; Lee, H.; Koh, W. Multi-Stimuli Responsive and Reversible Soft Actuator Engineered by Layered Fibrous Matrix and Hydrogel Micropatterns. *Chem. Eng. J.* **2022**, *427*, 130879. https://doi.org/10.1016/j.cej.2021.130879.

(129) Tzezana, R.; Zussman, E.; Levenberg, S. A Layered Ultra-Porous Scaffold for Tissue Engineering, Created via a Hydrospinning Method. *Tissue Eng. Part C* **2008**, *14* (4), 281–288.

(130) Xu, G.; Lee, J.; Kim, Y.; Lee, H.; Kim, H. S.; Kwon, S.-M. Thickness-Controllable Electrospun Fibers Promote Tubular Structure Formation by Endothelial Progenitor Cells. *Int. J. Nanomedicine* **2015**, *10*, 1189–1200.

(131) Mahjour, S. B.; Sefat, F.; Polunin, Y.; Wang, L.; Wang, H. Improved Cell Infiltration of Electrospun Nanofiber Mats for Layered Tissue Constructs. *J. Biomed. Mater. Res. Part A* **2016**, *104A*, 1479–1488. https://doi.org/10.1002/jbm.a.35676.

(132) McMahon, R. E.; Qu, X.; Jimenez-Vergara, A. C.; Bashur, C. A.; Guelcher, S. A.; Goldstein, A. S.; Hahn, M. S. Hydrogel – Electrospun Mesh Composites for Coronary Artery Bypass Grafts. *Tissue Eng. Part C* **2011**, *17* (4), 451–461. https://doi.org/10.1089/ten.tec.2010.0427.

(133) Nakielski, P.; Paw, S.; Rinoldi, C.; Ziai, Y.; Sio, L. De; Urbanek, O.; Zembrzycki, K.; Pruchniewski, M.; Lanzi, M.; Salatelli, E.; et al. Multifunctional Platform Based on Electrospun Nano Fi Bers and Plasmonic Hydrogel: A Smart Nanostructured Pillow for Near-Infrared Light-Driven Biomedical Applications. *ACS Appl. Bio Mater.* **2020**, *12*, 54328–54342. https://doi.org/10.1021/acsami.0c13266.

(134) Papaparaskeva, G.; Louca, M.; Voutouri, C.; Stylianopoulos, T.; Krasia-christoforou, T. Amalgamated Fiber/Hydrogel Composites Based on Semi-

Interpenetrating Polymer Networks and Electrospun Nanocomposite Fibrous Mats. *Eur. Polym. J.* **2020**. https://doi.org/10.1016/j.eurpolymj.2020.110041.

(135) Ekaputra, A. K.; Prestwich, G. D.; Cool, S. M.; Hutmacher, D. W. Combining Electrospun Scaffolds with Electrosprayed Hydrogels Leads to Three-Dimensional Cellularization of Hybrid Constructs. *Biomacromolecules* **2008**, *9*, 2097–2103.

(136) Martin, A.; Nyman, J. N.; Reinholdt, R.; Cai, J.; Schaedel, A.; va der Plas, M. J. A.; Malmsten, M.; Rades, T.; Heinz, A. In Situ Transformation of Electrospun Nanofibers into Nanofiber-Reinforced Hydrogels. *Nanomaterials* **2022**, *12*. https://doi.org/10.3390/nano12142437.

(137) Moroni, L.; Seliktar, D.; Elisseeff, J. Biomimetics of the Extracellular Matrix: An Integrated Three-Dimensional Fiber-Hydrogel Composite for Cartilage Tissue Engineering. *Smart Struct Syst* **2011**, *7* (3), 213–222.

(138) Nguyen, L. H.; Gao, M.; Lin, J.; Wu, W.; Wang, J.; Chew, S. Y. Three-Dimensional Aligned Nanofibers-Hydrogel Scaffold for Controlled Non-Viral Drug / Gene Delivery to Direct Axon Regeneration in Spinal Cord Injury Treatment. *Sci. Rep.* **2017**, *7*. https://doi.org/10.1038/srep42212.

(139) Matera, D. L.; DiLillo, K. M.; Smith, M. R.; Davidson, C. D.; Parikh, R.; Said, M.; Wilke, C. A.; Lombaert, I. M.; Arnold, K. B.; Moore, B. B.; et al. Microengineered 3D Pulmonary Interstitial Mimetics Highlight a Critical Role for Matrix Degradation in Myofibroblast Differentiation. *Sci. Adv.* **2020**, *6* (37), 1–15. https://doi.org/10.1126/sciadv.abb5069.

(140) Matera, D. L.; Wang, W. Y.; Smith, M. R.; Shikanov, A.; Baker, B. M. Fiber Density Modulates Cell Spreading in 3D Interstitial Matrix Mimetics. *ACS Biomater. Sci. Eng.* **2019**, *5*, 2965–2975. https://doi.org/https://doi.org/10.1021/acsbiomaterials.9b00141.

(141) Kent III, R. N.; Said, M.; Busch, M. E.; Poupard, E. R.; Tsai, A.; Xia, J.; Matera, D. L.; Wang, W. Y.; Depalma, S. J.; Hiraki, H. L.; et al. Physical and Soluble Cues Enhance Tendon Progenitor Cell Invasion into Injectable Synthetic Hydrogels. *Adv. Funct. Mater.* **2022**, *32*. https://doi.org/10.1002/adfm.202207556.

(142) Li, X.; Cho, B.; Martin, R.; Seu, M.; Zhang, C.; Zhou, Z.; Choi, J. S.; Jiang, X.; Chen, L.; Walia, G.; et al. Nanofiber-Hydrogel Composite–Mediated Angiogenesis for Soft Tissue Reconstruction. *Sci. Transl. Med.* **2019**, *11* (490), 1–12. https://doi.org/10.1126/scitranslmed.aau6210.

(143) Li, X.; Zhang, C.; Haggerty, A. E.; Yan, J.; Lan, M.; Seu, M.; Yang, M.; Marlow, M.

M.; Maldonado-lasunción, I.; Cho, B.; et al. The Effect of a Nanofiber-Hydrogel Composite on Neural Tissue Repair and Regeneration in the Contused Spinal Cord. *Biomaterials* **2020**, *245*. https://doi.org/10.1016/j.biomaterials.2020.119978.

(144) Haggerty, A. E.; Nitobe, Y.; Yamane, K.; Marlow, M. M.; You, H.; Zhang, C.; Cho, B.; Li, X.; Reddy, S.; Mao, H.; et al. The Effects of the Combination of Mesenchymal Stromal Cells and Nanofiber-Hydrogel Composite on Repair of the Contused Spinal Cord. *Cells* **2022**, *11*, 1–17.

(145) Davidson, M. D.; Prendergast, M. E.; Ban, E.; Xu, K. L.; Mickel, G.; Mensah, P.; Dhand, A.; Janmey, P. A.; Shenoy, V. B.; Burdick, J. A. Programmable and Contractile Materials through Cell Encapsulation in Fibrous Hydrogel Assemblies. *Sci. Adv.* **2021**, *7*, 1–14.

(146) Prendergast, M. E.; Davidson, M. D.; Burdick, J. A. A Biofabrication Method to Align Cells within Bioprinted Photocrosslinkable and Cell-Degradable Hydrogel Constructs via Embedded Fibers. *Biofabrication* **2021**, *13*.

(147) Prendergast, M. E.; Heo, S.-J.; Mauck, R. L.; Burdick, J. A. Suspension Bath Bioprinting and Maturation of Anisotropic Meniscal Constructs. *Biofabrication* **2023**, *15* (3). https://doi.org/10.1088/1758-5090/acc3c3.

(148) Hiraki, H. L.; Matera, D. L.; Rose, M. J.; Kent, R. N.; Todd, C. W.; Stout, M. E.; Wank, A. E.; Schiavone, M. C.; Depalma, S. J.; Zarouk, A. A.; et al. Magnetic Alignment of Electrospun Fiber Segments Within a Hydrogel Composite Guides Cell Spreading and Migration Phenotype Switching. *Front. Bioeng. Biotechnol.* **2021**, *9*, 1–14. https://doi.org/10.3389/fbioe.2021.679165.

(149) Doyle, A. D.; Carvajal, N.; Jin, A.; Matsumoto, K.; Yamada, K. M. Local 3D Matrix Microenvironment Regulates Cell Migration through Spatiotemporal Dynamics of Contractility-Dependent Adhesions. *Nat. Commun.* **2015**, *6*. https://doi.org/10.1038/ncomms9720.

(150) Ko, Y.-G.; Kwon, O. H. Reinforced Gelatin-Methacrylate Hydrogels Containing Poly(Lactic-Co-Glycolic Acid) Nanofiber Fragments for 3D Bioprinting. *J. Ind. Eng. Chem.* **2020**, *89*, 147–155. https://doi.org/https://doi.org/10.1016/j.jiec.2020.04.021.

(151) Shin, Y. M.; Kim, T. G.; Park, J.; Gwon, H.; Jeong, S. I.; Shin, H.; Kim, K.; Kim, D.; Yoon, M.; Lim, Y. Engineered ECM-like Microenvironment with Fibrous Particles for Guiding 3D Encapsulated HMSC Behaviours. *J. Mater. Chem. B* **2015**, *3*, 2732–2741. https://doi.org/10.1039/c3tb21830a.

(152) Matera, D. L.; Lee, A. T.; Hiraki, H. L.; Baker, B. M. The Role of Rho GTPases During Fibroblast Spreading, Migration, and Myofibroblast Differentiation in 3D Synthetic Fibrous Matrices. *Cell. Mol. Bioeng.* **2021**. https://doi.org/10.1007/s12195-021-00698-5.

(153) Hiraki, H. L.; Matera, D. L.; Wang, W. Y.; Prabhu, E. S.; Zhang, Z.; Midekssa, F.; Argento, A. E.; Buschhaus, J. M.; Humphries, B. A.; Luker, G. D.; et al. Fiber Density and Matrix Stiffness Modulate Distinct Cell Migration Modes in a 3D Stroma Mimetic Composite Hydrogel. *Acta Biomater.* **2022**. https://doi.org/10.1016/j.actbio.2022.09.043.

(154) Li, L.; Yao, Z.; Parian, A.; Yang, Y.; Chao, J.; Yin, J.; Salimian, K. J.; Reddy, S. K.; Zaheer, A.; Gearhart, S. L.; et al. A Nanofiber-Hydrogel Composite Improves Tissue Repair in a Rat Model of Crohn's Disease Perianal Fistulas. *Sci. Adv.* **2023**, *9*. https://doi.org/10.1126/sciadv.ade1067.

(155) Chen, K.; Ph, D.; Sivaraj, D.; Gurtner, G. C. Enrichment of Nanofiber Hydrogel Composite with Fractionated Fat Promotes Regenerative Macrophage Polarization and Vascularization for Soft-Tissue Engineering. *Plast. Reconstr. Surg.* **2022**, 433–444. https://doi.org/10.1097/PRS.0000000000008872.

(156) Daly, A. C.; Riley, L.; Segura, T.; Burdick, J. A. Hydrogel Microparticles for Biomedical Applications. *Nat. Rev. Mater.* **2020**, *5*, 20–43. https://doi.org/10.1038/s41578-019-0148-6.

(157) Riley, L.; Schirmer, L.; Segura, T. Granular Hydrogels: Emergent Properties of Jammed Hydrogel Microparticles and Their Applications in Tissue Repair and Regeneration. *Curr. Opin. Biotechnol.* **2019**, *60*, 1–8. https://doi.org/10.1016/j.copbio.2018.11.001.

(158) Highley, C. B.; Song, K. H.; Daly, A. C.; Burdick, J. A. Jammed Microgel Inks for 3D Printing Applications. *Adv. Sci.* **2019**, *6* (1801076), 1–6. https://doi.org/10.1002/advs.201801076.

(159) Qazi, T. H.; Wu, J.; Muir, V. G.; Weintraub, S.; Gullbrand, S. E.; Lee, D.; Issadore, D.; Burdick, J. A. Anisotropic Rod-Shaped Particles Influence Injectable Granular Hydrogel Properties and Cell Invasion. *Adv. Mater.* **2022**, *34*, 1–12. https://doi.org/10.1002/adma.202109194.

(160) Cho, K.; Lee, H. J.; Han, S. W.; Min, J. H.; Park, H.; Koh, W. Multi-Compartmental Hydrogel Microparticles Fabricated by Combination of Sequential Electrospinning and Photopatterning. *Angew. Chemie - Int. Ed.* **2015**, *756*, 11511–11515. https://doi.org/10.1002/anie.201504317.

(161) Rutte, J. M. De; Koh, J.; Carlo, D. Di. Scalable High-Throughput Production of Modular Microgels for In Situ Assembly of Microporous Tissue Scaffolds. *Adv. Funct. Mater.* **2019**, *29*, 1–10. https://doi.org/10.1002/adfm.201900071.

(162) Molley, T. G.; Hung, T.; Kilian, K. A. Cell-Laden Gradient Microgel Suspensions for Spatial Control of Differentiation During Biofabrication. *Adv. Healthc. Mater.* **2022**, *11* (24), 1–16. https://doi.org/10.1002/adhm.202201122.

(163) Yao, Z.; Yang, Y.; Kong, J.; Zhu, Y.; Li, L.; Chang, C.; Zhang, C.; Yin, J.; Chao, J.; Selaru, F. M.; et al. Biostimulatory Micro-Fragmented Nanofiber-Hydrogel Composite Improves Mesenchymal Stem Cell Delivery and Soft Tissue Remodeling. *Small* **2022**, *2202309*, 1–11. https://doi.org/10.1002/smll.202202309.

(164) Boda, S. K.; Chen, S.; Chu, K.; Kim, H. J.; Xie, J. Electrospraying Electrospun Nanofiber Segments into Injectable Microspheres for Potential Cell Delivery. *ACS Appl. Mater. Interfaces* **2018**, *10*, 25069–25079. https://doi.org/10.1021/acsami.8b06386.

(165) John, J. V; Choksi, M.; Chen, S.; Boda, S. K.; Su, Y.; Mccarthy, A.; Teusink, M. J.; Reinhardt, R. A.; Xie, J. Tethering Peptides onto Biomimetic and Injectable Nanofiber Microspheres to Direct Cellular Response. *Nanomedicine Nanotechnology, Biol. Med.* **2019**, *22*. https://doi.org/10.1016/j.nano.2019.102081.

(166) John, J. V; Mccarthy, A.; Wang, H.; Chen, S.; Su, Y.; Davis, E.; Li, X.; Park, J. S.; Reinhardt, R. A.; Xie, J. Engineering Biomimetic Nanofiber Microspheres with Tailored Size, Predesigned Structure, and Desired Composition via Gas Bubble – Mediated Coaxial Electrospray. *Small* **2020**, *16*, 1–9. https://doi.org/10.1002/smll.201907393.

(167) Miller, B.; Hansrisuk, A.; Highley, C. B.; Caliari, S. R. Guest − Host Supramolecular Assembly of Injectable Hydrogel Nanofibers for Cell Encapsulation. *ACS Biomater. Sci. Eng.* **2021**, *7*, 4164–4174. https://doi.org/10.1021/acsbiomaterials.1c00275.

(168) Miller, B.; Wolfe, W.; Gentry, J. L.; Grewal, M. G.; Highley, C. B.; Vita, R. De; Vaughan, M. H.; Caliari, S. R. Supramolecular Fibrous Hydrogel Augmentation of Uterosacral Ligament Suspension for Treatment of Pelvic Organ Prolapse. *Adv. Healthc. Mater.* **2023**, 1–14. https://doi.org/10.1002/adhm.202300086.

(169) Grewal, M. G.; Helein, G. T.; Sumey, J. L.; Caliari, S. R.; Highley, C. B. Packed Hydrogel Microfibers as a Granular Medium. *bioRxiv* **2023**.

CHAPTER 5: PACKED HYDROGEL MICROFIBERS AS A GRANULAR MEDIUM

5.1. Abstract

Particle-based (granular) hydrogels are an attractive class of biomaterials due to their unique properties and array of applications in the biomedical space – serving as platforms for extrusion printing and injecting as well as permissive materials for 3D cell culture. Physical properties of particle-based hydrogels are governed in part by contact forces between particles, which are limited to interactions with neighboring particles. Secondary annealing mechanisms are often used to increase mechanical properties and serve to link particles across the granular material volume. Here, we present a novel particle-based hydrogel where each "particle" is a discrete electrospun hydrogel microfiber that has been segmented to a length of 93 ± 51 μm, with a diameter of 1.6 ± 0.3 μm. The fibers are flexible and have aspect ratios that are greater than one order of magnitude larger than most traditional hydrogel microparticles. This enables long-range entanglements of discrete fibers following packing into a bulk material, yielding unique properties. Without crosslinking, these packed hydrogel microfiber materials are mechanically robust, they can stretch without breaking when strained, and they exhibit stress relaxation under constant strain. As a cell culture scaffold, shear-induced alignment of the individual fibers within 3D printed filaments confers contact guidance cues to cells and promotes anisotropic cellular morphologies. Packed hydrogel microfibers can also be used as 3D cell culture environments, with cells able to spread due to the permissive nature of the scaffold. Overall, this work introduces a particle-based material system

comprised of individual hydrogel microfibers that allows unique properties to be engineered into biomaterials that might be used in extrusion processes and cell cultures and, ultimately, in tissue engineering and regenerative medicine applications.

5.2. Introduction

In recent years, granular hydrogels – which are hydrogel materials comprised largely of discrete hydrogel microparticles (HMPs) held in place by particle-particle contact forces and, often, engineered interparticle interactions – have received increasing attention in biomaterials research[1]. Granular hydrogels are attractive for reasons that include properties that enable injection delivery as well as control over mechanics and degree of porosity[2–4]. Discrete HMPs, often spherical particles formed through microfluidic or emulsion approaches (on the order of 10^1-10^2 μm in diameter)[1,5], are packed to yield a macroscale construct held together by physical (e.g., contact)[6] or chemical (e.g., covalent)[7] interactions, or both. Physical interactions are commonly introduced through packing of individual HMPs via centrifugation or vacuum filtration where interstitial fluid between the particles is largely removed[1,5]. This places HMPs in direct physical contact where particle-particle contact interactions determine mechanical properties of the granular hydrogel as a whole[8,9]. These purely physical interparticle forces allow for the granular hydrogel to be stable at rest, but individual particles will begin to slide and flow when a force is applied that overwhelms contact interactions in the system (e.g., during extrusion)[6,10–12].

Chemical crosslinking, or annealing, between particles can improve mechanical stability in granular hydrogel systems[13–15]. Annealing can be employ covalent[2] or supramolecular[16] crosslinks between reactive moieties on the surface of discrete particles to stabilize the granular hydrogel. In injection applications into a tissue defect or wound, this stabilization has enabled a class of granular hydrogels known as microporous annealed particle (MAP) scaffolds to serve as injectable tissue regeneration platforms.

There has been considerable work tuning HMP properties, and therefore granular hydrogel behaviors, by varying crosslinking and secondary annealing mechanisms, introducing degradability, and using HMPs to deliver bioactive molecules post-delivery[7,12–18]. This degree of specificity over individual particles allows for engineered modularity[19] and control over physical and chemical heterogeneity in granular hydrogel materials.

Advanced strategies to tune the biomimicry of individual HMPs are largely predicated on spherical particles (aspect ratio ~ 1). Shifting away from spheres, studies leveraging particles with increased aspect ratios have elucidated some unique characteristics when assembled together into granular hydrogel scaffolds. For example, rod-shaped HMPs (aspect ratios ranging from ~ 2-20) enable larger, more interconnected pores throughout the scaffold, which facilitate greater cell migration and infiltration[20,21]. Increasing the size of HMPs while conserving the higher aspect ratios, leads to long, flexible hydrogel strands that can align and entangle when assembled into a granular hydrogel[22,23] – offering interactions at increased length scales compared to other, lower aspect ratio HMPs. These entanglements are useful for extrusion mechanisms[23–25] (e.g., injection and 3D printing) and also enable increased granular hydrogel structural fidelity without secondary annealing[23,26].

Decreasing the diameter of these high aspect ratio strands to sub-cellular length scales (~1 μm diameter "fibers") offers a granular hydrogel platform where cells are able to recruit individual fibers and reorganize the structure of the scaffold[27]. While these have been densely assembled and immobilized through designed annealing interactions[27–29], we sought to develop a materials strategy using dense combinations of hydrogel fibers

without secondary annealing mechanisms to yield granular hydrogels with high mechanical stability and high degrees of permissivity. To achieve this, we electrospin and segment hydrogel microfibers to yield discrete "particles" with sub-cellular length scale diameters and high aspect ratios, which are analogous to extracellular matrix (ECM) fibrous proteins like collagen[30–32]. These individual microfiber segments represent the "grains" that are packed through centrifugation to form the granular hydrogel scaffold – hereafter denoted as packed hydrogel microfiber (PHM) scaffolds. Herein, we demonstrate that PHM scaffolds allow the design of materials which are strain yielding and while exhibiting unique stretching properties. Furthermore, we show that these materials dissipate stress in response to applied strains similar to biological materials and maintain their mechanics with increasing interstitial fluid within the system (i.e., decreasing packing density). Finally, we show that PHM scaffolds can influence cell behaviors through topographical cues, which can be dictated via extrusion and bioprinting, as well as through their unique physical properties as 3D, permissive cell culture scaffolds.

5.3. Materials and Methods

All reagents were purchased from Millipore Sigma, unless otherwise stated.

5.3.1. Methacrylated hyaluronic acid (MeHA) synthesis

Hyaluronic acid (HA) was functionalized with methacrylates as previously discussed[33]. Briefly, sodium hyaluronate (Lifecore, 60 kDa) was dissolved in deionized water at 2% w/v. While maintaining the solution at a pH of ~ 8.5-9, methacrylic anhydride

(Sigma Aldrich, 4.83 mL per g HA) was added dropwise to the solution. The reaction mixture was maintained at a pH of 8.5-9 for 6 h on ice, then continued to react at room temperature overnight. The reaction was dialyzed against deionized water (SpectraPor, 6-8 kDa molecular weight cutoff) at room temperature for 5 days, then frozen and lyophilized to dryness. The final methacrylate functionalization was 100% by quantification with ^{1}H NMR (500 MHz Varian Inova 500) (**Figure S5.1**).

5.3.2. Electrospinning MeHA microfibers

To electrospin MeHA, solutions consisting of 3% w/v MeHA, 2.5% w/v polyethylene oxide (900 kDa), and 0.05% w/v 2-hydroxy-4'-(2-hydroxyethoxy)-2-methylpropiophenone (HHMP) were mixed overnight in DI H_2O. To fluorescently tag microfibers for characterization and visualization, 0.4% w/v fluorescein isothiocyanate-dextran (FITC-dextran) was included in the electrospinning solution. The MeHA solution was extruded through a 16-gauge needle at a rate of 0.5 ml h^{-1} with an applied voltage of 12-14 kV. Microfibers were collected on a negatively charged (-4 kV) rotating mandrel (DOXA Microfluidics) moving at a linear velocity of 10 m s^{-1}. Fiber batches were collected for 1 h before a 2 min UV crosslinking step (365 nm, 5 mW cm^{-2}, VWR UV Crosslinker) to stabilize fibers for subsequent segmentation steps.

5.3.3. Preparation of PHMs

Fibers were hydrated in PBS for at least 1 h and then comminuted through a series of extrusion steps to yield small fiber segments. Beginning with a 16-gauge needle, the fiber solution was passed up and down the needle 25x to preliminarily break up the fibers.

This process was repeated with an 18-gauge needle, and finally a 20-gauge needle to yield the final fiber segments. The resulting solution was then centrifuged, the supernatant was discarded to remove the PEO and unreacted HHMP, and the fibers were resuspended in a known volume of PBS to yield a stock concentration of 10% v/v. Fiber stock solutions were stored at 4 °C until further use. Fluorescently tagged MeHA fibers were diluted and imaged on a Leica DMi8 widefield fluorescence microscope to characterize fiber diameter and length (n>150 fibers) post-segmentation.

For cell culture assays, fibers were functionalized with a fibronectin-mimetic Arg-Gly-Asp (RGD)-containing adhesive peptide (GCGYG<u>RGD</u>SPG, Genscript) via the thiol-Michael addition reaction to promote integrin-mediated cellular interactions in the scaffold. Briefly, fibers were suspended at 10% v/v in the presence of 1 mM RGD, the pH of the solution was elevated to 8 using triethanolamine and allowed to react for 2 h at 37 °C. Fiber solutions were centrifuged and resuspended in PBS thrice to removed unreacted molecules prior to packing.

Fiber solutions were packed (condensed into a minimal volume with minimal solvent between the fibers) via centrifugation at 10,000 RCF for 10 min, with all remaining supernatant decanted to yield the shear-thinning and self-healing PHMs used within this work. PHMs were either used as is (denoted as PHM-100), or further diluted with known volumes of PBS to yield 90% v/v and 80% v/v (denoted as PHM-90 and PHM-80) relative to the original packing density to increase interstitial space between fibers.

5.3.4. Preparation of crosslinkable PHMs

For low crosslinking, fibers were treated with 250 mM cysteamine at pH 8 for 2 h at 37 °C to quench most pendant methacrylate groups and prevent significant crosslinking. For high crosslinking, the fibers were treated with 1 mM cysteamine at pH 8 for 2 h at 37 °C to mimic the RGD addition scheme, while leaving most pendant methacrylates free. Crosslinked fiber scaffolds were prepared by suspending the fiber segments at 10% v/v in a 0.1% w/v HHMP solution, packed via centrifugation as previously described, handled for the experiment (e.g., rheology or extrusion), then treated with 2 min of UV light at 5 mW cm^{-2} to induce crosslinking of the unquenched methacrylate groups.

5.3.5. Oscillatory rheological characterization

Mechanical properties of PHMs were determined via rheological measurements (Anton Paar MCR 302 rheometer) using a 25 mm parallel plate geometry, a solvent trap, and a gap height of 200 μm. Shear-thinning and self-healing properties were determined using oscillatory time sweeps that cyclically changed between low strain (1%) and high strain (250%) at 1 Hz. To assess the ink/support properties of PHMs for extrusion-based printing applications, strain sweeps (0.01-250%, 1 Hz) were conducted to elucidate yield strains (%). Rheological measurements were conducted in triplicate. Shear recovery for each dilution was analyzed using a paired T-test and dilutions compared against each other were assessed using a one-way ANOVA coupled with a Tukey HSD post-hoc test to determine statistical significance.

For characterization of PHM viscoelasticity, time sweeps were utilized to quantify storage and loss moduli. To assess the ability of PHMs to stress relax, a constant 15% strain was applied to the system and the resultant shear stress was recorded over time. Stress relaxation plots were smoothed using an exponential smoothing algorithm for clean presentation. For low and high crosslinkable scaffolds, the samples were irradiated for 2 min at 5 mW cm^{-2} before conducting the rest of the rheological measurements. Time sweeps for UV crosslinking of PHMs are shown in **Figure S5.4**. Viscoelasticity rheological assessments were conducted in duplicate, with representative data shown.

5.3.6. Extensional rheological characterization of PHMs

Extensibility of PHMs was determined via a modified filament stretching extensional rheology protocol[34] (FiSER, Anton Paar MCR 302 rheometer) using a 25 mm parallel plate geometry. Briefly, 500 μl of PHM scaffold was added to the rheometer stage and the gap height was lowered to 1 mm. A vertical strain rate of $\dot{\epsilon}$ = 1.2 s^{-1} was applied, and the normal force was tracked as the geometry height was increased. Filament failure was determined at the point where the material completely broke, and the height of failure was utilized to quantify the overall percentage stretch to failure relative to the original height. FiSER experiments were conducted in triplicate, and statistical significance was evaluated using a one-way ANOVA coupled with a Tukey HSD post-hoc test.

5.3.7. Extrusion printing of PHMs

A FELIX BIOprinter was used for all controlled extrusion of PHMs, and PHM-100 was utilized as the ink due to its robust mechanical properties compared to other dilutions.

Inks were loaded into 1 ml syringes (BD) equipped with a 22 G needle via centrifugation at 200 RCF for 1 min to ensure all air bubbles were removed prior to printing. Printer workflows were written using G-code commands that were actuated through the FELIX BIOprinter's software interface. Targeting filaments with 500 μm diameter, macroscale properties were determined by manipulation of the filament, and microscale properties were determined by printing PHM-100 on glass coverslips. For printed filaments used in cell culture, the glass coverslips were first modified to present methacrylate groups based on a previously described protocol[35] to allow for covalent conjugation of the filament to the coverslip. Videos of extrusion printing are included in **Figures S5.7-S5.8**.

5.3.8. Cell culture

Immortalized murine myoblasts (C2C12s, ATCC) were used for cell culture experiments (passages 6-7). Cells were cultured in standard growth media comprised of high glucose Dulbeccos's Modified Eagle's Medium (DMEM), 10% v/v fetal bovine serum (Gibco), and 1% v/v antibiotic/antimycotic (Gibco). Media was changed every 2 days during expansion and experiments.

For experiments with cells seeded atop printed filaments, the crosslinked scaffolds were first sterilized via irradiation with germicidal light for 2 h. Scaffolds were then hydrated in complete growth media for 1 h prior to seeding cells at a density of 1 x 10^5 cells per scaffold. Cells were cultured for 2 d prior to fixing and staining for analysis. For experiments with cells seeded within fibers as a support, fiber solutions (10% v/v in PBS) were sterilized under germicidal light for 2 h, packed via centrifugation, and the PBS supernatant was exchanged with sterile C2C12 growth media for at least 2 h prior to

packing for cell experiments. PHM-100 was prepared as described above and C2C12s were gently mixed into PHMs at a density of 1 x 10^7 cells/ml and cultured for 1 d in a PDMS mold prior to fixing and staining.

5.3.9. Cell staining

Prior to cell staining, C2C12s seeded on printed filaments were fixed in 10% v/v neutral buffered formalin for 15 min, permeabilized in 0.1% v/v Triton X-100 for 10 min, then blocked with 3% w/v bovine serum albumin for 2 h at room temperature. Cells were incubated with AlexaFluor-488 phalloidin for 1 h to visualize F-actin (1:600, Invitrogen). Samples were washed thrice in PBS to remove unbound molecules.

A similar protocol was utilized for experiments with C2C12s in PHMs supports. Cells were fixed for 1 h, permeabilized for 1 h, and blocked for 2 h using the same solution concentrations prior to tagging F-actin with AlexaFluor-488 phalloidin (1:200) for 2 h. Again, samples were washed in PBS thrice to remove unbound fluorophore.

5.3.10. Microscopy and image analysis

Fluorescence microscopy for fiber segmentation and printed filament analysis was conducted on a Leica DMi8 widefield fluorescent microscope. For cell imaging on filaments or within supports, a Leica Stellaris Confocal microscope was utilized to image Z-stacks, with representative maximum projections shown here. Fiber length, diameter, and directionality, as well as cell orientation and area were all quantified using built-in ImageJ functionalities.

5.4. Results and Discussion

5.4.1. Preparing packed hydrogel microfiber scaffolds

Packed hydrogel microfibers were fabricated from electrospun methacrylated hyaluronic acid (MeHA), which has demonstrated biocompatibility[36,37] and been previously used in electrospinning[38,39] (^{1}H NMR spectrum confirming MeHA synthesis shown in **Figure S5.1**). Electrospun MeHA fibers were designed to model endogenous ECMs both through the use of a material based on the native glycosaminoglycan, hyaluronic acid (HA), and its subsequent processing into hydrogel microfibers that mimic the natural protein fibers in the ECM[40–43]. Methacrylation enabled photomediated crosslinking to stabilize the fibers prior to hydration (**Figure 5.1A**) and, through reactive methacrylates that remain after photocrosslinking, coupling of the fibronectin-mimetic Arg-Gly-Asp (RGD) adhesive motif through a Michael addition reaction to a cysteine residue incorporated into the RGD-containing peptide[44].

To create segmented microfibers that can be packed together to form PHMs, crosslinked MeHA fibers were hydrated then segmented via a series of triturations through needles of decreasing inner diameter (16 G, 18 G, and 20 G)[27,28,45]. The resultant fiber segments (**Figure 5.1B**) were 1.6 ± 0.3 μm in diameter and 93 ± 51 μm in length (**Figures 5.1C** and **S5.2**). After packing the suspension of discrete fibers by centrifugation, they behaved as a bulk solid at rest (**Figure 5.1D**), similar to conventional granular hydrogels. Compared to granular materials based on spherical particles, the high length:diameter aspect ratio of the microfibers in a PHM scaffold allows for unique long-range entanglements. These long-range interactions allow for dilution of the "fully packed" scaffolds to increase inter-fiber fluid content and provide more space between individual

191
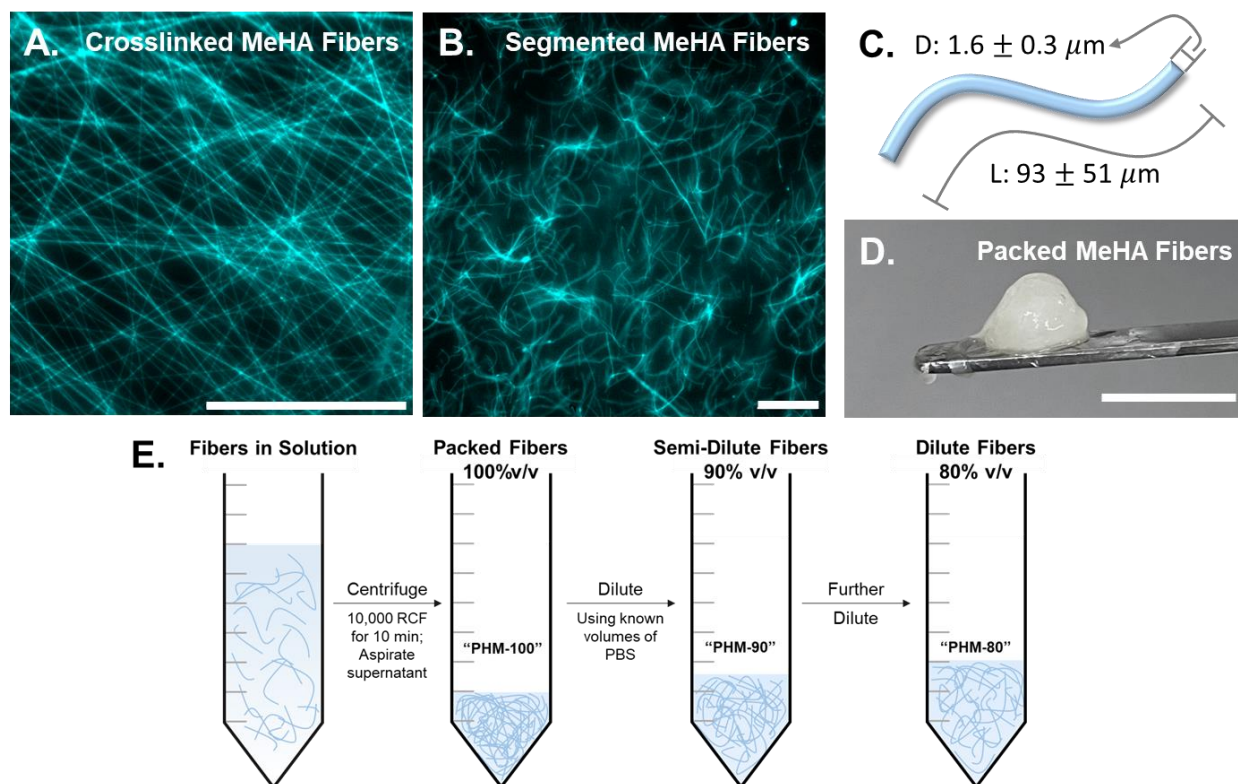
Figure 5.1. Fabrication of packed hydrogel microfiber-based hydrogel scaffolds. (A) Dry MeHA fibers containing a fluorophore for visualization immediately following the electrospinning and crosslinking processes. (B) Trituration yields fiber segments in solution that are (C) on the order of ~100 μm in length, with diameters on the order of ~1 μm. (D) Packing via centrifugation at 10,000 RCF for 10 minutes yields a packed hydrogel microfiber scaffold that behaves as a bulk solid at rest. (E) Schematic illustrating how PHM-100, PHM-90, and PHM-80 scaffolds were assembled, where more PBS added increases the inter-fiber fluid content while conserving total hydrogel microfiber content in each sample. *Scalebars (A-B) = 100 μm and (C) = 1 cm.*

fiber segments. Here, we define the "fully packed" scaffolds as consisting of 100% v/v of the material recovered from centrifugation. The fully packed material, hereafter referred to as "PHM-100", can be further diluted with known volumes of PBS to 90% v/v and 80% v/v, referred to as "PHM-90" and "PHM-80", respectively (shown in **Figure 5.1E**).

5.4.2. Mechanical Characterization of PHMs

PHM-100, PHM-90, and PHM-80 all exhibit characteristics that are important for particle-based hydrogels used for extrusion processes or in cell culture systems. Shear-thinning and self-healing were evidenced in all dilutions via oscillatory shear rheology (**Figure 5.2A**) through repeated cycling between low (1%) and high (250%) strains. In contrast to granular hydrogels based on spherical particles[6,46], the storage modulus recovered after removal of the high strain from the system was reduced (~60-70%) in all groups (**Figure 5.2B**). This reduction was statistically significant and observed between the first and second low-strain regimes, with no statistical significance in the percentage drop in modulus across dilutions. We attribute this PHM behavior to rearrangements of microfibers during rheometric analysis. After initial packing via centrifugation, the organization of the segmented fibers is likely maximumly entangled through random organization, giving rise to the initial mechanical properties of the scaffold. During the high-strain regimes, this organization is disrupted, and a portion of the long-range entanglements is irreversibly lost.

As in other granular hydrogel and shear thinning systems, the ability to convert from a solid to liquid-like state above a yield strain (defined as the crossover point between G' and G" in a strain sweep[17], **Figure 5.2C**) allows the solid-like material to be injected or extruded. The 136% yield strain (**Figure 5.2D**) for the 100% v/v group (PHM-100) is notably larger than other granular hydrogel systems[20]. Diluted fiber density in the PHM-90 and PHM-80 groups yielded statistically decreased yield strains of 56% and
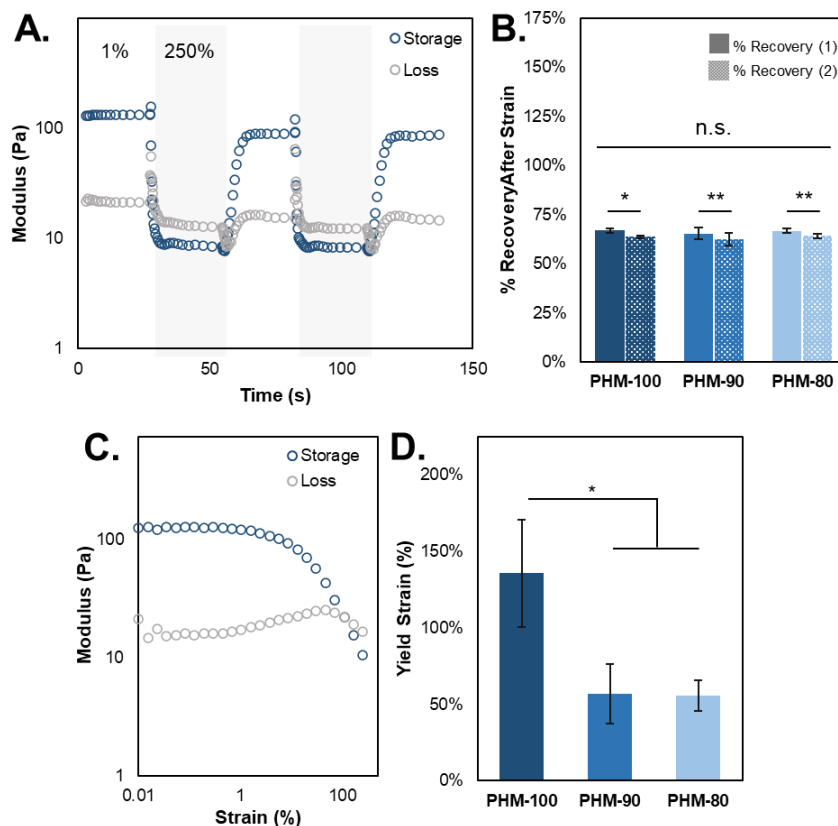
Figure 5.2. **Rheological characterization of packed hydrogel microfiber-based scaffolds.** (A) Cyclical application of high (250%, shaded regions) and low (1%) strains demonstrates shear-thinning and self-healing properties of PHM-100 (PHM-90 and PHM-80 shown in **Figure S5.3**). (B) Quantification of recovery after strain shows that PHM scaffolds recover ~60-70% of their initial modulus prior to the addition of high strain – suggesting that organization of discrete fibers influences overall mechanical properties. (C) Amplitude sweep for PHM-100 demonstrates shear-yielding properties of this group with (D) yield strains for diluted groups (PHM-90 and PHM-80 rheological data shown in **Figure S5.3**) significantly less than PHM-100. *$p < 0.05$; ** $p < 0.01$.

57%, respectively, which is consistent with yield strains of other reported granular hydrogel systems[20]. These data indicate that all test groups are shear-thinning and self-healing, with yield strains generally in ranges characteristic of granular hydrogels used in extrusion processes. Furthermore, increased yield strains are possible in PHM formulations, which indicate the potential for enhancing the stability of particle-based hydrogels through dense fiber-based formulations.

5.4.3. Evaluating the extensibility of PHM scaffolds

Anticipating that long-range interactions between microfibers in PHM scaffolds resulting from their high aspect ratios would offer unique bulk properties, we next examined the extensibility of the PHM-based materials. We conducted a modified version of filament stretching extensional rheology (FiSER)[47], in which a material can be stretched as a filament, allowing strain to failure to be observed as a measure of material extensibility or stretchability. We hypothesized that discrete fibers within the filament would participate in interactions at extended length scales compared to conventional granular materials, thus resulting in highly extensible PHM materials when stretched. Compared to spherical particle interactions, which would be restricted to engagements with a limited number of neighboring particles[1], we expected that a PHM scaffold would stretch more and appear less brittle as a bulk than a conventional granular hydrogel.

In modified FiSER testing, all groups of PHMs exhibited strain-to-break values of 2000-2500% (**Figure 5.3A**), indicating fibers maintain filament-stabilizing interactions in response to stretching. Notably, while PHM-100 exhibited the highest degree of stretchability (~2500%), there was no statistical difference between the groups. In these measurements, the normal forces sustained by the filaments during extension (**Figure 5.3B**) were observed to decrease with respect to hydrogel microfiber density. These observations combine to suggest that the extensibility of a PHM scaffold is dictated by fiber geometry, while the density of fiber-fiber interactions (i.e., the combination of entanglements and surface-surface interactions) drives the forces that can be sustained during stretching. Correspondingly, the normal force profiles for each group exhibit the same trend as they are stretched to failure, which occurs at % strains that exhibit no

statistical difference. We believe this extensibility (visualized during testing of PHM-100 in **Figure 5.3C**) is unique among particle-based hydrogels where there is no dissolved polymer between particles, and that it is driven by enhanced interactions among the discrete elements of the bulk material that result from the high-aspect ratios of the individual fibers in the PHM scaffold.
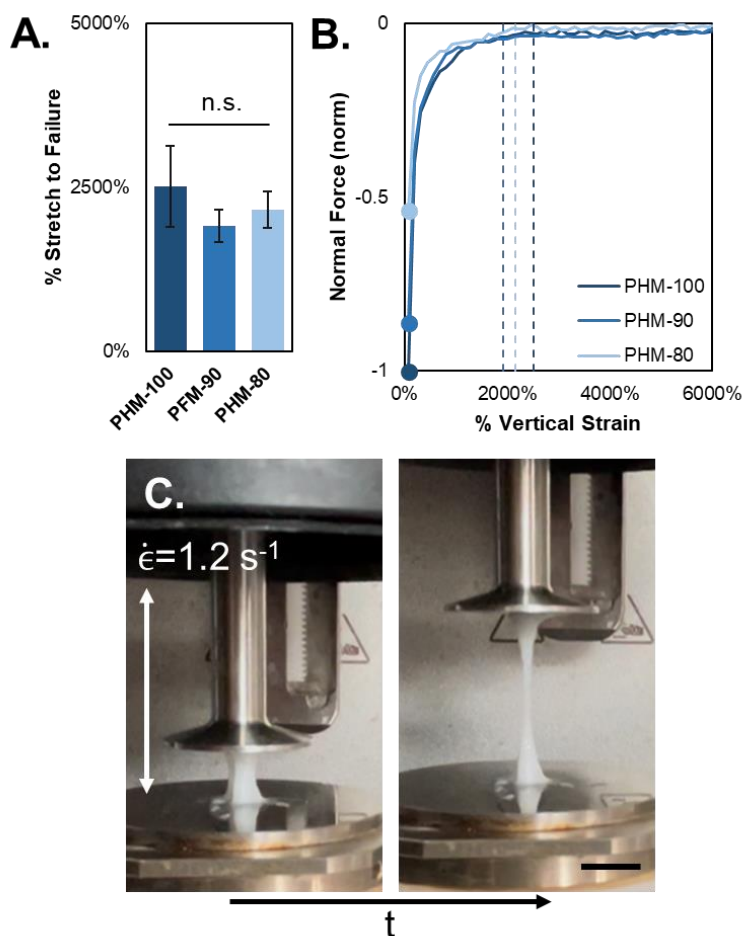
Figure 5.3. **Modified FiSER characterizes extensibility of packed hydrogel microfiber scaffolds.** (A) Percentage stretch to failure of PHM-100, PHM-90, and PHM-80 filaments indicates that all groups can stretch vertically to greater than 2000% of their original height with no statistical significance between groups. (B) Representative trends of normal force for each dilution (normalized to PHM-100) illustrates that although percentage stretch to failure is similar for all groups, the original normal force (indicated by filled circles at 0%) decreases as dilution increases. However, normal forces exhibit similar trends once the stretching begins. Dashed lines correspond to the average % stretch to failure values from A. (C) Representative images of PHM-100 being stretched using the modified FiSER setup. *Scalebar (C) = 1 cm.*

5.4.4. Characterizing viscoelasticity and stress relaxation of PHM scaffolds

Given observation of these dynamic behaviors of PHM hydrogels, we were interested in further characterizing their viscoelasticity and stress relaxation to determine whether they might offer new properties as cell and tissue culture scaffolds. Endogenous tissue exhibits a host of complex, time-dependent mechanical properties that are difficult to recapitulate in traditional hydrogel materials[48–50]. For example, ECM structural components like collagen fibers present in many native tissue microenvironments enable the dissipation of stress over time, thereby contributing to nonlinear viscoelasticity profiles[51]. Inspired by this and other long-standing observations of the similarities between the geometries of electrospun fibers and ECM fibrous proteins[30], we hypothesized that noncovalent interactions between individual fibers in 3D PHM materials would allow effective mimicking of the stress relaxation of native ECM in a synthetic system. As noted above, the previous characterization experiments suggested the ability of fibers within the PHM hydrogels to interact at rest but slide past each other and reorganize to dissipate forces applied to the materials.

To assess PHM scaffold viscoelasticity for comparison to biological tissues and materials[48], we measured the loss modulus (i.e., viscous component, G") versus storage modulus (i.e., elastic component, G') from rheometric time sweeps (**Figure 5.4A**). All PHM formulations exhibited relatively soft bulk storage moduli – ranging from ~50 Pa for PHM-80 to ~150 Pa for PHM-100, despite individual hydrogel microfibers having moduli many orders of magnitude greater than bulk fiber-based scaffolds[39]. Additionally, all groups demonstrated viscoelastic behavior with their storage moduli approximately 5x their loss moduli (grey dashed line in **Figure 5.4A** illustrates where $G' = 5 \times G''$).
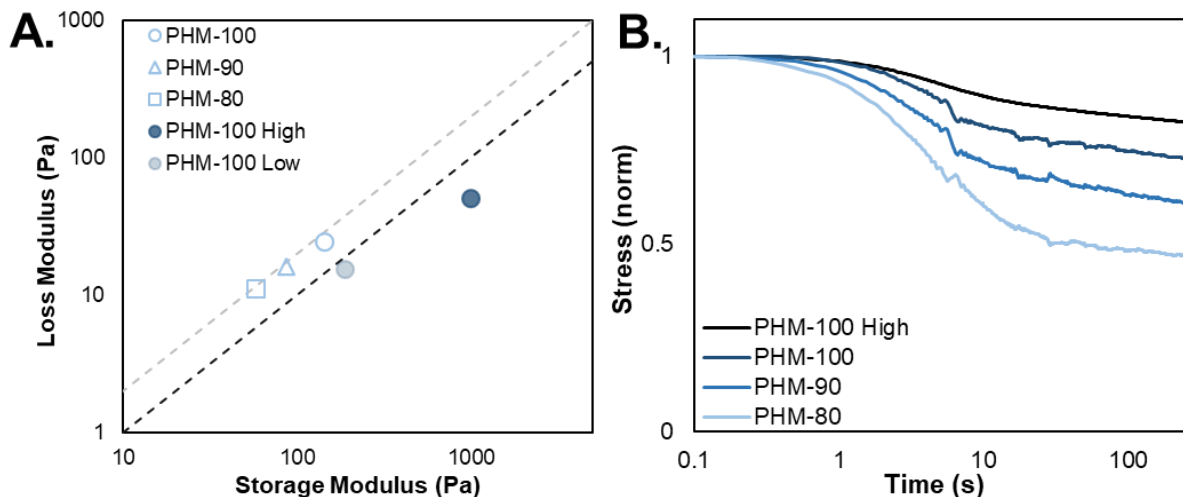
Figure 5.4. Characterization of viscoelasticity and stress relaxation properties. (A) Plot of shear loss modulus versus shear storage modulus of PHMs. Grey dashed line and black dashed line represent where G' is equivalent to 5x G'' and 10x G", respectively. Non-crosslinked groups reside near the 5x trend, whereas the addition of secondary annealing to stabilize the material shifts the viscoelasticity to the 10x trend, which is characteristic of many biological tissues[48]. (B) Plot of stress relaxation tests where a 15% constant shear strain was applied to the systems and resultant stress was observed as a function of time. All groups exhibit relatively rapid stress relaxation and mimic profiles characteristic of viscoelastic solids. PHM-100, PHM-90, and PHM-80 are compared with the PHM-100 High group.

Importantly, endogenous tissue typically possesses a higher elastic contribution, where the storage moduli are typically 10x the loss moduli[48]. We further postulated that we could achieve this 10x target via additional interfiber crosslinking (or annealing) of PHMs.

To test this, we designed PHMs to have residual methacrylate groups on the surfaces of individual microfibers that were not consumed during the initial fiber crosslinking process. Utilizing the PHM-100 formulation, we created "High" and "Low" crosslinkable fibers, where the "PHM-100 High" group was treated after fiber segmentation to remove some reactive methacrylate groups (to mimic RGD modification) but had most residual methacrylate groups available for crosslinking. The "PHM-100 Low" group was similarly treated after fiber segmentation to eliminate most, but not all, residual

methacrylate groups on the fibers. Therefore, PHM-100 High could achieve considerable annealing during a secondary crosslinking step by inducing methacrylate polymerization. Conversely, PHM-100 Low could undergo only a comparatively low degree of secondary crosslinking, resulting in reduced interfiber annealing compared to PHM-100 High (rheology for the secondary UV-initiated annealing step shown in **Figure S5.4**).

We observed in both groups (PHM-100 High and PHM-100 Low) that interfiber crosslinking shifted the G':G'' ratio towards 10:1 (**Figure 5.4A**, shaded circles, dashed black line represents $G' = 10 \times G''$). PHM-100 Low exhibited a stark decrease in G'' coupled with a marginal increase in G' compared to PHM-100. Interestingly, PHM-100 High exhibits a slight increase in the loss modulus coupled with a notable increase in the storage modulus, which also shifted the viscoelastic moduli toward the 10:1 ratio that characterizes many biological tissues. Taken together, these data suggest that the degree of secondary crosslinking afforded by available methacrylate groups can be utilized to controllably modulate the viscoelasticity of PHM hydrogel systems.

As previous tests pointed to dynamic responses to applied stress in PHM scaffolds, we next sought to evaluate their capacity to undergo stress relaxation. Time-dependent stress relaxation is a feature of many biological material systems that is observed to critically influence cellular behaviors[48,52]; however, it is challenging to engineer and control stress relaxation in many hydrogel systems. In this analysis, we applied a constant shear strain of 15% to the sample and recorded the resultant stress as a function of time to assess how the material relaxes in response to the applied strain. Plotted as the normalized stress in **Figure 5.4B**, PHM-100, PHM-90, and PHM-80 all exhibit varying degrees of stress relaxation, with increasing relaxation corresponding to increased

dilution with PBS. The enhanced relaxation for the diluted groups is attributed to more space for fibers to reorganize in response to the applied strain and reduced interactions between fibers on a per volume basis. PHM-100 experiences the highest degree of these interactions and the most confining interfiber space that slows or prevents fiber movement that results in PHM stress relaxation.

To observe the effects of interfiber crosslinking, we applied the same 15% strain to the PHM-100 High group. We observed that PHM-100 High dissipated stress modestly (**Figure 5.4B**). However, the covalent interfiber crosslinking restricted the ability of the microfibers to move and thus prevented the material from relaxing to the extent of the non-crosslinked groups (**Figure 5.4B**). Importantly, with respect to recapitulating the relaxation time scales of viscoelastic solids, the relaxation profiles of the PHM hydrogels began to plateau within 100 s of stress being applied. Through the use of a viscoelastic standard linear solid model (**Figure S5.5**), characteristic relaxation times (τ) were calculated[53]. All groups, including the PHM-100 High crosslinked material, exhibited most of their stress relaxation within a characteristic time of approximately 5-10 s, indicating that PHM systems respond to applied strains rapidly. From these data, we expect these non-crosslinked materials to be useful in engineering soft tissue systems *in vitro*, and in engineering both soft and stiffer tissues (via secondary crosslinking) to model physiological systems where ~100s and quicker relaxation times are desired.

5.4.5. Extrusion of PHM inks

As mentioned, the rheological and mechanical properties of PHM materials should enable diverse uses in applications where injectable or extrudable biomaterials are

desired, including in biomedical applications of 3D printing. We studied the responses to extrusion processes using a 3D printer (FELIX BIOPrinter). In controlled extrusions, we first printed a 2 cm vertical filament of PHM-100 through a 22 G needle (ID: 0.413 mm). This yielded a filament with a diameter of ~0.5 mm (**Figure 5.5Ai**). Towards observing the stability of PHM filament without interfiber crosslinking (a filament stabilized strictly by noncovalent interactions), we translated the vertical filament 1 cm horizontally without further extrusion (**Figure 5.5Aii**) and then back to the original position (**Figure 5.5Aiii**). The filament was easily manipulated without breakage. Additionally, the filament stretched noticeably as a result of undergoing dynamic stress relaxation when extended without extrusion (**Figure 5.5Aiii**, dashed circle). To further observe the extent to which the filament was extensible, the nozzle was moved vertically an additional 2 cm without extrusion. We attribute this high degree of extension to the long-range interactions among the individual microfibers, which provide additional stability in the filament that would not occur with other particle-based systems with smaller aspect ratios.

Finally, towards demonstrating the remarkable stability of the non-covalently annealed PHM filaments, we extruded filaments horizontally across the posts of a 2.5x2.5 cm inverted table (**Figure 5.5B**). The resultant filaments were mechanically stable, spanning these gaps without breaking while stabilized only by physical interparticle interactions. This demonstration of the strength of long-range interactions among individual fibers being sufficient to maintain filament integrity at longer scales is an exciting feature of the PHMs as a granular hydrogel system. These properties will have value in

numerous applications that use extrusion processes, including 3D printing, where structural fidelity of printed hydrogel inks remains a central consideration in developing new biomaterial inks.
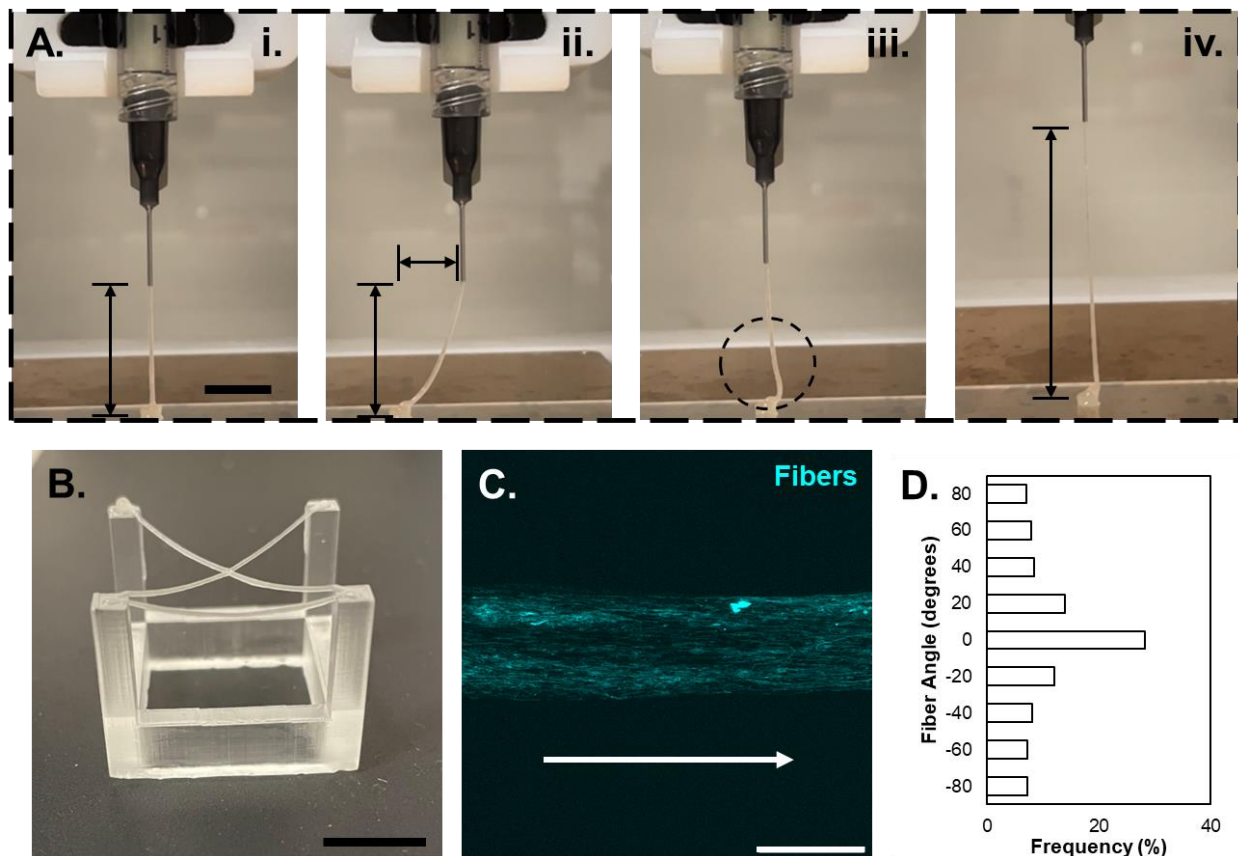
Figure 5.5. Extrusion of packed hydrogel microfiber inks. (A) (i) PHM-100 was extruded at a rate that yields a 2 cm vertical filament that is ~0.5 mm in diameter. (ii) Following extrusion, the filament was then manipulated to demonstrate the fidelity of PHM-100. The filament was translated 1 cm horizontally before (iii) returning to the original horizontal position. The dashed circle highlights filament sagging due to stretching. (iv) The filament was finally stretched another 2 cm vertically without breaking. (B) Macroscale extrusion of PHM-100 across 4 posts of a 2.5x2.5 cm table without secondary crosslinking. These demonstrations highlight the shear-thinning and self-healing properties that are desired for extrusion printing, with the high extensibility and long-range entanglements enabling stretching and filament fidelity at long ranges without additional annealing mechanisms. (C) Fluorescent image of the microscale topography of a printed filament illustrating shear-induced alignment (white arrow indicating direction of printing) of the fibers following extrusion. (D) Quantification of fiber direction indicates that a high percentage of fibers are aligned in the direction of shear (0 degrees corresponding to the direction of the white arrow). *Scalebar (A-B) = 1 cm, (C) = 500 μm.*

In addition to observing these macroscale characteristics of extruded filaments, we were interested in the effects of extrusion processing on the PHM filaments at the microscale, in particular the organization of the fibers after extrusion. From our previous rheological studies, we concluded that the organization of fibers within PHM scaffolds drives mechanical properties but can be influenced by high shear. Therefore, we hypothesized that the shear introduced by the extrusion process might disrupt fiber orientation and induce anisotropic alignment in the direction of shear. To assess this, we mixed nonfluorescent fibers with fluorophore-tagged fibers at a 10:1 ratio to enable visualization of the extruded material, and printed PHM-100 onto glass coverslips. Indeed, fibers aligned in the direction of the applied shear (**Figure 5.5C-D**). This result follows previously demonstrated shear-induced alignment of fibers embedded in bulk gels by Prendergast and coworkers[45], as well as alignment demonstrated by Kessel et al. using hydrogel microstrands[23] and Sather et al. utilizing self-assembled supramolecular nanofibers[54]. However, in the PHM materials used here, which consisted entirely of electrospun fibers with diameters on the order of 1 μm, there was a unique opportunity to directly control the surface topography to direct cell behaviors. The importance of microscale topography and contact guidance on cellular behaviors has been well studied and characterized[55–58], and the ability to dictate surface topography via extrusion using PHMs is an exciting opportunity to extend work using electrospun hydrogel fibers.

5.4.6. PHM scaffolds support 2D and 3D cell culture

Given the potential to use PHM materials in bioprinting to create materials with specified surface anisotropies and to design permissive 3D environments using PHMs, we next sought to examine cellular responses to these materials. To assess whether fiber alignment in filaments would provide microscale topographical cues to cells that interacted with these materials, we printed a PHM biomaterial ink and seeded cells onto it. We extruded PHM-100 with 1 mM RGD (analogous to PHM-100 High) that could undergo a secondary interfiber crosslinking onto glass coverslips and then irradiated with light to stabilize the filament through secondary crosslinking. Immortalized murine myoblasts (C2C12s), which are known to respond to alignment cues[55], were seeded atop the crosslinked PHM-100 filament (**Figure 5.6A**). Following a 2 d culture period, cytoskeletal staining showed that cells aligned with the direction of microfibers in the
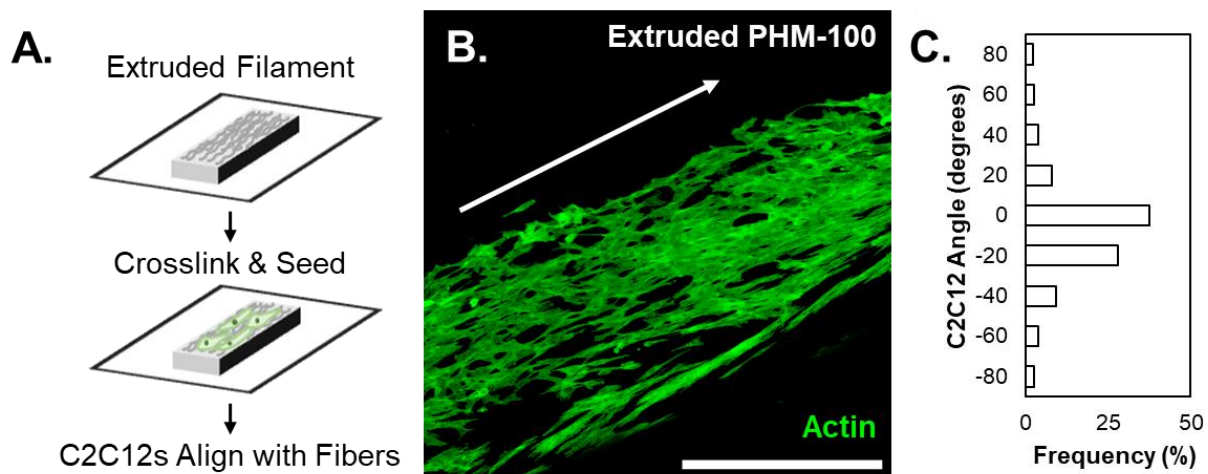
Figure 5.6. Extruded PHM scaffolds influence cell culture. (A) Process schematic for extruding PHM-100, crosslinking the individual fibers together to stabilize the filament, then seeding C2C12 cells on top of the scaffold. (B) Fluorescent micrograph of C2C12s tagged with AlexaFluor-488 phalloidin for visualization of cell alignment. (C) Quantification of cell alignment with 0 degrees corresponding to the direction of shear (white arrow). The microscale topography of the extruded filament induces alignment of C2C12 cells cultured on top of the scaffold. *Scalebar (B) = 500 μm.*

filament (**Figure 5.6B-C**), indicating that the microscale topography provided contact guidance that can influence cellular organization. Because fiber alignment responds to changes in needle direction (**Figure S5.6**), these results suggest the ability to influence cell directionality via the needle path during extrusion, with arbitrary 2D topography and cell alignment defined by the extrusion printing process when using PHMs as a biomaterial ink.

We next looked at how cells within a 3D PHM-based hydrogel would behave, given the dynamic properties measured previously. Since our most fiber-dense formulation (PHM-100) is soft and viscoelastic, we postulated that C2C12s would be able to reorganize the constituent fibers during proliferation, migration, and interactions with the environment. Over short time scales, we expected to see cell spreading within these materials as opposed to rounded morphologies typical of cells in 3D hydrogels that are not permissive[59,60]. To investigate this, C2C12s were gently mixed with PHM-100 which would undergo no interfiber crosslinking, in order to maintain the dynamic properties observed in previous experimentation. The C2C12+ PHM-100 was then placed into a PDMS mold and covered with 100 μm pore filter paper to prevent PHM-100 from disassociating in culture media (**Figure 5.7A**). After 1 d in culture, cytoskeletal staining showed that C2C12s were able to spread freely in PHM-100 (**Figure 5.7B**), with a wide range of projected cell areas, along with a loss of circularity (cell shape index) that would be expected in a covalently crosslinked hydrogel quantified in **Figure 5.7C-D**.
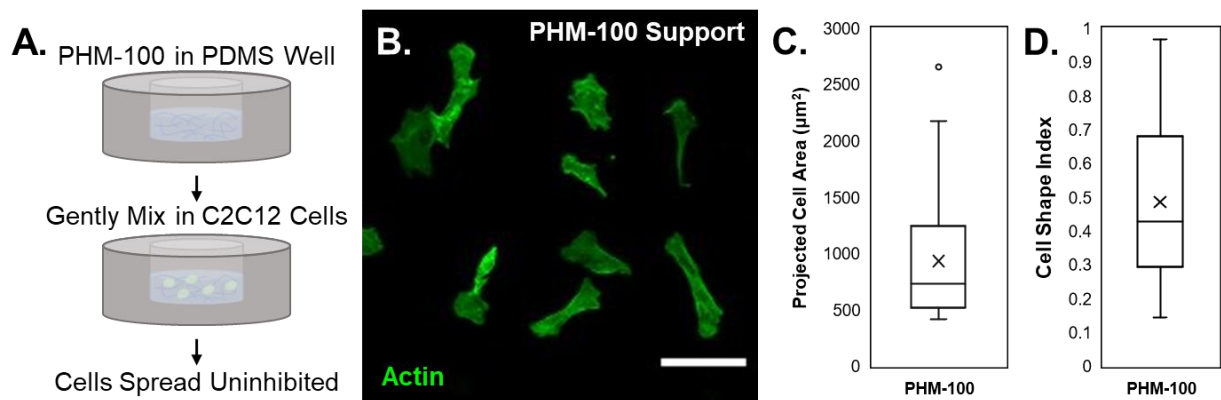
Figure 5.7. PHM scaffolds support 3D cell culture. (A) Process schematic for culturing C2C12 cells within a PHM-100 support using PDMS wells to contain the scaffolds. (B) C2C12s stained with AlexaFluor-488 phalloidin (1 d) spreading in the non-crosslinked PHM-100 scaffold. (C-D) Quantification of projected cell area and cell shape index reveal ranges of cell spreading and circularity, further supporting the permissivity of PHMs at short timescales. *Scalebar (B) = 100 μm.*

Our observations suggest that PHM-100, even absent interfiber crosslinking, supports 3D cellular activity. The cell spreading observed was in our most fiber-dense formulation, suggesting that PHMs yield in response to cells' movements and impose minimal spatial restrictions on the cells. We believe that because the microfiber elements of the material are soft and have diameters on the order of 1 µm, they might be uniquely permissive to cellular activity. In comparison to larger spherical particles used in other granular materials, whose diameters are on the order of 10^1-$10^2 \mu$m, PHMs may present an alternative physical environment to the cells incorporated into them *in vitro* or with cells that engage with them when applied *in vivo*. We postulate that opportunities to reorganize and move throughout 3D space exist in PHM-type systems that might be less accessible in granular materials with larger particle diameters, where particle movement in response to cellular activity would be limited, resulting in cells negotiating the surfaces of the particles and the spaces in between. PHMs offer exciting new opportunities within particle-based materials through their presentation of robust bulk properties emerging

from a microenvironment comprised of individual fibers that cells can readily interrogate, reorganize, and migrate around.

5.5. Conclusions and Future Outlook

In summary, we have developed a new class of particle-based hydrogels comprised solely of discrete electrospun microfibers. Packed hydrogel microfiber scaffolds (PHMs) are shear-thinning and self-healing, with strain yielding responses that will enable application in extrusion or injection processes. The high-aspect ratios of the fibers and long-range entanglements provide physical interactions in PHMs that result in robust materials that behave elastically as a bulk below a yield strain. These interactions also enable high degrees of extensibility in packed scaffolds. PHMs can be stretched to greater than 2000% of their original height; a phenomenon that is conserved across PHM scaffolds during dilution. PHM scaffolds are also viscoelastic and quickly (~10 s) dissipate stresses applied to them. Macroscale extrusion printing demonstrates filament fidelity and robust stability, even without secondary crosslinking to stabilize filaments. Shear-induced alignment of component microfibers during extrusion can be leveraged to direct cellular alignment when seeded on top of printed filaments. Cells seeded within these materials – or potentially infiltrating into these materials – experience permissive, 3D environments that they can interrogate and possibly remodel during migration and proliferation.

We envision this novel packed hydrogel microfiber system will provide an exciting new avenue for designing granular hydrogel media. The flexibility afforded by the PHM preparation process coupled with the ability to tailor individual fibers that comprise the

bulk scaffold will enable new approaches to engineering synthetic models of the ECM *in vitro* and new opportunities for engineering implantable biomaterials.

5.6. Acknowledgements

5.7. Supplementary Figures
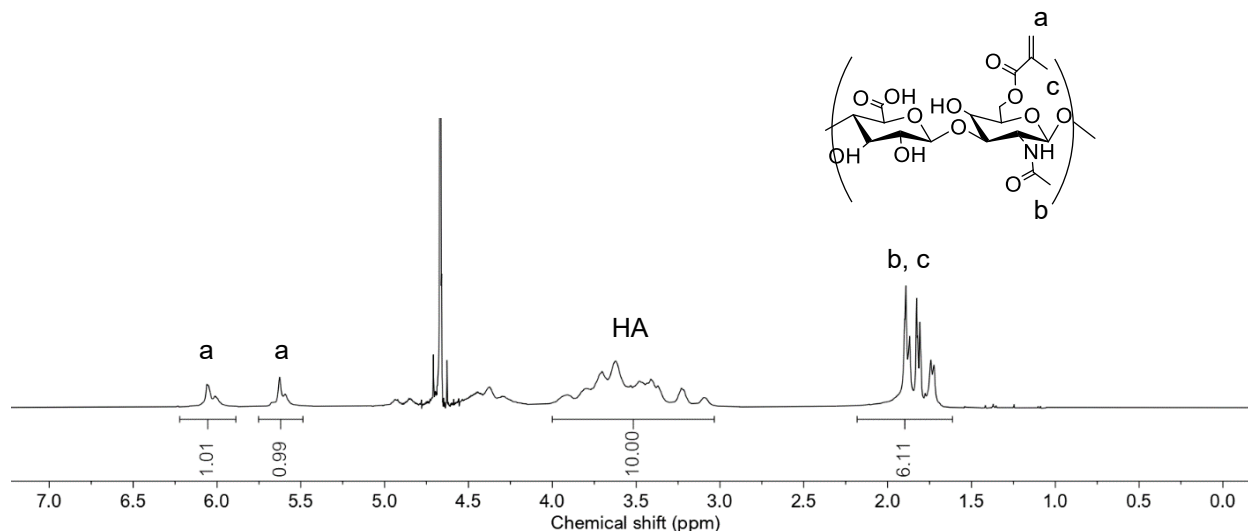
Figure S5.1. Methacrylate-functionalized hyaluronic acid (MeHA) ^{1}H NMR spectrum. The resultant NMR spectrum is normalized to the 10 hydrogens on the standard HA backbone (~3.0-4.0 ppm), and the degree of modification is determined based on the integral of the peaks corresponding to the methacrylate groups (~5.5-6.25 ppm). The above spectrum illustrates a modification of ~100%.
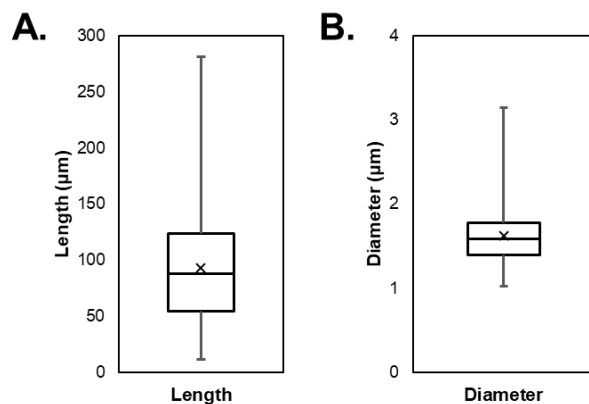
Figure S5.2. Quantification of fiber length and diameter. (A) Segmented fiber length was determined to be 93 ± 51 μm. (B) Segmented fiber diameter was determined to be 1.6 ± 0.3 μm. Fluorescent images of fiber solutions were utilized to quantify fiber segments.
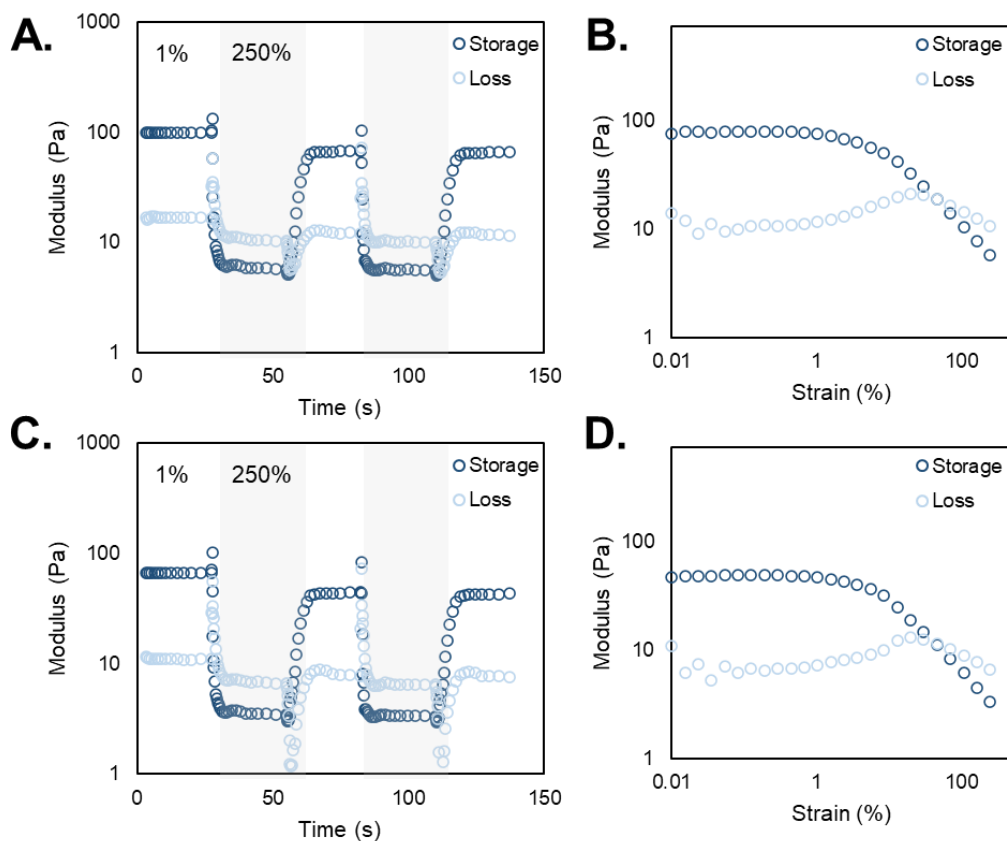
Figure S5.3. Rheological characterization of PHM-90 (A-B) and PHM-80 (C-D). (A, C) Shear-thinning and self-healing properties of PHM-90 and PHM-80, respectively. While modulus values are decreased compared to PHM-100, the trends are starkly similar, regardless of dilution. (B, D) Amplitude sweeps illustrate strain yielding properties of these diluted PHMs, with yield-strains significantly decreased compared to PHM-100 (shown in **Figure 5.2**, main text).
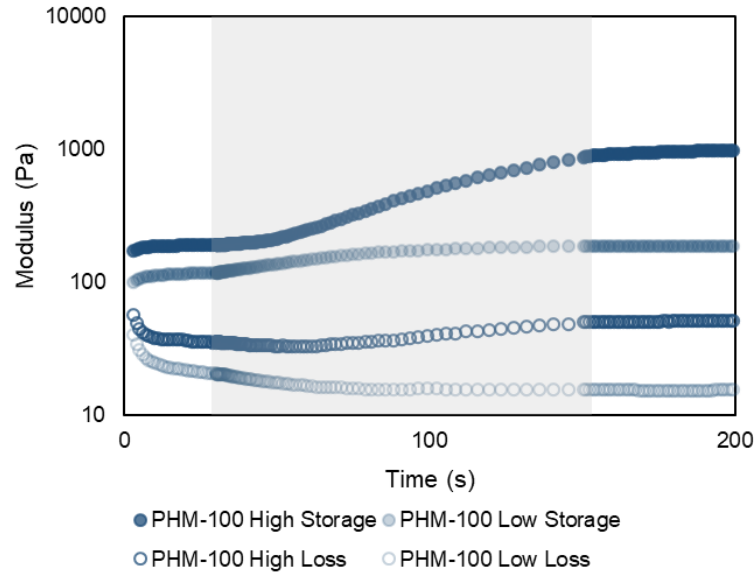
Figure S5.4. UV crosslinking of PHM-100 High and PHM-100 Low. Representative time sweeps including a UV cure step (shaded region). PHM-100 High, which has the most methacrylate groups available for crosslinking, exhibits a noticeable increase in storage modulus compared to the original pre-crosslinked state and the crosslinked PHM-100 Low as well. Importantly, both groups demonstrate a larger difference between their respective storage and loss moduli following the secondary crosslinking, which yields G' values that are ~10x the G" values.
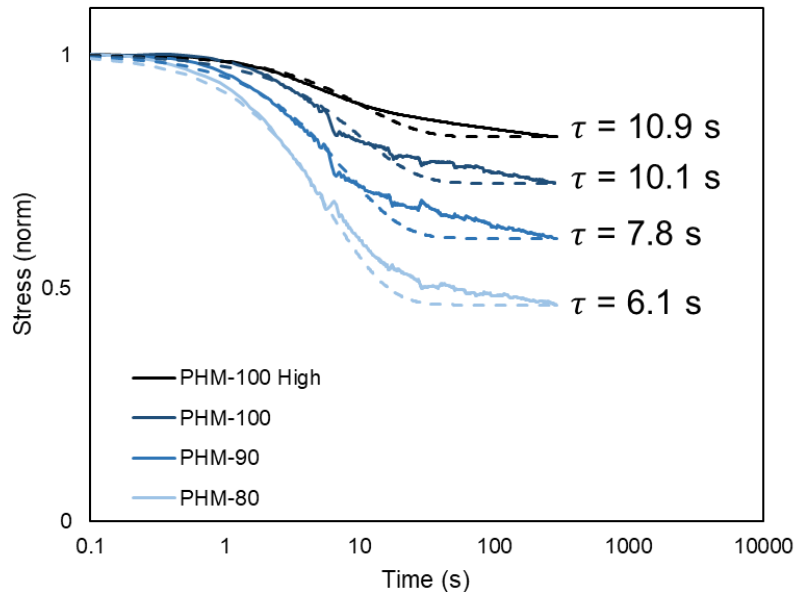
Figure S5.5. Modeling stress relaxation with a viscoelastic standard linear solid (SLS) model. Stress relaxation profiles of PHM-100, PHM-90, PHM-80, and PHM-100

High (solid lines) with corresponding SLS models (dashed lines). Representative relaxation time constants (τ) are shown adjacent to each group.

The stress relaxation profiles of PHMs exhibit behaviors similar to viscoelastic solids. Interestingly, work by Wingert and coworkers[53] demonstrated that Nylon-11 nanofiber meshes dissipated stress similarly to PHMs, albeit at much longer time scales (on the order of minutes). Therefore, we leverage the same viscoelastic standard linear solid (SLS) model to analyze the stress relaxation of PHMs that was utilized to model the Nylon-11 fibers. The basic SLS model is shown below as **Equation 5.1**, and the resultant τ values are shown in the figure corresponding to the PHM group.

$$\frac{\sigma(t)}{\sigma_0} = \beta + (1 - \beta)\, exp\left(-\frac{t}{\tau}\right) \tag{1}$$

Where:

$$\tau = \text{relaxation time constant}$$

$$\beta = \lim_{t \to \infty} \frac{\sigma(t)}{\sigma_0}$$
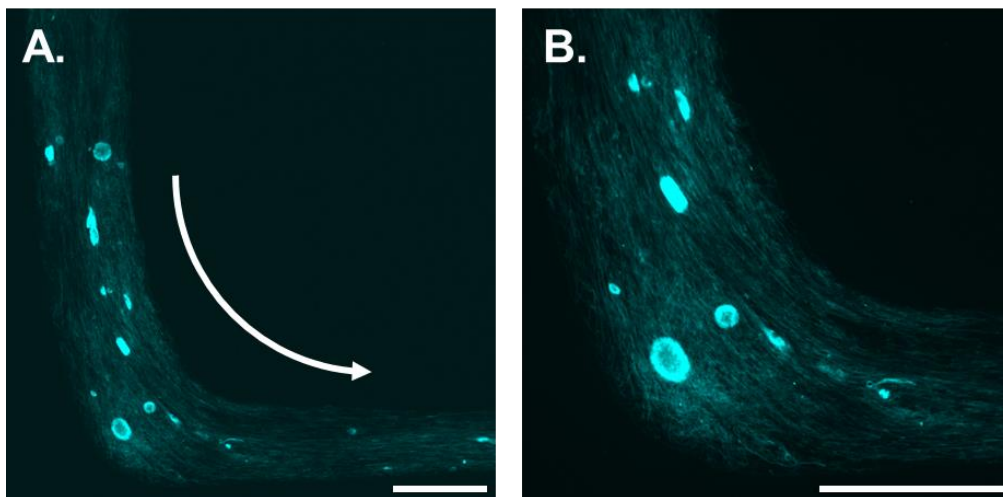
Figure S5.6. Fiber alignment during extrusion. The individual fiber segments within the PHM ink experience shear-induced alignment during extrusion printing processes. This microscale topography was demonstrated to provide contact guidance to C2C12 cells in the main text (**Figure 5.6**). This fiber alignment continues when the direction of extrusion changes. Shown in (A) and expanded in (B), fiber alignment continues with the curve as the direction of printing follows the white arrow in (A). It is important to note that the depicted filaments contain some aggregates of fibers. Overall, this demonstrated control over microscale topography enables the ability to arbitrarily define the surface topography of a substrate purely by extrusion design. *Scalebars = 500 μm.*

Video S7. Extrusion manipulation. Video corresponding to the images shown in **Figure 5.5A** of the main text. Video playback is 5x original speed.

Video S8. Extrusion across table. Video corresponding to the image of extruded filament across four corners of a table in **Figure 5.5B** of the main text. Video playback is 5x original speed.

5.8. References

(1) Daly, A. C.; Riley, L.; Segura, T.; Burdick, J. A. Hydrogel Microparticles for Biomedical Applications. *Nat. Rev. Mater.* **2020**, *5* (January), 20–43. https://doi.org/10.1038/s41578-019-0148-6.

(2) Griffin, D. R.; Weaver, W. M.; Scumpia, P. O.; Di Carlo, D.; Segura, T. Accelerated Wound Healing by Injectable Microporous Gel Scaffolds Assembled from Annealed Building Blocks. *Nat. Mater.* **2015**, *14*, 737–744. https://doi.org/10.1038/NMAT4294.

(3) Sideris, E.; Griffin, D. R.; Ding, Y.; Li, S.; Weaver, W. M.; Di Carlo, D.; Hsiai, T.; Segura, T. Particle Hydrogels Based on Hyaluronic Acid Building Blocks. *ACS Biomater. Sci. Eng.* **2016**, *2*, 2034–2041. https://doi.org/10.1021/acsbiomaterials.6b00444.

(4) Nih, L. R.; Sideris, E.; Carmichael, S. T.; Segura, T. Injection of Microporous Annealing Particle (MAP) Hydrogels in the Stroke Cavity Reduces Gliosis and Inflammation and Promotes NPC Migration to the Lesion. *Adv. Mater.* **2017**, *29* (1606471), 1–8. https://doi.org/10.1002/adma.201606471.

(5) Riley, L.; Schirmer, L.; Segura, T. Granular Hydrogels: Emergent Properties of Jammed Hydrogel Microparticles and Their Applications in Tissue Repair and Regeneration. *Curr. Opin. Biotechnol.* **2019**, *60*, 1–8. https://doi.org/10.1016/j.copbio.2018.11.001.

(6) Highley, C. B.; Song, K. H.; Daly, A. C.; Burdick, J. A. Jammed Microgel Inks for 3D Printing Applications. *Adv. Sci.* **2019**, *6* (1801076), 1–6. https://doi.org/10.1002/advs.201801076.

(7) Pfaff, B. N.; Pruett, L. J.; Cornell, N. J.; de Rutte, J.; Di Carlo, D.; Highley, C. B.; Griffin, D. R. Selective and Improved Photoannealing of Microporous Annealed Particle (MAP) Scaffolds. *ACS Biomater. Sci. Eng.* **2021**, *7* (2), 422–427. https://doi.org/10.1021/acsbiomaterials.0c01580.

(8) Behringer, R. P. Jamming in Granular Materials. *Comptes Rendus Phys.* **2015**, *16* (1), 10–25. https://doi.org/10.1016/j.crhy.2015.02.001.

(9) Kumar, N.; Luding, S. Memory of Jamming – Multiscale Models for Soft and Granular Matter. *Granul. Matter* **2016**, *18*, 1–21. https://doi.org/10.1007/s10035-016-0624-2.

(10) Feng, Q.; Li, Q.; Wen, H.; Chen, J.; Liang, M.; Huang, H.; Lan, D.; Dong, H.; Cao,

X. Injection and Self-Assembly of Bioinspired Stem Cell-Laden Gelatin/Hyaluronic Acid Hybrid Microgels Promote Cartilage Repair In Vivo. *Adv. Funct. Mater.* **2019**, *29* (1906690), 1–11. https://doi.org/10.1002/adfm.201906690.

(11) Seymour, A. J.; Shin, S.; Heilshorn, S. C. 3D Printing of Microgel Scaffolds with Tunable Void Fraction to Promote Cell Infiltration. *Adv. Healthc. Mater.* **2021**, *10* (2100644), 1–14. https://doi.org/10.1002/adhm.202100644.

(12) Muir, V. G.; Qazi, T. H.; Shan, J.; Groll, J.; Burdick, J. A. Influence of Microgel Fabrication Technique on Granular Hydrogel Properties. *ACS Biomater. Sci. Eng.* **2021**, *7*, 4269–4281. https://doi.org/10.1021/acsbiomaterials.0c01612.

(13) Molley, T. G.; Hung, T.; Kilian, K. A. Cell-Laden Gradient Microgel Suspensions for Spatial Control of Differentiation During Biofabrication. *Adv. Healthc. Mater.* **2022**, *11* (24), 1–16. https://doi.org/10.1002/adhm.202201122.

(14) Pruett, L.; Ellis, R.; McDermott, M.; Roosa, C.; Griffin, D. R. Spatially Heterogeneous Epidermal Growth Factor Release from Microporous Annealed Particle (MAP) Hydrogel for Improved Wound Closure. *J. Mater. Chem. B* **2021**, *9*, 7132–7139. https://doi.org/10.1039/d1tb00715g.

(15) Anderson, A. R.; Nicklow, E.; Segura, T. Particle Fraction Is a Bioactive Cue in Granular Scaffolds. *Acta Biomater.* **2022**, *150*, 111–127. https://doi.org/10.1016/j.actbio.2022.07.051.

(16) Mealy, J. E.; Chung, J. J.; Jeong, H.; Issadore, D.; Lee, D.; Atluri, P.; Burdick, J. A. Injectable Granular Hydrogels with Multifunctional Properties for Biomedical Applications. *Adv. Mater.* **2018**, *30*, 1–7. https://doi.org/10.1002/adma.201705912.

(17) Qazi, T. H.; Muir, V. G.; Burdick, J. A. Methods to Characterize Granular Hydrogel Rheological Properties , Porosity , and Cell Invasion. *ACS Biomater. Sci. Eng.* **2022**, *8*, 1427–1442. https://doi.org/10.1021/acsbiomaterials.1c01440.

(18) Kurt, E.; Segura, T. Nucleic Acid Delivery from Granular Hydrogels. *Adv. Healthc. Mater.* **2022**, *11*, 1–16. https://doi.org/10.1002/adhm.202101867.

(19) Miksch, C. E.; Skillin, N. P.; Kirkpatrick, B. E.; Hach, G. K.; Rao, V. V; White, T. J.; Anseth, K. S. 4D Printing of Extrudable and Degradable Poly(Ethylene Glycol) Microgel Scaffolds for Multidimensional Cell Culture. *Small* **2022**, *18* (2200951), 1–13. https://doi.org/10.1002/smll.202200951.

(20) Qazi, T. H.; Wu, J.; Muir, V. G.; Weintraub, S.; Gullbrand, S. E.; Lee, D.; Issadore, D.; Burdick, J. A. Anisotropic Rod-Shaped Particles Influence Injectable Granular

Hydrogel Properties and Cell Invasion. *Adv. Mater.* **2022**, *34*, 1–12. https://doi.org/10.1002/adma.202109194.

(21) Suturin, A. C.; Krüger, A. J. D.; Neidig, K.; Klos, N.; Dolfen, N.; Bund, M.; Gronemann, T.; Sebers, R.; Manukanc, A.; Yazdani, G.; et al. Annealing High Aspect Ratio Microgels into Macroporous 3D Scaffolds Allows for Higher Porosities and Effective Cell Migration. *Adv. Healthc. Mater.* **2022**, *11*, 1–12. https://doi.org/10.1002/adhm.202200989.

(22) Han, L.; Yu, S.; Wang, T.; Behn, A. W.; Yang, F. Microribbon-Like Elastomers for Fabricating Macroporous and Highly Flexible Scaffolds That Support Cell Proliferation in 3D. *Adv. Funct. Mater.* **2013**, *23*, 346–358. https://doi.org/10.1002/adfm.201201212.

(23) Kessel, B.; Lee, M.; Bonato, A.; Tinguely, Y.; Tosoratti, E.; Zenobi-wong, M. 3D Bioprinting of Macroporous Materials Based on Entangled Hydrogel Microstrands. *Adv. Sci.* **2020**, *7* (2001419), 1–13. https://doi.org/10.1002/advs.202001419.

(24) Pan, Z.; Nunes, J. K.; Duprat, C.; Shum, H. C.; Stone, H. A. Controlling Extrudate Volume Fraction through Poroelastic Extrusion of Entangled Looped Fibers. *Nat. Commun.* **2023**, *14* (1242), 1–9. https://doi.org/10.1038/s41467-023-36860-y.

(25) Shen, Y.; Liu, Y.; Nunes, J. K.; Wang, C.; Xu, M.; To, M. K.; Stone, H. A.; Shum, H. C. Fibro-Gel: An All-Aqueous Hydrogel Consisting of Microfibers with Tunable Release Profile and Its Application in Wound Healing. *Adv. Mater.* **2023**, *35* (19), 1–13. https://doi.org/10.1002/adma.202211637.

(26) Negi, V.; Picu, R. Soft Matter Tensile Behavior of Non-Crosslinked Networks of Athermal Fibers in the Presence of Entanglements and Friction. *Soft Matter* **2021**, *17*, 10186–10197. https://doi.org/10.1039/d0sm01297a.

(27) Davidson, M. D.; Prendergast, M. E.; Ban, E.; Xu, K. L.; Mickel, G.; Mensah, P.; Dhand, A.; Janmey, P. A.; Shenoy, V. B.; Burdick, J. A. Programmable and Contractile Materials through Cell Encapsulation in Fibrous Hydrogel Assemblies. *Sci. Adv.* **2021**, *7*, 1–14.

(28) Miller, B.; Hansrisuk, A.; Highley, C. B.; Caliari, S. R. Guest − Host Supramolecular Assembly of Injectable Hydrogel Nano Fi Bers for Cell Encapsulation. *ACS Biomater. Sci. Eng.* **2021**, *7*, 4164–4174. https://doi.org/10.1021/acsbiomaterials.1c00275.

(29) Miller, B.; Wolfe, W.; Gentry, J. L.; Grewal, M. G.; Highley, C. B.; Vita, R. De; Vaughan, M. H.; Caliari, S. R. Supramolecular Fibrous Hydrogel Augmentation of

Uterosacral Ligament Suspension for Treatment of Pelvic Organ Prolapse. *Adv. Healthc. Mater.* **2023**, *2300086*, 1–14. https://doi.org/10.1002/adhm.202300086.

(30) Grewal, M. G.; Highley, C. B. Electrospun Hydrogels for Dynamic Culture Systems: Advantages, Progress, and Opportunities. *Biomater. Sci.* **2021**, *9*, 4228–4245. https://doi.org/10.1039/d0bm01588a.

(31) Wade, R. J.; Burdick, J. A. Advances in Nanofibrous Scaffolds for Biomedical Applications: From Electrospinning to Self-Assembly. *Nano Today* **2014**, *9* (6), 722–742. https://doi.org/10.1016/j.nantod.2014.10.002.

(32) Grewal, M. G.; Gray, V. P.; Letteri, R. A.; Highley, C. B. User-Defined, Temporal Presentation of Bioactive Molecules on Hydrogel Substrates Using Supramolecular Coiled Coil Complexes. *Biomater. Sci.* **2021**, *9* (12), 4374–4387. https://doi.org/10.1039/d1bm00016k.

(33) Caliari, S. R.; Perepelyuk, M.; Cosgrove, B. D.; Tsai, S. J.; Lee, G. Y.; Mauck, R. L.; Wells, R. G.; Burdick, J. A. Stiffening Hydrogels for Investigating the Dynamics of Hepatic Stellate Cell Mechanotransduction during Myofibroblast Activation. *Sci. Rep.* **2016**, *6*, 1–10. https://doi.org/10.1038/srep21387.

(34) Grosskopf, A. K.; Mann, J. L.; Baillet, J.; Hernandez, H. L.; Autzen, A. A. A.; Yu, A. C.; Appel, E. A. Extreme Extensibility in Physically Cross-Linked Nanocomposite Hydrogels Leveraging Dynamic Polymer − Nanoparticle Interactions. *Macromolecules* **2022**, *55* (17), 7498–7511. https://doi.org/10.1021/acs.macromol.2c00649.

(35) Marklein, R. A.; Burdick, J. A. Spatially Controlled Hydrogel Mechanics to Modulate Stem Cell Interactions. *Soft Matter* **2009**, *6* (1), 136–143. https://doi.org/10.1039/b916933d.

(36) Burdick, J. A.; Prestwich, G. D. Hyaluronic Acid Hydrogels for Biomedical Applications. *Adv. Healthc. Mater.* **2011**, *23* (12), H41–H56. https://doi.org/10.1002/adma.201003963.

(37) Highley, C. B.; Prestwich, G. D.; Burdick, J. A. Recent Advances in Hyaluronic Acid Hydrogels for Biomedical Applications. *Curr. Opin. Biotechnol.* **2016**, *40*, 35–40. https://doi.org/10.1016/j.copbio.2016.02.008.

(38) Sundararaghavan, H. G.; Metter, R. B.; Burdick, J. A. Electrospun Fibrous Scaffolds with Multiscale and Photopatterned Porosity. *Macromol. Biosci.* **2010**, *10* (3), 265–270. https://doi.org/10.1002/mabi.200900363.

(39) Kim, I. L.; Khetan, S.; Baker, B. M.; Chen, C. S.; Burdick, J. A. Fibrous Hyaluronic Acid Hydrogels That Direct MSC Chondrogenesis through Mechanical and Adhesive Cues. *Biomaterials* **2013**, *34* (22), 5571–5580. https://doi.org/10.1016/j.biomaterials.2013.04.004.

(40) Frantz, C.; Stewart, K. M.; Weaver, V. M. The Extracellular Matrix at a Glance. *J. Cell Sci.* **2010**, *123* (24), 4195–4200. https://doi.org/https://doi.org/10.1242/jcs.023820.

(41) Lutolf, M. P.; Hubbell, J. A. Synthetic Biomaterials as Instructive Extracellular Microenvironments for Morphogenesis in Tissue Engineering. *Nat. Biotechnol.* **2005**, *23*, 47–55. https://doi.org/https://doi.org/10.1038/nbt1055.

(42) Wade, R. J.; Burdick, J. A. Engineering ECM Signals into Biomaterials. *Mater. Today* **2012**, *15* (10), 454–459. https://doi.org/https://doi.org/10.1016/S1369-7021(12)70197-9.

(43) Wade, R. J.; Bassin, E. J.; Rodell, C. B.; Burdick, J. A. Protease-Degradable Electrospun Fibrous Hydrogels. *Nat. Commun.* **2015**, *6*, 1–10. https://doi.org/https://doi.org/10.1038/ncomms7639.

(44) Davidson, M. D.; Song, K. H.; Lee, M. H.; Llewellyn, J.; Du, Y.; Baker, B. M.; Wells, R. G.; Burdick, J. A. Engineered Fibrous Networks to Investigate the Influence of Fiber Mechanics on Myofibroblast Differentiation. *ACS Biomater. Sci. Eng.* **2019**, *5* (8), 3899–3908. https://doi.org/https://doi.org/10.1021/acsbiomaterials.8b01276.

(45) Prendergast, M. E.; Davidson, M. D.; Burdick, J. A. A Biofabrication Method to Align Cells within Bioprinted Photocrosslinkable and Cell-Degradable Hydrogel Constructs via Embedded Fibers. *Biofabrication* **2021**, *13*, 044108.

(46) Menut, P.; Seiffert, S.; Sprakel, J.; Weitz, D. A. Does Size Matter? Elasticity of Compressed Suspensions of Colloidal- and Granular-Scale Microgels. *Soft Matter* **2012**, *8* (1), 156–164. https://doi.org/10.1039/c1sm06355c.

(47) Mckinley, G. H.; Sridhar, T. FILAMENT-STRETCHING RHEOMETRY OF COMPLEX FLUIDS. *Annu. Rev. Fluid Mech.* **2002**, *34*, 375–415.

(48) Chaudhuri, O.; Cooper-white, J.; Janmey, P. A.; Mooney, D. J.; Shenoy, V. B. Effects of Extracellular Matrix Viscoelasticity on Cellular Behaviour. *Nature* **2020**, *584* (December 2019), 535–546. https://doi.org/10.1038/s41586-020-2612-2.

(49) Chaudhuri, O.; Koshy, S. T.; Branco Da Cunha, C.; Shin, J. W.; Verbeke, C. S.;

Allison, K. H.; Mooney, D. J. Extracellular Matrix Stiffness and Composition Jointly Regulate the Induction of Malignant Phenotypes in Mammary Epithelium. *Nat. Mater.* **2014**, *13* (10), 970–978. https://doi.org/10.1038/nmat4009.

(50) Chaudhuri, O.; Gu, L.; Klumpers, D.; Darnell, M.; Bencherif, S. A.; Weaver, J. C.; Huebsch, N.; Lee, H.; Lippens, E.; Duda, G. N.; et al. Hydrogels with Tunable Stress Relaxation Regulate Stem Cell Fate and Activity. *Nat. Mater.* **2016**, *15*, 326–334. https://doi.org/10.1038/NMAT4489.

(51) Carvalho, E. M.; Kumar, S. Lose the Stress: Viscoelastic Materials for Cell Engineering. *Acta Bio* **2022**, *163*, 146–157. https://doi.org/10.1016/j.actbio.2022.03.058.

(52) Saraswathibhatla, A.; Indana, D.; Chaudhuri, O. Cell – Extracellular Matrix Mechanotransduction in 3D. *Nat. Rev. Mol. Cell Biol.* **2023**. https://doi.org/10.1038/s41580-023-00583-1.

(53) Wingert, M. C.; Jiang, Z.; Chen, R.; Cai, S. Strong Size-Dependent Stress Relaxation in Electrospun Polymer Nanofibers. *J. Appl. Phys.* **2017**, *121*, 1–7. https://doi.org/10.1063/1.4973486.

(54) Sather, N. A.; Sai, H.; Sasselli, I. R.; Sato, K.; Ji, W.; Synatschke, C. V; Zambrotta, R. T.; Edelbrock, J. F.; Kohlmeyer, R. R.; Hardin, J. O.; et al. 3D Printing of Supramolecular Polymer Hydrogels with Hierarchical Structure. *Small* **2021**, *17*, 1–14. https://doi.org/10.1002/smll.202005743.

(55) Basurto, I. M.; Mora, M. T.; Gardner, G. M.; Christ, G. J.; Caliari, S. R. Aligned and Electrically Conductive 3D Collagen Scaffolds for Skeletal Muscle Tissue Engineering. *Biomater. Sci.* **2021**, *9* (11), 4040–4053. https://doi.org/10.1039/d1bm00147g.

(56) Kador, K. E.; Alsehli, H. S.; Zindell, A. N.; Lau, L. W.; Andreopoulos, F. M.; Watson, B. D.; Goldberg, J. L. Retinal Ganglion Cell Polarization Using Immobilized Guidance Cues on a Tissue-Engineered Scaffold. *Acta Biomater.* **2014**, *10* (12), 4939–4946. https://doi.org/10.1016/j.actbio.2014.08.032.

(57) Christopherson, G. T.; Song, H.; Mao, H. The Influence of Fiber Diameter of Electrospun Substrates on Neural Stem Cell Differentiation and Proliferation. *Biomaterials* **2009**, *30* (4), 556–564. https://doi.org/https://doi.org/10.1016/j.biomaterials.2008.10.004.

(58) Lim, S. H.; Liu, X. Y.; Song, H.; Yarema, K. J.; Mao, H. The Effect of Nanofiber-Guided Cell Alignment on the Preferential Differentiation of Neural Stem Cells.

Biomaterials **2010**, *31* (34), 9031–9039.
https://doi.org/10.1016/j.biomaterials.2010.08.021.

(59) Madl, C. M.; Lesavage, B. L.; Dewi, R. E.; Dinh, C. B.; Stowers, R. S.; Khariton,
M.; Lampe, K. J.; Nguyen, D.; Chaudhuri, O.; Enejder, A.; et al. Maintenance of
Neural Progenitor Cell Stemness in 3D Hydrogels Requires Matrix Remodelling.
Nat. Mater. **2017**, *16* (12), 1233–1242. https://doi.org/10.1038/nmat5020.

(60) Khetan, S.; Guvendiren, M.; Legant, W. R.; Cohen, D. M.; Chen, C. S.; Burdick, J.
A. Degradation-Mediated Cellular Traction Directs Stem Cell Fate in Covalently
Crosslinked Three-Dimensional Hydrogels. *Nat. Mater.* **2013**, *12*, 458–465.
https://doi.org/10.1038/nmat3586.

CHAPTER 6: PACKED HYDROGEL MICROFIBERS WITH TUNABLE STRESS RELXATION PROFILES

6.1. Foreword

This chapter was developed as an extension of Chapter 6 where MeHA microfibers were segmented and assembled into packed hydrogel microfibers (PHMs). Herein, we describe a MeHA fiber-based PHM analog comprised of segmented polyethylene glycol (PEG) microfibers. Notably, utilizing this new material system enabled increased throughput of fiber fabrication due to the more favorable performance of PEG in the electrospinning process – thus, affording increased scalability compared to MeHA-based PHMs. We report on porosity and mechanics of PEG-based PHMs with a particular focus on tunability of stress relaxation and compare PHM properties to granular hydrogels comprised of spherical particles with matched volume and matched dimension. We further demonstrate that PEG-based PHMs offer unique control over mechanics through the use of different fiber subpopulations that enable selective annealing of the PHM scaffold. Overall, this Chapter aims to introduce an improved PHM system comprised of segmented PEG fibers that enables matching of complex extracellular matrix mechanics in a previously unrealized manner.

6.2. Abstract

Viscoelasticity and stress relaxation are critical ECM properties that are known to influence cell behaviors, thereby driving the recent emphasis on incorporating these complex mechanics into 3D hydrogel culture models. Granular hydrogels are an emerging class of 3D scaffolds due to their inherent viscoelasticity, as well as their micro-to-mesoscale void space within the scaffold, which provides cells with degrees of migratory

freedom that are not possible in conventional 3D bulk hydrogels. Traditional hydrogel microparticles (HMPs) are often spherical (aspect ratio ~1) and thus restricted to only contacting immediately adjacent HMPs. This limited number of interactions between particles complicates the ability to tune time-dependent mechanics like stress relaxation because particles easily shift past each other in response to strain. In response, we describe a system that leverages segmented hydrogel microfibers (aspect ratio ~15) as the individual "grains" within the granular hydrogel, which enables these interactions at increased length scales compared to their spherical analogs. Our packed hydrogel microfiber (PHM) scaffolds exhibit viscoelasticity, shear-thinning and self-healing properties, and injectability – like all other classes of granular hydrogels. This increased length scale of interaction allows for fibers to entangle and slide past each other, which enables tunable stress relaxation profiles ($T_{1/2}$ ~ 1-100+ s) across a range of applied strains (σ ~ 2.5-50%) in a packing density-dependent fashion – behaviors that were not seen with spherical particles with matched volume and matched dimension. We also demonstrate the ability to selectively anneal a small subset of fibers within the PHMs to bolster scaffold mechanics. Taken together, PHMs offer an intriguing alternative to traditional granular hydrogels due to their unique mechanics and offer a promising solution to engineering complex 3D scaffolds for cell culture applications.

6.3. Introduction

Mechanotransduction of extracellular matrix (ECM) mechanics is widely considered to be a critical driver of many fundamental cell behaviors, such as proliferation, migration, and differentiation[1,2]. The components of the ECM are fairly well characterized, along with their contribution to overall mechanical properties, thereby providing a blueprint of desired characteristics when engineering *in vitro* models of various tissue systems[3–6]. The most well-described and studied ECM mechanical property is its stiffness or elasticity[7]; however, natural tissue is not purely elastic, with viscous contributions (i.e., viscoelasticity) and strain- and stress-dependent behaviors[8–11]. These characteristics are exploited by cells within the environment during routine processes[12]. More specifically, cells within the ECM exert protrusion and traction forces during migration where they reorganize the ECM and contribute to localized nonlinear stiffening of the matrix[11–13]. Therefore, when developing an *in vitro* biomaterial system to model natural tissue, the resultant scaffold must yield to cell forces to provide an environment that recapitulates endogenous complex matrix mechanics.

Hydrogel-forming biomaterials are widely leveraged to engineer ECM-mimetics due to their ability to match many of the biophysical and biochemical attributes of natural tissue[14,15]. While there are numerous proven strategies to directly control hydrogel stiffness, these are commonly implemented as 2D tissue culture substrates[15,16]. Indeed, much of the established knowledge surrounding fundamental cellular functions is predicated on 2D studies utilizing static hydrogel microenvironments[15–17]. Due to the increased appreciation for the complexity of ECM mechanics in 3D[18], there has been a shift to developing hydrogels that enable more dynamic microenvironments for use as 3D

tissue models[17,19–21]. Naturally-derived materials like collagen and fibrin offer a simple platform for introducing viscoelasticity and stress relaxation into hydrogels[8,11,22–24], but their low overall modulus frustrates their utility as tunable biomaterials systems[1]. These challenges have inspired a shift towards developing materials systems with advanced chemical crosslinking strategies that enable more complex mechanical profiles. Engineering controlled viscoelasticity and stress relaxation into hydrogels is perhaps the most common strategy for increasing the dynamicity of 3D culture environments, and prevalent examples include dynamic guest-host chemistries grafted onto various polymer backbones[25–28] and physical (ionic) chelation of polymers like alginate[10–12,29]. When coupled with covalent crosslinking mechanisms, these reversible interactions allow for increased control over various ECM-mimetic mechanics, providing useful platforms for 3D cell culture[30]. Importantly, while these strategies enable a tunable approach to engineering viscoelasticity into 3D hydrogel environments, they sometimes require intense material design and can be challenging to implement, thus motivating the development of other techniques to afford these properties.

Granular hydrogels are a class of 3D hydrogel environments that allow dynamic properties to be introduced into many hydrogel systems via particle-based formulations, and there has been considerable work utilizing these materials for 3D cell culture[31–33]. These hydrogel systems are comprised of discrete hydrogel microparticles (HMPs) that are packed together and immobilized strictly by contact forces between discrete particles[31–35], and they enable unique modular design through the combination of different particle population[36]. The micro-to-mesoscale space between the particles enables cells to migrate throughout the overall construct in ways that are challenging in bulk 3D

hydrogels[37–39]. While granular hydrogel scaffolds provide a more facilitative environment for migratory processes, the ability to tune viscoelasticity and stress relaxation is largely governed by the minimal length scale of interactions (i.e., contact forces between particles) between individual HMPs compared to the crosslinked polymer chains in bulk hydrogels[40,41]. Interparticle annealing enables force transmission across multiple particles rather than restricting interactions to those between immediate neighbors only[42]; however, this often reduces the permissive nature of the scaffold by covalently immobilizing particles in place.

In light of these challenges, we sought to develop a hydrogel system with uniquely tunable viscoelasticity and control over time-dependent stress relaxation utilizing hydrogel microfibers. Hydrogel microfibers can form a unique granular system, which like spherical HMPs, might be formulated with independence from the hydrogel backbone[43], but unlike spherical HMPs, have increased interparticle interactions between individual fibers that influence strain responses and allow stabilization without secondary annealing. These interparticle interactions can be defined as both the number of other fibers that a single fiber can interact and entangle with, along with the length scale in which these interactions occur, afforded by the flexible, high-aspect ratio hydrogel microfibers. Herein, we report on a packed hydrogel microfiber (PHM) system comprised of electrospun polyethylene glycol (PEG) derivatives that exhibits packing density-mediated viscoelasticity and stress relaxation in response to physiologically-relevant forces and strains. These behaviors are unique to this new class of granular hydrogels, where spherical particles with matched volume and matched dimension (i.e., particle diameter ~ fiber length) are unable to exhibit similar properties under the same conditions designed

for this study. PHMs are soft and tunable, suggesting their utility as 3D *in vitro* models of soft tissue types, with the possibility of selective covalent annealing to increase mechanics and model systems with greater stiffnesses.

6.4. Materials and Methods

All reagents were purchased from Millipore Sigma, unless otherwise stated.

6.4.1. Peptide Synthesis

The fluorescent peptide (GCDDD-fluorophore) utilized to visualize microfibers and microgels in this study was synthesized with a cysteine residue to permit thiol-ene conjugation to residual norbornenes during the fiber- and particle-making processes (Liberty Blue automated, microwave-assisted solid phase peptide synthesizer, CEM). The peptide was built from C-terminus to N-terminus on Rink amide resin using Fmoc-protected amino acids (resin and amino acids were sourced from Advanced Chemtech), with 5(6)-carboxyfluorescein (FAM, Sigma Aldrich) added last to the N-terminus. The resultant peptide was cleaved off the resin using a cocktail of trifluoroacetic acid, triisopropylsilane, 2.2'-(ethylenedioxy) diethanethiol (all were sourced from Sigma Aldrich), and DI water at a 92.5/2.5/2.5/2.5 mixing ratio, respectively. The freed peptide was then isolated via precipitation in cold diethyl ether (Sigma Aldrich), dried under vacuum, resuspended in DI water, and lyophilized to yield the final product. Peptide synthesis was confirmed using MALDI-TOF spectrometry (**Figure S6.1**).

6.4.2. Electrospinning and segmenting PEGNB microfibers

To electrospin PEGNB, solutions comprised of 10% w/v PEGNB (20 kDa, JenKem Technology), 7% w/v PEGSH (10 kDa, JenKem Technology), 5% polyethylene oxide (PEO, 400 kDa, Sigma Aldrich), and 0.05% w/v 2-hydroxy-4'-(2-hydroxyethoxy)-2-methylpropiophenone (HHMP, Sigma Aldrich) in DI water were mixed overnight. Quantity of PEGSH was determined to enable a stoichiometric mismatch between norbornene and thiol groups to avail residual norbornenes for coupling with thiolated peptides. 0.5 mM of thiolated FAM peptide (GCDDD-FAM) was included in the electrospinning precursor solution to enable fluorescent imaging of microfibers for visualization and characterization. A second electrospinning solution designed to be co-spun with the PEGNB solution comprised of 5% PEO (900 kDa, Sigma Aldrich) in DI water was also mixed overnight. This solution was intended to yield sacrificial fibers that would introduce space between PEGNB fibers during the electrospinning process, but dissolve away after the crosslinking step to prevent welding of PEGNB fibers.

The PEGNB and sacrificial fiber solutions were both extruded through 16-gauge needles positioned 18 cm away from a rotating mandrel collector at rates of 0.4 ml/hr and 0.5 ml/hr, respectively. The needles were charged with 11-12 kV for the PEGNB solution and 5.5-6.5 kV for the sacrificial fiber solution. The mandrel was charged with -4 kV to focus the electrical field and set to rotate at 1000 RPM to align fibers and minimize welding. Fiber batches were collected for 1 hr each, crosslinked under nitrogen for 15 min at 5 mW/cm^2 (VWR UV Crosslinker) to stabilize the PEGNB fibers, then hydrated in PBS to hydrate PEGNB fibers while simultaneously dissolving away the sacrificial fibers. Fiber batches were hydrated overnight to ensure sufficient swelling of the hydrogel network and

removal of undesired components from the electrospinning process (i.e., PEO and unreacted photoinitiator).

Hydrated fiber mats were suspended in PBS at ~10% v/v, segmented via homogenization (IKA T25) at 10k RPM for 2 min, and filtered through a 40 μm mesh to remove welded fiber aggregates. Final solutions were centrifuged thrice to remove all undesired components, and fibers were resuspended at 10% v/v and stored at 4 °C until use. Fiber length and diameter were characterized using ridge detection in ImageJ based on thresholded confocal images of dilute fiber solutions (BioTek Cytation C10, Agilent Technologies).

For crosslinkable PEGVS fibers, the electrospinning solution was prepared similarly to the PEGNB solution, with 10% w/v PEGVS (10 kDa, Jenkem Technology) replacing both the PEGNB and PEGSH since PEGVS crosslinks readily with itself without a crosslinker molecule. PEGVS was electrospun utilizing the same parameters as PEGNB, crosslinked for 5 min at 5 mW/cm^2, then subsequently processed using the same protocol established for the PEGNB fibers. PEGVS microfiber characterization is included in **Figure S6.2**.

6.4.3. Aqueous two-phase PEGNB hydrogel microparticle synthesis

To form PEGNB hydrogel microparticles via aqueous two-phase suspension, solutions of dextran from *Leuconostoc* spp. (70 kDa, dextran(70), Sigma Aldrich) were mixed with PEGNB hydrogel precursor solutions at a 4:1 ratio of continuous(dextran):disperse(PEGNB) phases. Here, we targeted 2 separate sizes for the spherical HMPs: spheres with matched dimension (i.e., particle diameter ~ fiber

length) and spheres with matched volume – hereafter "spheres (D)" and "spheres (V)", respectively. For spheres (V), 800 μl of 40% w/v dextran and 0.05% HHMP in DI water was mixed with 200 μl of a solution comprised of 6% PEGNB, 4.2% PEGSH, and 0.05% HHMP in DI water. 0.5 mM of GCDDD-FAM peptide was included in both phases as well when preparing particles for fluorescence imaging. This mixture was vortexed at maximum speed for 1 min prior to crosslinking under UV light at 20 mW/cm^2 (Omnicure) for 5 min. For spheres (D), the continuous dextran phase was modified to 25% w/v and the stir rate was reduced to 800 RPM, but all other parameters were conserved compared to spheres (V). Following the crosslinking step, the resultant particles were suspended in 15x volume of PBS to thermodynamically favor a single-phase solution and centrifuged twice to remove dextran and other unreacted materials. Spheres (V) and spheres (D) were filtered through 20 μm and 40 μm meshes, respectively, and centrifuged once more to yield the final particles used within this study. Particles were also stored at 10% v/v in 4 °C until further use. Similar to fibers, particle size was characterized using ImageJ based on thresholded confocal images of dilute particle solutions (BioTek Cytation C10, Agilent Technologies).

6.4.4. Forming granular hydrogels

Two classes of granular hydrogels were designed for this study: those comprised of segmented PEGNB fibers and those comprised of spherical PEGNB microparticles. Fibrous granular hydrogels were assembled via centrifugation at 5k, 10k, and 15k RCF for 5 min to yield low, medium, and high packing densities, respectively. Spheres (V) and spheres (D) were packed at the medium packing density to enable direct comparisons

with the fibrous assemblies packed at medium density. Following centrifugation, the supernatant was carefully aspirated to avoid disrupting the granular hydrogel and the pellet was manipulated using a spatula thereafter.

6.4.5. Granular hydrogel characterization

To characterize void space in these granular hydrogel assemblies, fibers and spheres were resuspended in 2 mg/ml FITC-dextran (2 MDa) then subsequently centrifuged to yield the desired packing density. In this scheme, the fluorescent regions represent the void space within the assembly. Packed granular hydrogels were then transferred to a 96 well plate and Z-stacks of each sample were acquired at random ROIs on a Leica Stellaris 8 confocal microscope. Images were thresholded on ImageJ and void space was quantified using the built-in Analyze Particles functionality. Void space was determined as the average pixel intensity of the fluorescent regions with respect to the total pixel volume of the micrograph for each group.

Mechanical properties of granular hydrogel assemblies were assessed via oscillatory shear rheology (DHR-3, TA Instruments) using a 20 mm parallel plate geometry, a 500 μm gap distance, and a 25 °C testing temperature. Time sweeps (0.5% strain, 1 Hz) were utilized to assess viscoelasticity of granular hydrogels. Cyclical addition of high and low strains (low: 0.5%, 1 Hz; high: 250%, 1 Hz) were leveraged to demonstrate shear recovery. Strain sweeps (0.01%-500% strain) helped elucidate strain yielding and critical strain values. Finally, constant application of strain (ranging from 2.5%-50%, depending on the trial) was utilized to investigate stress relaxation characteristics of granular hydrogel assemblies.

For annealed particle systems using varied quantities of PEGVS, the Peltier plate base was replaced with a glass base that enables UV curing. Fibrous assemblies were resuspended in a 0.05% w/v HHMP solution, centrifuged to yield the medium packing density, then transferred to the rheometer. Time sweeps (0.5%, 1 Hz) with UV curing at 5 mW/cm^2 (either 10 s or 120 s, Omnicure) were utilized to assess the crosslinked scaffold mechanics, followed by a 15% constant strain to record stress relaxation capabilities of partially-annealed scaffolds. Noisy stress relaxation data were smoothed using an exponential smoothing algorithm.

6.5. Results and Discussion

6.5.1. Preparing granular hydrogels

The two types of granular hydrogels utilized in this study were both prepared using modified polyethylene glycol (PEG) backbone chains. PEG is a hydrophilic polyether that is readily modifiable with functional groups for various crosslinking mechanisms[44]. Furthermore, PEG is relatively bioinert – lending itself as a "blank-slate" material that offers user-defined tuning of the biochemical profile through the installed reactive groups[15,45–47]. Here, we selected PEG-norbornene (PEGNB) and PEG-thiol (PEGSH) as the modified PEG derivatives due to the stoichiometric nature of the photomediated step-growth thiol-ene click reaction mechanism[48–51]. This chemical scheme allows for residual norbornene groups following the crosslinking process to enable additional thiol-ene conjugation of thiol-containing fluorophores and bioactive peptides[52]. For packed hydrogel microfiber scaffolds (PHMs), we utilized segmented electrospun PEGNB microfibers as the individual grains (**Figure 6.1a-b**). As comparisons, spherical hydrogel

231

microparticles were prepared via an aqueous two-phase separation technique[53–56] (ATPS, **Figure 6.1d-e**) to yield particles with matched dimension (i.e., particle diameter ~ fiber length) and matched volume (assuming spherical for particles and cylindrical for fibers) – hereafter "spheres (D)" and "spheres (V)", respectively (**Figure 6.1c** and **6.1f**).

Electrospinning is an effective platform for fabricating hydrogel fibers with diameters on the order of hundreds of nanometers to single microns[57]. Here, the electrospinning setup was modified such that the resultant hydrated fibers were >1 μm in diameter (average diameter = 2.41 μm, **Figure 6.1f**). Previous methods to segment electrospun hydrogel fibers include repeated aspiration and extrusion steps[58–61], photopatterning[62–64], and cryomilling[65–67]; however, we employed a simple and scalable homogenization step where fiber solutions were agitated at 10k RPM for 2 min, then filtered to remove aggregates. Following the processing steps, the resultant fibers were measured to be approximately 37.3 μm in length (**Figure 6.1c**). The aspect ratio (L/D) of ~15 is considerably larger than most hydrogel microparticles used for granular hydrogel scaffolds.
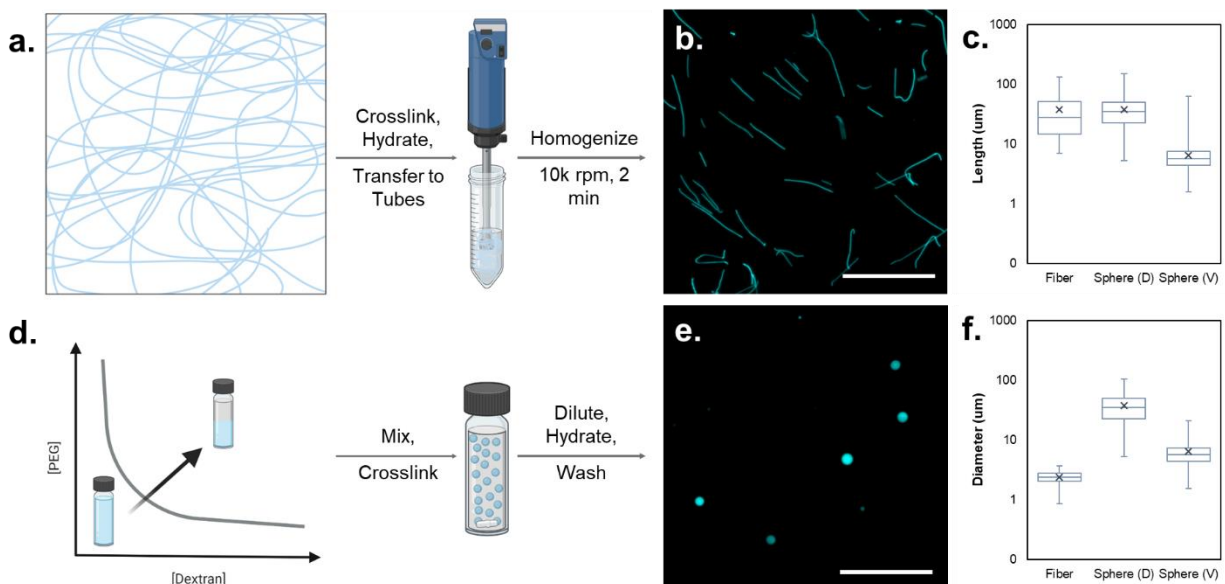
Figure 6.1. Preparation of granular hydrogel units. (a) Electrospun PEGNB fibers were crosslinked, hydrated, and homogenized to segment fibers in a fast, scalable fashion. (b) Fluorescent micrograph of segmented PEGNB fibers. (c) Quantification of fiber and sphere length illustrating matching of fiber and sphere dimension in spheres (D) group. (d): Schematic of a binodal curve for PEG and dextran, where two phases occur in the regime above the curve. The ATPS system was then mixed to form dispersed PEGNB spheres within the continuous dextran phase, the hydrogel microparticles were crosslinked, diluted to form a single phase, and finally washed. (f) Quantification of fiber and sphere diameter illustrates the disparity in the dimensions between fibers and spheres. The aspect ratio of spheres was assumed to be ~1, so length and diameter was assumed to be equal for these groups. Scalebars in b and e = 200 μm; n > 300 for all groups.

In order to compare PHMs to more traditional hydrogel microparticles, PEGNB spheres (D) and spheres (V) were produced using an ATPS technique. This process leverages PEG-rich and dextran-rich aqueous solutions that are thermodynamically immiscible when mixed at high enough concentrations[53]. A systematic approach to determine experimental concentrations of PEGNB/PEGSH and dextran solutions was leveraged to form PEGNB hydrogel microparticles (summary of different processing variables shown in **Figure S6.3-S6.5**). Spheres (D) have an average diameter 37.2 μm which matches the average length of the electrospun fibers, and spheres (V) have an

average diameter of 6.4 μm which approximately matches the volume of the electrospun fibers. Matching these dimensional characteristics of the electrospun fibers allows for investigating how the increased aspect ratio of PEGNB fibers affects mechanical properties of resultant granular hydrogels when compared to spherical hydrogel microparticles.

6.5.2. Influence of particle size and shape on granular hydrogel properties

Granular hydrogels were formed via centrifugation-mediating packing at different speeds to yield low, medium, and high packing densities – hereafter "Low-Fiber", "Med-Fiber", and "High-Fiber", respectively. Fibers were packed at all three densities whereas spheres (V) and spheres (D) were only packed at the medium density for comparison to fibers ("Med-Sphere (V)" and "Med-Sphere (D)"). To investigate differences in porosity of the granular hydrogels, particles were packed with high-molecular weight FITC-dextran and confocal microscopy was leveraged to visualize the fluorescent signal within pores (**Figure 6.2a**). Consistent with previous findings in other types of granular hydrogel systems[33,68], increasing packing density of fibers resulted in decreased void space (from 21% for Low-Fiber to 15% for High-Fiber). Both Med-Sphere (V) and Med-Sphere (D) possessed larger quantities of void space in the granular hydrogel (22% and 27%, respectively) when compared to the fibers. This is likely due to the small diameters and flexibility of the fibers allowing for fibers to fold and fill more void space following centrifuge-mediated packing when compared to spheres that maintain their defined shape following packing.
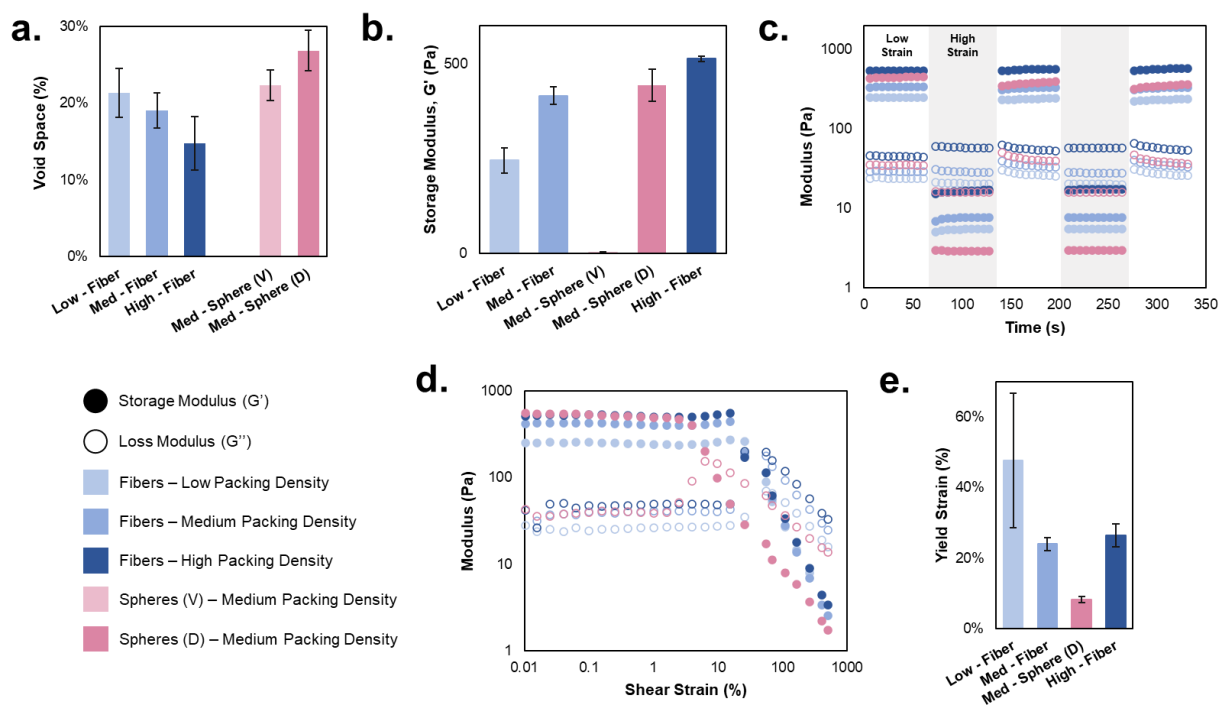
Figure 6.2. Particle size and shape influences overall granular hydrogel properties. (a) Granular hydrogels following centrifuge-mediated packing exhibit void spaces in both a packing density- and particle shape-dependent manner. (b) Storage moduli indicate that all groups exhibit solid-like behaviors at low strains, except for Med-Sphere (V) where there was no appreciable storage modulus, likely due to insufficient contact forces between particles. Generally, increased packing density yielded greater elastic contribution in granular hydrogels, with Med-Fiber and Med-Sphere (D) exhibiting similar stiffnesses due to similar characteristic dimensions defining the system.

It is evident that all packing densities for fibers behave like solids at rest as illustrated by their storage modulus ranging from ~245-513 Pa (**Figure 6.2b**). Similarly, Med-Sphere (D) exhibit storage moduli values of ~440 Pa, which is consistent with the moduli seen with the Med-Fiber group. Conversely, Med-Sphere (V) did not exhibit an appreciable storage modulus (< 5 Pa). These results suggest that at the packing densities investigated, the characteristic dimension of the fibers and spheres (D) is the main contributor to the storage moduli at low strains, with the smaller diameters of spheres (V) unable to generate sufficient interparticle contact forces to sustain solid-like behavior.

Thus, for the rest of the rheological analyses, only spheres (D) were analyzed in parallel with fibers.

A favorable characteristic of granular hydrogels is their ability to be manipulated via pipetting or injecting due to their shear-thinning and self-healing behaviors. When cycling between low strain (0.5%) and high strain (250%) regimes, all granular hydrogels demonstrated shear-thinning and self-healing properties and were able to restore a majority of their original mechanics, regardless of particle shape (**Figure 6.2c**). Additionally, all groups of granular hydrogels are shear-yielding (**Figure 6.2d-e**), with yield strains (% strain where G' <G") affected in both a packing density- and particle shape-dependent manner. More specifically, the yield strain (~48%) for the Low-Fiber group trended higher than the yield strains for the Med-Fiber and High-Fiber groups (24% and 26%, respectively). We attribute this phenomenon to the higher interstitial fluid content in the Low-Fiber group enabling movement via rearrangement of fibers in response to the increasing strain without notable alteration at points of entanglement or interaction. Denser networks require yielding at these points of entanglement in order for rearrangements to occur, thus they yield and fluidize at lower strains. Conversely, Med-Sphere (D) exhibited yield strains considerably lower than all fiber groups (~8%). We hypothesize that this difference is due to the inability of spherical microparticles to interact with more particles besides those immediately adjacent, thus limiting longer-range interactions. Alternatively, fibers are able to entangle and interact with many other fibers at longer ranges due to their aspect ratios compared to spheres, even if the characteristic length of both particle types are consistent (fiber length ~ sphere diameter).

6.5.3. Viscoelasticity of granular hydrogels

Towards understanding the viscoelastic properties, which are critical to cellular responses to their environments[1,9,11], we sought to quantify the elastic and viscous contributions to the overall mechanics of the granular hydrogels described here using oscillatory shear rheology. We hypothesized that the increased interparticle interactions afforded by the electrospun fibers would allow for enhanced viscoelasticity over their spherical counterparts – due to the ability of the fibers to slide and reorganize their numerous interactions compared to spheres shifting past each other in response to applied strains (schematic in **Figure 6.3a**).

Elastic and viscous contributions to the mechanical properties of natural tissue and ECM-mimetics are often visualized by plotting their storage modulus versus their loss modulus (**Figure 6.3b**). Many tissues exhibit an elastic contribution that is ~10x the viscous contribution[11] (shown as the gray dashed line in **Figure 6.3b**), so that is the target criterion when designing these granular hydrogels. Indeed, PHMs all demonstrate storage moduli that are ~10x the loss moduli, therefore achieving that desired design criterion. Med-Spheres (D) have an increased elastic contribution as illustrated by their deviation from the 10x trendline in **Figure 6.3b**, suggesting that the sliding and reorganizing abilities of PHMs contribute to their viscoelasticity. This phenomenon is likely analogous to reversible chemistries that are known to increase viscoelasticity of bulk hydrogels. For example, a hydrogel system crosslinked via a supramolecular guest-host mechanism (e.g., adamantane-β-cyclodextrin) would exhibit increased viscous behavior as applied forces disrupt that guest-host interaction, but this is reversible if the force is removed
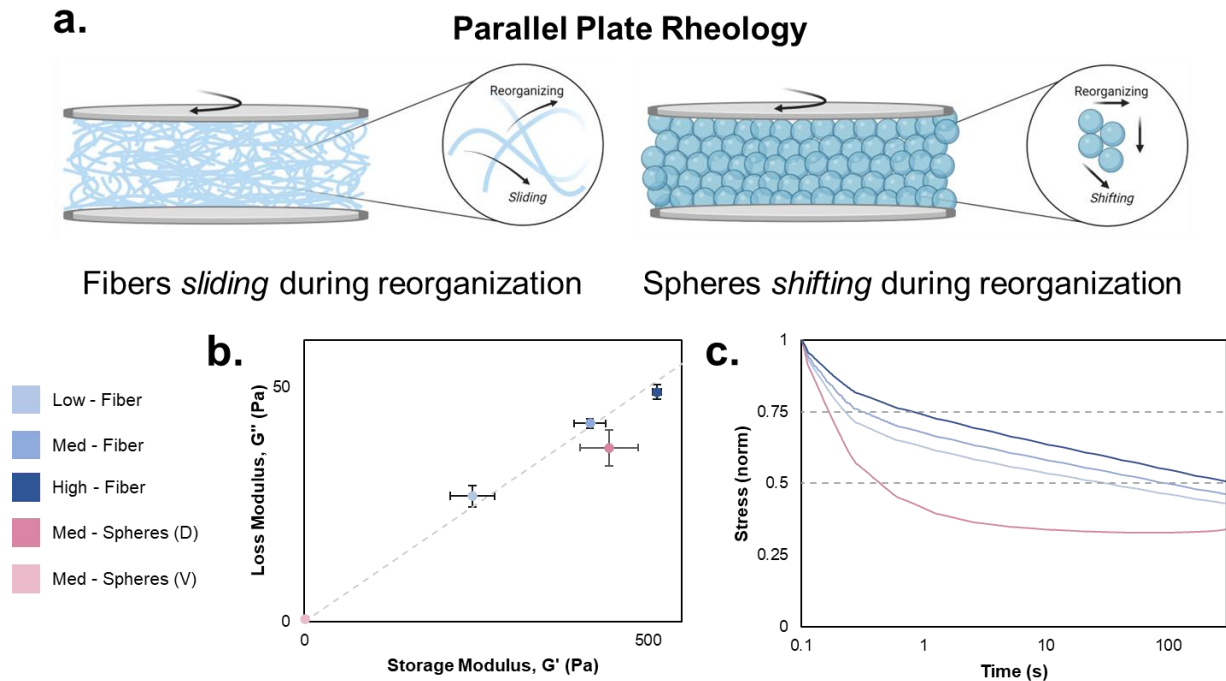
Figure 6.3. Viscoelasticity and time-dependent stress relaxation of granular hydrogels. (a) schematic of the parallel plate oscillatory shear rheology testing platform. The increased length scale of interactions between fibers enables sliding and reorganization in response to applied strains whereas particles will begin to shift in response to applied strains. (b) Plotting loss vs. storage modulus illustrates both viscous and elastic contributions to the mechanics of granular hydrogels. PHMs exhibit storage moduli that are ~10x loss moduli (illustrated by gray dashed trendline), which is consistent with many natural tissue types. Conversely, Med-Spheres (D) have a lesser viscous contribution and thus deviate from this 10x trend. Med-Spheres (V) illustrate negligible storage and loss moduli. (c) Time-dependent stress relaxation profiles at 15% applied strain of granular hydrogels. PHMs are able to dissipate stress over time as fibers slide and reorganize in response to the applied strain as illustrated by the slow decrease in normalized stress ($T_{1/2}$ on the order of 10-100+ s). Spheres (D) are unable to reorganize effectively and seemingly shift and fracture before reorganizing into a granular hydrogel as illustrated by the sharp drop in normalized stress ($T_{1/2} < 1$ s).

before the polymeric network has undergone substantial rearrangement to relax the applied stress[26,27,69]. We postulate that PHMs exhibit similar response – except at the microscale as opposed to the nanoscale – where fibers begin to slide in response to applied forces but return to rest due to contact and entanglement forces when the force is removed.

238

Time-dependent stress relaxation is thus another important ECM mechanical property that is closely related to viscoelasticity. Natural tissue dissipates stress at relaxation times ($T_{1/2}$, defined as the time it takes for a tissue or material to relax to 50% of the peak stress under constant strain) ranging from 1-1000 s[11]. Using a constant applied shear strain of 15%, we found that all packing densities of PHMs were able to dissipate stress with $T_{1/2}$ >10 s (**Figure 6.3c**). Additionally, $T_{1/2}$ demonstrates a positive correlation with packing density, where the relaxation time is longest for the High-Fiber group. In comparison, Med-Spheres (D) exhibited a sharp drop off in normalized stress with a $T_{1/2}$ <1 s. This is likely due to the limited number of interactions between spheres preventing them from sliding against each other and instead shifting past each other. Stress relaxation occurs within an elastic-dominated regime and based on the yield strains reported for Med-Spheres (D) (~8%, **Figure 6.2e**), there are smaller strain ranges in which this can occur due to the transition to fluid-like behaviors at lower strains.

6.5.4. Strain-dependence of granular hydrogel stress relaxation

Preliminary analysis of time-dependent stress relaxation of granular hydrogels in this study demonstrated that Med-Spheres (D) relax at time scales on the order of 10^{-1} s. We next investigated how Med-Spheres (D) responded to a range of applied strains (2.5-50% strain), with a particular focus on strains that do not supersede their yield strain (**Figure 6.4ai**). We also sought to compare the stress-dissipation behaviors of PHMs within this same range, aiming to identify a relationship between yield strain and relaxation time similar to Med-Spheres (D) (**Figure 6.4aii-iv**). Importantly, we utilize a different definition of relaxation time here, $T_{1/4}$, which is when the material system only
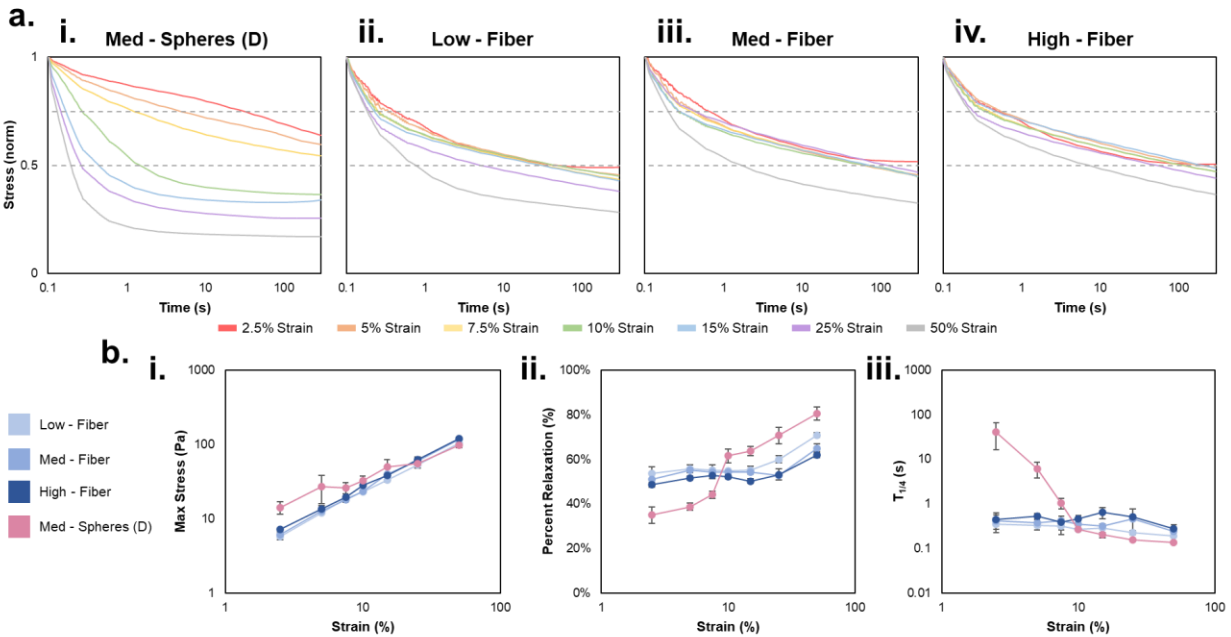
Figure 6.4. Strain-dependence of granular hydrogel stress relaxation. (a) Granular hydrogels demonstrate that (i) Med-Spheres (D) exhibit a stronger strain-dependence on stress relaxation when compared to all packing densities of PHMs (ii-iv). Med-Spheres (D) are able to reorganize and dissipate stress when the applied strain is below their yield strain (~8%), whereas PHMs exhibit a more muted relationship between stress relaxation and applied strain, seemingly regardless of their yield strains. (b) These relationships are quantified where (i) all groups exhibit increasing max stress with increasing strain, with Med-Spheres (D) generally exhibiting higher max stresses than fibers at low strains. (ii) Interestingly, Med-Spheres (D) do not relax to the same level as PHM groups at strains below their yield strain, indicating that they store more stress than fibers during the time scale investigated if the applied strain is not sufficient to cause them to reorganize and flow. However, there is a sharp increase once the applied strain surpasses their yield strain as they begin to flow. Notably, all fiber groups exhibit a modest positive correlation in total relaxation with respect to applied strain. (iii) Finally, consistent with the previous results of total relaxation, $T_{1/4}$ is considerably longer for Med-Spheres (D) when the applied strain is below the yield strain, with a sharp decrease as the applied strain is increased beyond this threshold. Conversely, PHMs exhibit a marginal decrease in relaxation time as applied strain is increased.

relaxes 25% of the max stress value. This different relaxation time allows for us to draw

comparisons across groups that do not exhibit a $T_{1/2}$ value within the 300 s test parameter

utilized here.

Illustrated in **Figure 6.4ai**, it is evident that there is a distinct strain-dependent relationship for the stress relaxation profiles for Med-Spheres (D). As previously demonstrated, we observed a yield strain of ~8% for the Med-Spheres (D) granular hydrogel. For applied strains <8%, Med-Spheres (D) are able to slowly relax as spheres slide in place to dissipate stress. However, once the applied strain reaches 10% and above, Med-Spheres (D) exhibit a sharp decrease in normalized stress as sphere-sphere surface contact is effectively disrupted in response to applied strains greater than their yield strain. Critically, the range of strains in which Med-Spheres (D) relax in $T_{1/4}$ values greater than 1 s is outside the range of strains considered relevant for most cell activity (10-50%)[41], suggesting that further modifications might be necessary to engineer ECM-mimetic environments using the Med-Spheres (D) scaffolds described here.

In comparison, all packing densities of PHMs exhibit a muted relationship between applied strain and stress relaxation (**Figure 6.4aii-iv**). This observation is particularly noticeable for strains ranging from 2.5-15% strain for all packing densities, with deviations beginning at 25% strain for the Low-Fiber group and 50% strain for the Med-Fiber and High-Fiber groups. Again, we attribute these phenomena to the high aspect ratio of the fibers entangling within the granular hydrogel at increased length scales, enabling sliding and reorganizing in response to applied stress. Additionally, while there is a slight change in behavior of $T_{1/4}$ around the yield strains of fibers, we do not observe as noticeable a decrease in normalized stress when compared to Med-Spheres (D). This result could be explained by the ability of fibers to reorganize under a constant applied strain near their yield strain in a manner in which spheres are unable to replicate.

The unique properties of the interactions within PHMs allow for relaxation of stress at higher strains without flow compared to Med-Spheres (D). In light of these results, we next sought to quantify these relationships to further discern how PHM packing density influences time-dependent stress relaxation behaviors. Interestingly, when comparing the max stress value for all groups, they exhibit the same linear trend where max stress increases with applied strain (**Figure 6.4bi**). It is noteworthy that Med-Spheres (D) exhibit a higher max stress than fibers at low strains, but this trend begins to diminish once applied strains surpass the yield strain of the spheres. When analyzing the percent relaxation (**Figure 6.4bii**), we observe similar trends across all fiber groups where total relaxation increases modestly at low applied strains, but sharply increases once the applied strain surpasses the yield strain. Consistent with previous results, the percent relaxation for Med-Spheres (D) is considerably lower than fibers until the strain surpasses their yield strain where total relaxation starkly increases due to spheres shifting and potentially causing microscale fracturing of the granular hydrogel in response to the applied perturbation. Finally, quantifying $T_{1/4}$ for all granular hydrogel groups affirms the previously described differences between fibers and spheres. Across all strains for PHMs, there is a generally a modest decrease in $T_{1/4}$ in response to increasing strain. Conversely, Med-Spheres (D) exhibit $T_{1/4}$ values that drastically decrease with increasing strain, then begin to level out once the yield strain is exceeded. These results indicate that yield strain influences the stress relaxation behavior in a strain-dependent manner for the sphere-based granular hydrogels more so than the PHMs described here.

6.5.5. Selective annealing of packed hydrogel microfibers

PHMs have thus far demonstrated favorable properties for use as permissive 3D cell culture environments that mimic many properties of natural tissues. They form soft, viscoelastic 3D scaffolds (G' on the order of 100 Pa) that are mechanically robust. However, most natural tissues are stiffer (G' on the order of 1+ kPa)[70], which might limit their utility in modeling many ECM types. Thus, we sought to increase the mechanical properties of PHMs while potentially maintaining their viscoelasticity and time-dependent stress relaxation properties demonstrated thus far. There exists an exciting possibility to control crosslinking within a PHM scaffold by incorporating subpopulations of fibers that are able to participate in secondary annealing mechanisms within fibers that are unable to do so. We propose that this would enable fabrication of an elastically annealed fibrous architecture that supports the unannealed fibers within and surrounding the network.

To achieve this, we leveraged a PEG-vinyl sulfone (PEGVS) derivative to form photoreactive electrospun fibers that could be mixed in with PEGNB fibers are predetermined ratios (PEGVS fibers characterized in **Figure S6.2**). PEGNB fibers were crosslinked with PEGSH in a stoichiometric mismatch, theoretically exhausting all thiol groups – thereby rendering PEGNB fibers theoretically non-photoreactive for further annealing processes. Conversely, PEGVS fibers form kinetic chains during crosslinking which allows crosslinks to propagate when exposed to UV light[71]. This enables a modular system design where the quantity of annealable fibers in PHMs can be dictated directly by the ratio of PEGVS:PEGNB fibers in the scaffold (schematic shown in **Figure 6.5a**). The PEGVS form covalent crosslinks between fibers that stabilize the system (contributing to matrix elasticity) and PEGNB fibers are unincorporated in this covalent
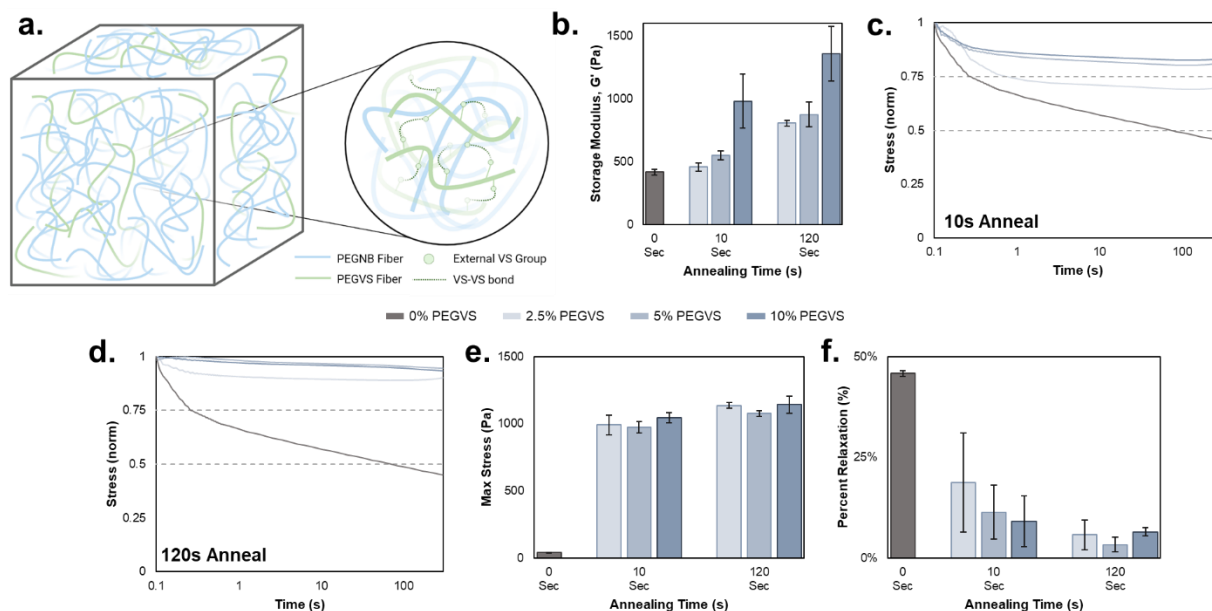
Figure 6.5. Modular addition of PEGVS fibers to PEGNB PHMs to increase mechanical properties. (a) Schematic of incorporating PEGVS fibers into PEGNB PHMs. PEGVS fibers form kinetic chains with each other when exposed to UV light, forming a reinforcing structure, while leaving PEGNB fibers essentially unincorporated. This strategy allows PEGNB fibers to theoretically continue to reorganize and respond to external perturbations with PEGVS providing mechanical stability. (b) Incorporating PEGVS fibers at low volumes (2.5%-10% v/v) increases granular hydrogel storage moduli for both 10 s and 120 s annealing times compared to 0% PEGVS, with a larger effect at the longer annealing duration. (c-d) Annealing PEGVS fibers in these granular hydrogels diminishes the stress relaxation capabilities of the scaffolds in both PEGVS content-dependent and annealing time-mediated fashions. (e-f) Annealing all quantities of PEGVS fibers for both annealing times revealed that the max stress of the scaffolds when 15% strain was applied increased with a related reduction in their ability to dissipate stress in response to that applied strain. It is hypothesized that the PEGVS network within the PHMs might allow for local stress relaxation at the microscale due to PEGNB fibers sliding and reorganizing, with PEGVS fibers contributing to the elasticity of the scaffold at the macroscale.

network, and thus are still able to slide and reorganize around the PEGVS fibers (contributing to matrix viscosity).

PEGVS fibers were added into PHMs at 2.5%, 5%, and 10% v/v compared to PEGNB fibers and annealed at 5 mW/cm^2 for either 10 s or 120 s. All groups exhibited PEGVS content- and annealing time-mediated increases in their respective storage

moduli compared to the 0% PEGVS fiber control (**Figure 6.5b**), with the 10% PEGVS groups eclipsing the 1 kPa threshold for both annealing times. Additionally, all groups exhibited both PEGVS content-dependent and annealing time-mediated stress relaxation profiles (**Figure 6.5c-d**). This is grounded conceptually in the formation of kinetic chains when annealing VS groups together. Increasing the volume of PEGVS fibers or the annealing duration enables more crosslinks to form, which increases the magnitude of reinforcement provided by PEGVS fibers in the granular hydrogel scaffold. Accordingly, PEGV (2.5% v/v) coupled with only 10 s of UV irradiation yielded the most stress relaxation out of all groups tested. It is noteworthy, however, that any incorporation of PEGVS drastically increased the max stress of the scaffold upon the introduction of 15% strain (**Figure 6.5e**) and also reduced the ability of the granular hydrogel to relax at the global scale compared to the 0% PEGVS group (**Figure 6.5f**). PEGVS fibers theoretically crosslink orthogonally, thereby not covalently interacting with the PEGNB fibers. Thus, PEGVS fibers might provide a covalent scaffolding (i.e., similar to rebar in concrete) that influences mechanical properties at the macroscale, while still enabling the scaffold to exhibit soft, time-dependent stress relaxation properties at the microscale as PEGNB fibers slide and reorganize within and around the annealed structure. Future work will test this hypothesis by investigating cellular responses at the microscale in scaffolds with varying quantities of annealed PEGVS fibers.

6.6. Conclusions and Future Outlook

Viscoelasticity and stress relaxation are important characteristics of natural tissue that are well-appreciated to influence cell behaviors including migration, proliferation, and

differentiation[1,11]. These complex matrix mechanical properties are often difficult to engineer into traditional 3D bulk hydrogel scaffolds, with granular hydrogels offering some advantages due to their ability to behave like solids[34], but then reorganize in response to applied forces – features that are analogous to viscoelasticity. This study explores a new class of ECM-mimetic, packed hydrogel microfiber scaffold with tunable viscoelasticity using high aspect ratio (~15) electrospun PEGNB microfibers. The higher length/diameter ratio enables increased interparticle interactions between discrete fibers which uniquely contribute to complex scaffold mechanics in ways that were previously unrealized by conventional spherical microparticles (aspect ratios of ~1).

We demonstrate that PHMs are viscoelastic with shear-thinning and self-healing capabilities, which are properties consistent with other classes of granular hydrogels. Interestingly, particles with matched volume to the fibers ("Med-Spheres (V)") are unable to form a scaffolding system with an appreciable storage modulus, indicating that the spherical dimensions to yield the desired volume are insufficient to provide enough contact forces to form a solid-like system at rest using the processing parameters defined here. Further, the increased interparticle interactions between individual fibers enable higher yield strains for PHMs when compared to spherical-based systems with matched volume and matched dimension. These fiber-fiber entanglements seemingly enable a packing density-dependent stress relaxation profile for PHMs within cell-relevant strain regimes, thereby providing tunability when designing the granular hydrogel system for cell culture applications. Conversely, spherical-based scaffolds are less tunable and exhibit rapid stress relaxation when the applied strain is above their yield strain. Finally, PHMs can be selectively annealed via the incorporation of photoreactive PEGVS fibers

to increase the macroscale mechanics of the scaffold. We hypothesize that small amounts (<10%) of PEGVS fibers provides a reinforcing network that penetrates throughout the granular hydrogel, with PEGNB fibers still able to slide and reorganize at the microscale to contribute to the viscoelasticity and stress relaxation that cells might perceive in their environment.

While this study has focused on the mechanical characterization of PHMs compared to scaffolds formed from spheres with matched volume and matched dimension, it is important to contextualize this work as a 3D, permissive cell culture scaffold. Perhaps the most notable property of PHMs is their tunable stress relaxation that is largely independent from yield strain, with $T_{1/2}$ values ranging from 1-100+ s, depending on packing density. These timescales are physiologically relevant for many tissue types, thereby offering user-defined design control over the time-dependent mechanics of the tissue culture scaffold.

Additionally, the subcellular length scale diameters of these PEGNB fibers might offer a more permissive granular hydrogel environment compared to spherical particles that are commonly sized to be on the same order of magnitude as cells, or larger[32] – possibly providing the ability for cells to navigate their environment without hindrances introduced by the particles. Cells within the ECM are known to exert protrusion and traction forces during migration on the order of 10^{-1}-10^{1} kPa, coupled with 10-50% strains where they reorganize the ECM[12,41,72–76]. Within the design parameters of this study, we report that PHMs are able to withstand strains within this range without yielding at the global/bulk scale, but it is possible that they yield at the microscale, and further investigation using atomic force microscopy or traction force microscopy is required to

confirm this hypothesis. Nevertheless, the demonstrated bulk mechanical properties of PHMs are analogous to natural tissues where a soft, viscoelastic hydrogel occupies most of the space in the ECM. We postulate that these advantages might lend themselves to modeling tissue systems – like brain tissue – where the amorphous hydrogel dominates the mechanical properties of the environment and cells are known to migrate and grow independently of adhesion forces[77].

Many natural tissue types also contain protein fibers that mechanically strengthen the amorphous, viscoelastic hydrogel that occupies the ECM[6]. This inspired the inclusion of PEGVS fibers within the PEGNB PHM to covalently stabilize the network. In addition to the mechanical support offered by the annealed PEGVS fibers, they might provide immobilized anchoring points for cells to engage with and exert traction forces like they would in many endogenous tissue environments. Importantly, both PEGNB fibers and PEGVS fibers are readily modifiable with protein-mimetic and adhesive peptide ligands to increase the bioactivity of PEG to support cell engagement with the granular hydrogel network[78].

Overall, packed hydrogel microfibers offer an intriguing alternative to traditional granular hydrogels comprised of spherical microparticles. Their mechanical tunability to match complex matrix properties of different tissue types offers a promising solution to engineering 3D scaffolds for cell culture applications. While the focus of this study was to characterize their range of physical properties, we expect that this new class of granular hydrogels will lead to further exploration into their utility as a cell culture scaffold for both *in vitro* and *in vivo* applications.

6.7. Acknowledgements

6.8. Supplementary Figures
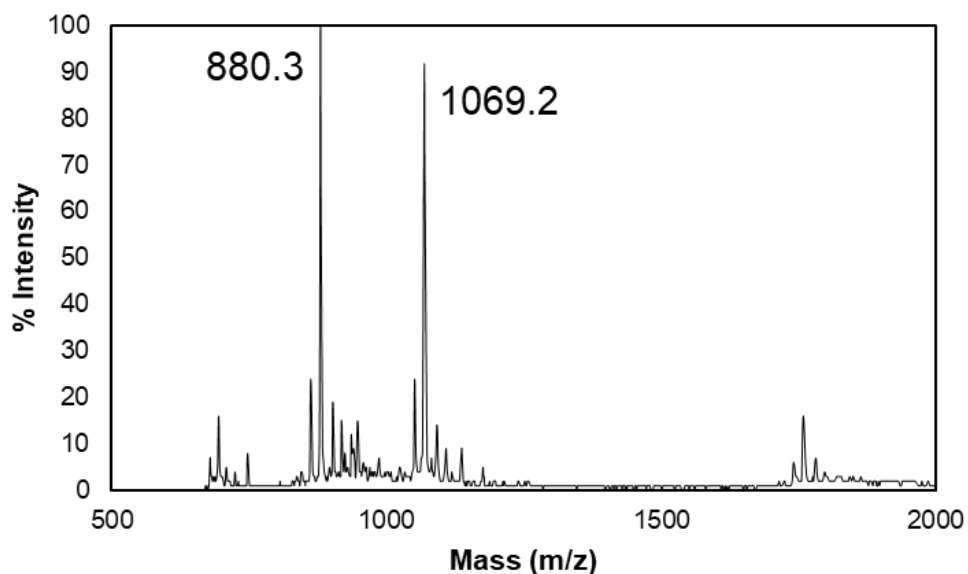
Figure S6.1. MALDI-TOF spectrum of GCDDD-FAM peptide. Confirmation of fluorescent peptide synthesis. Expected molecular weight: 881.8 Da; MALDI-TOF molecular weights: 880.3 Da and 1069.2 Da. Both peaks suggest successful synthesis, with the 1069.2 peak likely corresponding to the combined molecular weights of the peptide and the matrix utilized for MALDI-TOF.
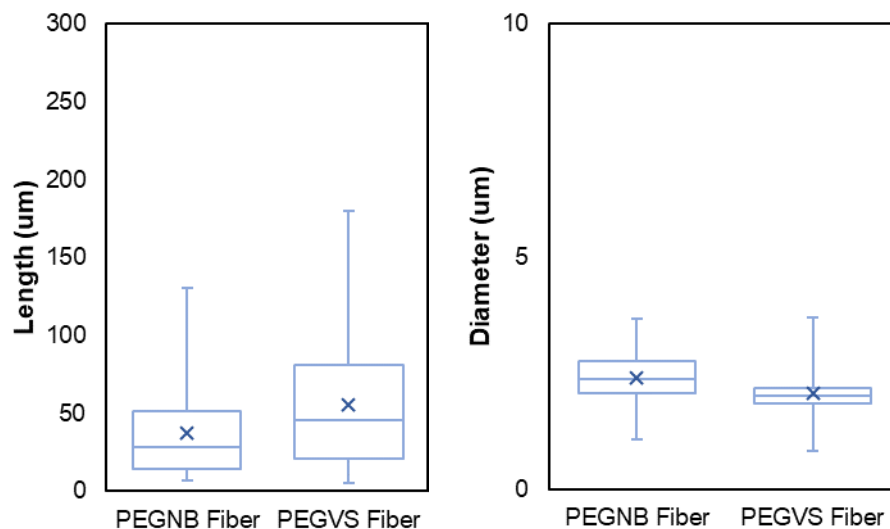
Figure S6.2. PEGVS fiber quantification. Comparisons between PEGNB fibers and PEGVS fibers show marginal differences in length and diameter. However, we determined that these values were sufficiently close to be considered interchangeable for this study – especially at the low concentrations (% v/v) of PEGVS fibers in the PEGNB fiber-based granular hydrogels (0-10% v/v).
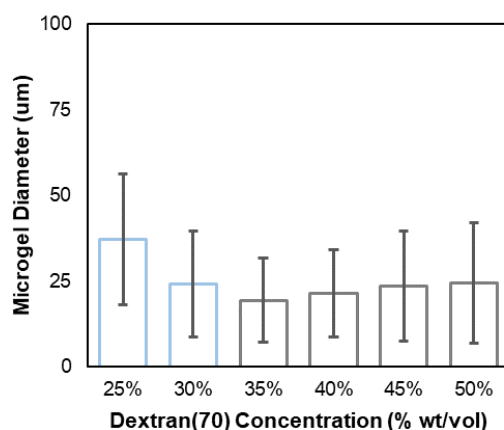
Figure S6.3. Effect of continuous phase concentration (dextran) on resultant microgel diameter. To determine the effect of the continuous phase concentration, the following variables were held constant: 6% w/v PEGNB, 4.2% w/v PEGSH (corresponding to [-SH]:[-NB]=0.7), and 800 RPM stir rate. We originally observed decreasing microgel diameter as dextran(70) concentration was increased from 25% to 30% w/v, then we saw a marginal increasing trend in diameter with increasing dextran(70) concentration above 30% w/v. This is likely due to the disperse phase aggregating in lower viscosity dextran(70) solutions to form larger droplets, with increasing viscosity (i.e., higher dextran(70) concentrations) supporting larger independent disperse phase droplets. Importantly, 25% w/v was the chosen continuous phase concentration for spheres (D) used in this study and 40% w/v was utilized for spheres (V).
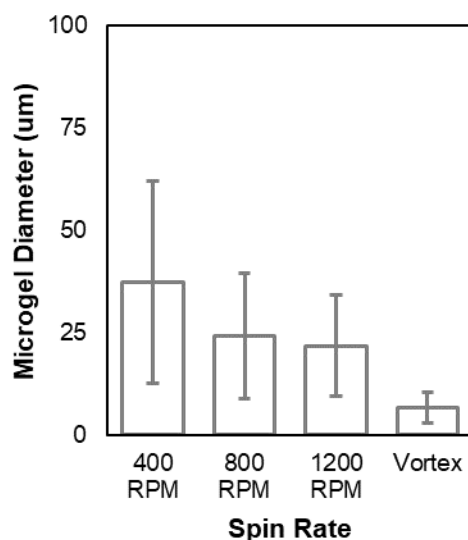
Figure S6.4. Effect of spin rate on resultant microgel diameter. To determine the effect of the spin rate, the following variables were held constant: 6% w/v PEGNB, 4.2% w/v PEGSH (corresponding to [-SH]:[-NB]=0.7), and 30% dextran(70). Overall, microgel diameter decreased with increasing spin rate. 800 RPM was utilized for spheres (D) in

this study and spheres (V) were fabricated via vortexing at maximum speed rather than using a stir plate.
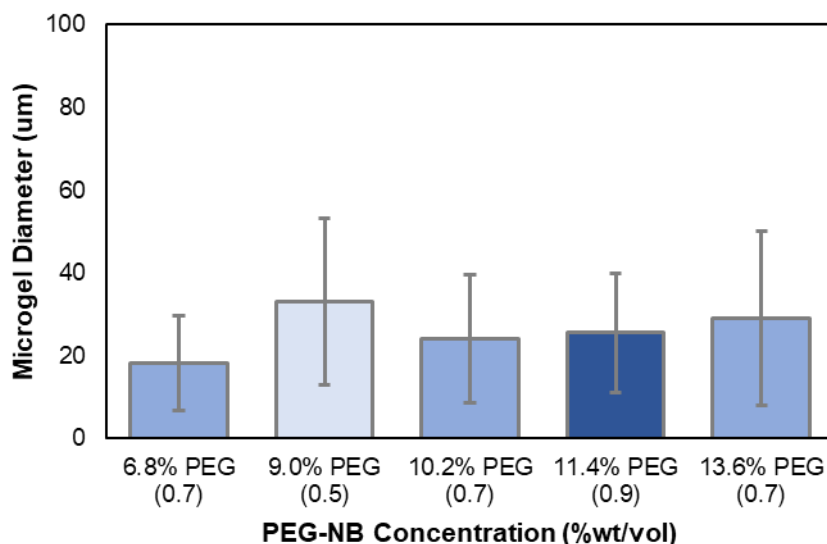
Figure S6.5. Effect of disperse phase concentration (PEGNB and PEGSH) on resultant microgel diameter. To determine the effect of the disperse phase concentration, the following variables were held constant: 30% dextran(70) and 800 RPM stir rate. The concentrations shown in the figure correspond to total % w/v between PEGNB and PEGSH, with the [-SH]:[-NB] ratio indicated below. Generally, increasing PEG concentration resulted in marginally larger microgel diameters, except for 9% PEG with [-SH]:[-NB]=0.5, which had the largest diameter due to the lowest crosslinking density allowing for the greatest swelling. 10.2% PEG – 6% PEGNB and 4.2% PEGSH – was utilized in this study for all microparticles.

6.9. References

(1)   Saraswathibhatla, A.; Indana, D.; Chaudhuri, O. Cell – Extracellular Matrix
        Mechanotransduction in 3D. *Nat. Rev. Mol. Cell Biol.* **2023**, *24*, 495–516.
        https://doi.org/10.1038/s41580-023-00583-1.

(2)   Miller, A. E.; Hu, P.; Barker, T. H. Feeling Things Out: Bidirectional Signaling of
        the Cell–ECM Interface, Implications in the Mechanobiology of Cell Spreading,
        Migration, Proliferation, and Differentiation. *Adv. Healthc. Mater.* **2020**, *9*
        (1901445), 1–24. https://doi.org/10.1002/adhm.201901445.

(3)   Hynes, R. O. The Extracellular Matrix: Not Just Pretty Fibrils. *Science (80-.).*
        2009, *326* (5957), 1216–1219. https://doi.org/10.1126/science.1176009.

(4)   Yue, B. Biology of the Extracellular Matrix: An Overview. *J. Glaucoma* **2014**, 1–8.
        https://doi.org/10.1097/IJG.0000000000000108.Biology.

(5)   Frantz, C.; Stewart, K. M.; Weaver, V. M. The Extracellular Matrix at a Glance. *J.
        Cell Sci.* **2010**, *123* (24), 4195–4200.
        https://doi.org/https://doi.org/10.1242/jcs.023820.

(6)   Rozario, T.; Desimone, D. W. The Extracellular Matrix in Development and
        Morphogenesis : A Dynamic View. *Dev. Biol.* **2010**, *341* (1), 126–140.
        https://doi.org/10.1016/j.ydbio.2009.10.026.

(7)   Engler, A. J.; Sen, S.; Sweeney, H. L.; Discher, D. E. Matrix Elasticity Directs
        Stem Cell Lineage Specification. *Cell* **2006**, *126*, 677–689.
        https://doi.org/10.1016/j.cell.2006.06.044.

(8)   Chaudhuri, O. Viscoelastic Hydrogels for 3D Cell Culture. *Biomater. Sci.* **2017**, *5*,
        1480–1490. https://doi.org/10.1039/c7bm00261k.

(9)   Hui, E.; Gimeno, K. I.; Guan, G.; Caliari, S. R. Spatiotemporal Control of
        Viscoelasticity in Phototunable Hyaluronic Acid Hydrogels. *Biomacromolecules*
        2019, *20* (11), 4126–4134.
        https://doi.org/https://doi.org/10.1021/acs.biomac.9b00965.

(10)   Chaudhuri, O.; Gu, L.; Darnell, M.; Klumpers, D.; Bencherif, S. A.; Weaver, J. C.;
        Huebsch, N.; Mooney, D. J. Substrate Stress Relaxation Regulates Cell
        Spreading. *Nat. Commun.* **2015**, 1–7. https://doi.org/10.1038/ncomms7365.

(11)   Chaudhuri, O.; Cooper-white, J.; Janmey, P. A.; Mooney, D. J.; Shenoy, V. B.
        Effects of Extracellular Matrix Viscoelasticity on Cellular Behaviour. *Nature* **2020**,

584 (December 2019), 535–546. https://doi.org/10.1038/s41586-020-2612-2.

(12)   Nam, S.; Chaudhuri, O. Mitotic Cells Generate Protrusive Extracellular Forces to Divide in Three-Dimensional Microenvironments. *Nat. Phys.* **2018**, *14* (June). https://doi.org/10.1038/s41567-018-0092-1.

(13)   Adebowale, K.; Gong, Z.; Hou, J. C.; Wisdom, K. M.; Garbett, D.; Lee, H.; Nam, S.; Meyer, T.; Odde, D. J.; Shenoy, V. B.; et al. Enhanced Substrate Stress Relaxation Promotes Filopodia-Mediated Cell Migration. *Nat. Mater.* **2021**, *20*, pages1290–1299. https://doi.org/10.1038/s41563-021-00981-w.

(14)   Tibbitt, M. W.; Anseth, K. S. Hydrogels as Extracellular Matrix Mimics for 3D Cell Culture. *Biotechnol. Bioeng.* **2009**, *103* (4), 655–663. https://doi.org/https://doi.org/10.1002/bit.22361.

(15)   Caliari, S. R.; Burdick, J. A. A Practical Guide to Hydrogels for Cell Culture. *Nat. Methods* **2016**, *13* (5), 405–414. https://doi.org/10.1038/nmeth.3839.

(16)   Baker, B. M.; Chen, C. S. Deconstructing the Third Dimension – How 3D Culture Microenvironments Alter Cellular Cues. *J. Cell Sci.* **2012**, *125* (13), 3015–3024. https://doi.org/https://doi.org/10.1242/jcs.079509.

(17)   Burdick, J. A.; Murphy, W. L. Moving from Static to Dynamic Complexity in Hydrogel Design. *Nat. Commun.* **2012**, *3*, 1–8. https://doi.org/10.1038/ncomms2271.

(18)   Yamada, K. M.; Doyle, A. D.; Lu, J. Cell – 3D Matrix Interactions : Recent Advances and Opportunities. *Trends Cell Biol.* **2022**, *32* (10), 883–895. https://doi.org/10.1016/j.tcb.2022.03.002.

(19)   Zhang, Y. S.; Khademhosseini, A. Advances in Engineering Hydrogels. *Science (80-.).* **2017**, *356* (6337), 1–27. https://doi.org/10.1126/science.aaf3627.

(20)   Moroni, L.; Burdick, J. A.; Highley, C.; Lee, S. J.; Morimoto, Y.; Takeuchi, S.; Yoo, J. J. Biofabrication Strategies for 3D in Vitro Models and Regenerative Medicine. *Nat. Rev. Mater.* **2018**, *3*, 21–37. https://doi.org/https://doi.org/10.1038/s41578-018-0006-y.

(21)   Rosales, A. M.; Anseth, K. S. The Design of Reversible Hydrogels to Capture Extracellular Matrix Dynamics. *Nat. Rev. Mater.* **2016**, *1*, 1–15. https://doi.org/10.1038/natrevmats.2015.12.

(22) Janmey, P. A.; Winer, J. P.; Weisel, J. W. Fibrin Gels and Their Clinical and Bioengineering Applications. *J. R. Soc. Interface* **2009**, *6*, 1–10. https://doi.org/10.1098/rsif.2008.0327.

(23) Carvalho, E. M.; Kumar, S. Lose the Stress: Viscoelastic Materials for Cell Engineering. *Acta Bio* **2022**, *163*, 146–157. https://doi.org/10.1016/j.actbio.2022.03.058.

(24) Ma, Y.; Lin, M.; Huang, G.; Li, Y.; Wang, S.; Bai, G.; Lu, T. J.; Xu, F. 3D Spatiotemporal Mechanical Microenvironment: A Hydrogel-Based Platform for Guiding Stem Cell Fate. *Adv. Mater.* **2018**, *30* (49), 1–27. https://doi.org/10.1002/adma.201705911.

(25) Uman, S.; Dhand, A.; Burdick, J. A. Recent Advances in Shear-Thinning and Self-Healing Hydrogels for Biomedical Applications. *J. Appl. Polym. Sci.* **2020**, *48668*, 1–20. https://doi.org/10.1002/app.48668.

(26) Loebel, C.; Rodell, C. B.; Chen, M. H.; Burdick, J. A. Shear-Thinning and Self-Healing Hydrogels as Injectable Therapeutics and for 3D-Printing. *Nat. Protoc.* **2017**, *12* (8), 1521–1541. https://doi.org/10.1038/nprot.2017.053.

(27) Rodell, C. B.; Kaminski, A. L.; Burdick, J. A. Rational Design of Network Properties in Guest − Host Assembled and Shear-Thinning Hyaluronic Acid Hydrogels. *Biomacromolecules* **2013**, *14*, 4125–4134.

(28) Rodell, C. B.; Wade, R. J.; Purcell, B. P.; Dusaj, N. N.; Burdick, J. A. Selective Proteolytic Degradation of Guest − Host Assembled, Injectable Hyaluronic Acid Hydrogels. *ACS Biomater. Sci. Eng.* **2015**, *1*, 277–286. https://doi.org/10.1021/ab5001673.

(29) Chaudhuri, O.; Gu, L.; Klumpers, D.; Darnell, M.; Bencherif, S. A.; Weaver, J. C.; Huebsch, N.; Lee, H.; Lippens, E.; Duda, G. N.; et al. Hydrogels with Tunable Stress Relaxation Regulate Stem Cell Fate and Activity. *Nat. Mater.* **2016**, *15*, 326–334. https://doi.org/10.1038/NMAT4489.

(30) Loebel, C.; Ayoub, A.; Galarraga, J. H.; Kossover, O.; Simaan-yameen, H.; Seliktar, D.; Burdick, J. A. Tailoring Supramolecular Guest–Host Hydrogel Viscoelasticity with Covalent Fibrinogen Double Networks. *J. Mater. Chem. B* **2019**, *7*, 1753–1760. https://doi.org/10.1039/c8tb02593b.

(31) Daly, A. C.; Riley, L.; Segura, T.; Burdick, J. A. Hydrogel Microparticles for Biomedical Applications. *Nat. Rev. Mater.* **2020**, *5*, 20–43. https://doi.org/10.1038/s41578-019-0148-6.

(32) Riley, L.; Schirmer, L.; Segura, T. Granular Hydrogels: Emergent Properties of Jammed Hydrogel Microparticles and Their Applications in Tissue Repair and Regeneration. *Curr. Opin. Biotechnol.* **2019**, *60*, 1–8. https://doi.org/10.1016/j.copbio.2018.11.001.

(33) Qazi, T. H.; Burdick, J. A. Granular Hydrogels for Endogenous Tissue Repair. *Biomater. Biosyst.* **2021**, *1*, 1–3. https://doi.org/10.1016/j.bbiosy.2021.100008.

(34) Highley, C. B.; Song, K. H.; Daly, A. C.; Burdick, J. A. Jammed Microgel Inks for 3D Printing Applications. *Adv. Sci.* **2019**, *6* (1801076), 1–6. https://doi.org/10.1002/advs.201801076.

(35) Kumar, N.; Luding, S. Memory of Jamming – Multiscale Models for Soft and Granular Matter. *Granul. Matter* **2016**, *18*, 1–21. https://doi.org/10.1007/s10035-016-0624-2.

(36) Molley, T. G.; Hung, T.; Kilian, K. A. Cell-Laden Gradient Microgel Suspensions for Spatial Control of Differentiation During Biofabrication. *Adv. Healthc. Mater.* **2022**, *11* (24), 1–16. https://doi.org/10.1002/adhm.202201122.

(37) Griffin, D. R.; Weaver, W. M.; Scumpia, P. O.; Di Carlo, D.; Segura, T. Accelerated Wound Healing by Injectable Microporous Gel Scaffolds Assembled from Annealed Building Blocks. *Nat. Mater.* **2015**, *14*, 737–744. https://doi.org/10.1038/NMAT4294.

(38) Qazi, T. H.; Wu, J.; Muir, V. G.; Weintraub, S.; Gullbrand, S. E.; Lee, D.; Issadore, D.; Burdick, J. A. Anisotropic Rod-Shaped Particles Influence Injectable Granular Hydrogel Properties and Cell Invasion. *Adv. Mater.* **2022**, *34*, 1–12. https://doi.org/10.1002/adma.202109194.

(39) Muir, V. G.; Qazi, T. H.; Weintraub, S.; Maldonado, B. O. T.; Arratia, P. E.; Burdick, J. A. Sticking Together: Injectable Granular Hydrogels with Increased Functionality via Dynamic Covalent Inter-Particle Crosslinking. *Small* **2022**, 1–14. https://doi.org/10.1002/smll.202201115.

(40) Emiroglu, D. B.; Bekcic, A.; Dranseikiene, D.; Zhang, X.; Zambelli, T.; Andrew, J.; Tibbitt, M. W. Building Block Properties Govern Granular Hydrogel Mechanics through Contact Deformations. *Sci. Adv.* **2022**, *8*, 1–15.

(41) Bertsch, P.; Andrée, L.; Besheli, N. H.; Leeuwenburgh, S. C. G. Colloidal Hydrogels Made of Gelatin Nanoparticles Exhibit Fast Stress Relaxation at Strains Relevant for Cell Activity. *Acta Biomater.* **2022**, *138*, 124–132. https://doi.org/10.1016/j.actbio.2021.10.053.

(42) Pfaff, B. N.; Pruett, L. J.; Cornell, N. J.; de Rutte, J.; Di Carlo, D.; Highley, C. B.; Griffin, D. R. Selective and Improved Photoannealing of Microporous Annealed Particle (MAP) Scaffolds. *ACS Biomater. Sci. Eng.* **2021**, *7* (2), 422–427. https://doi.org/10.1021/acsbiomaterials.0c01580.

(43) Grewal, M. G.; Helein, G. T.; Sumey, J. L.; Caliari, S. R.; Highley, C. B. Packed Hydrogel Microfibers as a Granular Medium. *bioRxiv* **2023**.

(44) Aisenbrey, E. A.; Murphy, W. L. Synthetic Alternatives to Matrigel. *Nat. Rev. Mater.* **2020**, *5* (7), 539–551. https://doi.org/10.1038/s41578-020-0199-8.Synthetic.

(45) Kloxin, A. M.; Kloxin, C. J.; Bowman, C. N.; Anseth, K. S. Mechanical Properties of Cellularly Responsive Hydrogels and Their Experimental Determination. *Adv. Mater.* **2010**, *22* (31), 3484–3494. https://doi.org/10.1002/adma.200904179.

(46) Yavitt, F. M.; Brown, T. E.; Hushka, E. A.; Brown, M. E.; Gjorevski, N.; Dempsey, P. J.; Lutolf, M. P.; Anseth, K. S. The Effect of Thiol Structure on Allyl Sulfide Photodegradable Hydrogels and Their Application as a Degradable Scaffold for Organoid Passaging. *Adv. Mater.* **2020**. https://doi.org/10.1002/adma.201905366.

(47) Grim, J. C.; Brown, T. E.; Aguado, B. A.; Chapnick, D. A.; Viert, A. L.; Liu, X.; Anseth, K. S. A Reversible and Repeatable Thiol–Ene Bioconjugation for Dynamic Patterning of Signaling Proteins in Hydrogels. *ACS Cent. Sci.* **2018**, *4*, 909–916. https://doi.org/https://doi.org/10.1021/acscentsci.8b00325.

(48) Hoyle, C. E.; Bowman, C. N. Thiol – Ene Click Chemistry. *Angew. Chemie* **2010**, *49*, 1540–1573. https://doi.org/https://doi.org/10.1002/anie.200903924.

(49) Wade, R. J.; Bassin, E. J.; Gramlich, W. M.; Burdick, J. A. Nanofibrous Hydrogels with Spatially Patterned Biochemical Signals to Control Cell Behavior. *Adv. Mater.* **2015**, *27* (8), 1356–1362. https://doi.org/https://doi.org/10.1002/adma.201404993.

(50) Xin, S.; Alge, D. L.; Chimene, D.; Garza, J. E.; Gaharwar, A. K. Clickable PEG Hydrogel Microspheres as Building Blocks for 3D Bioprinting. *Biomater. Sci.* **2019**, *7*, 1179–1187. https://doi.org/10.1039/c8bm01286e.

(51) Gramlich, W. M.; Kim, I. L.; Burdick, J. A. Synthesis and Orthogonal Photopatterning of Hyaluronic Acid Hydrogels with Thiol-Norbornene Chemistry. *Biomaterials* **2013**, *34* (38), 9803–9811. https://doi.org/10.1016/j.biomaterials.2013.08.089.

(52) Grewal, M. G.; Gray, V. P.; Letteri, R. A.; Highley, C. B. User-Defined, Temporal

Presentation of Bioactive Molecules on Hydrogel Substrates Using Supramolecular Coiled Coil Complexes. *Biomater. Sci.* **2021**, *9* (12), 4374–4387. https://doi.org/10.1039/d1bm00016k.

(53)   Fraser, A. K.; Ki, C. S.; Lin, C. PEG-Based Microgels Formed by Visible-Light-Mediated Thiol-Ene Photo-Click Reactions. *Macromol. Chem. Phys.* **2014**, *215*, 507–515.

(54)   Becker, M.; Gurian, M.; Schot, M.; Leijten, J. Aqueous Two-Phase Enabled Low Viscosity 3D (LoV3D) Bioprinting of Living Matter. **2023**, *2204609*, 1–12. https://doi.org/10.1002/advs.202204609.

(55)   King, W. J.; Toepke, M. W.; Murphy, W. L. Facile Formation of Dynamic Hydrogel Microspheres for Triggered Growth Factor Delivery. *Acta Biomater.* **2011**, 7 (3), 975–985. https://doi.org/10.1016/j.actbio.2010.10.026.

(56)   Impellitteri, N. A.; Toepke, M. W.; Lan Levengood, S. K.; Murphy, W. L. Specific VEGF Sequestering and Release Using Peptide- Functionalized Hydrogel Microspheres. *Biomaterials* **2013**, *33* (12), 3475–3484. https://doi.org/10.1016/j.biomaterials.2012.01.032.Specific.

(57)   Grewal, M. G.; Highley, C. B. Electrospun Hydrogels for Dynamic Culture Systems: Advantages, Progress, and Opportunities. *Biomater. Sci.* **2021**, *9*, 4228–4245. https://doi.org/10.1039/d0bm01588a.

(58)   Davidson, M. D.; Prendergast, M. E.; Ban, E.; Xu, K. L.; Mickel, G.; Mensah, P.; Dhand, A.; Janmey, P. A.; Shenoy, V. B.; Burdick, J. A. Programmable and Contractile Materials through Cell Encapsulation in Fibrous Hydrogel Assemblies. *Sci. Adv.* **2021**, *7*, 1–14.

(59)   Prendergast, M. E.; Davidson, M. D.; Burdick, J. A. A Biofabrication Method to Align Cells within Bioprinted Photocrosslinkable and Cell-Degradable Hydrogel Constructs via Embedded Fibers. *Biofabrication* **2021**, *13*.

(60)   Prendergast, M. E.; Heo, S.-J.; Mauck, R. L.; Burdick, J. A. Suspension Bath Bioprinting and Maturation of Anisotropic Meniscal Constructs. *Biofabrication* **2023**, *15* (3). https://doi.org/10.1088/1758-5090/acc3c3.

(61)   Miller, B.; Hansrisuk, A.; Highley, C. B.; Caliari, S. R. Guest − Host Supramolecular Assembly of Injectable Hydrogel Nanofibers for Cell Encapsulation. *ACS Biomater. Sci. Eng.* **2021**, *7*, 4164–4174. https://doi.org/10.1021/acsbiomaterials.1c00275.

(62)   Matera, D. L.; Wang, W. Y.; Smith, M. R.; Shikanov, A.; Baker, B. M. Fiber Density Modulates Cell Spreading in 3D Interstitial Matrix Mimetics. *ACS Biomater. Sci. Eng.* **2019**, *5*, 2965–2975. https://doi.org/https://doi.org/10.1021/acsbiomaterials.9b00141.

(63)   Matera, D. L.; Lee, A. T.; Hiraki, H. L.; Baker, B. M. The Role of Rho GTPases During Fibroblast Spreading, Migration, and Myofibroblast Differentiation in 3D Synthetic Fibrous Matrices. *Cell. Mol. Bioeng.* **2021**. https://doi.org/10.1007/s12195-021-00698-5.

(64)   Hiraki, H. L.; Matera, D. L.; Rose, M. J.; Kent, R. N.; Todd, C. W.; Stout, M. E.; Wank, A. E.; Schiavone, M. C.; Depalma, S. J.; Zarouk, A. A.; et al. Magnetic Alignment of Electrospun Fiber Segments Within a Hydrogel Composite Guides Cell Spreading and Migration Phenotype Switching. *Front. Bioeng. Biotechnol.* **2021**, *9*, 1–14. https://doi.org/10.3389/fbioe.2021.679165.

(65)   Li, X.; Cho, B.; Martin, R.; Seu, M.; Zhang, C.; Zhou, Z.; Choi, J. S.; Jiang, X.; Chen, L.; Walia, G.; et al. Nanofiber-Hydrogel Composite–Mediated Angiogenesis for Soft Tissue Reconstruction. *Sci. Transl. Med.* **2019**, *11* (490), 1–12. https://doi.org/10.1126/scitranslmed.aau6210.

(66)   Li, L.; Yao, Z.; Parian, A.; Yang, Y.; Chao, J.; Yin, J.; Salimian, K. J.; Reddy, S. K.; Zaheer, A.; Gearhart, S. L.; et al. A Nanofiber-Hydrogel Composite Improves Tissue Repair in a Rat Model of Crohn ' s Disease Perianal Fistulas. *Sci. Adv.* **2023**, *9*. https://doi.org/10.1126/sciadv.ade1067.

(67)   Haggerty, A. E.; Nitobe, Y.; Yamane, K.; Marlow, M. M.; You, H.; Zhang, C.; Cho, B.; Li, X.; Reddy, S.; Mao, H.; et al. The Effects of the Combination of Mesenchymal Stromal Cells and Nanofiber-Hydrogel Composite on Repair of the Contused Spinal Cord. *Cells* **2022**, *11*, 1–17.

(68)   Mealy, J. E.; Chung, J. J.; Jeong, H.; Issadore, D.; Lee, D.; Atluri, P.; Burdick, J. A. Injectable Granular Hydrogels with Multifunctional Properties for Biomedical Applications. *Adv. Mater.* **2018**, *30*, 1–7. https://doi.org/10.1002/adma.201705912.

(69)   Highley, C. B.; Rodell, C. B.; Burdick, J. A. Direct 3D Printing of Shear-Thinning Hydrogels into Self-Healing Hydrogels. *Adv. Mater.* **2015**, *27* (34), 5075–5079. https://doi.org/10.1002/adma.201501234.

(70)   Barnes, J. M.; Przybyla, L.; Weaver, V. M. Tissue Mechanics Regulate Brain Development , Homeostasis and Disease. *J. Cell Sci.* **2017**, *130*, 71–82. https://doi.org/10.1242/jcs.191742.

(71)　Ifkovits, J. L.; Burdick, J. A. Review: Photopolymerizable and Degradable Biomaterials for Tissue Engineering Applications. *Tissue Eng.* **2007**, *13* (10), 2369–2385. https://doi.org/10.1089/ten.2007.0093.

(72)　Wisdom, K. M.; Adebowale, K.; Chang, J.; Lee, J. Y.; Nam, S.; Desai, R.; Rossen, N. S.; Rafat, M.; West, R. B.; Hodgson, L.; et al. Matrix Mechanical Plasticity Regulates Cancer Cell Migration through Confining Microenvironments. *Nat. Commun.* **2018**, *9*. https://doi.org/10.1038/s41467-018-06641-z.

(73)　Legant, W. R.; Miller, J. S.; Blakely, B. L.; Cohen, D. M.; Genin, G. M.; Chen, C. S. Measurement of Mechanical Tractions Exerted by Cells in Three-Dimensional Matrices. *Nat. Methods* **2010**, *7* (12), 969–971. https://doi.org/10.1038/NMETH.1531.

(74)　Prass, M.; Jacobson, K.; Mogilner, A.; Radmacher, M. Direct Measurement of the Lamellipodial Protrusive Force in a Migrating Cell. **2006**, *174* (6), 767–772. https://doi.org/10.1083/jcb.200601159.

(75)　Roure, O.; Saez, A.; Buguin, A.; Austin, R. H.; Chavrier, P.; Silberzan, P.; Ladoux, B. Force Mapping in Epithelial Cell Migration. *PNAS* **2005**, *102*, 2390–2395. https://doi.org/10.1073/pnas.0408482102.

(76)　Piotrowski-daspit, A. S.; Nerger, B. A.; Wolf, A. E.; Sundaresan, S.; Nelson, C. M. Dynamics of Tissue-Induced Alignment of Fibrous Extracellular Matrix. *Biophys. J.* **2017**, *113* (3), 702–713. https://doi.org/10.1016/j.bpj.2017.06.046.

(77)　Santos, T. E.; Schaffran, B.; Broguiere, N.; Meyn, L.; Zenobi-wong, M.; Bradke, F. Axon Growth of CNS Neurons in Three Dimensions Is Amoeboid and Independent of Adhesions. *Cell Rep.* **2020**, *32*, 1–12. https://doi.org/10.1016/j.celrep.2020.107907.

(78)　Sharma, S.; Floren, M.; Ding, Y.; Stenmark, K. R.; Tan, W.; Bryant, S. J. A Photoclickable Peptide Microarray Platform for Facile and Rapid Screening of 3-D Tissue Microenvironments. *Biomaterials* **2017**, *143*, 17–28. https://doi.org/10.1016/j.biomaterials.2017.07.025.

CHAPTER 7: A BIOFABRICATION TECHNOLOGY FOR ACHIEVING NEAR-SINGLE-CELL RESOLUTION IN CELL-DENSE, MACROSCALE TISSUE CONSTRUCTS

7.1. Abstract

Across biomedical sciences in broad scientific, engineering, and medical disciplines, efforts to understand biology and improve health have included the development and application of tissue-like constructs that recapitulate features of cellular and physiological systems, tissues, and organs. There are numerous established biofabrication platforms that enable design of some important features of tissue systems, such as material and cellular localization (e.g., 3D bioprinting) and fibrous architecture (e.g., electrospinning); however, state-of-the-art technologies still face hurdles in recreating the complexity of biological structures across multiple length scales. Given the appreciation for how local environments influence individual cell fates, the ability to assemble cells within material environments where cellular and material architecture is controlled at near-single-scale resolution will enable the directed formation of desired biological structures. Thus, we identified a potential strategy that might enable these requirements: a layer-by-layer assembly of thin hydrogel fiber scaffolds with spatially patternable biomolecules, cells, and materials through the thiol-ene reaction scheme. Herein, we demonstrate initial steps towards the development of this biofabrication platform – through photomediated patterning mechanisms to modify electrospun hydrogels, utilizing thin film support substrates to enhance the stability of these 2D scaffolds, and precise layering of these scaffolds to begin forming constructs in the Z direction. While only preliminarily demonstrated here, future extension of these steps will enable the desired control of cellular and material composition at the microscale throughout 3D, macroscale constructs.

7.2. Introduction

Throughout the history of tissue engineering and regenerative medicine, our collective understanding of fundamental biological processes has been closely coupled with the available techniques to develop and apply tissue-mimetic constructs that recapitulate targeted features of physiological systems[1]. Accordingly, the advancement of biofabrication processes – fabrication processes that aim to engineer the cellular and material environment of tissue-mimetics with precise spatiotemporal control in 3D space – has received considerable attention in recent years[2]. This has resulted in well-demonstrated use cases of cell- and material-based constructs, including for the interrogation of stem cell niches[3], the design of systems that support and influence developmental and morphogenic processes[4–6], the creation of drug screening platforms for personalized medicine[7], and the engineering of replacement tissue[2,8]. These approaches harness a variety of sophisticated technologies that enable researchers to approach modeling the endogenous complexity of the cellular and extracellular environments seen *in vivo* through controlled positioning of cells and materials. While *de novo* creation of fully functional patient-specific tissues and organs remain an important (and currently aspirational) objective for tissue engineering and regenerative medicine, technologies that advance our capabilities in isolating specific variables when modeling native biology are having immediate impacts on human health by furthering our understanding of biological development, function, and dysfunction[9].

Defining cellular and material structures with high microscale (<100 μm) resolution throughout macroscale 3D space (>1mm^3) remain central considerations in tissue engineering efforts and are motivating factors in biofabrication technologies. Hydrogel

materials are commonly used in tissue engineering, owing to properties that mirror – and can be modulated to further recapitulate – characteristics of the endogenous extracellular matrix (ECM)[10–12]. Indeed, diverse techniques have been explored to attempt to achieve biomimetic structure and function in synthetically engineered hydrogels. These techniques have been applied to cell suspensions and cells embedded within hydrogels with dimensions ranging from the microscale to the mesoscale (100 μm – 1 mm) and include: fluidic patterning[13]; electric fields[14]; organization of microgels[15–21]; sound waves[22]; magnetism[23]; and molding[24]. Hydrogels are also amenable to chemical functionalization strategies that enable post-crosslinking modifications for further specification of the biomimetic heterogeneity of the resultant construct[25–31]. Often, focused light is utilized to pattern microscale extracellular features with high precision into hydrogel systems[32–34]. Examples include, but are not limited to, photomediated patterning of biochemical functionalities[35], mechanical cues[34], viscoelasticity[36], and topologies that might direct cell behaviors[37,38].

Despite the recent progress in biofabrication technologies, there are still technique-dependent hurdles in simultaneously addressing critical challenges that are central to building tissue constructs with multiscale complexity. In particular, the ability to specify arbitrary cellular and material composition at single-cell-scale resolution must be achieved throughout 3D space at the macroscale. Currently, no biofabrication or tissue engineering platform has demonstrated this capability[39]. Generally, sophisticated techniques allowing high-resolution control over construct composition have demonstrated the ability to control the positions of cells or the material structure, but typically not both. These techniques also face challenges in scaling towards macroscale

263

structures for various reasons. For example, 3D printing faces significant challenges in specifying structures at the single-cell level. Although position capabilities are high, the maximum resolution of printed structures is typically in the mesoscale range. Print times also scale exponentially with increasing resolution, which poses a significant hurdle to 3D printing approaches towards cell-scale resolution in macroscale constructs. Additionally, and perhaps most notably, cells experience higher shear forces from 3D printing processes, where cell viability is inversely correlated with print resolution[40,41].

In response, we have identified a potential biofabrication strategy for tissue engineering that might be capable of positioning cells and extracellular material throughout 3D space with <100 μm spatial resolution. This technique employs thin, planar substrates comprised of electrospun hydrogel fibers, which have shown considerable promise as substrates for cell adhesion and also possess reactive functional groups for spatially controlled crosslinking and post-crosslinking biochemical modification using established photochemistries[42]. These planar substrates are subsequently layered to form a 3D construct comprised of many 2D layers. Using a layer-by-layer approach enables independent processing of each layer, with seeded cells allowed to reach confluency before assembling into a cell-dense construct. This biofabrication platform is preliminarily demonstrated here; however, the ability to control both cellular and material composition at near-cell-scale in macroscale 3D constructs is an unparalleled strength of this technique that is applicable to any tissue system of interest.

7.3. Materials and Methods

All reagents were purchased from Millipore Sigma, unless otherwise stated.

7.3.1. Preparation of support materials for electrospun substrates

Thin films (~50μm thick) of cyclic olefin copolymer (COC, ZeonorFilm) were identified as the support substrate for each layer of electrospun hydrogel fibers. COC films are generally inert off-the-shelf but are amenable to modifications. First, COC films were cut using a CO_2 laser to introduce void spaces in the support material for fibers to span across. The films were then chemically functionalized with 3-(mercaptopropyl) trimethoxysilane (MTS) to enable covalent bonding between electrospun fibers and the COC surface. Briefly, COC film surfaces were activated using air plasma (Harrick Plasma) for 5 min, and MTS was added dropwise to the surface prior to being baked at 60 °C for 1 h in an exhausted oven. COC films were then washed twice in 70% ethanol in water and DI water and stored under nitrogen until use.

For preliminary cell patterning experiments, glass coverslips were utilized as the substrate for fiber adhesion. Glass coverslips were modified with MTS as described in Chapter 3.

7.3.2. Synthesis of methacrylate-modified HA (MeHA) and norbornene-modified HA (NorHA)

NorHA was synthesized as previously described in Chapter 3. Similarly, MeHA was synthesized as described in Chapter 5. The degree of modification was determined to be

~25% for NorHA and ~100% for MeHA by ^{1}H NMR spectra (**Figures S3.1** and **S5.1**, respectively).

7.3.3. Peptide synthesis

All fluorescent peptides utilized in this study were synthesized identically to the methods outlined in Chapters 3, 5, and 6. Here, two fluorescent peptides were used – one with a 5(6)-carboxyfluorescein appended to the N-terminus and one with a rhodamine B appended to the N-terminus (GCDDD-FAM and GCDDD-RhoB). The cysteine residue within both peptides provides a thiol group for photomediated thiol-ene conjugation to methacrylate and norbornene groups. For cell adhesion, a thiolated RGD peptide (GCGYGRGDSPG) was purchased from Genscript.

7.3.4. Fabrication of planar electrospun hydrogel fiber substrates

Both MeHA and NorHA were chosen to preliminarily demonstrate this biofabrication platform. While the norbornene groups on NorHA facilitate a more stoichiometric crosslinking reaction compared to the methacrylates on MeHA, both HA derivatives utilized here enable spatially-controlled, photomediated ligation of biomolecules to the stabilized fibers. Prior to electrospinning, MTS-modified COC films or glass coverslips were secured to a rotating mandrel collector (DOXA Microfluidics) which was set to rotate at 1000 RPM.

MeHA was electrospun according to the protocols outlined in Chapter 5. NorHA was electrospun using a solution comprised of 3.5% w/v NorHA, 2.5% w/v PEO (900 kDa), 0.05% w/v HHMP, and sufficient dithiothreitol (DTT) such that the ratio of thiol groups from DTT to norbornenes on NorHA equaled 0.6 ([-SH]:[nor]=0.6). Both polymers

were electrospun with flow rates varying from 0.4-0.6 mL/hr and applied voltages ranging from 10-15 kV. A constant negative voltage of -4 kV was applied to the mandrel to focus the electrical field during the electrospinning process. If homogenous fluorescence of fibers were desired, 1 mM of the FAM peptide was included in the electrospinning precursor solution. Fibers were collected for ~45 min prior to being removed from the mandrel and crosslinked at 10 mW/cm^2 (Omnicure) for 5 min for MeHA and 15 min for NorHA. All fiber samples were hydrated in PBS for at least 1 hr before further modifications.

7.3.5. Photoligation of fluorescent peptides to hydrogel fibers

Prior to photopatterning experiments, all fiber samples were hydrated in 1% w/v BSA in PBS for at least 30 min. For spatially-controlled patterning of the fluorescent peptide to hydrogel fibers, a solution consisting of 1 mM fluorescent peptide (either RhoB or FAM), 1 % BSA, and 1 mM LAP was added to the fiber surface. Next, a photomask (CAD/Art Services) was added on top of the fiber scaffold and the entire system was irradiated with UV light (10 mW/cm^2) for 2 min. The same protocol was followed for conjugating the cell-adhesive, fibronectin-mimetic Arg-Gly-Asp (RGD) peptide to fibers, with 1 mM of the RGD peptide added to the patterning solution in addition to the fluorescent peptide for visualization of RGD+ regions. Following the photopatterning process, fiber samples were washed thrice in PBS to remove unreacted peptides and stored at room temperature in PBS until required for further experimentation. Scaffolds patterned with just the fluorescent peptide were imaged directly following the washing steps on a Leica DMi8 Widefield microscope, and resultant images were processed and

analyzed using ImageJ. Scaffolds with patterned RGD were then moved into the cell culture pipeline for patterning cells in RGD+ regions.

7.3.6. Cell culture, seeding, and staining

Immortalized murine myoblasts (C2C12s, ATCC) and human umbilical vein endothelial cells (hUVECs, Lonza) were used for cell culture experiments (passages 5-8). C2C12s were cultured in standard growth media comprised of high glucose Dulbecco's Modified Eagle's Medium (DMEM) fortified with 10% v/v fetal bovine serum (Gibco) and 1% antibiotic/antimycotic (Gibco). hUVECs were cultured using an Endothelial Growth Medium-2 BulletKit (Lonza) according to the manufacturer's protocol. Media was changed every 2 days for both cell types.

Prior to cell seeding, RGD+ scaffolds were sterilized with germicidal light for 1 h. The PBS was then exchanged with the desired complete growth media for at least 30 min to displace PBS with the nutrient-rich media. Cells were then seeded on top of the fibrous scaffolds at a density of 1 x 10^5 cells per scaffold and were given 30 min to adhere to the RGD+ regions. Scaffolds were then gently washed with PBS to remove unadhered cells from the fibers. Following a 3 d culture period, cells were fixed in 10% v/v neutral buffered formalin for 15 min, permeabilized with 0.1% v/v Triton X-100 for 10 min, then blocked with 3% w/v BSA for 90 min at room temperature. F-actin was tagged with AlexaFluor-488 phalloidin (1:600, Invitrogen) for 2h and nuclei were counterstained with DAPI (1:10000) for 1 min. Scaffolds were washed thrice in PBS to remove unreacted molecules. Cells were imaged on a Leica DMi8 Widefield Microscope and fluorescent micrographs

were processed and analyzed on ImageJ to determine cell localization with respect to RGD+ regions.

7.4. Results and Discussion

7.4.1. Spatially-controlled photopatterning electrospun hydrogel fibers

Electrospun fibrous scaffolds were fabricated using both NorHA and MeHA – both of which have demonstrated biocompatibility and been established for electrospinning processes (^{1}H NMR spectra confirming successful syntheses shown in **Figures S3.1** and **S5.1**)[33,43,44]. Electrospun fibers have seen extensive use in the tissue engineering space due to their ability to mimic the fibrous content of endogenous ECM[42,45,46], and the use of HA as the base material is additionally advantageous due to its prevalence in natural tissue[47,48]. Both the methacrylate and norbornene functional groups enable a photomediated crosslinking mechanism to stabilize fibers; however, they are not used to exhaustion during crosslinking, thereby providing sites for biomolecule adhesion through
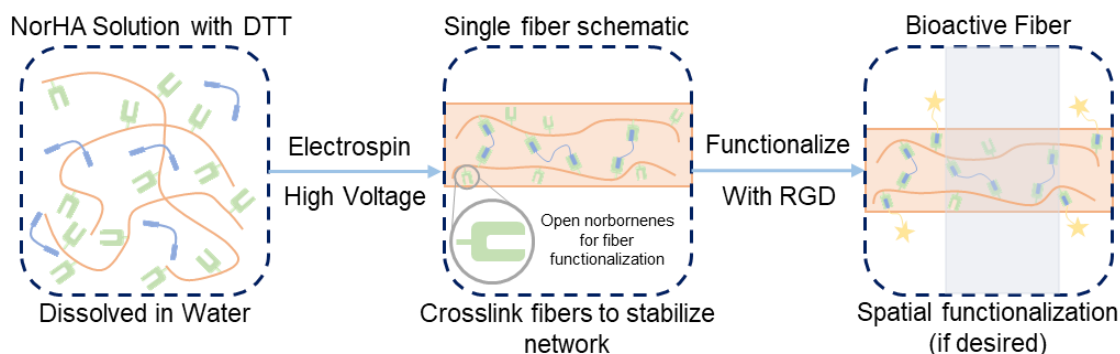
Scheme 7.1. Schematic of electrospinning NorHA fibers with photopatterned bioactivity. (left): The aqueous NorHA electrospinning solution contains a crosslinker molecule (here, DTT) that enables (middle) photomediated crosslinking of individual fibers following the electrospinning process. (right): The fibers contain residual norbornene groups that allow for further functionalization with bioactive molecules (such as RGD) through the thiol-ene reaction mechanism. Importantly, while this schematic illustrates the process for NorHA, MeHA generally follows the same scheme, except methacrylate groups crosslink together rather than through a dithiol crosslinker molecule.

additional thiol-ene reactions with thiolated peptides. The thiol-ene reaction is light-mediated[49], so spatial control is afforded by dictating where light engages with the scaffold during the conjugation process (**Scheme 7.1**)[33,34,43].

Since high-resolution, light-based techniques are typically physically constrained by light spreading, we first sought to examine the limitations of the thiol-ene mechanism when photopatterning features with decreasing sizes. We utilized a photomask with vertical stripes that decrease in width from 600 μm down to 20 μm, which is approximately the size of a single cell (**Figure 7.1A**). Interestingly, as stripe size decreased, there was a correlated decrease in signal intensity, which might be attributed to the amount of light contacting the scaffold allowing the reaction to proceed (**Figure 7.1B**). When analyzing the resultant stripe sizes following the patterning process, we were able to discern a relationship between expected stripe width (i.e., the size of the photomask) and the actual stripe width (i.e., the size of the patterned stripe on the scaffold). Plotting the expected width versus the actual width, the slope of the line should theoretically be 1; however, it was expected that the slope might deviate from 1 at smaller features due to light spreading. Indeed, the expected versus actual values were essentially equivalent at large stripe widths (**Figure 7.1C**), with deviations beginning at widths below ~70 μm (**Figure 7.1D**), indicating that we can achieve patterns that are sized within the same order of magnitude as most cells.
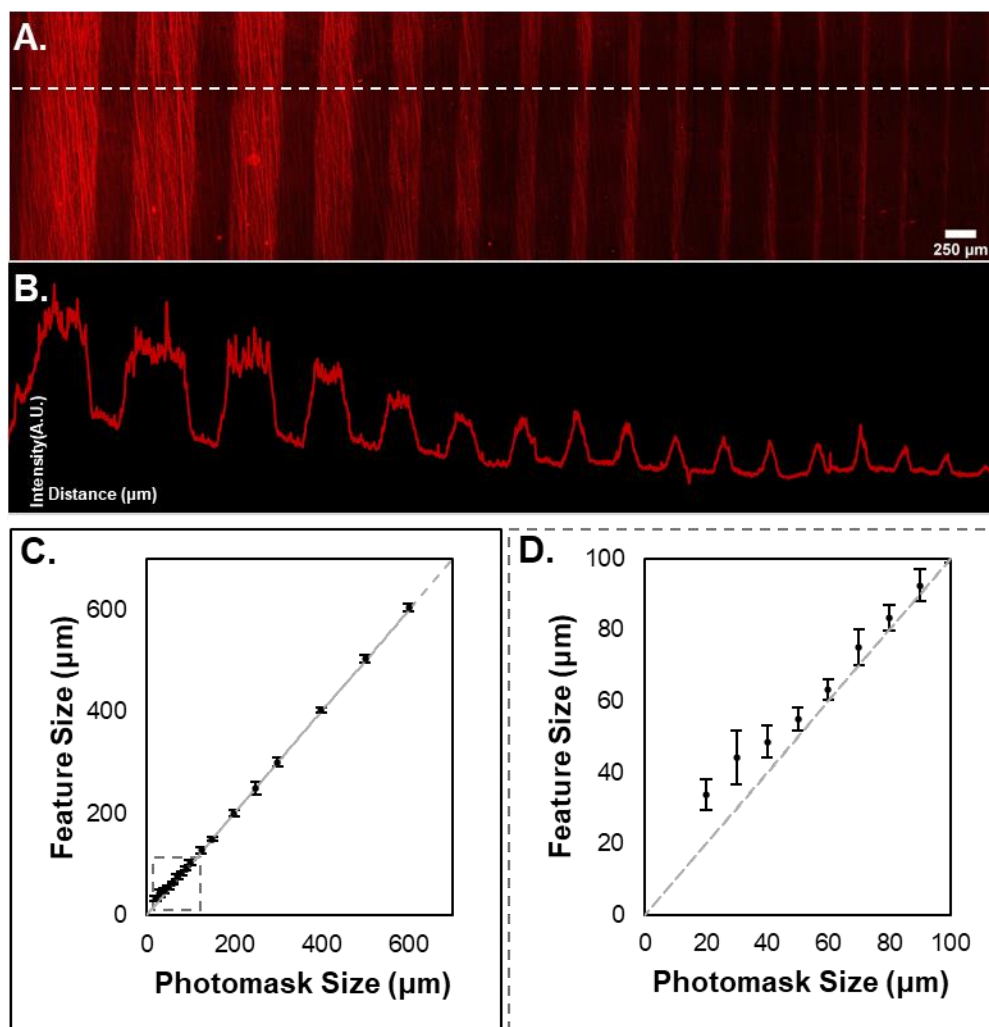
Figure 7.1. Investigating the limitations of light-based patterning. (A) Patterned stripes using a thiolated rhodamine B peptide with decreasing stripe width from 600 μm to 20 μm. White dashed line corresponds to the intensity profile (B) that illustrates decreasing stripe intensity as feature size decreases – possibly due to less light contacting the scaffold. (C) Expected versus actual feature width showing that actual stripes are essentially equivalent to the photomask size at larger stripe sizes (> ~70 μm, grey dashed line corresponds to equivalency). (D) Inset from (C) illustrating where actual stripe widths are larger than expected, likely due to light spreading. Scalebar = 250 μm.

7.4.2. Localizing cell adhesion by photopatterning thiolated adhesive ligands

To localize cell adhesion on 2D electrospun scaffolds, a thiolated peptide containing a fibronectin-mimetic RGD motif[50] was photopatterned onto the hydrogel fibers (support by glass coverslips) using a photomask with 100 μm wide stripes. Both

immortalized murine myoblasts (C2C12s) and human umbilical vein endothelial cells (hUVECs) were selected to demonstrate the flexibility of this patterning platform for multiple cell types. In this scheme, the RGD peptide was photopatterned along with the rhodamine B peptide to enable visual confirmation of RGD localization following the ligation and washing steps (**Figure 7.2A-B** and **7.2D-E**). Indeed, both the seeded C2C12s and hUVECs preferentially adhered to the patterned RGD+ regions (**Figure 7.2C** and **7.2F**), thereby demonstrating spatial control over cell localization on 2D fibrous substrates. The ability to control biomolecule localization (**Figure 7.1**) along with the position of cells (**Figure 7.2**) on a singular 2D electrospun hydrogel substrate is the first step towards a layer-by-layer assembly biofabrication platform, and this technique is theoretically grounded in the ability to repeat this process for multiple layers prior to stacking and forming a 3D construct. Thus, the next step is to translate this preliminary technique towards the layer-by-layer goal by developing a thin film substrate system that will support layering of fibrous scaffolds on top of each other.
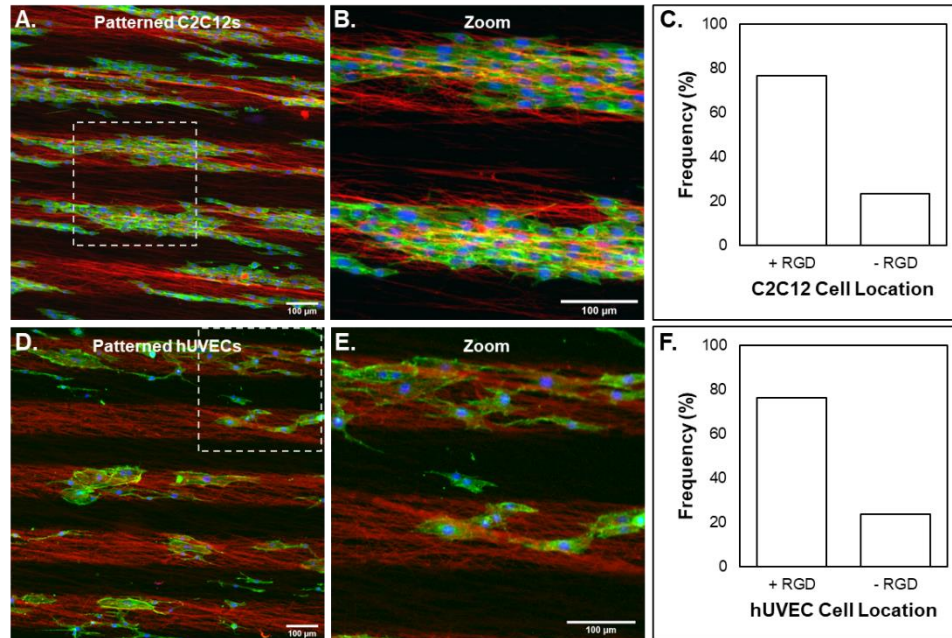
Figure 7.2. Controlling cell localization on fibrous substrates. (A) C2C12 cells preferentially adhering to the RGD+ regions (marked red by the rhodamine B peptide). (B) Zoomed in image of C2C12s within the patterned regions. (C) Quantification of cells in the RGD+ and RGD- regions indicating that C2C12s adhered primarily to the RGD+ regions. (D) hUVECs adhering preferentially to RGD+ regions (marked red by the rhodamine B peptide). (E) Zoomed in image of hUVECs within the patterned regions. (F) Quantification of cells in the RGD+ and RGD- regions indicating that hUVECs mostly adhered the RGD+ regions. Scalebars = 100 μm.

7.4.3. Developing a substrate system that enables layering of fibrous scaffolds

Thus far, we have demonstrated the ability to control the localization of biomolecules and cells on fibrous substrates supported by glass coverslips. To enable a layering system where the fibrous layers come in direct contact, we sought to develop a thin film substrate system that can be selectively ablated using a laser to create void spaces in the substrate that fibers can span across (**Figure 7.3A-C**). This step is critical because the void spaces in the substrate theoretically allow for fibers that span the wells to be layered directly on top of each other. To achieve this, we identified cyclic olefin copolymer (COC, ZeonorFilm) thin films that are 50 μm thick. COC films are

273

advantageous as substrates since they are bioinert, transparent, and enable facile laser ablation with a CO_2 laser[51]. Additionally, COC films are amenable to surface modification with thiol groups to enable covalent conjugation of electrospun fibers to the films for immobilization during further processing steps (e.g., photopatterning, cell culture, and layering). COC films were designed such that there would be 9 holes laser cut into each film sample in a 3x3 grid. The outside 8 holes are designated for sample alignment during the layering process, and the middle hole is the "working area", which is where the biomolecules and cells would be patterned onto fibers (**Figure 7.3A**).
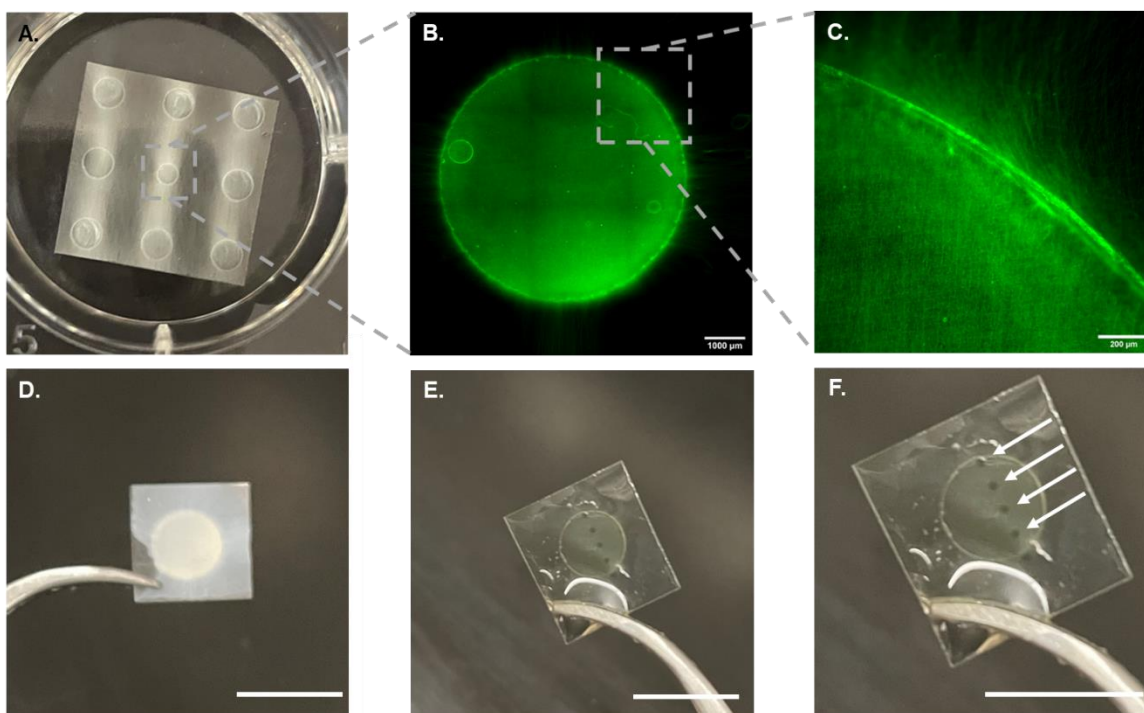
Figure 7.3. Cyclic olefin copolymer substrates for fibrous scaffolds that span wells.
(A) COC films are designed to have a 3x3 grid of holes, where the outside 8 holes support alignment during future layering processes. These COC films are modified to present thiols for covalent immobilization of fibers to the films. (B) FAM-tagged fibers that span the middle hole in the 3x3 grid. (C) Zoomed in image of fibers at the edge of the hole in the COC film. (D) Dry fibers that span a well in a COC film that has been crosslinked with a photomask that shields light in 250 μm circles. (E) Hydrated fibers in (D) that show the selective crosslinking capabilities where the shielded circles during crosslinking dissolve away upon hydration. (F) Zoomed in image of (E) with white arrows indicating dissolved regions. Scalebars: (B) = 1000 μm; (C) = 200 μm, (D-F) = 1 cm.

An advantageous feature of this scheme is that since both MeHA and NorHA fibers allow for photomediated crosslinking mechanisms, the localization of crosslinking can be controlled via selective shielding of fiber regions using photomasks (identical to the photopatterning of thiolated peptides)[43]. This is particularly noteworthy because if holes are patterned into fibers during crosslinking, those regions would dissolve when hydrated (**Figure 7.3D-F**), thus leaving holes in the middle of the fibers that span the void space of the COC film. If multiple substrates with the same hole patterns are layered on top of each other, then those holes would align and form a channel in 3D space. These channels can be utilized as a material structure to help with nutrient diffusion or can possibly be lined with endothelial cells that might fuse into a vessel-like structure in the 3D construct.

7.4.4. Layering fiber scaffolds with precise alignment

With the demonstrated abilities to control the localization of biomolecules, cells, and fibers on both COC thin film and glass substrates, the next step towards this layer-by-layer assembly biofabrication platform is to establish a technique that layers these individual scaffolds with high degrees of precision. To achieve this, we 3D printed a base plate with alignment posts (schematic in **Figure 7.4A**) that correspond to the outside 8 laser ablated holes in the COC films (refer to **Figure 7.3A**). Preliminary experiments utilized 2 photomasks that require precise alignment of the patterned shapes to reveal the complete design. Similar to the COC films and 3D printed base plate, both photomasks used for this study were also laser cut to provide holes for alignment. For alignment with high degrees of precision, the first layer was added to the base plate along with the desired photomask. From there, the same UV patterning process was completed

to conjugate the thiolated peptide to the fibers. This step was repeated for the second layer. Finally, the photomasks were removed, and the fiber layers were stacked on top of each other using the base plate to align them. The full process schematic is shown in **Figure 7.4A**.

Indeed, this process design was successful in precisely layering 2 scaffolds together to show the full design across both layers, where the University of Virginia's "Split-V" logo was patterned with the "V" on Layer 1 and "Virginia" on Layer 2 (**Figure 7.4B**). It is important to note that while this process was demonstrated with a FAM-tagged peptide on both layers, each layer can be independently patterned with different biomolecules to engineer biochemical heterogeneity across layers. Furthermore, it is possible to pattern multiple different biomolecules on the same layer due to the flexibility of the thiol-ene reaction mechanism, which has been previously demonstrated by Wade
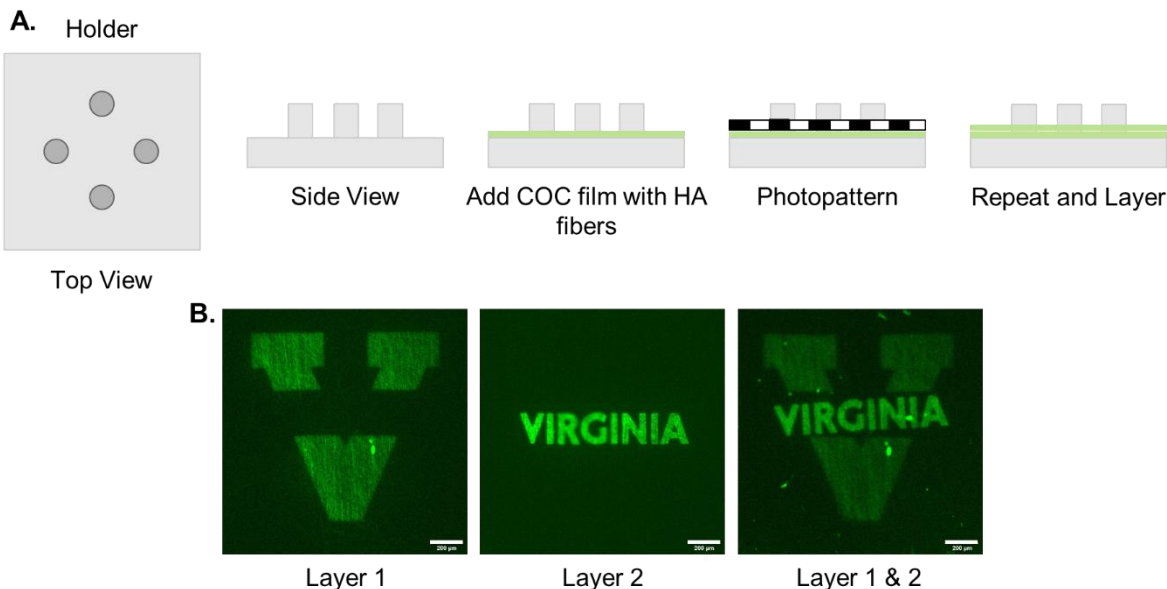
Figure 7.4. Precise layering of planar fibrous scaffolds with high precision. (A) Process schematic of using a 3D printed base plate to secure COC films with HA fibers during the photopatterning process. Precise layering is achieved using the same alignment posts to stack COC layers on top of each other. (B) 2 separately patterned layers form the University of Virginia's "Split-V" logo when stacked together. Scalebars = 200 μm.

and coworkers[33]. Finally, these techniques are the same as those used to add cells, as demonstrated in **Figure 7.2**. We therefore believe it would be possible to use this approach to introduce a user-defined cellular architecture that spans each layer and across layers in 3D space.

7.5. Conclusions and Future Outlook

In summary, we have successfully demonstrated preliminary proof-of-concept steps towards a layer-by-layer biofabrication platform that enables multiscale resolution in cell-dense, macroscale tissue constructs with control over the material and cellular heterogeneity in 3D space. MeHA and NorHA electrospun fibers act as substrates for cell culture, with the thiol-ene reaction scheme enabling localization of biomolecules that influence cell behavior and positioning at resolution length scales approaching that of a single cell (<70 µm). Using COC films as the support substrate for these fibers, holes can be laser cut such that fibers span over a void space. These unsupported fibers allow for each layer of fibers and cells to be stacked in direct contact when assembling the overall 3D macroscale construct. We finally demonstrate preliminary layering of 2 scaffolds with high precision such that photopatterned biomolecules form an overall design following stacking of the layers. Importantly, the demonstrated data address the main steps required for the process flow of the proposed biofabrication technology; however, the steps must be applied to systems with >2 layers to fully illustrate the generalizable flexibility of the platform. Future work includes designing intricate systems with multiple biomolecules, cells, and patterned channels across multiple layers to investigate the feasibility and scalability of a layer-by-layer biofabrication strategy.

Successful development of a biofabrication technology that enables near-single-cell resolution in cell-dense macroscale constructs would have significant implications in the tissue engineering community. For example, the perivascular neural stem cell niche is a tightly regulated environment where the maintenance of stemness is dictated by spatial arrangements of cells and signals at the microscale[52]. The ability to model this tissue system-specific stem cell niche might allow for more advanced studies of the underlying biology of these cells in their microenvironment. From a translational perspective, volumetric muscle loss is a potential application of this tool because functional regeneration would require densely cellularized structures that are innervated and supplied by vasculature[53] – complex challenges that are potentially addressable by this technology. These examples provide potential applications in both the research and translational spaces; however, this generalizable platform would enable the directed formation and subsequent study of biological structures, from models of specific cellular niches and replacement tissues (such as the two above examples), to models of dysfunctional tissue and synthetic multicellular systems with engineered functions.

7.6. References

(1)   Caliari, S. R.; Burdick, J. A. A Practical Guide to Hydrogels for Cell Culture. *Nat. Methods* **2016**, *13* (5), 405–414. https://doi.org/10.1038/nmeth.3839.

(2)   Moroni, L.; Burdick, J. A.; Highley, C.; Lee, S. J.; Morimoto, Y.; Takeuchi, S.; Yoo, J. J. Biofabrication Strategies for 3D in Vitro Models and Regenerative Medicine. *Nat. Rev. Mater.* **2018**, *3*, 21–37. https://doi.org/https://doi.org/10.1038/s41578-018-0006-y.

(3)   Ma, Y.; Lin, M.; Huang, G.; Li, Y.; Wang, S.; Bai, G.; Lu, T. J.; Xu, F. 3D Spatiotemporal Mechanical Microenvironment: A Hydrogel-Based Platform for Guiding Stem Cell Fate. *Adv. Mater.* **2018**, *30* (49), 1–27. https://doi.org/10.1002/adma.201705911.

(4)   Hughes, A. J.; Miyazaki, H.; Coyle, M. C.; Zhang, J.; Laurie, M. T.; Chu, D.; Vavrusova, Z.; Schneider, R. A.; Klein, O. D.; Gartner, Z. J. Engineered Tissue Folding by Mechanical Compaction of the Mesenchyme. *Dev. Cell* **2018**, *44*, 165–178. https://doi.org/10.1016/j.devcel.2017.12.004.

(5)   Viola, J. M.; Porter, C. M.; Gupta, A.; Alibekova, M.; Prahl, L. S.; Hughes, A. J. Guiding Cell Network Assembly Using Shape-Morphing Hydrogels. *Adv. Mater.* **2020**, *2002195*, e2002195. https://doi.org/10.1002/adma.202002195.

(6)   Laurent, J.; Blin, G.; Chatelain, F.; Vanneaux, V.; Fuchs, A.; Larghero, J.; Théry, M. Convergence of Microengineering and Cellular Self-Organization towards Functional Tissue Manufacturing. *Nat. Biomed. Eng.* **2017**, *1* (12), 939–956. https://doi.org/10.1038/s41551-017-0166-x.

(7)   Ahadian, S.; Civitarese, R.; Bannerman, D.; Mohammadi, M. H.; Lu, R.; Wang, E.; Davenport-huyer, L.; Lai, B.; Zhang, B.; Zhao, Y.; et al. Organ-On-A-Chip Platforms : A Convergence of Advanced Materials , Cells , and Microscale Technologies. *Adv. Healthc. Mater.* **2018**, *7* (1700506). https://doi.org/10.1002/adhm.201700506.

(8)   Xing, F.; Xu, J.; Yu, P.; Zhou, Y.; Zhe, M.; Luo, R.; Liu, M.; Xiang, Z.; Duan, X.; Ritz, U. Recent Advances in Biofabrication Strategies Based on Bioprinting for Vascularized Tissue Repair and Regeneration. *Mater. Des.* **2023**, *229*, 111885. https://doi.org/10.1016/j.matdes.2023.111885.

(9)   Bian, S.; Repic, M.; Guo, Z.; Kavirayani, A.; Burkard, T.; Bagley, J. A.; Krauditsch, C.; Knoblich, J. A. Genetically Engineered Cerebral Organoids Model Brain Tumor Formation. *Nat. Methods* **2018**, *15* (8), 631–639.

https://doi.org/10.1038/s41592-018-0070-7.

(10) Lutolf, M. P.; Hubbell, J. A. Synthetic Biomaterials as Instructive Extracellular Microenvironments for Morphogenesis in Tissue Engineering. *Nat. Biotechnol.* **2005**, *23*, 47–55. https://doi.org/https://doi.org/10.1038/nbt1055.

(11) Seliktar, D. Designing Cell-Compatible Hydrogels for Biomedical Applications. *Science (80-.).* **2012**, *336* (6085), 1124–1129. https://doi.org/10.1126/science.1214804.

(12) Burdick, J. A.; Murphy, W. L. Moving from Static to Dynamic Complexity in Hydrogel Design. *Nat. Commun.* **2012**, *3*, 1–8. https://doi.org/10.1038/ncomms2271.

(13) El-ali, J.; Sorger, P. K.; Jensen, K. F. Cells on Chips. *Nature* **2006**, *442*, 403–411. https://doi.org/10.1038/nature05063.

(14) Albrecht, D. R.; Underhill, G. H.; Wassermann, T. B.; Sah, R. L.; Bhatia, S. N. Probing the Role of Multicellular Organization in Three-Dimensional Microenvironments. *Nat. Methods* **2006**, *3* (5), 369–375. https://doi.org/10.1038/NMETH873.

(15) Eng, G.; Lee, B. W.; Parsa, H.; Chin, C. D.; Schneider, J.; Linkov, G.; Sia, S. K.; Vunjak-Novakovic, G. Assembly of Complex Cell Microenvironments Using Geometrically Docked Hydrogel Shapes. *PNAS* **2013**, *110* (12), 4551–4556. https://doi.org/10.1073/pnas.1300569110.

(16) Du, Y.; Lo, E.; Ali, S.; Khademhosseini, A. Directed Assembly of Cell-Laden Microgels for Fabrication of 3D Tissue Constructs. *PNAS* **2008**, *105* (28), 9522–9527. https://doi.org/10.1073/pnas.0801866105.

(17) Todhunter, M. E.; Jee, N. Y.; Hughes, A. J.; Coyle, M. C.; Cerchiari, A.; Farlow, J.; Garbe, J. C.; Labarge, M. A.; Desai, T. A.; Gartner, Z. J. Programmed Synthesis of Three-Dimensional Tissues. *Nat. Methods* **2015**, *12* (10), 975–981. https://doi.org/10.1038/nmeth.3553.

(18) Harada, A.; Kobayashi, R.; Takashima, Y.; Hashidzume, A.; Yamaguchi, H. Macroscopic Self-Assembly through Molecular Recognition. *Nat. Chem.* **2011**, *3* (1), 34–37. https://doi.org/10.1038/nchem.893.

(19) Qi, H.; Ghodousi, M.; Du, Y.; Grun, C.; Bae, H.; Yin, P.; Khademhosseini, A. DNA-Directed Self-Assembly of Shape-Controlled Hydrogels. *Nat. Commun.* **2013**, *4*. https://doi.org/10.1038/ncomms3275.

(20) Muir, V. G.; Qazi, T. H.; Weintraub, S.; Maldonado, B. O. T.; Arratia, P. E.; Burdick, J. A. Sticking Together: Injectable Granular Hydrogels with Increased Functionality via Dynamic Covalent Inter-Particle Crosslinking. *Small* **2022**, 1–14. https://doi.org/10.1002/smll.202201115.

(21) Qazi, T. H.; Wu, J.; Muir, V. G.; Weintraub, S.; Gullbrand, S. E.; Lee, D.; Issadore, D.; Burdick, J. A. Anisotropic Rod-Shaped Particles Influence Injectable Granular Hydrogel Properties and Cell Invasion. *Adv. Mater.* **2022**, *34*, 1–12. https://doi.org/10.1002/adma.202109194.

(22) Guo, F.; Mao, Z.; Chen, Y.; Xie, Z.; Lata, J. P.; Li, P.; Ren, L.; Liu, J.; Yang, J.; Dao, M.; et al. Three-Dimensional Manipulation of Single Cells Using Surface Acoustic Waves. *Proc. Natl. Acad. Sci. U. S. A.* **2016**, *113* (6), 1522–1527. https://doi.org/10.1073/pnas.1524813113.

(23) Tasoglu, S.; Yu, C. H.; Gungordu, H. I.; Guven, S.; Vural, T.; Demirci, U. Guided and Magnetic Self-Assembly of Tunable Magnetoceptive Gels. *Nat. Commun.* **2014**, *5* (4702), 1–11. https://doi.org/10.1038/ncomms5702.

(24) Stevens, K. R.; Ungrin, M. D.; Schwartz, R. E.; Ng, S.; Carvalho, B.; Christine, K. S.; Chaturvedi, R. R.; Li, C. Y.; Zandstra, P. W.; Chen, C. S.; et al. InVERT Molding for Scalable Control of Tissue Microarchitecture. *Nat. Commun.* **2013**, *4*, 1–10. https://doi.org/10.1038/ncomms2853.

(25) Burdick, J. A.; Prestwich, G. D. Hyaluronic Acid Hydrogels for Biomedical Applications. *Adv. Healthc. Mater.* **2011**, *23* (12), H41–H56. https://doi.org/10.1002/adma.201003963.

(26) Highley, C. B.; Prestwich, G. D.; Burdick, J. A. Recent Advances in Hyaluronic Acid Hydrogels for Biomedical Applications. *Curr. Opin. Biotechnol.* **2016**, *40*, 35–40. https://doi.org/10.1016/j.copbio.2016.02.008.

(27) Davidson, C. D.; Jayco, D. K. P.; Wang, W. Y.; Shikanov, A.; Baker, B. M. Fiber Crimp Confers Matrix Mechanical Nonlinearity, Regulates Endothelial Cell Mechanosensing, and Promotes Microvascular Network Formation. *J. Biomech. Eng.* **2020**, *142* (11), 1–9. https://doi.org/10.1115/1.4048191.

(28) Davidson, C. D.; Jayco, D. K. P.; Matera, D. L.; DePalma, S. J.; Hiraki, H. L.; Wang, W. Y.; Baker, B. M. Myofibroblast Activation in Synthetic Fibrous Matrices Composed of Dextran Vinyl Sulfone. *Acta Biomater.* **2020**, *105*, 78–86. https://doi.org/https://doi.org/10.1016/j.actbio.2020.01.009.

(29) Wang, W. Y.; Davidson, C. D.; Lin, D.; Baker, B. M. Actomyosin Contractility-

Dependent Matrix Stretch and Recoil Induces Rapid Cell Migration. *Nat. Commun.* **2019**, *10*, 1–12. https://doi.org/10.1038/s41467-019-09121-0.

(30)   Wingate, K.; Bonani, W.; Tan, Y.; Bryant, S. J.; Tan, W. Compressive Elasticity of Three-Dimensional Nanofiber Matrix Directs Mesenchymal Stem Cell Differentiation to Vascular Cells with Endothelial or Smooth Muscle Cell Markers. *Acta Biomater.* **2012**, *8* (4), 1440–1449. https://doi.org/10.1016/j.actbio.2011.12.032.

(31)   Lin-Gibson, S.; Jones, R. L.; Washburn, N. R.; Horkay, F. Structure-Property Relationships of Photopolymerizable Poly(Ethylene Glycol) Dimethacrylate Hydrogels. *Macromolecules* **2005**, *38* (7), 2897–2902. https://doi.org/https://doi.org/10.1021/ma0487002.

(32)   Grewal, M. G.; Gray, V. P.; Letteri, R. A.; Highley, C. B. User-Defined, Temporal Presentation of Bioactive Molecules on Hydrogel Substrates Using Supramolecular Coiled Coil Complexes. *Biomater. Sci.* **2021**, *9* (12), 4374–4387. https://doi.org/10.1039/d1bm00016k.

(33)   Wade, R. J.; Bassin, E. J.; Gramlich, W. M.; Burdick, J. A. Nanofibrous Hydrogels with Spatially Patterned Biochemical Signals to Control Cell Behavior. *Adv. Mater.* **2015**, *27* (8), 1356–1362. https://doi.org/https://doi.org/10.1002/adma.201404993.

(34)   Gramlich, W. M.; Kim, I. L.; Burdick, J. A. Synthesis and Orthogonal Photopatterning of Hyaluronic Acid Hydrogels with Thiol-Norbornene Chemistry. *Biomaterials* **2013**, *34* (38), 9803–9811. https://doi.org/10.1016/j.biomaterials.2013.08.089.

(35)   Deforest, C. A.; Polizzotti, B. D.; Anseth, K. S. Sequential Click Reactions for Synthesizing and Patterning Three-Dimensional Cell Microenvironments. *Nat. Mater.* **2009**, *8* (8), 659–664. https://doi.org/10.1038/nmat2473.

(36)   Hui, E.; Gimeno, K. I.; Guan, G.; Caliari, S. R. Spatiotemporal Control of Viscoelasticity in Phototunable Hyaluronic Acid Hydrogels. *Biomacromolecules* **2019**, *20* (11), 4126–4134. https://doi.org/https://doi.org/10.1021/acs.biomac.9b00965.

(37)   Chen, C. S.; Mrksich, M.; Huang, S.; Whitesides, G. M.; Ingber, D. E. Geometric Control of Cell Life and Death. *Science (80-.).* **1997**, *276* (5317), 1425–1428. https://doi.org/10.1126/science.276.5317.1425.

(38)   Kloxin, A. M.; Kasko, A. M.; Salinas, C. N.; Anseth, K. S. Photodegradable Hydrogels for Dynamic Tuning of Physical and Chemical Properties. *Science (80-.*

). **2009**, *324* (5923), 59–63.

(39) Velasco-Hogan, A.; Xu, J.; Meyers, M. A. Additive Manufacturing as a Method to Design and Optimize Bioinspired Structures. *Adv. Mater.* **2018**, *30* (1800940), 1–26. https://doi.org/https://doi.org/10.1002/adma.201800940.

(40) Murphy, S. V; De Coppi, P.; Atala, A. Opportunities and Challenges of Translational 3D Bioprinting. *Nat. Biomed. Eng.* **2020**, *4*, 370–380.

(41) Highley, C. B.; Rodell, C. B.; Burdick, J. A. Direct 3D Printing of Shear-Thinning Hydrogels into Self-Healing Hydrogels. *Adv. Mater.* **2015**, *27* (34), 5075–5079. https://doi.org/10.1002/adma.201501234.

(42) Grewal, M. G.; Highley, C. B. Electrospun Hydrogels for Dynamic Culture Systems: Advantages, Progress, and Opportunities. *Biomater. Sci.* **2021**, *9*, 4228–4245. https://doi.org/10.1039/d0bm01588a.

(43) Sundararaghavan, H. G.; Metter, R. B.; Burdick, J. A. Electrospun Fibrous Scaffolds with Multiscale and Photopatterned Porosity. *Macromol. Biosci.* **2010**, *10* (3), 265–270. https://doi.org/10.1002/mabi.200900363.

(44) Kim, I. L.; Khetan, S.; Baker, B. M.; Chen, C. S.; Burdick, J. A. Fibrous Hyaluronic Acid Hydrogels That Direct MSC Chondrogenesis through Mechanical and Adhesive Cues. *Biomaterials* **2013**, *34* (22), 5571–5580. https://doi.org/10.1016/j.biomaterials.2013.04.004.

(45) Prendergast, M. E.; Davidson, M. D.; Burdick, J. A. A Biofabrication Method to Align Cells within Bioprinted Photocrosslinkable and Cell-Degradable Hydrogel Constructs via Embedded Fibers. *Biofabrication* **2021**, *13*.

(46) Davidson, M. D.; Prendergast, M. E.; Ban, E.; Xu, K. L.; Mickel, G.; Mensah, P.; Dhand, A.; Janmey, P. A.; Shenoy, V. B.; Burdick, J. A. Programmable and Contractile Materials through Cell Encapsulation in Fibrous Hydrogel Assemblies. *Sci. Adv.* **2021**, *7*, 1–14.

(47) Nih, L. R.; Sideris, E.; Carmichael, S. T.; Segura, T. Injection of Microporous Annealing Particle (MAP) Hydrogels in the Stroke Cavity Reduces Gliosis and Inflammation and Promotes NPC Migration to the Lesion. *Adv. Mater.* **2017**, *29* (1606471), 1–8. https://doi.org/10.1002/adma.201606471.

(48) Kwon, M. Y.; Wang, C.; Galarraga, J. H.; Puré, E.; Han, L.; Burdick, J. A. Influence of Hyaluronic Acid Modification on CD44 Binding towards the Design of Hydrogel Biomaterials. *Biomaterials* **2019**, *222* (119451), 1–9.

https://doi.org/https://doi.org/10.1016/j.biomaterials.2019.119451.

(49)   Hoyle, C. E.; Bowman, C. N. Thiol – Ene Click Chemistry. *Angew. Chemie* **2010**, *49*, 1540–1573. https://doi.org/https://doi.org/10.1002/anie.200903924.

(50)   Sharma, S.; Floren, M.; Ding, Y.; Stenmark, K. R.; Tan, W.; Bryant, S. J. A Photoclickable Peptide Microarray Platform for Facile and Rapid Screening of 3-D Tissue Microenvironments. *Biomaterials* **2017**, *143*, 17–28. https://doi.org/10.1016/j.biomaterials.2017.07.025.

(51)   Agha, A.; Waheed, W.; Alamoodi, N.; Mathew, B.; Alnaimat, F.; Abu-Nada, E.; Abderrahmane, A.; Alazzam, A. A Review of Cyclic Olefin Copolymer Applications in Microfluidics and Microdevices. *Macromol. Mater. Eng.* **2022**, *307* (8), 1–34. https://doi.org/10.1002/mame.202200053.

(52)   David T. Scadden. The Stem-Cell Niche as an Entity of Action. *Nature* **2006**, *441*, 1075–1079.

(53)   Basurto, I. M.; Mora, M. T.; Gardner, G. M.; Christ, G. J.; Caliari, S. R. Aligned and Electrically Conductive 3D Collagen Scaffolds for Skeletal Muscle Tissue Engineering. *Biomater. Sci.* **2021**, *9* (11), 4040–4053. https://doi.org/10.1039/d1bm00147g.

CHAPTER 8: CONCLUSIONS AND FUTURE DIRECTIONS

8.1. Summary

The work reported herein focused on the development of biofabrication platforms that build upon the dimensionality of electrospun hydrogel fibers. Historically, electrospun fibers were reduced to static, 2D substrates that served to provide nano-to-microscale topography to cells seeded on the top of the scaffold. However, electrospun hydrogel fibers are analogous to the fibrous proteins in native ECM, which is a characteristic that has motivated a paradigm shift towards increasing the dynamic complexities of hydrogel fibers past just being static substrates. In this dissertation, we aimed to modify the biochemical and biophysical profiles of electrospun hydrogel fibers (comprised of HA and PEG derivatives) to increase their dimensionality in both time and space. Importantly, while the reported biofabrication platforms here are in their relative infancy and were developed with generalizability as the main goal, we envision that they will be applicable to virtually any tissue system of interest – providing platforms to further our collective understanding of biological processes like development, function, and dysfunction.

8.2. Conclusions and Future Directions

8.2.1. User-defined, temporal presentation of bioactive molecules on hydrogel substrates using supramolecular coiled coil complexes

In Chapter 3, we sought to develop a platform that enables user-defined, reversible presentation of biomolecules on hydrogel substrates (both isotropic and fibrous), with the goal of providing the capability to temporally dictate bioactivity. To achieve this, we identified a suite of peptides that were previously demonstrated to form heterodimeric

coiled coils[1] and modified them to enable spatially-controlled tethering to NorHA and PEGNB hydrogels and hydrogel fibers. Essentially, this system leverages three peptides: the peptide that is conjugated to the substrate (T-peptide), the bioactive peptide (A-peptide), and the disruptor peptide (D-peptide). A-peptide will interact with both T- and D-peptides, but preferentially binds to the D-peptide. Therefore, the T:A complex introduces bioactivity to the substrate and introduction of the D-peptide will strip the A-peptide away from the T-peptide, thereby rendering the substrate inert. This process was modulated by peptide affinities and reversibility was afforded through toehold-mediated strand displacement.

Through isothermal titration calorimetry, we were able to elucidate relative binding affinities that facilitated biomolecule presentation and reversibility. This strategy was demonstrated to be similarly efficacious in presenting biomolecules when compared to covalent conjugation mechanisms, with removal occurring simply via the addition of the competing D-peptide. Appending an RGD motif to the end of the A-peptide enables cell spreading, and subsequent removal of the RGD peptide results in decreased cell areas. Importantly, this scheme is repeatable, with multiple rounds of functionalization possible following removal of the original biomolecule – providing flexibility in the temporal presentation of multiple biomolecules to dictate the biochemical profile of the hydrogel and hydrogel fiber substrates.

While the biological demonstrations of this technique were limited to cell adhesion and spreading for proof-of-concept work, this system is generalizable and simple to implement for any number of biomolecules. The only required step to change the biological context of the scheme is to modify the bioactive motif that is appended to the

A-peptide. There are numerous well-studied peptide motifs that confer different modes of bioactivity to the microenvironment. In addition to the fibronectin-mimetic RGD motif[2], other common adhesive peptides include the laminin-mimetic IKVAV and YIGSR sequences that have demonstrated success with neural cell types[3]. There has also been significant research in the isolation and application of growth factor-mimetic peptide motifs. For example, VEGF[4] and FGF-2[5] are two common growth factors with identified bioactive sequences that can be synthesized as short peptides ($\leq$15 amino acid residues). These sequences could possibly be appended to the end of the A-peptide to confer angiogenic properties[4] (in the case of VEGF) or mitogenic activity to neural stem cells[5] (in the case of FGF-2). The ability to modulate both adhesion and growth factor-like molecules in a time-dependent manner is a powerful advantage of this reversible peptide platform.

This platform was demonstrated on 2D isotropic and fibrous hydrogel substrates, but all tissues exist in 3D[6]. Therefore, an outstanding question with this reversible peptide technique is how it will perform in 3D constructs where diffusion is an extra variable that will affect the rates (and possibly the effectiveness) of reversibility. Coupled with diffusion into the hydrogel network, the effect of peptide size and charge might be implicated in the rate and performance of reversibility[7]. Further studies are required to determine how this system performs in 3D. It is possible that this system could be combined with the layer-by-layer biofabrication platform introduced in Chapter 7, where the discrete layers that are stacked to form a hydrogel might allow for increased diffusion between layers compared to a bulk, isotropic hydrogel. Additionally, this layering technique potentially

allows for deconstruction of the system to enable reversible processing of each layer independently prior to being re-stacked into the 3D construct again.

Finally, this peptide system has applications that extend beyond the biochemical activity of a hydrogel system. Reversible interactions are attractive strategies to enable supramolecularly crosslinked hydrogels[8–10]. Two of the most common strategies are the use of β-cyclodextrin-adamantane complexes and cucurbituril-based guest-host complexes and have reported K_D values of 10^{-5} M^{11} and 10^{-11}-10^{-12} M^{12}, respectively. Our system exhibits K_D values on the order of 10^{-8}-10^{-9} M^1, indicating that it might provide an intermediate supramolecular crosslinking strategy compared to β-cyclodextrin- and cucurbituril-based modes. Additionally, the relatively facile synthesis of peptides and their photomediated conjugation to hydrogels could provide an easier pathway to introducing supramolecular crosslinks than other strategies that require intensive chemical processing[13]. Overall, this peptide-based platform for user-defined reversibility of bioactivity on hydrogel substrates offers great potential in the tissue engineering and regenerative medicine spaces.

8.2.2. Fiber-based granular hydrogels with increased interparticle interactions for robust mechanical properties and tunable viscoelasticity and stress relaxation

In Chapters 5 and 6, we sought to develop a granular hydrogel medium comprised of discrete electrospun fibers that would enable increased interparticle interactions between constituent fibers, yielding unique properties compared to conventional granular hydrogels made of spherical (or nearly spherical) particles. To achieve this, we electrospun MeHA fibers (Chapter 5) and PEGNB fibers (Chapter 6) and segmented them

via mechanical agitation processes. Discrete fiber segments were then packed via centrifugation to form packed hydrogel microfiber (PHM) scaffolds and bulk mechanical properties were assessed via oscillatory shear rheology and filament stretching extensional rheology.

Chapter 5 aimed to characterize MeHA-based PHMs as shear-thinning and self-healing biomaterial inks that would enable injection and extrusion printing processes. Owing to the high-aspect ratios of the fibers, individual fibers are able to entangle and interact with other fibers within the granular hydrogel, resulting in mechanically robust materials that behave like bulk solids at rest. These entanglements also enable extreme extensibility of these materials (stretching to >2000% of their original heights). These PHMs are also viscoelastic and exhibit rapid stress relaxation properties (~10 s). Importantly, PHMs can be diluted to increase interfiber fluid content, and these unique mechanical phenomena were conserved at all dilutions investigated. We next demonstrated through macroscale extrusion printing that PHMs are favorable biomaterial inks for extrusion-based processes. The resultant filaments are mechanically robust and are easily manipulated – likely owing to the entanglements between fibers affording extensibility. These filaments do not require secondary annealing processes and can span length scales previously unrealized by other granular hydrogel media without covalent interactions between discrete particles. Interestingly, extruding PHMs results in shear-induced alignment of individual fibers, which confers contact guidance cues to cells. Finally, MeHA-based PHMs are permissive, 3D environments that are suitable for encapsulation cell culture, with cells likely able to interrogate and possibly remodel the scaffold.

Chapter 6 leveraged PEG-based PHMs and demonstrated their viscoelasticity and time-dependent stress relaxation profiles compared to conventional granular hydrogels comprised of spherical PEG particles. The increased interparticle interactions within PEG-based PHMs allows for fibers to entangle with each other and slide during reorganization, resulting in tunable time-dependent stress relaxation profiles ($T_{1/2}$ ~ 1-100+ s) across a range of applied strains. These behaviors were reported to be unique to PHMs, with conventional granular hydrogels comprised of spheres with matched volume and dimension unable to replicate these complex mechanical properties. Finally, PHM mechanics can be increased via the addition of fiber subpopulations that can participate in secondary annealing processes. The modular design of fiber subpopulations theoretically enables the addition of an elastic reinforcement structure to the otherwise unannealed PHM, with nonannealed fibers still able to slide and reorganize around this annealed scaffolding.

The mechanical characterization of PHMs was primarily conducted using oscillatory shear rheology to determine bulk mechanical properties at the macroscale. To further understand how these materials would present to cells at the microscale, additional characterization is needed. Atomic force microscopy is a powerful technique that enables more localized investigation of mechanical properties[14] and would provide useful information regarding how cells might perceive a PHM environment. Additionally, more cellular studies would elucidate how PHMs perform as 3D cell culture scaffolds. From an extrusion printing perspective, the shear-induced alignment might be advantageous for applications where cells are known to align to form structures. Examples for this include the formation of vasculature[15] or muscle fibers[16], and the ability

to 3D bioprint filaments that offer anisotropic contact guidance cues might enable direct design of structures that promote the formation of vessel-like or muscle-like structures.

The viscoelasticity of PHMs might also offer advantages when utilizing them as 3D, permissive scaffolds. For example, PEG-based PHMs generally exhibited soft, viscoelastic properties, which might be advantageous for modeling brain tissue where the amorphous material component dominates tissue mechanics. Additionally, brain-specific cell types have been shown to migrate and grow largely independent of adhesion forces[17], and PHMs might be a useful platform to study those behaviors. As another example, dynamic hydrogels are known to facilitate the formation of vasculature *in vitro*[18], suggesting the utility of PHMs for morphogenic processes like angiogenesis.

There is also room for improvement in PHM design. Both the MeHA fiber-based and PEG fiber-based PHMs are relatively static from a fiber-design perspective. One of the most common ways to introduce dynamic complexity into hydrogel fibers is to crosslink them using a molecule that is susceptible to enzyme-mediated degradation[13]. There are established crosslinkers designed to be cleaved by specific cell-secreted matrix metalloproteinases and can be incorporated into the electrospinning precursor solution to fabricate fibers that degrade over time in the presence of cells[19]. Engineering PHMs with controlled degradation profiles is an important step prior to *in vivo* work. PHMs have demonstrated mechanical stability due to their high degrees of interparticle interactions, so if they are designed such that they degrade and can be cleared by cells *in vivo*, it would enhance their utility as injectable biomaterials scaffolds. Relatedly, future *in vivo* work would enable evaluation of PHM performance as tools for regeneration and should logically follow further *in vitro* biological experiments – such as the aforementioned

possibilities. Overall, PHMs exhibit exciting potential as both injectable/extrudable biomaterials and 3D, permissive scaffolds, and future work will continue to demonstrate their utility in the tissue engineering and regenerative medicine space.

8.2.3. A layer-by-layer biofabrication technology for achieving near-single-cell resolution in cell dense, macroscale tissue constructs

In Chapter 7, we sought to develop a biofabrication platform that allows arbitrary definition of cellular and material composition of 3D, macroscale constructs with microscale resolution that approaches near-single-cell level precision. To achieve this, we identified a potential strategy that leverages a layer-by-layer assembly of thin hydrogel scaffolds comprised of spatially-patternable electrospun fibers. These fibers were fabricated using both NorHA and MeHA, and enabled specification of the localization of biomolecules, cells, and materials through the thiol-ene reaction scheme. Preliminary photopatterning experiments revealed patterned features with high fidelity, with limitations of light-based spatial control occurring at feature sizes <70 μm, which is within the same order of magnitude of most cell types. Through the same patterning process, except with the addition of a thiolated RGD peptide, cell localization was restricted to RGD+ regions, thereby demonstrating control over cellular architecture on a 2D scaffold.

To enable layering of these planar electrospun scaffolds to form a 3D macroscale construct, thin films of cyclic olefin copolymer (COC) were identified as the support substrate for the electrospun fibers. COC films were ablated using a CO_2 laser to yield void spaces for fibers to span across. These "unsupported" regions where fibers span across the void spaces allow direct contact of fibers following layering. They also allow

holes to be patterned into electrospun fibers that might form channels as multiple scaffolds with holes are stacked together[20]. Finally, since each layer of electrospun fibers can be independently processed, different photomasks can be utilized to pattern heterogeneity (that might relate to other layers) throughout 3D space following layering of individual scaffolds. This concept was preliminarily demonstrated using photomasks designed to pattern different features across 2 layers that come together upon layering to reveal the University of Virginia's "Split-V" logo.

While the major steps required to achieve this biofabrication platform were established and preliminarily demonstrated here, there is still considerable work needed to fully establish this tool. First, and perhaps most importantly, the ability to control the localization of cells on fibers that span void spaces on COC films is a critical assumption using this system. This assumption is theoretically grounded in previous work that has demonstrated cells adhering to fibers that span wells in PDMS substrates[21,22]. Controlling the spatial localization of cells on independent layers would allow a "co-culture" system upon layering, but it is also desirable to control cellular heterogeneity on each layer. This might be enabled by subsequent thiol-ene reactions, or the use of the peptide system described in Chapter 3. Similarly, utilizing photomasks to introduce holes[20] that can be aligned to form channels upon stacking would be advantageous to improve nutrient diffusion into the scaffold – a pervasive challenge in 3D hydrogels[23]. Finally, the layering concept was limited to 2 layers here; however, future work should include multiple layers to build out a construct from the bottom up to create 3D macroscale constructs with microscale resolution in the cellular and material heterogeneity.

This biofabrication platform has exciting potential once it is fully developed with the future work suggestions described above. The ability to control the cellular and material profile of a 3D construct with high resolution would enable fabrication of tissue-mimetics with previously unrealized features. One possible example would be engineering artificial lymph node tissue. Lymph node tissue is highly regulated and possesses an innate reticular structure that could potentially be recapitulated with a layer-by-layer assembly of electrospun hydrogel fiber scaffolds[24]. The perivascular neural stem cell niche is another example of a tightly regulated tissue system that could benefit from a biofabrication platform that enables specificity of the material and cellular design. This niche controls how neural stem cells behave through its design and presentation of relevant signals[25]. Finally, from a translational perspective, muscle tissue is highly aligned and cell-dense, and in the event of a traumatic event like volumetric muscle loss, needs an exogenous scaffold to support regeneration[16]. This biofabrication platform should enable the creation of cell-dense constructs by allowing cells on each layer to become confluent prior to layering, and if the electrospun hydrogel fibers contain a protease-sensitive crosslinker[19], then the fibrous layers between cells would degrade over time. Overall, this biofabrication platform is an innovative and exciting new tool for engineering tissue models with precise control over the material and cellular composition in 3D, macroscale constructs, with considerable possible applications in the tissue engineering and regenerative medicine spaces.

8.3. References

(1)   Grçger, K.; Gavins, G.; Seitz, O. Molecular Recognition Strand Displacement in Coiled-Coil Structures: Controlled Induction and Reversal of Proximity. *Angew. Chemie - Int. Ed.* **2017**, *56*, 14217–14221. https://doi.org/10.1002/anie.201705339.

(2)   Sharma, S.; Floren, M.; Ding, Y.; Stenmark, K. R.; Tan, W.; Bryant, S. J. A Photoclickable Peptide Microarray Platform for Facile and Rapid Screening of 3-D Tissue Microenvironments. *Biomaterials* **2017**, *143*, 17–28. https://doi.org/10.1016/j.biomaterials.2017.07.025.

(3)   Smith Callahan, L. A.; Xie, S.; Barker, I. A.; Zheng, J.; Reneker, D. H.; Dove, A. P.; Becker, M. L. Directed Differentiation and Neurite Extension of Mouse Embryonic Stem Cell on Aligned Poly(Lactide) Nanofibers Functionalized with YIGSR Peptide. *Biomaterials* **2013**, *34* (36), 9089–9095. https://doi.org/https://doi.org/10.1016/j.biomaterials.2013.08.028.

(4)   Wang, G.; Yuan, N.; Li, N.; Wei, Q.; Qian, Y.; Zhang, J.; Qin, M.; Wang, Y.; Dong, S. Vascular Endothelial Growth Factor Mimetic Peptide and Parathyroid Hormone (1-34) Delivered via a Blue-Light-Curable Hydrogel Synergistically Accelerate Bone Regeneration. *ACS Appl. Mater. Interfaces* **2022**, *14* (31), 35319–35332. https://doi.org/10.1021/acsami.2c06159.

(5)   Ray, J.; Baird, A.; Gage, F. H. A 10-Amino Acid Sequence of Fibroblast Growth Factor 2 Is Sufficient for Its Mitogenic Activity on Neural Progenitor Cells. *Proc. Natl. Acad. Sci. U. S. A.* **1997**, *94* (13), 7047–7052. https://doi.org/10.1073/pnas.94.13.7047.

(6)   Baker, B. M.; Chen, C. S. Deconstructing the Third Dimension – How 3D Culture Microenvironments Alter Cellular Cues. *J. Cell Sci.* **2012**, *125* (13), 3015–3024. https://doi.org/https://doi.org/10.1242/jcs.079509.

(7)   Pauletti, G. M.; Okumu, F. W.; Borchardt, R. T. Effect of Size and Charge on the Passive Diffusion of Peptides across Caco-2 Cell Monolayers via the Paracellular Pathway. *Pharm. Res.* **1997**, *14* (2), 164–168. https://doi.org/10.1023/A:1012040425146.

(8)   Mann, J. L.; Yu, A. C.; Agmon, G.; Appel, E. A. Supramolecular Polymeric Biomaterials. *Biomater. Sci.* **2018**, *6* (1), 10–37. https://doi.org/10.1039/c7bm00780a.

(9)   Highley, C. B.; Rodell, C. B.; Burdick, J. A. Direct 3D Printing of Shear-Thinning Hydrogels into Self-Healing Hydrogels. *Adv. Mater.* **2015**, *27* (34), 5075–5079. https://doi.org/10.1002/adma.201501234.

(10)   Feliciano, A. J.; Blitterswijk, C. Van; Moroni, L.; Baker, M. B. Realizing Tissue Integration with Supramolecular Hydrogels. **2021**, *124*, 1–14. https://doi.org/10.1016/j.actbio.2021.01.034.

(11)   Boekhoven, J.; Rubert Pérez, C. M.; Sur, S.; Worthy, A.; Stupp, S. I. Dynamic

Display of Bioactivity through Host-Guest Chemistry. *Angew. Chemie - Int. Ed.*
2013, *52* (46), 12077–12080.
https://doi.org/https://doi.org/10.1002/anie.201306278.

(12)	Appel, E. A.; Biedermann, F.; Rauwald, U.; Jones, S. T.; Zayed, J. M.; Scherman,
O. A. Supramolecular Cross-Linked Networks via Host - Guest Complexation with
Cucurbit[8]Uril. *J. Am. Chem. Soc.* **2010**, *132* (40), 14251–14260.
https://doi.org/https://doi.org/10.1021/ja106362w.

(13)	Grewal, M. G.; Gray, V. P.; Letteri, R. A.; Highley, C. B. User-Defined, Temporal
Presentation of Bioactive Molecules on Hydrogel Substrates Using
Supramolecular Coiled Coil Complexes. *Biomater. Sci.* **2021**, *9* (12), 4374–4387.
https://doi.org/10.1039/d1bm00016k.

(14)	Matera, D. L.; DiLillo, K. M.; Smith, M. R.; Davidson, C. D.; Parikh, R.; Said, M.;
Wilke, C. A.; Lombaert, I. M.; Arnold, K. B.; Moore, B. B.; et al. Microengineered
3D Pulmonary Interstitial Mimetics Highlight a Critical Role for Matrix Degradation
in Myofibroblast Differentiation. *Sci. Adv.* **2020**, *6* (37), 1–15.
https://doi.org/10.1126/sciadv.abb5069.

(15)	Varhue, W. B.; Rane, A.; Castellanos-Sanchez, R.; Peirce, S. M.; Christ, G.;
Swami, N. S. Perfusable Cell-Laden Micropatterned Hydrogels for Delivery of
Spatiotemporal Vascular-like Cues to Tissues. *Organs-on-a-Chip* **2022**, *4*, 1–10.
https://doi.org/10.1016/j.ooc.2022.100017.

(16)	Basurto, I. M.; Mora, M. T.; Gardner, G. M.; Christ, G. J.; Caliari, S. R. Aligned
and Electrically Conductive 3D Collagen Scaffolds for Skeletal Muscle Tissue
Engineering. *Biomater. Sci.* **2021**, *9* (11), 4040–4053.
https://doi.org/10.1039/d1bm00147g.

(17)	Santos, T. E.; Schaffran, B.; Broguiere, N.; Meyn, L.; Zenobi-wong, M.; Bradke, F.
Axon Growth of CNS Neurons in Three Dimensions Is Amoeboid and
Independent of Adhesions. *Cell Rep.* **2020**, *32*, 1–12.
https://doi.org/10.1016/j.celrep.2020.107907.

(18)	Wei, Z.; Schnellmann, R.; Pruitt, H. C.; Gerecht, S. Hydrogel Network Dynamics
Regulate Vascular Morphogenesis. *Stem Cell* **2020**, *27* (5), 798–812.
https://doi.org/10.1016/j.stem.2020.08.005.

(19)	Wade, R. J.; Bassin, E. J.; Rodell, C. B.; Burdick, J. A. Protease-Degradable
Electrospun Fibrous Hydrogels. *Nat. Commun.* **2015**, *6*, 1–10.
https://doi.org/https://doi.org/10.1038/ncomms7639.

(20)	Sundararaghavan, H. G.; Metter, R. B.; Burdick, J. A. Electrospun Fibrous
Scaffolds with Multiscale and Photopatterned Porosity. *Macromol. Biosci.* **2010**,
10 (3), 265–270. https://doi.org/10.1002/mabi.200900363.

(21)	Baker, B. M.; Trappmann, B.; Wang, W. Y.; Sakar, M. S.; Kim, I. L.; Shenoy, V.
B.; Burdick, J. A.; Chen, C. S. Cell-Mediated Fibre Recruitment Drives
Extracellular Matrix Mechanosensing in Engineered Fibrillar Microenvironments.
Nat. Mater. **2015**, *14*, 1262–1268.

https://doi.org/https://doi.org/10.1038/nmat4444.

(22) Davidson, M. D.; Song, K. H.; Lee, M. H.; Llewellyn, J.; Du, Y.; Baker, B. M.;
      Wells, R. G.; Burdick, J. A. Engineered Fibrous Networks to Investigate the
      Influence of Fiber Mechanics on Myofibroblast Differentiation. *ACS Biomater. Sci.
      Eng.* **2019**, *5* (8), 3899–3908.
      https://doi.org/https://doi.org/10.1021/acsbiomaterials.8b01276.

(23) Miller, J. S.; Stevens, K. R.; Yang, M. T.; Baker, B. M.; Nguyen, D. T.; Cohen, D.
      M.; Toro, E.; Chen, A. A.; Galie, P. A.; Yu, X.; et al. Rapid Casting of Patterned
      Vascular Networks for Perfusable Engineered Three-Dimensional Tissues. *Nat.
      Mater.* **2012**, *11*, 768–774. https://doi.org/10.1038/nmat3357.

(24) Liao, S.; Padera, T. P. Lymphatic Function and Immune Regulation in Health and
      Disease. *Lymphat. Res. Biol.* **2013**, *11* (3), 136–143.
      https://doi.org/10.1089/lrb.2013.0012.

(25) David T. Scadden. The Stem-Cell Niche as an Entity of Action. *Nature* **2006**, *441*,
      1075–1079.